Discrete Dynamics in Nature and Society

Complex Discrete Nonlinear Dynamics: Chaos and Its Applications

Guest Editors: Qingdu Li, Timothy J. Healey, Xiao-Song Yang, and Xiaofeng Liao

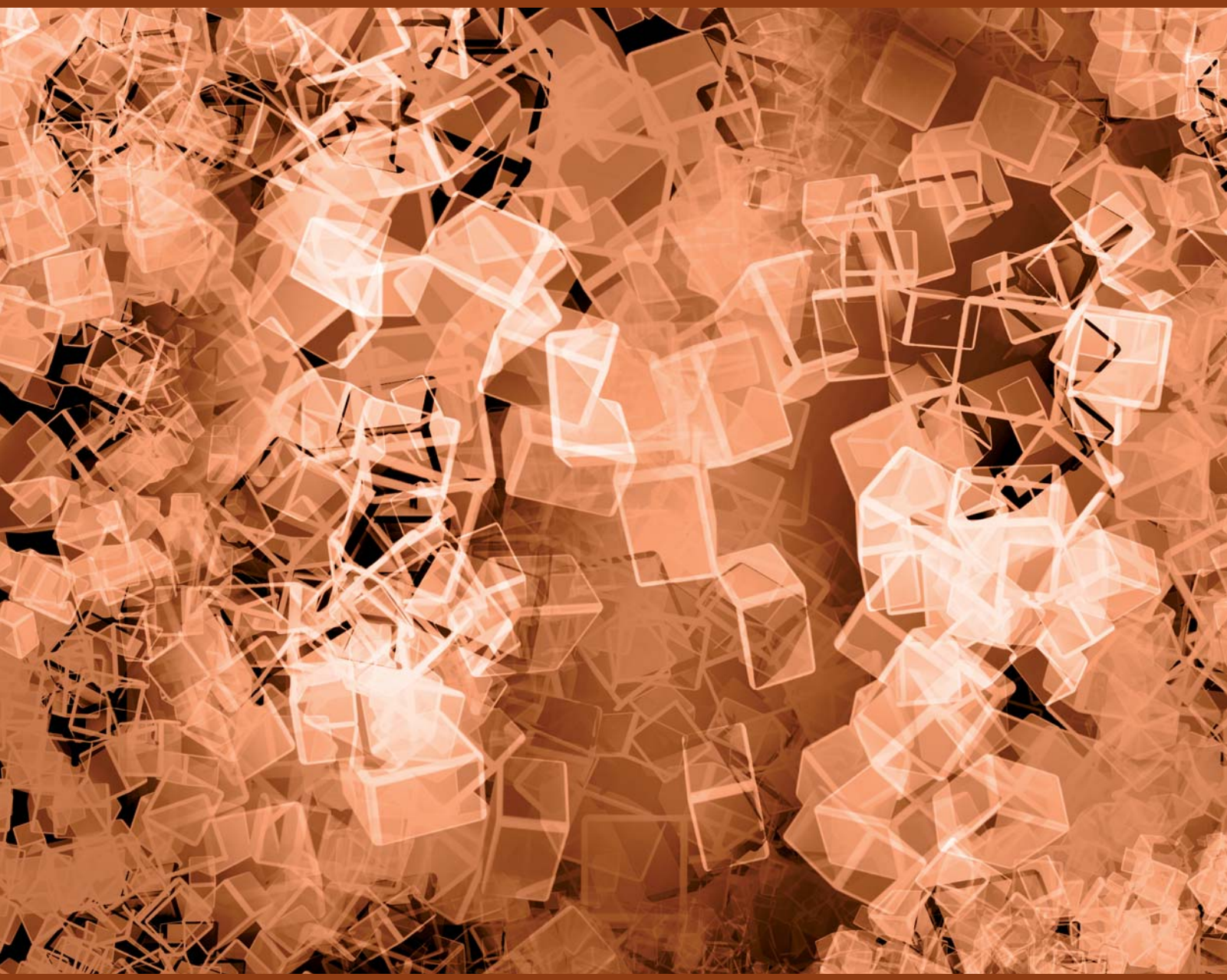

Complex Discrete Nonlinear Dynamics: Chaos and Its Applications

Discrete Dynamics in Nature and Society

Complex Discrete Nonlinear Dynamics: Chaos and Its Applications

Guest Editors: Qingdu Li, Timothy J. Healey, Xiao-Song Yang, and Xiaofeng Liao

Editorial Board

Contents

Complex Discrete Nonlinear Dynamics: Chaos and Its Applications, Qingdu Li, Timothy J. Healey, Xiao-Song Yang, and Xiaofeng Liao
Volume 2013, Article ID 806876, 2 pages

Multipulse Heteroclinic Orbits and Chaotic Dynamics of the Laminated Composite Piezoelectric Rectangular Plate, Minghui Yao and Wei Zhang
Volume 2013, Article ID 958219, 27 pages

Modeling a Tumor Growth with Piecewise Constant Arguments, F. Bozkurt
Volume 2013, Article ID 841764, 8 pages

Bifurcation and Chaos in a Price Game of Irrigation Water in a Coastal Irrigation District, Baogui Xin and Yuting Li
Volume 2013, Article ID 408904, 10 pages

Bifurcation of Limit Cycles of a Class of Piecewise Linear Differential Systems in $\mathbb{R}^4$ with Three Zones, Yanyan Cheng
Volume 2013, Article ID 385419, 9 pages

Bifurcation and Chaotic Behavior of a Discrete-Time SIS Model, Junhong Li and Ning Cui
Volume 2013, Article ID 705601, 8 pages

Horseshoe Chaos in a 3D Neural Network with Different Activation Functions, Fangyan Yang, Song Tang, and Guilan Xu
Volume 2013, Article ID 430963, 6 pages

Perturbation of Stochastic Boussinesq Equations with Multiplicative White Noise, Chunde Yang and Xin Zhao
Volume 2013, Article ID 875749, 6 pages

A Fractional-Order Chaotic System with an Infinite Number of Equilibrium Points, Ping Zhou, Kun Huang, and Chun-de Yang
Volume 2013, Article ID 910189, 6 pages

Complexity Analysis of a Cournot-Bertrand Duopoly Game Model with Limited Information, Hongwu Wang and Junhai Ma
Volume 2013, Article ID 287371, 6 pages

Dynamics Evolution of Credit Risk Contagion in the CRT Market, Tingqiang Chen, Jianmin He, and Qunyao Yin
Volume 2013, Article ID 206201, 9 pages

Hindawi Publishing Corporation
Discrete Dynamics in Nature and Society
Volume 2013, Article ID 806876, 2 pages
http://dx.doi.org/10.1155/2013/806876

Editorial

Complex Discrete Nonlinear Dynamics: Chaos and Its Applications

Qingdu Li,[1] Timothy J. Healey,[2] Xiao-Song Yang,[3] and Xiaofeng Liao[4]

[1] *Key Laboratory of Network Control & Intelligent Instrument, Ministry of Education, Chongqing University of Posts and Telecommunications, Chongqing 400065, China*
[2] *Department of Mathematics, Cornell University, Ithaca, NY 14850, USA*
[3] *Department of Mathematics, Huazhong University of Science and Technology, Wuhan 430074, China*
[4] *School of Electronic and Information Engineering, Southwest University, Chongqing 400715, China*

Correspondence should be addressed to Qingdu Li; liqd@cqupt.edu.cn

Received 31 July 2013; Accepted 31 July 2013

Nonlinear and chaotic behavior appears widely and naturally in many discrete dynamical systems; its study has led to vast multidisciplinary research in fields ranging from the natural sciences (mechanics, chemistry, biology, ecology, etc.) to the social sciences (economics, sociology, etc.) and engineering (electronics, control, communication, security, etc.). Recent advances in dynamical systems theory and computational methodologies have provided new ways of understanding such complex phenomena via novel tools and applications of discrete nonlinear dynamics.

This special issue contains ten papers, of which eight study chaotic behavior in some practical models from interesting fields, such as a Cournot-Bertrand duopoly game model, a price game model of irrigation water, a susceptible-infected-susceptible (SIS) model, the credit risk transfer (CRT) market model, a tumor growth model, a fractional-order system, a small neural network, and rectangular plates. There are also two theoretical papers focusing on the bifurcation of limit cycles from periodic orbits and the existence and uniqueness of the global solution for the stochastic Boussinesq equations, respectively.

Two game models are studied in detail in this special issue as typical discrete-time systems. "*Complexity analysis of a Cournot-Bertrand duopoly game model with limited information*" by H. Wang and J. Ma proposes a Cournot-Bertrand mixed game model, where the market has linear demand and two firms have the same fixed marginal cost, and shows complex dynamics, such as bifurcation scenarios and route to chaos, as well as parameter basin by numerical experiment. "*Bifurcation and chaos in a price game of irrigation water in a coastal irrigation district*" by B. Xin and Y. Li emphatically discusses the stability and codimension-two period-doubling (flip) bifurcation in a price game model with numerical bifurcation-based continuation methods, and the 0-1 test algorithm is used to compute the median value of correlation coefficient to indicate chaotic dynamics.

Mathematical models in the real world are often time-continuous systems or hybrid systems. To study their nonlinear dynamics, one frequently converts them to discrete systems. A common method is discretizing time with a well-chosen stepsize. "*Bifurcation and chaotic behavior of a discrete-time SIS model*" by J. Li and N. Cui obtains a discrete-time epidemic model with the Euler method, and shows rich and complex dynamical behaviors, such as transcritical bifurcation, flip bifurcation, Hopf bifurcation, and chaos. "*Dynamics evolution of credit risk contagion in the CRT market*" by T. Chen et al. introduces a nonlinear dynamics model to depict the dynamic behavior characteristics of evolution of credit risk contagion through numerical simulation and reports a series of Hopf bifurcations and chaotic phenomena in the process of credit risk contagion. "*Modeling a tumor growth with piecewise constant arguments*" by F. Bozkurt constructs two models of a tumor growth and shows that the increase of the population growth rate

decreases the local stability of the positive equilibrium point. "*A fractional-order chaotic system with an infinite number of equilibrium points*" by P. Zhou et al. studies chaos in a new 4-dimensional fractional-order system, which has an infinite number of equilibrium points, and also presents a chaotic synchronization scheme.

Another common method to discretize time-continuous systems is using Poincaré return maps. "*Multipulse heteroclinic orbits and chaotic dynamics of the laminated composite piezoelectric rectangular plate*" by M. Yao and W. Zhang demonstrates how to employ the energy phase method to analyze the Shilnikov type multipulse heteroclinic bifurcations and chaotic dynamics of high-dimensional nonlinear systems in engineering applications. "*Horseshoe chaos in a 3d neural network with different activation functions*" by F. Yang et al. studies a small neural network with three neurons. Although the network is a simple hybrid system with all subsystems being exponentially stable, they find that the network can exhibit very complex dynamics such as limit cycles and chaos, which implies that chaos is more related to its weight matrix than the type of activation functions.

Limit cycles, as well as their number and distribution, are significant for understanding the geometrical structures of the state space. "*Bifurcation of limit cycles of a class of piecewise linear differential systems in R^4 with three zones*" by Y. Cheng studies the bifurcation of limit cycles from periodic orbits of a four-dimensional system by the averaging method, and shows that when the parameter is sufficiently small, at most six limit cycles can bifurcate from periodic orbits in a class of asymmetric piecewise linear perturbed systems.

The existence and uniqueness of the solution are a fundamental problem for each dynamical system. "*Perturbation of stochastic Boussinesq equations with multiplicative white noise*" by C. Yang and X. Zhao studies the Boussinesq equations perturbed by multiplicative white noise, and shows the existence and uniqueness of the global solution. They also obtain some regularity results for the unique solution.

The topics of the selected papers in this issue do not of course cover this entire multidisciplinary field. Rather they represent rich and many-faceted results that we have the pleasure of sharing with the readers.

Since most dynamical systems have no explicit solution, it is often a hard task to theoretically analyze complex discrete nonlinear behavior. Although numerical methods works for most systems, it is often criticized because of numerical errors and increasing computational cost. Combining theoretical and numerical studies, like some of the aforementioned papers is perhaps a powerful approach. With interval algorithms on massive computing devices, nonlinear behavior, such as limit cycles, homoclinic/heteroclinic orbits, and even chaos, can be studied rigorously, and the complex geometrical structure of the state space and the parameter space may also be analyzed to reveal mechanisms behind the complex behavior, which are important for scientific and engineering purposes.

Acknowledgments

We would like to express our appreciation to the authors for their excellent contributions and patience in assisting us. The fundamental work of all reviewers on these papers is also very greatly acknowledged. In addition, Q. Li also would like to thank the National Natural Science Foundation of China (61104150) and Science Fund for Distinguished Young Scholars of Chongqing (cstc2013jcyjjq40001).

Qingdu Li
Timothy J. Healey
Xiao-Song Yang
Xiaofeng Liao

Hindawi Publishing Corporation
Discrete Dynamics in Nature and Society
Volume 2013, Article ID 958219, 27 pages
http://dx.doi.org/10.1155/2013/958219

Research Article

Multipulse Heteroclinic Orbits and Chaotic Dynamics of the Laminated Composite Piezoelectric Rectangular Plate

Minghui Yao and Wei Zhang

College of Mechanical Engineering, Beijing University of Technology, Beijing 100124, China

Correspondence should be addressed to Minghui Yao; ymh@bjut.edu.cn

Received 21 March 2013; Accepted 21 May 2013

Academic Editor: Qingdu Li

This paper investigates the multipulse global bifurcations and chaotic dynamics for the nonlinear oscillations of the laminated composite piezoelectric rectangular plate by using an energy phase method in the resonant case. Using the von Karman type equations, Reddy's third-order shear deformation plate theory, and Hamilton's principle, the equations of motion are derived for the laminated composite piezoelectric rectangular plate with combined parametric excitations and transverse excitation. Applying the method of multiple scales and Galerkin's approach to the partial differential governing equation, the four-dimensional averaged equation is obtained for the case of $1:2$ internal resonance and primary parametric resonance. The energy phase method is used for the first time to investigate the Shilnikov type multipulse heteroclinic bifurcations and chaotic dynamics of the laminated composite piezoelectric rectangular plate. The paper demonstrates how to employ the energy phase method to analyze the Shilnikov type multipulse heteroclinic bifurcations and chaotic dynamics of high-dimensional nonlinear systems in engineering applications. Numerical simulations show that for the nonlinear oscillations of the laminated composite piezoelectric rectangular plate, the Shilnikov type multipulse chaotic motions can occur. Overall, both theoretical and numerical studies suggest that chaos for the Smale horseshoe sense in motion exists.

1. Introduction

A piezoelectric material subjected to the mechanical force produces an electrical charge which is called the direct piezoelectric effect. Conversely, the material under an electrical field can generate mechanical stress which is called converse piezoelectric effect. In the development of intelligent structures, piezoelectric materials are widely designed as sensors and actuators for the active control of structures. Piezoelectric materials are usually clung to structural laminates used as devices to control deformation, shape, and vibration. There has been the model proposed for analysis of laminated composite plates containing active and passive piezoelectric layers. In aerospace applications, these smart structures are generally lightweight and have relatively large structural flexibility, and their flexibility can induce large deformation. Due to small material damping or the lack of environmental damping in space, fast motion or high-speed operation of laminated composite piezoelectric plates often generates the large amplitude vibration or geometrical nonlinearity. The complex nonlinear motions are strongly incited under the certain ranges of exciting frequency. Therefore, it is important to investigate large deformation and geometrically nonlinear effects of laminated composite piezoelectric plates in order to accurately design and effectively control structures.

Most of the studies on piezoelectric structures are based on linear piezoelectricity and linear elasticity theories, while research on the nonlinear dynamics of the piezoelectric structures is less. Lee et al. [1] incorporated the piezoelectric effect into the classical laminate plate theory and derived the distributed sensors and actuators which are capable of sensing and controlling the modal vibration of the cantilever plate. Tzou and Bao [2] formulated a new theory on thick anisotropic composite piezoelectric shell transducer laminates. This theory is applicable to a variety of composite piezoelectric structures. Reddy and Mitchell [3] developed geometrically nonlinear theories of laminated composite plates with piezoelectric laminae and used Hamilton's principle to derive equations of motion and boundary conditions of these theories. Hagood IV and McFarland [4] employed

the Rayleigh-Ritz mode energy method to study the distributed piezoceramics and the traveling wave dynamics of the stator. Sadri et al. [5] presented the theoretical vibration model of the piezoelectric plate and used the Rayleigh-Ritz method to obtain the governing nonlinear equations of the piezoelectric plate. Vel and Batra [6] utilized Eshelby-Stroh formalism to analyze the quasistatic deformations of linear piezoelectric laminated plates. Yu and Hodges [7] took advantage of the variational-asymptotic method to construct a Reissner-Mindlin model for the laminated composite piezoelectric plates subjected to mechanical, thermal, and electric loads. Huang and Shen [8] exploited the higher order shear deformation plate theory and von Karman-type equation to investigate the nonlinear vibration and dynamic response of the laminated piezoelectric plates subjected to mechanical, electrical, and thermal loads. Della and Shu [9] gave a review on the various analytical models and numerical analyses for free vibration of delaminated composites including composite piezoelectric laminates under axial loads. Zhang et al. [10] made use of Reddy's third-order shear deformation plate theory to analyze the bifurcations and chaotic dynamics of the four-edge simply supported, laminated composite piezoelectric rectangular plate in the case of 1 : 2 internal resonances. Sarangi and Ray [11] analyzed geometrically nonlinear transient vibrations of doubly curved laminated composite piezoelectric shells.

The global bifurcations and chaotic dynamics of high-dimensional nonlinear systems have been at the forefront of nonlinear dynamics for the past two decades. There are two ways of solutions on the Shilnikov type chaotic dynamics of high-dimensional nonlinear systems. One is Shilnikov type single-pulse chaotic dynamics and the other is the Shilnikov type multipulse chaotic dynamics. Most researchers focused on the Shilnikov type single-pulse chaotic dynamics of high-dimensional nonlinear systems. Wiggins [12] used the Melnikov method to investigate the global bifurcations and chaotic dynamics of three types high-dimensional perturbed Hamiltonian systems. With the aid of new global perturbation technique, Kovačič [13, 14] investigated the existence of the orbits homoclinic to resonance bands for the Hamiltonian systems and dissipative systems. Yagasaki [15] used the extended subharmonic Melnikov method and the modified homoclinic Melnikov method to examine periodic orbits and homoclinic motions in the coupled oscillators. Feng and Liew [16] canvassed the existence of the Shilnikov type single-pulse homoclinic orbits in the averaged equation which represents the modal interactions between two modes and influence of the fast mode on the slow mode. The global bifurcations and chaotic dynamics were investigated by Zhang et al. [17, 18] for the simply supported rectangular thin plates subjected to the parametrical-external excitation and the parametrical excitation. Yeo and Lee [19] employed the global perturbation technique to probe into the global dynamics of an imperfect circular plate with one-to-one internal resonance and obtained the criteria for chaotic motions of homoclinic orbits. Vakakis [20] adopted subharmonic and homoclinic Melnikov theory to study the strong nonlinear dynamic in a lattice and a lightweight of a nonlinear oscillator with nonlinearity stiffness.

Most research is on the Shilnikov type single-pulse global bifurcations and chaotic dynamics of high-dimensional nonlinear systems, but there are researchers investigating the Shilnikov type multipulse homoclinic and heteroclinic bifurcations and chaotic dynamics. So far, there are two theories of the Shilnikov type multipulse chaotic dynamics. One is the energy phase method and the other theory is the extended Melnikov method. Much achievement is made in the former theory of high-dimensional nonlinear systems. Haller and Wiggins [21] first established a simple energy-phase criterion which combined geometric singular perturbation theory, higher-dimensional Melnikov method, and transversality theory. Haller [22] derived a normal form for weak-strong resonance junctions in n-degree-of-freedom, nearly integrable Hamiltonian systems. Haller [23] proposed a new unified theory of orbits homoclinic to resonance bands in a class of near-integrable dissipative systems. Subsequently, Haller and Wiggins [24, 25] further developed the energy phase method to examine the existence of the multipulse homoclinic orbits in the damped-forced nonlinear Schrodinger equation and perturbed the Hamiltonian systems. Haller and Wiggins [26] proved the existence of the Shilnikov type multipulse homoclinic orbits to invariant 3 spheres and utilized the energy-phase method to investigate chaotic dynamics near resonant equilibria in three-degree-of-freedom Hamiltonian systems. Haller [27] derived a universal homoclinic tree describing the bifurcations of the multipulse homoclinic orbits near the intersection of a weaker and a stronger resonance in n-degree-of-freedom, nearly integrable Hamiltonian systems. Haller [28, 29] developed the energy-phase method to detect the existence of the Shilnikov-type multipulse orbits that repeatedly leave and come back to an invariant manifold with two different time scales in the perturbed nonlinear Schrodinger equation. Haller et al. [30] verified the existence of the Shilnikov-type multipulse homoclinic orbits to a spatially independent invariant torus in two coupled nonlinear Schrodinger equations with the damping and the quasiperiodical force. In book [31] published by Haller in 1999, they summarized the energy-phase method and presented a detailed procedure of the application to several problems in mechanics, which include the Shilnikov type multipulse homoclinic and heteroclinic orbits and chaotic dynamics.

Up to present, few researchers have made use of the energy phase method to study the Shilnikov type multipulse homoclinic and heteroclinic orbits and chaotic dynamics of high-dimensional nonlinear systems in engineering applications. Malhotra et al. [32] used the energy-phase method to investigate multipulse homoclinic orbits and chaotic dynamics for the motion of flexible spinning discs. McDonald and Namachchivaya [33] applied the Melnikov method, the Shilnikov method, and the energy-phase method to detect the presence of chaotic dynamics of parametrically excited pipes conveying fluid near a zero-to-one resonance. Yao and Zhang [34, 35] utilized the energy-phase method to analyze the Shilnikov type multipulse heteroclinic or homoclinic orbits and chaotic dynamics in a parametrically and externally excited rectangular thin plate and a laminated composite piezoelectric rectangular plate. Yu and Chen [36, 37] made

use of the energy-phase method to examine the Shilnikov type multipulse homoclinic orbits of a nonlinear cyclic system and a harmonically excited circular plate. Zhang et al. [38] extended the energy-phase method to six-dimensional system from four-dimensional system. They adopted the energy-phase method for six-dimensional system to delve into multipulse chaotic dynamics of a composite laminated piezoelectric rectangular plate subjected to the transverse, in-plane excitations and the piezoelectric excitation.

The study on the second theory of the Shilnikov type multipulse chaotic dynamics was stated by Kovačič and Wettergren [39]. They presented the extended Melnikov method to investigate the existence of the multipulse jumping of homoclinic orbits and chaotic dynamics in resonantly forced coupled pendula. Furthermore, Kaper and Kovačič [40] studied the existence of several classes of the multi-bump orbits homoclinic to resonance bands for completely integrable Hamiltonian systems subjected to small Hamiltonian amplitude and damped perturbations. Camassa et al. [41] applied the extended Melnikov method to analyze the multipulse jumping of homoclinic and heteroclinic orbits in a class of perturbed Hamiltonian systems. Until recently, Zhang and Yao [42, 43] introduced the extended Melnikov method to the engineering field. They came up with a simplification of the extended Melnikov method in the resonant case and utilized it to analyze the Shilnikov type multipulse homoclinic bifurcations and chaotic dynamics for the nonlinear nonplanar oscillations of the cantilever beam subjected to a harmonic axial excitation and two transverse excitations at the free end. Yao et al. [44] made use of the extended Melnikov method and numerical method to investigate multipulse chaotic dynamics in nonplanar motion of parametrically excited viscoelastic moving belt.

Despite extensive research of nonlinear dynamics in the laminated composite piezoelectric plate, multipulse chaotic dynamics has been studied rarely. Few researchers utilized the energy-phase method to investigate the Shilnikov type multipulse chaotic dynamics of high-dimensional nonlinear systems in engineering applications in the past several years. We have previously studied homoclinic bifurcations and multipulse chaotic dynamics of the laminated composite piezoelectric plate under the case of 1 : 3 internal resonances by applying the energy-phase method. In this paper, we have used the energy-phase method to investigate heteroclinic bifurcations and multipulse chaotic dynamics of the laminated composite piezoelectric plate under the case of 1 : 2 internal resonances.

It is the purpose of this paper to fill the research gap by investigating the Shilnikov type multipulse chaotic dynamics in the complex motion of the laminated composite piezoelectric plate. Based on the von Karman type equations and the Reddy's third-order shear deformation plate theory, the Hamilton's principle is employed to obtain the governing nonlinear equations of the laminated composite piezoelectric rectangular plate with combined parametric excitation and transverse load. We apply the method of multiple scales and Galerkin's approach to the partial differential governing equations to obtain the four-dimensional averaged equation

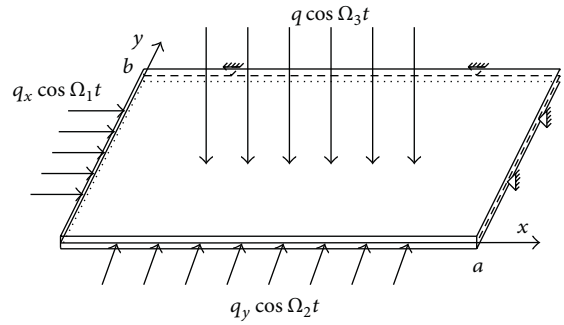

Figure 1: The model of a laminated composite piezoelectric rectangular plate is given.

for the case of 1 : 2 internal resonances and primary parametric resonance. From the averaged equation, the theory of normal form is used to find the explicit formulas of normal form. Finally, we employ the energy-phase method to analyze the Shilnikov type multipulse orbits and chaotic dynamics in the laminated composite piezoelectric plate. The analysis indicates that there exist the Shilnikov type multipulse jumping orbits in the perturbed phase space for the averaged equations. The results from numerical simulation also show that the chaotic motion can occur in the motion of the laminated composite piezoelectric plate, which verifies the analytical prediction. The Shilnikov type multipulse orbits are discovered from the results of numerical simulation. In summary, both theoretical and numerical studies demonstrate that chaos for the Smale horseshoe sense in the motion exists.

2. Equations of Motion and Perturbation Analysis

We consider a four-edge simply supported laminated composite piezoelectric rectangular plate, where the length, the width, and the thickness are denoted by a, b, and h, respectively. The laminated composite piezoelectric rectangular plate is subjected to in-plane excitation, transverse excitation, and piezoelectric excitation, as shown in Figure 1. We consider the laminated composite piezoelectric rectangular plate as regular symmetric cross-ply laminates with n layers with respect to principal material coordinates alternatively oriented at 0° and 90° to the laminate coordinate axes. Some of the layers are made of the piezoelectric materials as actuators, and the other layers are made of fiber-reinforced composite materials. It is assumed that different layers of the symmetric cross-ply composite laminated piezoelectric rectangular plate are perfectly clung to each other, and piezoelectric actuator layers are embedded in the plate. The fiber direction of odd-numbered layers is the x-direction of the laminate. The fiber direction of even-numbered layers is the y-direction of the laminate. Simply supported plate with immovable edges satisfies the symmetry requirement that eliminates the coupling between bending and extension. However, the displacement of x is free to move at the edge of $y = 0$, and the displacement of y is free to move at the edge of $x = 0$.

Therefore, the membrane stress is smaller and there exists the coupling between bending and extension. A Cartesian coordinate system $Oxyz$ is located on the middle surface of the composite laminated piezoelectric rectangular plate. Assume that (w, v, u) and (w_0, v_0, u_0) describe the displacements of an arbitrary point and a point on the middle surface of the composite laminated piezoelectric rectangular plate in the x, y, and z directions, respectively. It is also assumed that in-plane excitations of the composite laminated piezoelectric rectangular plate are loaded along the y-direction at $x = 0$ and the x-direction at $y = 0$ with the form of $q_0 + q_x \cos \Omega_1 t$ and $q_1 + q_y \cos \Omega_2 t$, respectively. Transverse excitation loaded to the composite laminated piezoelectric rectangular plate is expressed as $q = q_3 \cos \Omega_3 t$. The dynamic electrical loading is represented by $E_z = E_z \cos \Omega_4 t$.

In this paper, Reddy's third-order shear deformation description of the displacement field is adopted:

$$u(x, y, z, t) = u_0(x, y, t) + z\phi_x(x, y, t) - z^3 \frac{4}{3h^2}\left(\phi_x + \frac{\partial w_0}{\partial x}\right), \tag{1a}$$

$$v(x, y, z, t) = v_0(x, y, t) + z\phi_y(x, y, t) - z^3 \frac{4}{3h^2}\left(\phi_y + \frac{\partial w_0}{\partial y}\right), \tag{1b}$$

$$w(x, y, z, t) = w_0(x, y, t), \tag{1c}$$

where (u_0, v_0, w_0) are the deflection of a point on the middle surface, (u, v, w) are the displacement components along the (x, y, z) coordinate directions, and ϕ_x and ϕ_y denote the rotation components of normal to the middle surface about the y and x axes, respectively.

The nonlinear strain-displacement relations are assumed to have the following form:

$$\varepsilon_{xx} = \frac{\partial u}{\partial x} + \frac{1}{2}\left(\frac{\partial w}{\partial x}\right)^2, \qquad \varepsilon_{xz} = \frac{1}{2}\left(\frac{\partial u}{\partial z} + \frac{\partial w}{\partial x}\right),$$
$$\varepsilon_{xy} = \frac{1}{2}\left(\frac{\partial u}{\partial y} + \frac{\partial v}{\partial x} + \frac{\partial w}{\partial x}\frac{\partial w}{\partial y}\right)$$
$$\varepsilon_{yy} = \frac{\partial v}{\partial y} + \frac{1}{2}\left(\frac{\partial w}{\partial y}\right)^2, \qquad \varepsilon_{yz} = \frac{1}{2}\left(\frac{\partial v}{\partial z} + \frac{\partial w}{\partial y}\right), \tag{2}$$
$$\varepsilon_{zz} = \frac{\partial w}{\partial z}.$$

Stress constitutive relations are presented as follows:

$$\sigma_{ij} = \sigma^s_{ijkl}\varepsilon_{kl} - e_{ijk}E_k, \quad (i, j, k, l = x, y, z), \tag{3}$$

where σ_{ij} and ε_{kl} denote the mechanical stresses and strains in extended vector notation, σ^s_{ijkl} represents the elastic stiffness tensor, E_k stands for the electric field vector, and e_{ij} is the piezoelectric tensor.

According to Hamilton's principle, the nonlinear governing equations of motion for the composite laminated piezoelectric rectangular plate are given in the previou studies as follows [10, 35]:

$$\frac{\partial N_{xx}}{\partial x} + \frac{\partial N_{xy}}{\partial y} = I_0\ddot{u}_0 + J_1\ddot{\phi}_x - c_1 I_3 \frac{\partial \ddot{w}_0}{\partial x}, \tag{4a}$$

$$\frac{\partial N_{xy}}{\partial x} + \frac{\partial N_{yy}}{\partial y} = I_0\ddot{v}_0 + J_1\ddot{\phi}_y - c_1 I_3 \frac{\partial \ddot{w}_0}{\partial y}, \tag{4b}$$

$$\frac{\partial \overline{Q}_x}{\partial x} + \frac{\partial \overline{Q}_y}{\partial y} + \frac{\partial}{\partial x}\left(N_{xx}\frac{\partial w_0}{\partial x} + N_{xy}\frac{\partial w_0}{\partial y}\right) + \frac{\partial}{\partial y}\left(N_{xy}\frac{\partial w_0}{\partial x} + N_{yy}\frac{\partial w_0}{\partial y}\right) + c_1\left(\frac{\partial^2 P_{xx}}{\partial x^2} + 2\frac{\partial^2 P_{xy}}{\partial x \partial y} + \frac{\partial^2 P_{yy}}{\partial y^2}\right) - \gamma\dot{w}_0 + q = I_0\ddot{w}_0 - c_1^2 I_6\left(\frac{\partial^2 \ddot{w}_0}{\partial x^2} + \frac{\partial^2 \ddot{w}_0}{\partial y^2}\right) + c_1\left[I_3\left(\frac{\partial \ddot{u}_0}{\partial x} + \frac{\partial \ddot{v}_0}{\partial y}\right) + I_4\left(\frac{\partial \ddot{\phi}_x}{\partial x} + \frac{\partial \ddot{\phi}_y}{\partial y}\right)\right], \tag{4c}$$

$$\frac{\partial \overline{M}_{xx}}{\partial x} + \frac{\partial \overline{M}_{xy}}{\partial y} - \overline{Q}_x = J_1\ddot{u}_0 + k_2\ddot{\phi}_x - c_1 J_4 \frac{\partial \ddot{w}_0}{\partial x}, \tag{4d}$$

$$\frac{\partial \overline{M}_{xy}}{\partial x} + \frac{\partial \overline{M}_{yy}}{\partial y} - \overline{Q}_y = J_1\ddot{v}_0 + k_2\ddot{\phi}_y - c_1 J_4 \frac{\partial \ddot{w}_0}{\partial y}, \tag{4e}$$

where the dot represents the partial differentiation with respect to time t, the comma denotes the partial differentiation with respect to a specified coordinate, γ is the damping coefficient, and all kinds of inertias in (4a), (4b), (4c), (4d), and (4e) are calculated by

$$I_i = \sum_{k=1}^{N}\int_{z_k}^{z_{k+1}} \rho^k z^i \, dz, \qquad J_i = I_i - c_1 I_{i+2}, \qquad K_2 = I_2 - 2c_1 I_4. \tag{5}$$

In addition, the stress resultants are represented as follows:

$$N_{xx} = A_{11}\left[\frac{\partial u_0}{\partial x} + \frac{1}{2}\left(\frac{\partial w_0}{\partial x}\right)^2\right] + A_{12}\left[\frac{\partial v_0}{\partial y} + \frac{1}{2}\left(\frac{\partial w_0}{\partial y}\right)^2\right] - N^p_{xx}, \tag{6a}$$

$$N_{yy} = A_{21}\left[\frac{\partial u_0}{\partial x} + \frac{1}{2}\left(\frac{\partial w_0}{\partial x}\right)^2\right] + A_{22}\left[\frac{\partial v_0}{\partial y} + \frac{1}{2}\left(\frac{\partial w_0}{\partial y}\right)^2\right] - N^p_{yy}, \tag{6b}$$

$$N_{xy} = A_{66}\left(\frac{\partial v_0}{\partial x} + \frac{\partial w_0}{\partial x}\frac{\partial w_0}{\partial y} + \frac{\partial u_0}{\partial y}\right) - N^p_{xy}, \tag{6c}$$

$$M_{xx} = \left(D_{11} - c_1F_{11}\right)\frac{\partial \phi_x}{\partial x} + \left(D_{12} - c_1F_{12}\right)\frac{\partial \phi_y}{\partial y} - c_1F_{11}\frac{\partial^2 w_0}{\partial x^2} - c_1F_{12}\frac{\partial^2 w_0}{\partial y^2} - M_{xx}^p, \tag{6d}$$

$$M_{yy} = \left(D_{21} - c_1F_{21}\right)\frac{\partial \phi_x}{\partial x} + \left(D_{22} - c_1F_{22}\right)\frac{\partial \phi_y}{\partial y} - c_1F_{21}\frac{\partial^2 w_0}{\partial x^2} - c_1F_{22}\frac{\partial^2 w_0}{\partial y^2} - M_{yy}^p, \tag{6e}$$

$$M_{xy} = \left(D_{66} - c_1F_{66}\right)\left(\frac{\partial \phi_x}{\partial x} + \frac{\partial \phi_y}{\partial y}\right) - 2c_1F_{66}\frac{\partial^2 w_0}{\partial x \partial y} - M_{xy}^p, \tag{6f}$$

$$P_{xx} = \left(F_{11} - c_1H_{11}\right)\frac{\partial \phi_x}{\partial x} + \left(F_{12} - c_1H_{12}\right)\frac{\partial \phi_y}{\partial y} - c_1H_{11}\frac{\partial^2 w_0}{\partial x^2} - c_1H_{12}\frac{\partial^2 w_0}{\partial y^2}, \tag{6g}$$

$$P_{yy} = \left(F_{21} - c_1\nu H_{21}\right)\left(\frac{\partial \phi_x}{\partial x} + \frac{\partial \phi_y}{\partial y}\right) - c_1H_{21}\frac{\partial^2 w_0}{\partial x^2} - c_1H_{22}\frac{\partial^2 w_0}{\partial y^2}, \tag{6h}$$

$$P_{xy} = \left(P_{66} - c_1H_{66}\right)\left(\frac{\partial \phi_x}{\partial x} + \frac{\partial \phi_y}{\partial y}\right) - 2c_1H_{66}\frac{\partial^2 w_0}{\partial x \partial y}, \tag{6i}$$

$$\overline{Q}_x = \left(A_{44} - c_2D_{44}\right)\phi_x + \left(A_{44} - c_2D_{44}\right)\frac{\partial w_0}{\partial y}, \tag{6j}$$

$$\overline{Q}_y = \left(A_{55} - c_2D_{55}\right)\phi_x + \left(A_{55} - c_2D_{55}\right)\frac{\partial w_0}{\partial x}, \tag{6k}$$

$$N_x^P = \sum_{k=1}^{N}\int_{z_k}^{z_{k+1}} \overline{Q}_{11}^k e_{31}^k E_z\, dz, \tag{6l}$$

$$N_y^P = \sum_{k=1}^{N}\int_{z_k}^{z_{k+1}} \overline{Q}_{22}^k e_{32}^k E_z\, dz, \tag{6m}$$

where $N_i^P = N_i^P \cos(\Omega_4 t)$ $(i = x, y)$ represent the piezoelectric stress resultants, e_{31} and e_{32} are piezoelectric constants, E_z denotes electric field, and A_{ij}, B_{ij}, D_{ij}, E_{ij}, F_{ij}, and H_{ij} are, respectively, the stiffness elements of the laminated composite piezoelectric rectangular plate, which are denoted as

$$\left(A_{ij}, B_{ij}, D_{ij}, E_{ij}, F_{ij}, H_{ij}\right) = \sum_{k=1}^{N}\int_{z_k}^{z_{k+1}} \overline{Q}_{ij}^k \left(1, z, z^2, z^3, z^4, z^6\right) dz, \quad (i, j = 1, 2, 6), \tag{7a}$$

$$\left(A_{ij}, D_{ij}, F_{ij}\right) = \sum_{k=1}^{N}\int_{z_k}^{z_{k+1}} \overline{Q}_{ij}^k \left(1, z^2, z^4\right) dz, \quad (i, j = 4, 5). \tag{7b}$$

Substituting (6a), (6b), (6c), (6d), (6e), (6f), (6g), (6h), (6i), (6j), (6k), (6l), and (6m) into (4a), (4b), (4c), (4d), and (4e) yields governing equations of motion in terms of generalized displacements $(u_0, v_0, w_0, \phi_x, \phi_y)$ as follows:

$$A_{11}\frac{\partial^2 u_0}{\partial x^2} + A_{66}\frac{\partial^2 u_0}{\partial y^2} + \left(A_{12} + A_{66}\right)\frac{\partial^2 v_0}{\partial x \partial y} + A_{11}\frac{\partial w_0}{\partial x}\frac{\partial^2 w_0}{\partial x^2} + A_{66}\frac{\partial w_0}{\partial x}\frac{\partial^2 w_0}{\partial y^2} + \left(A_{12} + A_{66}\right)\frac{\partial w_0}{\partial y}\frac{\partial^2 w_0}{\partial x \partial y} = I_0\ddot{u}_0 + J_1\ddot{\phi}_x - c_1I_3\frac{\partial \ddot{w}_0}{\partial x}, \tag{8a}$$

$$A_{66}\frac{\partial^2 v_0}{\partial x^2} + A_{22}\frac{\partial^2 v_0}{\partial y^2} + \left(A_{21} + A_{66}\right)\frac{\partial^2 u_0}{\partial x \partial y} + A_{66}\frac{\partial w_0}{\partial y}\frac{\partial^2 w_0}{\partial x^2} + A_{22}\frac{\partial w_0}{\partial y}\frac{\partial^2 w_0}{\partial y^2} + \left(A_{21} + A_{66}\right)\frac{\partial w_0}{\partial x}\frac{\partial^2 w_0}{\partial x \partial y} = I_0\ddot{v}_0 + J_1\ddot{\phi}_y - c_1I_3\frac{\partial \ddot{w}_0}{\partial y}, \tag{8b}$$

$$A_{66}\frac{\partial w_0}{\partial x}\frac{\partial^2 u_0}{\partial y^2} - H_{22}c_1^2\frac{\partial^4 w_0}{\partial y^4} + c_1\left(2F_{66} + F_{12} - 2H_{66}c_1 - H_{12}c_1\right)\frac{\partial^3 \phi_y}{\partial y \partial x^2} + c_1\left(F_{22} - H_{22}c_1\right)\frac{\partial^3 \phi_y}{\partial y^3} - H_{11}c_1^2\frac{\partial^4 w_0}{\partial x^4} + A_{11}\frac{\partial w_0}{\partial x}\frac{\partial^2 u_0}{\partial x^2} + \left(F_{44}c_2^2 - 2D_{44}c_2 + A_{44}\right)\frac{\partial \phi_y}{\partial y} + c_1\left(F_{21} + 2F_{66} - H_{21}c_1 - 2H_{66}c_1\right)\frac{\partial^3 \phi_x}{\partial y^2 \partial x} - c_1^2\left(H_{21} + 4H_{66} + H_{12}\right)\frac{\partial^4 w_0}{\partial y^2 \partial x^2} + \left(A_{44} - N_y^P\cos\left(\Omega_4 t\right) + F_{44}c_2^2 - 2D_{44}c_2\right)\frac{\partial^2 w_0}{\partial y^2} - \frac{\partial N_y^P}{\partial y}\cos\left(\Omega_2 t\right)\frac{\partial w_0}{\partial y} + \left(A_{21} + 4A_{66} + A_{12}\right)\frac{\partial w_0}{\partial x}\frac{\partial w_0}{\partial y}\frac{\partial^2 w_0}{\partial y \partial x} + c_1\left(F_{11} - H_{11}c_1\right)\frac{\partial^3 \phi_x}{\partial x^3} + \left(A_{21} + A_{66}\right)\frac{\partial w_0}{\partial y}\frac{\partial^2 u_0}{\partial y \partial x}$$

$$
\begin{aligned}
&+ A_{21}\frac{\partial u_0}{\partial x}\frac{\partial^2 w_0}{\partial y^2} A_{66}\frac{\partial w_0}{\partial y}\frac{\partial^2 v_0}{\partial x^2} + A_{22}\frac{\partial w_0}{\partial y}\frac{\partial^2 v_0}{\partial y^2} \\
&+ \frac{1}{2}\left(A_{12} + 2A_{66}\right)\left(\frac{\partial w_0}{\partial y}\right)^2\frac{\partial^2 w_0}{\partial x^2} \\
&+ A_{22}\frac{\partial^2 w_0}{\partial y^2}\frac{\partial v_0}{\partial y} + \left(A_{12} + A_{66}\right)\frac{\partial w_0}{\partial x}\frac{\partial^2 v_0}{\partial y \partial x} \\
&+ \frac{1}{2}\left(A_{21} + 2A_{66}\right)\frac{\partial^2 w_0}{\partial y^2}\left(\frac{\partial w_0}{\partial x}\right)^2 + \frac{3}{2}A_{11}\left(\frac{\partial w_0}{\partial x}\right)^2\frac{\partial^2 w_0}{\partial x^2} \\
&+ A_{11}\frac{\partial^2 w_0}{\partial x^2}\frac{\partial u_0}{\partial x} + A_{12}\frac{\partial^2 w_0}{\partial x^2}\frac{\partial v_0}{\partial y} + 2A_{66}\frac{\partial^2 w_0}{\partial y \partial x}\frac{\partial v_0}{\partial x} \\
&+ 2A_{66}\frac{\partial^2 w_0}{\partial y \partial x}\frac{\partial u_0}{\partial y} + \frac{3}{2}A_{22}\left(\frac{\partial w_0}{\partial y}\right)^2\frac{\partial^2 w_0}{\partial y^2} \\
&+ \left(A_{55} + q_x\cos\left(\Omega_1 t\right) - N_x^P\cos\left(\Omega_4 t\right)\right. \\
&\quad \left. + F_{55}c_2^2 - 2D_{55}c_2\right)\frac{\partial^2 w_0}{\partial x^2} \\
&- \frac{\partial N_x^P}{\partial x}\cos\left(\Omega_3 t\right)\frac{\partial w}{\partial x} + \left(F_{55}c_2^2 - 2D_{55}c_2 + A_{55}\right)\frac{\partial \phi_x}{\partial x} \\
&- q\cos\left(\Omega_3 t\right) + kf\frac{\partial w_0}{\partial t} \\
&= I_0\ddot{w}_0 - c_1^2 I_6\left(\frac{\partial^2 \ddot{w}_0}{\partial x^2} + \frac{\partial^2 \ddot{w}_0}{\partial y^2}\right) + c_1 I_3\left(\frac{\partial \ddot{u}_0}{\partial x} + \frac{\partial \ddot{v}_0}{\partial y}\right) \\
&+ c_1 J_4\left(\frac{\partial \ddot{\phi}_x}{\partial x} + \frac{\partial \ddot{\phi}_y}{\partial y}\right),
\end{aligned}
\tag{8c}
$$

$$
\begin{aligned}
&\left(D_{11} - 2F_{11}c_1 + H_{11}c_1^2\right)\frac{\partial^2 \phi_x}{\partial x^2} + \left(D_{66} - 2F_{66}c_1 + H_{66}c_1^2\right)\frac{\partial^2 \phi_x}{\partial y^2} \\
&- c_1\left(F_{11} - H_{11}c_1\right)\frac{\partial^3 w_0}{\partial x^3} \\
&- \left(F_{55}c_2^2 - 2D_{55}c_2 + A_{55}\right)\frac{\partial w_0}{\partial x} \\
&+ \left(D_{12} + D_{66} + H_{66}c_1^2 - 2F_{66}c_1 + H_{12}c_1^2 - 2F_{12}c_1\right)\frac{\partial^2 \phi_y}{\partial y \partial x} \\
&- c_1\left(2F_{66} + F_{12} - 2H_{66}c_1 - H_{12}c_1\right)\frac{\partial^3 w_0}{\partial y^2 \partial x} \\
&+ \left(2D_{55}c_2 - A_{55} - F_{55}c_2^2\right)\phi_x \\
&= J_1\ddot{u}_0 + K_2\ddot{\phi}_x - c_1 J_4\frac{\partial \ddot{w}_0}{\partial x},
\end{aligned}
\tag{8d}
$$

$$
\begin{aligned}
&\left(D_{66} - 2F_{66}c_1 + H_{66}c_1^2\right)\frac{\partial^2 \phi_y}{\partial x^2} \\
&- c_1\left(F_{21} + 2F_{66} - H_{21}c_1 - 2H_{66}c_1\right)\frac{\partial^3 w_0}{\partial y \partial x^2} \\
&+ \left(H_{21}c_1^2 + D_{66} + D_{21} - 2F_{21}c_1 + H_{66}c_1^2 - 2F_{66}c_1\right)\frac{\partial^2 \phi_x}{\partial y \partial x} \\
&+ \left(H_{22}c_1^2 + D_{22} - 2F_{22}c_1\right)\frac{\partial^2 \phi_y}{\partial y^2} \\
&- c_1\left(F_{22} - H_{22}c_1\right)\frac{\partial^3 w_0}{\partial y^3} - \left(F_{44}c_2^2 - 2D_{44}c_2 + A_{44}\right)\frac{\partial w_0}{\partial y} \\
&+ \left(2D_{44}c_2 - F_{44}c_2^2 - A_{44}\right)\phi_y \\
&= J_1\ddot{v}_0 + K_2\ddot{\phi}_y - c_1 J_4\frac{\partial \ddot{w}_0}{\partial y}.
\end{aligned}
\tag{8e}
$$

The simply supported boundary conditions of the composite laminated piezoelectric rectangular plate can be represented as follows [10, 35, 45]:

$$x = 0 : w = 0, \quad \phi_y = 0, \quad N_{xy} = 0, \quad M_{xx} = 0, \tag{9a}$$

$$x = a : w = 0, \quad \phi_y = 0, \quad N_{xy} = 0, \quad M_{xx} = 0, \tag{9b}$$

$$y = 0 : w = 0, \quad \phi_x = 0, \quad N_{xy} = 0, \quad M_{yy} = 0, \tag{9c}$$

$$y = b : w = 0, \quad \phi_x = 0, \quad N_{xy} = 0, \quad M_{yy} = 0, \tag{9d}$$

$$\int_0^h N_{xx}|_{x=0}\,dz = -\int_0^h \left(q_0 + q_x\cos\Omega_1 t\right)dz, \tag{9e}$$

$$\int_0^h N_{yy}|_{y=0}\,dz = -\int_0^h \left(q_1 + q_y\cos\Omega_2 t\right)dz. \tag{9f}$$

The boundary condition (9f) includes the influence of the in-plane load. We consider complicated nonlinear dynamics of the composite laminated piezoelectric rectangular plate in the first two modes of u_0, v_0, w_0, ϕ_x, and ϕ_y. It is desirable that we select an appropriate mode function to satisfy the boundary condition. Thus, we can write u_0, v_0, w_0, ϕ_x, and ϕ_y in the following forms:

$$u_0 = u_1(t)\cos\frac{\pi x}{2a}\cos\frac{\pi y}{2b} + u_2(t)\cos\frac{3\pi x}{2a}\cos\frac{\pi y}{2b}, \tag{10a}$$

$$v_0 = v_1(t)\cos\frac{\pi y}{2b}\cos\frac{\pi x}{2a} + v_2(t)\cos\frac{\pi y}{2b}\cos\frac{3\pi x}{2a}, \tag{10b}$$

$$w_0 = w_1(t)\sin\frac{\pi x}{a}\sin\frac{\pi y}{b} + w_2(t)\sin\frac{3\pi x}{a}\sin\frac{\pi y}{b}, \tag{10c}$$

$$\phi_x = \phi_1(t)\cos\frac{\pi x}{a}\sin\frac{\pi y}{b} + \phi_2(t)\cos\frac{3\pi x}{a}\sin\frac{\pi y}{b}, \quad (10d)$$

$$\phi_y = \phi_3(t)\cos\frac{\pi y}{b}\sin\frac{\pi x}{a} + \phi_4(t)\cos\frac{\pi y}{b}\sin\frac{3\pi x}{a}. \quad (10e)$$

Based on the study given by Nosir and Reddy and Bhimaraddi [46, 47], we neglect the in-plane and rotary inertia terms in (8a), (8b), (8d), and (8e) since their influences are small compared to the transverse inertia term. By means of the Galerkin method, substituting (10a), (10b), (10c), (10d), and (10e) into (8a), (8b), (8c), (8d), and (8e), integrating and neglecting all inertia terms in (8a), (8b), (8d), and (8e), we obtain the expressions of u_1, u_2, v_1, v_2, ϕ_1, ϕ_2, ϕ_3, and ϕ_4 in terms of w_1 and w_2 as follows:

$$u_1 = k_1 w_1^2 + k_2 w_2^2 + k_3 w_1 w_2, \quad (11a)$$

$$u_2 = k_4 w_1^2 + k_5 w_2^2 + k_6 w_1 w_2, \quad (11b)$$

$$v_1 = k_7 w_1^2 + k_8 w_2^2 + k_9 w_1 w_2, \quad (11c)$$

$$v_2 = k_{10} w_1^2 + k_{11} w_2^2 + k_{12} w_1 w_2, \quad (11d)$$

$$\phi_1 = k_{19} w_1, \qquad \phi_2 = k_{20} w_2, \quad (11e)$$

$$\phi_3 = k_{21} w_1, \qquad \phi_4 = k_{22} w_2, \quad (11f)$$

where the coefficients presented in (11a), (11b), (11c), (11d), (11e), and (11f) can be found in Appendix A.

In order to obtain the dimensionless governing equations of motion, we introduce the transformations of the variables and parameters:

$$\overline{u} = \frac{u_0}{a}, \quad \overline{v} = \frac{v_0}{b}, \quad \overline{w} = \frac{w_0}{h}, \quad \overline{\phi}_x = \phi_x,$$

$$\overline{\phi}_y = \phi_y, \quad \overline{x} = \frac{x}{a}, \quad \overline{y} = \frac{y}{b}, \quad \overline{q} = \frac{b^2}{Eh^3}q,$$

$$\overline{q}_x = \frac{b^2}{Eh^3}q_x, \quad \overline{q}_y = \frac{b^2}{Eh^3}q_y, \quad \overline{t} = \pi^2\left(\frac{E}{ab\rho}\right)^{1/2}t,$$

$$\overline{\Omega}_i = \frac{1}{\pi^2}\left(\frac{ab\rho}{E}\right)^{1/2}\Omega_i \quad (i = 1, 2),$$

$$\overline{A}_{ij} = \frac{(ab)^{1/2}}{Eh^2}A_{ij}, \quad \overline{B}_{ij} = \frac{(ab)^{1/2}}{Eh^3}B_{ij},$$

$$\overline{D}_{ij} = \frac{(ab)^{1/2}}{Eh^4}D_{ij}, \quad \overline{E}_{ij} = \frac{(ab)^{1/2}}{Eh^5}E_{ij},$$

$$\overline{F}_{ij} = \frac{(ab)^{1/2}}{Eh^6}F_{ij}, \quad \overline{H}_{ij} = \frac{(ab)^{1/2}}{Eh^8}H_{ij},$$

$$\overline{I}_i = \frac{1}{(ab)^{(i+1)/2}\rho}I_i. \quad (12)$$

Based on the practical work condition of laminated composite rectangular plates, and theoretical and experimental studies obtained by Reddy and Mitchell [3, 45], it is known that the nonlinear transverse vibration of laminated composite rectangular plates occupies the main aspect of the dynamical characteristics. The transverse vibration is far greater than the other additional vibrations in the u_0 and v_0 directions, respectively. Therefore, the equations for u_0 and v_0 can be neglected. We mainly consider the nonlinear transverse vibration of laminated composite rectangular plates.

For simplicity, we drop the overbar in the following analysis. Substituting ((9a), (9b), (9c), (9d), (9e), and (9f))–(12) into (8c) and applying the Galerkin procedure, we obtain the governing equations of motion of the composite laminated piezoelectric rectangular plate for the dimensionless as follows:

$$\ddot{w}_1 + \mu_1\dot{w}_1 + \omega_1^2 w_1 + \left(a_2\cos\Omega_1 t + a_3\cos\Omega_2 t - a_4\cos\Omega_4 t\right)w_1 + a_5 w_1^2 w_2 + a_6 w_2^2 w_1 + a_7 w_1^3 + a_8 w_2^3 = f_1\cos\Omega_3 t, \quad (13a)$$

$$\ddot{w}_2 + \mu_2\dot{w}_2 + \omega_2^2 w_2 + \left(b_2\cos\Omega_1 t + b_3\cos\Omega_2 t + b_4\cos\Omega_4 t\right)w_2 + b_5 w_2^2 w_1 + b_6 w_1^2 w_2 + b_7 w_2^3 + b_8 w_1^3 = f_2\cos\Omega_3 t, \quad (13b)$$

where the coefficients presented in (13a) and (13b) are given in Appendix B.

The above equations include the cubic terms, in-plane excitation, transverse excitation, and piezoelectric excitation. Equations (13a) and (13b) can describe the nonlinear transverse oscillations of the composite laminated piezoelectric rectangular plate. We only study the case of primary parametric resonance and 1 : 2 internal resonances. In this resonant case, there are the following resonant relations:

$$\omega_1^2 = \frac{\omega^2}{4} + \varepsilon\sigma_1, \quad \omega_2^2 = \omega^2 + \varepsilon\sigma_2, \quad \Omega_3 = \omega, \quad \Omega_1 = \Omega_2 = \Omega_4 = \omega, \quad \omega_2 \approx 2\omega_1, \quad (14)$$

where σ_1 and σ_2 are two detuning parameters.

The method of multiple scales [48] is employed in (13a) and (13b) to find the uniform solutions in the following form:

$$w_1(t,\varepsilon) = x_0(T_0, T_1) + \varepsilon x_1(T_0, T_1) + \cdots, \quad (15a)$$

$$w_2(t,\varepsilon) = y_0(T_0, T_1) + \varepsilon y_1(T_0, T_1) + \cdots, \quad (15b)$$

where $T_0 = t$, $T_1 = \varepsilon t$.

Substituting (14), (15a), and (15b) into (13a) and (13b) and balancing the coefficients of the corresponding powers of ε on the left-hand and right-hand sides of equations, the four-dimensional averaged equations in the Cartesian form are obtained as follows:

$$\dot{x}_1 = -\frac{1}{2}\mu_1 x_1 - \frac{1}{2}\sigma_1 x_2 + \frac{1}{4}\left(a_2 + a_3 - a_4\right)x_2 - a_6 x_2\left(x_3^2 + x_4^2\right) - \frac{3}{2}a_7 x_2\left(x_1^2 + x_2^2\right), \quad (16a)$$

$$\dot{x}_2 = -\frac{1}{2}\mu_1 x_2 + \frac{1}{2}\sigma_1 x_1 + \frac{1}{4}\left(a_2 + a_3 - a_4\right)x_1 + a_6 x_1\left(x_3^2 + x_4^2\right) + \frac{3}{2}a_7 x_1\left(x_1^2 + x_2^2\right), \tag{16b}$$

$$\dot{x}_3 = -\frac{1}{2}\mu_2 x_3 - \frac{1}{4}\sigma_2 x_4 - \frac{1}{2}b_6 x_4\left(x_1^2 + x_2^2\right) - \frac{3}{4}b_7 x_4\left(x_3^2 + x_4^2\right), \tag{16c}$$

$$\dot{x}_4 = -\frac{1}{2}\mu_2 x_4 + \frac{1}{4}\sigma_2 x_3 + \frac{1}{2}b_6 x_3\left(x_1^2 + x_2^2\right) + \frac{3}{4}b_7 x_3\left(x_3^2 + x_4^2\right) - \frac{1}{8}f_2. \tag{16d}$$

3. Computation of Normal Form

In order to assist the analysis of the Shilnikov type multipulse orbits and chaotic dynamics of the laminated composite piezoelectric rectangular plate, it is necessary to reduce the averaged equations (16a), (16b), (16c), and (16d) to a simpler normal form. It is found that there are $Z_2 \oplus Z_2$ and D_4 symmetries in the averaged equations (16a), (16b), (16c), and (16d) without the parameters. Therefore, these symmetries are also held in normal form.

We take into account the excitation amplitude f_2 as a perturbation parameter. Amplitude f_2 can be considered as an unfolding parameter when the Shilnikov type multipulse orbits are investigated. Obviously, when we do not consider the perturbation parameter, (16a), (16b), (16c), and (16d) become

$$\dot{x}_1 = -\frac{1}{2}\mu_1 x_1 + \left(f_0 - \frac{1}{2}\sigma_1\right)x_2 - a_6 x_2\left(x_3^2 + x_4^2\right) - \frac{3}{2}a_7 x_2\left(x_1^2 + x_2^2\right), \tag{17a}$$

$$\dot{x}_2 = -\frac{1}{2}\mu_1 x_2 + \left(f_0 + \frac{1}{2}\sigma_1\right)x_1 + a_6 x_1\left(x_3^2 + x_4^2\right) + \frac{3}{2}a_7 x_1\left(x_1^2 + x_2^2\right), \tag{17b}$$

$$\dot{x}_3 = -\frac{1}{2}\mu_2 x_3 - \frac{1}{4}\sigma_2 x_4 - \frac{1}{2}b_6 x_4\left(x_1^2 + x_2^2\right) - \frac{3}{4}b_7 x_4\left(x_3^2 + x_4^2\right), \tag{17c}$$

$$\dot{x}_4 = -\frac{1}{2}\mu_2 x_4 + \frac{1}{4}\sigma_2 x_3 + \frac{1}{2}b_6 x_3\left(x_1^2 + x_2^2\right) + \frac{3}{4}b_7 x_3\left(x_3^2 + x_4^2\right), \tag{17d}$$

where $f_0 = (1/4)(a_2 + a_3 - a_4)$.

It is obviously known that (17a), (17b), (17c), and (17d) have a trivial zero solution $(x_1, x_2, x_3, x_4) = (0, 0, 0, 0)$ at which the Jacobian matrix can be written as

$$\mathbf{J} = D_x X = \begin{bmatrix} -\frac{1}{2}\mu_1 & f_0 - \frac{1}{2}\sigma_1 & 0 & 0 \\ f_0 + \frac{1}{2}\sigma_1 & -\frac{1}{2}\mu_1 & 0 & 0 \\ 0 & 0 & -\frac{1}{2}\mu_2 & -\frac{1}{4}\sigma_2 \\ 0 & 0 & \frac{1}{4}\sigma_2 & -\frac{1}{2}\mu_2 \end{bmatrix}. \tag{18}$$

The characteristic equation corresponding to the trivial zero solution is

$$\left(\lambda^2 + \mu_1\lambda + \frac{1}{4}\mu_1^2 + \frac{1}{4}\sigma_1^2 - f_0^2\right) \times \left(\lambda^2 + \mu_2\lambda + \frac{1}{4}\mu_2^2 + \frac{1}{16}\sigma_2^2\right) = 0. \tag{19}$$

Let

$$\Delta_1 = \frac{1}{4}\mu_1^2 + \frac{1}{4}\sigma_1^2 - f_0^2, \qquad \Delta_2 = \frac{1}{4}\mu_2^2 + \frac{1}{16}\sigma_2^2. \tag{20}$$

When $\mu_1 = \mu_2 = 0$, $\Delta_1 = 0$, and $\Delta_2 = (1/16)\sigma_2^2 > 0$ are satisfied simultaneously, (17a), (17b), (17c), and (17d) have one nonsemisimple double zero and a pair of pure imaginary eigenvalues:

$$\lambda_{1,2} = 0, \qquad \lambda_{3,4} = \pm i\overline{\omega}, \tag{21}$$

where $\overline{\omega}^2 = (1/16)\sigma_2^2$.

Considering $\overline{\sigma}_1$, μ_1, μ_2, and f_2 as the perturbation parameters, letting $\sigma_1 = 2(\overline{\sigma}_1 - f_0)$, and setting $f_0 = 1/2$, then, averaged equations (17a), (17b), (17c), and (17d) without the perturbation parameters become the following forms:

$$\dot{x}_1 = x_2 - a_6 x_2\left(x_3^2 + x_4^2\right) - \frac{3}{2}a_7 x_2\left(x_1^2 + x_2^2\right), \tag{22a}$$

$$\dot{x}_2 = a_6 x_1\left(x_3^2 + x_4^2\right) + \frac{3}{2}a_7 x_1\left(x_1^2 + x_2^2\right), \tag{22b}$$

$$\dot{x}_3 = -\frac{1}{4}\sigma_2 x_4 - \frac{1}{2}b_6 x_4\left(x_1^2 + x_2^2\right) - \frac{3}{4}b_7 x_4\left(x_3^2 + x_4^2\right), \tag{22c}$$

$$\dot{x}_4 = \frac{1}{4}\sigma_2 x_3 + \frac{1}{2}b_6 x_3\left(x_1^2 + x_2^2\right) + \frac{3}{4}b_7 x_3\left(x_3^2 + x_4^2\right). \tag{22d}$$

According to (22a), (22b), (22c), and (22d), we have

$$A = \begin{bmatrix} 0 & 1 & 0 & 0 \\ 0 & 0 & 0 & 0 \\ 0 & 0 & 0 & -\frac{1}{4}\sigma_2 \\ 0 & 0 & \frac{1}{4}\sigma_2 & 0 \end{bmatrix}. \tag{23}$$

Executing the Maple program given by Zhang et al. [49], the 3-order normal form of (22a), (22b), (22c), and (22d) is obtained as

$$\dot{y}_1 = y_2, \tag{24a}$$

$$\dot{y}_2 = a_6 y_1 \left(y_3^2 + y_4^2\right) + \frac{3}{2} a_7 y_1^3, \tag{24b}$$

$$\dot{y}_3 = -\frac{1}{4}\sigma_2 y_4 - \frac{1}{2} b_6 y_1^2 y_4 - \frac{3}{4} b_7 y_4 \left(y_3^2 + y_4^2\right), \tag{24c}$$

$$\dot{y}_4 = \frac{1}{4}\sigma_2 y_3 + \frac{1}{2} b_6 y_1^2 y_3 + \frac{3}{4} b_7 y_3 \left(y_3^2 + y_4^2\right). \tag{24d}$$

The nonlinear transformation used here is given as follows:

$$x_1 = y_1 - \frac{1}{4} a_7 y_1^3, \tag{25a}$$

$$x_2 = y_2 + \frac{3}{2} a_7 y_2^3 + \frac{3}{4} a_7 y_1^2 y_2 + a_6 y_2 y_3^2 + a_6 y_2 y_4^2, \tag{25b}$$

$$x_3 = y_3 - \frac{1}{2} b_6 y_1 y_2 y_4, \tag{25c}$$

$$x_4 = y_4 + \frac{1}{2} b_6 y_1 y_2 y_3. \tag{25d}$$

The above nonlinear transformation is computed through the Maple program given by Zhang et al. [49], and completely agrees with those presented by Yu et al. [50]. Therefore, a simpler 3-order normal form with the parameters for the averaged equations (16a), (16b), (16c), and (16d) is obtained as follows:

$$\dot{y}_1 = -\overline{\mu}_1 y_1 + \left(1 - \overline{\sigma}_1\right) y_2, \tag{26a}$$

$$\dot{y}_2 = \overline{\sigma}_1 y_1 - \overline{\mu}_1 y_2 + a_6 y_1 \left(y_3^2 + y_4^2\right) + \frac{3}{2} a_7 y_1^3, \tag{26b}$$

$$\dot{y}_3 = -\overline{\mu}_2 y_3 - \overline{\sigma}_2 y_4 - \frac{1}{2} b_6 y_1^2 y_4 - \frac{3}{4} b_7 y_4 \left(y_3^2 + y_4^2\right), \tag{26c}$$

$$\dot{y}_4 = \overline{\sigma}_2 y_3 - \overline{\mu}_2 y_4 + \frac{1}{2} b_6 y_1^2 y_3 + \frac{3}{4} b_7 y_3 \left(y_3^2 + y_4^2\right) - \overline{f}_2, \tag{26d}$$

where the coefficients are $\overline{\mu}_1 = (1/2)\mu_1$, $\overline{\mu}_2 = (1/2)\mu_2$, $\overline{\sigma}_2 = (1/4)\sigma_2$, and $\overline{f}_2 = (1/8) f_2$, respectively.

Further, let

$$y_3 = I\cos\gamma, \qquad y_4 = I\sin\gamma. \tag{27}$$

Substituting (27) into (26a), (26b), (26c), and (26d) yields

$$\dot{y}_1 = -\overline{\mu}_1 y_1 + \left(1 - \overline{\sigma}_1\right) y_2, \tag{28a}$$

$$\dot{y}_2 = \overline{\sigma}_1 y_1 - \overline{\mu}_1 y_2 + a_6 y_1 I^2 + \frac{3}{2} a_7 y_1^3, \tag{28b}$$

$$\dot{I} = -\overline{\mu}_2 I - \overline{f}_2 \sin\gamma, \tag{28c}$$

$$I\dot{\gamma} = \overline{\sigma}_2 I + \frac{1}{2} b_6 y_1^2 I + \frac{3}{4} b_7 I^3 - \overline{f}_2 \cos\gamma. \tag{28d}$$

In order to get the unfolding of (28a), (28b), (28c), and (28d), a linear transformation is introduced:

$$\begin{bmatrix} y_1 \\ y_2 \end{bmatrix} = \sqrt{2}\frac{\sqrt{|a_6|}}{\sqrt{|b_6|}} \begin{bmatrix} 1 - \overline{\sigma}_1 & 0 \\ \overline{\mu}_1 & 1 \end{bmatrix} \begin{bmatrix} u_1 \\ u_2 \end{bmatrix}. \tag{29}$$

Substituting (29) into (28a), (28b), (28c), and (28d), and canceling nonlinear terms including the parameter $\overline{\sigma}_1$ yield the unfolding as follows:

$$\dot{u}_1 = u_2, \tag{30a}$$

$$\dot{u}_2 = -\mu u_1 - \mu_3 u_2 + \eta_1 u_1^3 + a_6 u_1 I^2, \tag{30b}$$

$$\dot{I} = -\overline{\mu}_2 I - \overline{f}_2 \sin\gamma, \tag{30c}$$

$$I\dot{\gamma} = \overline{\sigma}_2 I + a_6 u_1^2 I + \alpha_2 I^3 - \overline{f}_2 \cos\gamma, \tag{30d}$$

where $\mu = \overline{\mu}_1^2 - \overline{\sigma}_1(1 - \overline{\sigma}_1)$, $\mu_3 = 2\overline{\mu}_1$, $\eta_1 = 3a_6 a_7 / b_6$, and $\alpha_2 = (3/4) b_7$.

The scale transformations to be introduced into (30a), (30b), (30c), and (30d) are

$$\begin{gathered} \overline{\mu}_2 \longrightarrow \varepsilon\overline{\mu}_2, \qquad \mu_3 \longrightarrow \varepsilon\mu_3, \qquad \overline{f}_2 \longrightarrow \varepsilon\overline{f}_2, \\ \eta_1 \longrightarrow \eta_1, \qquad \alpha_2 \longrightarrow \alpha_2, \qquad a_6 \longrightarrow a_6. \end{gathered} \tag{31}$$

Then, the normal forms (30a), (30b), (30c), and (30d) can be rewritten in the form with the perturbations as follows:

$$\dot{u}_1 = \frac{\partial H}{\partial u_2} + \varepsilon g^{u_1} = u_2, \tag{32a}$$

$$\dot{u}_2 = -\frac{\partial H}{\partial u_1} + \varepsilon g^{u_2} = -\mu u_1 + \eta_1 u_1^3 + a_6 u_1 I^2 - \varepsilon\mu_3 u_2, \tag{32b}$$

$$\dot{I} = \frac{\partial H}{\partial \gamma} + \varepsilon g^{I} = -\varepsilon\overline{\mu}_2 I - \varepsilon\overline{f}_2 \sin\gamma, \tag{32c}$$

$$I\dot{\gamma} = -\frac{\partial H}{\partial I} + \varepsilon g^{\gamma} = \overline{\sigma}_2 I + \alpha_2 I^3 + a_6 I u_1^2 - \varepsilon\overline{f}_2 \cos\gamma, \tag{32d}$$

where the Hamiltonian function H is of the following form:

$$\begin{aligned} H\left(u_1, u_2, I, \gamma\right) = {} & \frac{1}{2}u_2^2 + \frac{1}{2}\mu u_1^2 - \frac{1}{4}\eta_1 u_1^4 - \frac{1}{2}a_6 I^2 u_1^2 \\ & - \frac{1}{2}\overline{\sigma}_2 I^2 - \frac{1}{4}\alpha_2 I^4, \end{aligned} \tag{33}$$

and g^{u_1}, g^{u_2}, g^I, and g^γ are the linear perturbation terms induced by the dissipative effects:

$$g^{u_1} = 0, \qquad g^{u_2} = -\mu_3 u_2, \qquad g^I = -\overline{\mu}_2 I, \qquad g^\gamma = 0. \tag{34}$$

4. Heteroclinic Bifurcations

In this section, we focus on studying the nonlinear dynamics characteristic of the unperturbed system. When $\varepsilon = 0$, it can be seen that the system from (32a), (32b), (32c), and (32d) is

an uncoupled two-degree-of-freedom nonlinear system. The variable I in the subspace (u_1, u_2) of (32a), (32b), (32c), and (32d) becomes a parameter since $\dot{I} = 0$. Consider the first two decoupled equations of (32a), (32b), (32c), and (32d),

$$\dot{u}_1 = u_2, \tag{35a}$$

$$\dot{u}_2 = -\mu u_1 + \eta_1 u_1^3 + a_6 I^2 u_1. \tag{35b}$$

Since $\eta_1 > 0$, (35a) and (35b) can exhibit the heteroclinic bifurcations. It is obvious from (35a) and (35b) that when $\mu - a_6 I^2 < 0$, the only solution to (35a) and (35b) is the trivial zero solution, $(u_1, u_2) = (0, 0)$, which is the saddle point. On the curve defined by $\mu = a_6 I^2$, that is,

$$\overline{\mu}_1^2 = \overline{\sigma}_1 \left(1 - \overline{\sigma}_1\right) + a_6 I^2, \tag{36}$$

or

$$I_{1,2} = \pm \left[\frac{\overline{\mu}_1^2 - \overline{\sigma}_1 (1 - \overline{\sigma}_1)}{a_6} \right]^{1/2}, \tag{37}$$

the trivial zero solution bifurcates into three solutions through a pitchfork bifurcation, which are given by $q_0 = (0, 0)$ and $q_\pm(I) = (B, 0)$, respectively, where

$$B = \pm \left\{ \frac{1}{\eta_1} \left[\overline{\mu}_1^2 - \overline{\sigma}_1 \left(1 - \overline{\sigma}_1\right) - a_6 I^2 \right] \right\}^{1/2}. \tag{38}$$

From the Jacobian matrix evaluated at the nonzero solutions, it can be found that the singular points $q_\pm(I)$ are the saddle points. It is observed that I and γ actually represent the amplitude and the phase of vibrations, respectively. Therefore, we assume that $I \geq 0$ and (37) become

$$I_1 = 0, \qquad I_2 = \left[\frac{\overline{\mu}_1^2 - \overline{\sigma}_1 (1 - \overline{\sigma}_1)}{a_6} \right]^{1/2}, \tag{39}$$

such that for all $I \in [I_1, I_2]$, (35a) and (35b) have two hyperbolic saddle points, $q_\pm(I)$, which are connected by a pair of heteroclinic orbits, $u_\pm^h(T_1, I)$, that is, $\lim_{T_1 \to \pm\infty} u_\pm^h(T_1, I) = q_\pm(I)$. Thus, in the full four-dimensional phase space, the set defined by

$$M = \left\{ (u, I, \gamma) \mid u = q_\pm (I),\ I_1 < I < I_2,\ 0 \leq \gamma < 2\pi \right\} \tag{40}$$

is a two-dimensional invariant manifold. From the results obtained by Kovačič [13, 14], it is known that the two-dimensional invariant manifold M is normally hyperbolic. The two-dimensional normally hyperbolic invariant manifold M has the three-dimensional stable and unstable manifolds represented as $W^s(M)$ and $W^u(M)$, respectively. The existence of the heteroclinic orbit of (35a) and (35b) to $q_\pm(I) = (B, 0)$ indicates that $W^s(M)$ and $W^u(M)$ intersect nontransversally along a three-dimensional heteroclinic manifold denoted by Γ, which can be written as

$$\begin{aligned} \Gamma = \Big\{ & (u, I, \gamma) \mid u = u_\pm^h (T_1, I),\ I_1 < I < I_2, \\ & \gamma = \int_0^{T_1} D_I H \left(u_\pm^h (T_1, I), I \right) ds + \gamma_0 \Big\}. \end{aligned} \tag{41}$$

We analyze the dynamics of the unperturbed system of (32a), (32b), (32c), and (32d) restricted to M. Considering the unperturbed system of (32a), (32b), (32c), and (32d) restricted to M yields

$$\dot{I} = 0, \tag{42a}$$

$$I\dot{\gamma} = D_I H \left(q_\pm (I), I \right), \quad I_1 < I < I_2, \tag{42b}$$

where

$$D_I H \left(q_\pm (I), I \right) = -\frac{\partial H \left(q_\pm (I), I \right)}{\partial I} = \overline{\sigma}_2 I + \alpha_2 I^3 + a_6 I q_\pm^2 (I). \tag{43}$$

From the results obtained by Kovačič [13, 14], it is known that if $D_I H(q_\pm(I), I) \neq 0$; then I = constant is called a periodic orbit, and if $D_I H(q_\pm(I), I) = 0$; then I = constant is known as a circle of the singular points. Any value of $I \in [I_1, I_2]$ at which $D_I H(q_\pm(I), I) = 0$ is a resonant value I and these singular points are resonant singular points. We denoted a resonant value by I_r such that

$$\begin{aligned} D_I H \left(q_\pm (I), I \right) = {} & \overline{\sigma}_2 I_r + \alpha_2 I_r^3 \\ & + \frac{a_6}{\eta_1} \left[\overline{\mu}_1^2 - \overline{\sigma}_1 \left(1 - \overline{\sigma}_1\right) - a_6 I_r^2 \right] I_r = 0. \end{aligned} \tag{44}$$

Then, we obtain

$$I_r = \pm \left\{ \frac{\overline{\sigma}_2 \eta_1 + a_6 [\overline{\mu}_1^2 - \overline{\sigma}_1 (1 - \overline{\sigma}_1)]}{a_6^2 - \alpha_2 \eta_1} \right\}^{1/2}. \tag{45}$$

Figure 2 shows the geometry structure of the stable and unstable manifolds of M in the full four-dimensional phase space for the unperturbed system of (32a), (32b), (32c), and (32d). Since γ represents the phase of oscillations, when $I = I_r$, the phase shift $\Delta\gamma$ of oscillations is defined by

$$\Delta\gamma = \gamma \left(+\infty, I_r\right) - \gamma \left(-\infty, I_r\right). \tag{46}$$

The physical interpretation of the phase shift is the phase difference between the two end points of the orbit. In the subspace (u_1, u_2), there exists a pair of the heteroclinic orbits connecting to the two saddles. Therefore, the homoclinic orbit in subspace (I, γ) represents, in fact, a heteroclinic connecting in the full four-dimensional space (u_1, u_2, I, γ). The phase shift denotes the difference of the value γ as a trajectory leaving and returning to the basin of the attraction of M. We will use the phase shift in the subsequent analysis to obtain the condition for the existence of the Shilnikov type multipulse orbit. The phase shift will be calculated later in the heteroclinic orbit analysis.

We consider the heteroclinic orbits of (35a) and (35b). Let $\varepsilon_1 = \mu - a_6 I^2$ and let $\mu_3 = \varepsilon_2$; then (35a) and (35b) can be rewritten as

$$\dot{u}_1 = u_2, \tag{47a}$$

$$\dot{u}_2 = -\varepsilon_1 u_1 + \eta_1 u_1^3 - \varepsilon\varepsilon_2 u_2. \tag{47b}$$

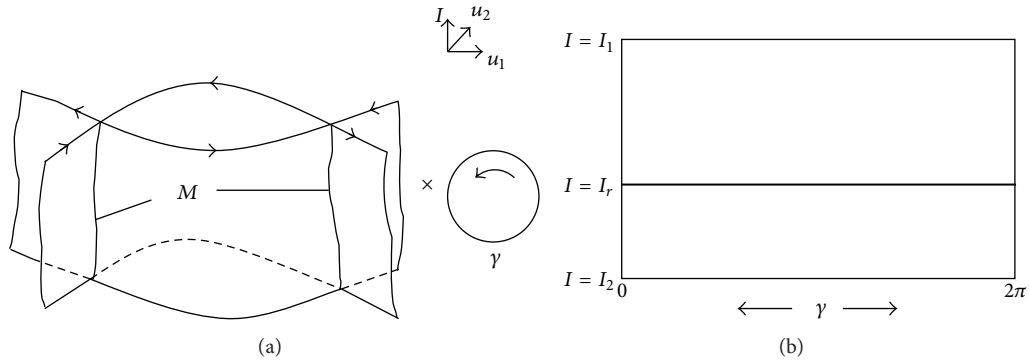

Figure 2: The geometric structure of manifolds M; $W^s(M)$ and $W^u(M)$ are given in the full four-dimensional phase space.

Set $\varepsilon = 0$; then (47a) and (47b) are a system with the Hamiltonian function:

$$\overline{H}(u_1, u_2) = \frac{1}{2}u_2^2 + \frac{1}{2}\varepsilon_1 u_1^2 - \frac{1}{4}\eta_1 u_1^4. \tag{48}$$

When $\overline{H} = \varepsilon_1^2/(4\eta_1)$, there exists a heteroclinic loop Γ^0 which consists of the two hyperbolic saddles $q_\pm$ and a pair of heteroclinic orbits $u_\pm(T_1)$. In order to calculate the phase shift and the energy difference function, we obtain the equations of a pair of heteroclinic orbits given by

$$u_1(T_1) = \pm\sqrt{\frac{\varepsilon_1}{\eta_1}}\tanh\left(\frac{\sqrt{2\varepsilon_1}}{2}T_1\right), \tag{49a}$$

$$u_2(T_1) = \pm\frac{\varepsilon_1}{\sqrt{2\eta_1}}\operatorname{sech}^2\left(\frac{\sqrt{2\varepsilon_1}}{2}T_1\right). \tag{49b}$$

We turn our attention to the computation of the phase shift. Substituting the first equation of (49a) and (49b) into the fourth equation of the unperturbed system of (32a), (32b), (32c), and (32d) yields

$$\dot{\gamma} = \overline{\sigma}_2 + \alpha_2 I^2 + \frac{a_6\varepsilon_1}{\eta_1}\tanh^2\left(\frac{\sqrt{2\varepsilon_1}}{2}T_1\right). \tag{50}$$

Integrating (50) yields

$$\gamma(T_1) = \omega_r T_1 - \frac{a_6\sqrt{2\varepsilon_1}}{\eta_1}\tanh\left(\frac{\sqrt{2\varepsilon_1}}{2}T_1\right) + \gamma_0, \tag{51}$$

where $\omega_r = \overline{\sigma}_2 + \alpha_2 I^2 + (\varepsilon_1 a_6/\eta_1)$.

At $I = I_r$, there is $\omega_r \equiv 0$. Therefore, the phase shift may be expressed as

$$\begin{aligned}\Delta\gamma &= \left[-\frac{2a_6\sqrt{2\varepsilon_1}}{\eta_1}\right]_{I=I_r} \\ &= -\frac{2a_6}{\eta_1}\sqrt{2\left[\overline{\mu}_1^2 - \overline{\sigma}_1(1-\overline{\sigma}_1) - a_6 I_r^2\right]}.\end{aligned} \tag{52}$$

5. Dissipative Perturbations of Homoclinic Loop

In this section, the effects of small perturbation terms on the unperturbed system are analyzed in detail. We now analyze dynamics of the perturbed system and the effect of small perturbations on M. Based on the analysis given by Kovačič [13, 14], it is known that M along with its stable and unstable manifolds is invariant under small, sufficiently differentiable perturbations. It is noticed that $q_\pm(I)$ in (35a) and (35b) maintain the characteristic of the hyperbolic singular point under small perturbations, in particular, $M \to M_\varepsilon$. Therefore, we obtain

$$M = M_\varepsilon = \left\{(u, I, \gamma) \mid u = q_\pm(I), I_1 < I < I_2, 0 \le \gamma < 2\pi\right\}. \tag{53}$$

Considering the last two equations of (32a), (32b), (32c), and (32d) yields

$$\dot{I} = -\overline{\mu}_2 I - \overline{f}_2 \sin\gamma, \tag{54a}$$

$$\dot{\gamma} = \overline{\sigma}_2 + \alpha_2 I^2 + a_6 u_1^2 - \frac{\overline{f}_2\cos\gamma}{I}. \tag{54b}$$

It is known from the above analysis that the last two equations of (32a), (32b), (32c), and (32d) are of a pair of pure imaginary eigenvalues. Therefore, the resonance can occur in (54a) and (54b). Also introduce the scale transformations

$$\begin{aligned}&\overline{\mu}_2 \longrightarrow \varepsilon\overline{\mu}_2, \qquad I = I_r + \sqrt{\varepsilon}h, \\ &\overline{f}_2 \longrightarrow \varepsilon\overline{f}_2, \qquad T_1 \longrightarrow \frac{T_1}{\sqrt{\varepsilon}}.\end{aligned} \tag{55}$$

Substituting the above transformations into (54a) and (54b) yields

$$\dot{h} = -\overline{\mu}_2 I_r - \overline{f}_2\sin\gamma - \sqrt{\varepsilon}\overline{\mu}_2 h, \tag{56a}$$

$$\dot{\gamma} = -\frac{2\delta}{\eta_1}I_r h - \sqrt{\varepsilon}\left(\frac{\overline{f}_2}{I_r}\cos\gamma + \frac{\delta}{\eta_1}h^2\right), \tag{56b}$$

where $\delta = a_6^2 - \alpha_2\eta_1$.

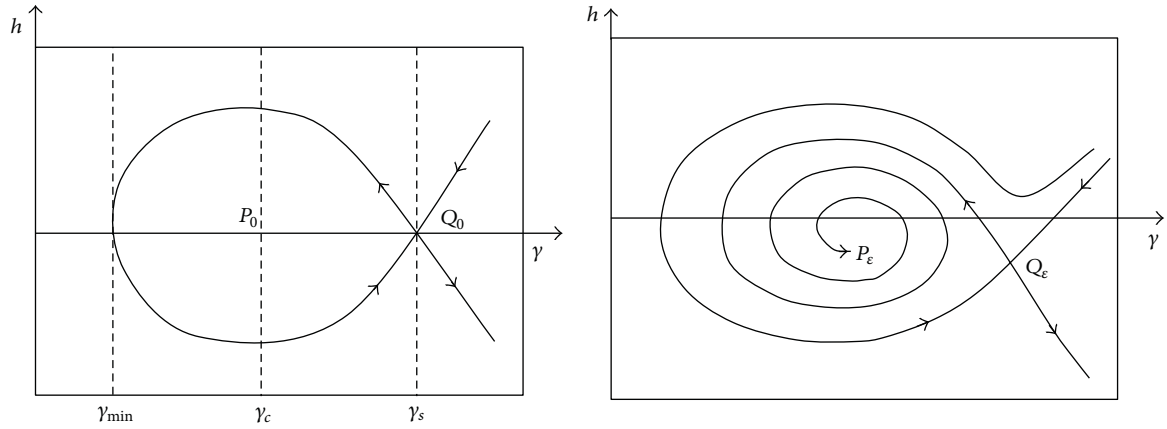

FIGURE 3: Dynamics on the normally hyperbolic manifold is described; (a) the unperturbed case; (b) the perturbed case.

When $\varepsilon = 0$, (56a) and (56b) become

$$\dot{h} = -\overline{\mu}_2 I_r - \overline{f}_2 \sin\gamma, \tag{57a}$$

$$\dot{\gamma} = -\frac{2\delta}{\eta_1} I_r h. \tag{57b}$$

The unperturbed system from (57a) and (57b) is a Hamilton system with the following function:

$$\widehat{H}_D(h,\gamma) = -\overline{\mu}_2 I_r \gamma + \overline{f}_2 \cos\gamma + \frac{\delta}{\eta_1} I_r h^2. \tag{58}$$

The singular points of (57a) and (57b) are represented as

$$\begin{aligned} P_0 &= (0,\gamma_c) = \left(0, -\arcsin\frac{\overline{\mu}_2 I_r}{\overline{f}_2}\right), \\ Q_0 &= (0,\gamma_s) = \left(0, \pi + \arcsin\frac{\overline{\mu}_2 I_r}{\overline{f}_2}\right). \end{aligned} \tag{59}$$

Based on the characteristic equations evaluated at the two singular points P_0 and Q_0, we can know the stabilities of these singular points. The Jacobian matrix of (57a) and (57b) is

$$J = \begin{bmatrix} 0 & -\overline{f}_2 \cos\gamma \\ -\dfrac{2\delta}{\eta_1} I_r & 0 \end{bmatrix}. \tag{60}$$

The characteristic equation corresponding to the singular point P_0 is obtained as

$$\lambda^2 - \frac{2\delta}{\eta_1} I_r \overline{f}_2 \cos\gamma_c = 0. \tag{61}$$

When the condition $(2\delta/\eta_1)\overline{f}_2 I_r \cos\gamma_c < 0$ is satisfied, (57a) and (57b) have a pair of pure imaginary eigenvalues. Therefore, it is known that the singular point P_0 is a center point.

The characteristic equation corresponding to the singular point Q_0 is represented by

$$\lambda^2 - \frac{2\delta}{\eta_1} \overline{f}_2 I_r \cos\gamma_s = 0. \tag{62}$$

When the condition $(2\delta/\eta_1)\overline{f}_2 I_r \cos\gamma_s > 0$ is satisfied, (57a) and (57b) have two real, unequal, and opposite sign eigenvalues. Therefore, the singular point Q_0 is a saddle which is connected to itself by a homoclinic orbit. The phase portrait of the system from (57a) and (57b) is shown in Figure 3(a).

It is found that for the sufficiently small parameter ε, the singular point Q_0 remains a hyperbolic singular point Q_ε of the saddle stability type. It is known that the Jacobian matrix of the linearization of (56a) and (56b) is of the following form:

$$J_{p_\varepsilon} = \begin{bmatrix} -\sqrt{\varepsilon}\overline{\mu}_2 & -\overline{f}_2 \cos\gamma_c \\ -\dfrac{2\delta}{\eta_1} I_r - \dfrac{2\delta}{\eta_1} h\sqrt{\varepsilon} & \sqrt{\varepsilon}\dfrac{\overline{f}_2}{I_r} \sin\gamma_c \end{bmatrix}. \tag{63}$$

or

$$J_{p_\varepsilon} = \begin{bmatrix} -\sqrt{\varepsilon}\overline{\mu}_2 & -\overline{f}_2 \cos\gamma_c \\ -\dfrac{2\delta}{\eta_1} I_r & -\sqrt{\varepsilon}\overline{\mu}_2 \end{bmatrix}. \tag{64}$$

Based on (64), we find that the leading order term of the trace in the linearization of (56a) and (56b) is less than zero inside the homoclinic loop. Therefore, for small perturbations, the singular point P_0 becomes a hyperbolic sink P_ε. The phase portrait of the perturbed system from (56a) and (56b) is also depicted in Figure 3(b).

Using the function (58), at $h = 0$, the estimate of the basin of attractor for $\gamma_{\min}$ is obtained as

$$-\overline{\mu}_2 I_r \gamma_{\min} + \overline{f}_2 \cos\gamma_{\min} = -\overline{\mu}_2 I_r \gamma_s + \overline{f}_2 \cos\gamma_s. \tag{65}$$

Substituting γ_s in (59) into (65) yields

$$\gamma_{\min} - \frac{\overline{f}_2}{\overline{\mu}_2 I_r} \cos\gamma_{\min} = \pi + \arcsin\frac{\overline{\mu}_2 I_r}{\overline{f}_2} + \frac{\sqrt{\overline{f}_2^2 - \overline{\mu}_2^2 I_r^2}}{\overline{\mu}_2 I_r}. \tag{66}$$

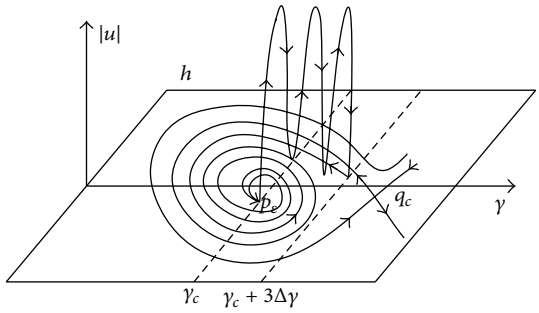

Figure 4: The Shilnikov type three-pulse homoclinic orbits are obtained.

Define an annulus A_ε near $I = I_r$ as

$$A_\varepsilon = \left\{(u_1, u_2, I, \gamma) \mid u_1 = B, u_2 = 0, |I - I_r| < \sqrt{\varepsilon}C, \gamma \in T^l\right\}, \tag{67}$$

where C is a constant and is sufficiently large so that the unperturbed homoclinic orbit is enclosed within the annulus.

It is noticed that the three-dimensional stable and unstable manifolds of A_ε, denoted as $W^s(A_\varepsilon)$ and $W^u(A_\varepsilon)$, are subsets of $W^s(M_\varepsilon)$ and $W^u(M_\varepsilon)$, respectively. We will indicate that for the perturbed system, the saddle focus P_ε on A_ε has the multipulse orbits which come out of the annulus A_ε and can return to the annulus in the full four-dimensional space. These orbits, which are asymptotic to some invariant manifolds in the slow manifold M_ε, leave and enter a small neighborhood of M_ε multiple times, and, finally, return and approach an invariant set in M_ε asymptotically, as shown in Figure 4. In Figure 4, this is an example of the three-pulse jumping orbit which depicts the formation mechanism of the multipulse orbits.

6. Energy Difference Function

In this section, the energy-phase method developed by Haller and Wiggins [21–31] is utilized to discover the existence of the Shilnikov type multipulse orbits and chaotic dynamics of nonlinear vibration for the laminated composite piezoelectric rectangular plate with combined parametric excitation and transverse load. The energy-phase method, which was first presented by Haller and Wiggins [21], is a new global perturbation method, which is different from the global perturbation technique developed by Kovačič and Wiggins [12–14]. Haller and Wiggins [21–31] gave the unperturbed system expressed by a mixture of action-angle variables, which can describe homoclinic and heteroclinic behavior. The key feature of their analysis is that the unperturbed system has a resonance with the action-angle variables. The unperturbed integrable system contains a normally hyperbolic invariant two-dimensional manifold, which has three-dimensional stable and unstable manifolds coinciding along a branch. Action-angle variables illustrate the dynamics on the normally hyperbolic two-dimensional manifold. The situation of the resonance leads to a circle of fixed points on the two-dimensional manifold. Two different points on the circle of fixed points are connected by a heteroclinic orbit. These heteroclinic orbits consist of part of a foliation of the three-dimensional stable and unstable manifolds on the normally hyperbolic two-dimensional manifold. Obviously, the perturbation can dramatically alter the dynamics near the circle of fixed points. Thus, the dynamics restricted to the normally hyperbolic two-dimensional manifold near the resonance becomes hyperbolic fixed points with periodic orbits surrounding homoclinic or heteroclinic trajectories. Each homoclinic or heteroclinic trajectory connects with the hyperbolic points. Haller and Wiggins [21–31] gave conditions for the existence of homoclinic or heteroclinic orbits created near the resonance in the full four-dimensional phase space.

The energy-phase method has three steps in the process in this paper. The first step involves analyzing the perturbed dynamics restricted to the normally hyperbolic invariant two-dimensional manifold near the resonance. The used approach is based on nonlinear oscillation theory. The second step requires manifesting the existence of heteroclinic orbits to the normally hyperbolic invariant two-dimensional manifold. A higher-dimensional Melnikov theory is mainly used in the analysis process of this step. The final step is the most difficult and represents the most innovative part of the energy-phase method. Based on the Haller and Wiggins study in [21–31], we prove the existence of multipulse heteroclinic orbits to specific orbits on the two-dimensional manifold in this step. The analysis is complicated by perturbations of nontransversal intersections of manifolds. According to the investigation given by Haller and Wiggins [21–31], we use the geometric singular perturbation theory of Fenichel to analyze the existence of heteroclinic orbits in the full four-dimensional phase space. Based on foliations of stable and unstable manifolds, Fenichel's theory combines with energy-type arguments which are suited for the Hamiltonian systems. The analysis shows that the existence of heteroclinic orbits depends only on an energy-phase criterion which is obtained from a reduced, one-degree-of-freedom Hamiltonian system. Therefore, the energy-phase method is combined with geometric singular perturbation theory, higher-dimensional Melnikov method, and transversality theory.

The energy-phase method can be utilized to detect the Shilnikov type multipulse heteroclinic orbits to slow manifolds of near-integrable four-dimensional or higher-dimensional nonlinear systems. The key to energy-phase method is the calculation of the energy difference function, which is actually the difference of the Hamiltonian function. Based on the higher-dimensional Melnikov theory and the transversality theory, Haller and Wiggins [21] derived the expression of the energy difference function. In order to illustrate the existence of the multipulse orbits, it is important to obtain the expression of the energy difference function. Using the general expression derived by Haller and Wiggins [21–31] for the class of systems, the energy difference function for the dissipative case is given as follows:

$$\Delta^n \widehat{H}_D(\gamma) = \widehat{H}_D(h, \gamma + n\Delta\gamma) - \widehat{H}_D(h, \gamma)$$

$$- n \int_A \left[\frac{d}{du_1} g^{u_1}(u_1, u_2, I_r, \gamma) + \frac{d}{du_2} g^{u_2}(u_1, u_2, I_r, \gamma) \right] du_1\, du_2 - n \int_{\partial A_l} g^I\, d\gamma, \tag{68}$$

where

$$\widehat{H}_D(h, \gamma + n\Delta\gamma) - \widehat{H}_D(h, \gamma) = -n\overline{\mu}_2 I_r \Delta\gamma + \overline{f}_2 \left[\cos(\gamma + n\Delta\gamma) - \cos\gamma\right], \tag{69}$$

where A denotes the area enclosed by a pair of heteroclinic orbits in plane (u_1, u_2), ∂A_l is the boundary of the area A, and $\Delta\gamma$ is the phase difference.

The coordinate transformation introduced by Haller and Wiggins [21–31] changes the topology structure of heteroclinic orbits when they used the energy-phase method to calculate the energy difference function. In the paper, we did not apply this transformation to calculate the energy difference function in order to maintain the consistency of the topology structure. We directly calculate the energy differential function on the area enclosed by a pair of heteroclinic orbits. These studies are innovations and contributions of this paper.

The energy difference function gives the leading order energy difference between the taking off and landing points of an n-pulse orbit. This function contains the phase-type information from the unperturbed part and the energy-type information from the perturbed part of systems (32a), (32b), (32c), (32d).

Computing (68) leads to the following expression for the dissipative energy difference function:

$$\Delta^n \widehat{H}_D(\gamma) = \overline{f}_2 \left[\cos(\gamma + n\Delta\gamma) - \cos\gamma\right] - \frac{2n\mu_3\varepsilon_1\Delta\gamma}{3a_6}. \tag{70}$$

We define a dissipative factor $d = \mu_3/\overline{f}_2$ such that d gives the relative measure of the dissipative effect with respect to the excitation amplitude. Equation (70) can be rewritten as

$$\Delta^n \widehat{H}_D(\gamma) = \overline{f}_2 \left[-2\sin\left(\gamma + \frac{n\Delta\gamma}{2}\right) \sin\frac{n\Delta\gamma}{2} - \frac{2nd\varepsilon_1\Delta\gamma}{3a_6} \right]. \tag{71}$$

The zeroes of $\Delta^n \widehat{H}_D(\gamma)$ are obtained by solving the following equation:

$$\sin\left(\gamma + \frac{n\Delta\gamma}{2}\right) = \frac{-nd\varepsilon_1\Delta\gamma}{3a_6 \sin(n\Delta\gamma/2)}. \tag{72}$$

Based on (72), the upper bound on the value of the dissipative factor is obtained as follows:

$$|d| < d_{\max} = \frac{3a_6}{n\varepsilon_1} \left| \frac{\sin(n\Delta\gamma/2)}{\Delta\gamma} \right|. \tag{73}$$

For a given value of the dissipative factor d, the multipulse orbits for all values of the pulse number n are not possible. In the presence of small dissipative effects $d < 1$, we have an upper bound on the maximum number of pulses:

$$n < n_{\max} = \left| \frac{3a_6}{\varepsilon_1 d\Delta\gamma} \right|. \tag{74}$$

It is obviously known from (74) that the upper bound $n_{\max}$ is inversely proportional to the value of the dissipative factor d.

7. Zeroes of the Energy Difference Function

The main aim of the following research focuses on identifying the transverse zeroes of the energy difference function. Define a set that contains all such transverse zeroes:

$$\widehat{Z}_-^n = \left\{ (h, \gamma) \mid \Delta^n \widehat{H}_D(\gamma) = 0, D_\gamma \Delta^n \widehat{H}_D(\gamma) \neq 0 \right\}. \tag{75}$$

The transverse zeroes of the dissipative energy difference function $\Delta^n \widehat{H}_D(\gamma)$ are given by the following equation:

$$\gamma + \frac{n\Delta\gamma}{2} = 2m\pi + (-1)^m \alpha, \tag{76}$$

where $m \in \mathrm{Z}$ and

$$\alpha = -\arcsin \frac{nd\varepsilon_1\Delta\gamma}{3a_6 \sin(n\Delta\gamma/2)}. \tag{77}$$

For any n satisfying $\Delta\gamma \neq 4l\pi$ ($l = 0, 1, 2, \ldots$), there are two transverse zeroes of the dissipative energy difference function in the interval $\gamma \in [-\pi/2, 3\pi/2]$, that is:

$$\gamma_{0,1}^n = \frac{3\pi}{2} - \left(\frac{n\Delta\gamma}{2} + \alpha \right) \bmod 2\pi, \tag{78a}$$

$$\gamma_{0,2}^n = \frac{3\pi}{2} - \left(\pi + \frac{n\Delta\gamma}{2} - \alpha \right) \bmod 2\pi. \tag{78b}$$

In order to classify these internal orbits, we can use the fact that each orbit has a unique energy level associated with it. The energy level associated with the homoclinic connection is $\overline{h}_0$. The energy level of the center type singular point is represented by $\overline{h}_\infty$. Any periodic orbit enclosed inside the homoclinic connections has an energy level $\overline{h}_n$. The energy sequence at the different energy levels is defined as

$$\overline{h}_0 = \widehat{H}_D(0, \gamma^s) = \frac{1}{2}\overline{f}_2 \left[-kdI_r \left(\pi + \arcsin\frac{1}{2}kdI_r \right) - \sqrt{4 - k^2 d^2 I_r^2} \right], \tag{79a}$$

$$\overline{h}_n = \min\left[\widehat{H}_D\left(0, \gamma_{0,1}^n\right), \widehat{H}_D\left(0, \gamma_{0,2}^n\right) \right], \tag{79b}$$

$$\overline{h}_\infty = \widehat{H}_D(0, \gamma^c) = \frac{1}{2}\overline{f}_2 \left[kdI_r \arcsin\frac{1}{2}kdI_r + \sqrt{4 - k^2 d^2 I_r^2} \right], \tag{79c}$$

where $\mu_2/\mu_1 = k$, $\overline{\mu}_2/\overline{f}_2 = (1/2)kd$.

From (79a), (79b), and (79c), it is found that there exists the relation $\bar{h}_0 < \bar{h}_n < \bar{h}_\infty$ in the energy sequence, which means that the energy increases monotonically as the orbits move towards the center type singular point.

Due to the existence of the dissipative perturbations, the center type singular point becomes a hyperbolic sink or a saddle focus. It is known that the existence of the multipulse orbits, which are homoclinic to internal periodic orbits in the slow manifold M_ε, implies the existence of the chaos for the Smale horseshoe sense in the simply supported laminated composite piezoelectric rectangular plate [24, 25].

8. Existence of Multipulse Shilnikov Orbits

In this section, the main interest lies in finding the existence of the multipulse Shilnikov orbits. It is known that the existence of multipulse orbits, which are homoclinic to internal periodic orbits in the slow manifold M_ε, was studied by Haller and Wiggins [21–31]. There are no such internal periodic orbits that lie on the slow manifold in the case of the dissipative perturbations. Due to the existence of the dissipative perturbations, the center type singular point becomes a hyperbolic sink or a saddle focus. In the following analysis, we look for multipulse orbits which are homoclinic to the saddle focus, that is, the Shilnikov type multipulse orbits are negatively and positively asymptotic to the saddle focus itself in full four-dimensional phase space when the dissipative perturbations exist. It is indicated that the presence of N-pulse Shilnikov orbits leads to chaotic dynamics in the sense of the Smale horseshoes. In order to determine the existence of such orbits, we apply the results given by Haller and Wiggins [21–31] to the following research.

First, we require the existence of nondegenerate equilibrium points for $\widehat{H}_D$. In the (h, γ) phase space, based on (59) and $\mu_2/\mu_1 = k$, it is known that this singular point is given by

$$P^c = (h^c, \gamma^c) = \left(0, -\arcsin\frac{kdI_r}{2}\right). \tag{80}$$

Next, we need to compute the zeroes of the dissipative energy difference function at the saddle center $(B, 0, 0, \gamma^c)$ in full four-dimensional phase space (u_1, u_2, h, γ). In order to obtain the zeroes of $\Delta^n \widehat{H}_D(\gamma^c)$, we solve the following equation:

$$\Delta^n \widehat{H}_D(\gamma^c) = -2\overline{f}_2 \sin\left(\gamma + \frac{n\Delta\gamma}{2}\right)\sin\frac{n\Delta\gamma}{2} - \frac{2n\mu_3\varepsilon_1\Delta\gamma}{3a_6} = 0. \tag{81}$$

Equation (81) leads to

$$\sqrt{1 - \frac{k^2d^2I_r^2}{4}}\left[1 - \cos(n\Delta\gamma)\right] = \frac{1}{2}d\left[kI_r\sin(n\Delta\gamma) - \frac{4n\varepsilon_1\Delta\gamma}{3a_6}\right]. \tag{82}$$

Based on (82), we obtain the following dissipative parameter:

$$d = \frac{\mu_3}{\overline{f}_2} = \frac{2\left[1 - \cos(n\Delta\gamma)\right]}{\sqrt{k^2I_r^2\left[1 - \cos(n\Delta\gamma)\right]^2 + \left[kI_r\sin(n\Delta\gamma) - 4n\varepsilon_1\Delta\gamma/3a_6\right]^2}}. \tag{83}$$

The results obtained above are only valid when the nonzero damping exists, that is,

$$\Delta\gamma \neq \frac{2m\pi}{n}, \quad m \in \mathrm{Z}. \tag{84}$$

In order to indicate the existence of the multipulse Shilnikov type orbits in (32a), (32b), (32c), and (32d), it is also necessary to satisfy the following two nondegeneracy conditions:

$$D_d\Delta^n\widehat{H}_D(\gamma^c) \neq 0, \qquad D_{\gamma^c}\Delta^n\widehat{H}_D(\gamma^c) \neq 0, \tag{85}$$

whenever (83) and (84) hold.

The first condition in (85) can be rewritten as

$$D_d\left[\cos\left(-\arcsin\frac{kdI_r}{2} + n\Delta\gamma\right) - \cos\left(-\arcsin\frac{kdI_r}{2}\right) - \frac{2nd\varepsilon_1\Delta\gamma}{3a_6}\right] \neq 0. \tag{86}$$

Carrying out the differentiation with respect to d in (86), it is seen that the above condition is violated only if

$$\sqrt{1 - \frac{k^2d^2I_r^2}{4}}\left[kI_r\sin(n\Delta\gamma) - \frac{4n\varepsilon_1\Delta\gamma}{3a_6}\right] = \frac{k^2dI_r^2}{2}\left[\cos(n\Delta\gamma) - 1\right]. \tag{87}$$

It is obviously found that (82) and (87) cannot be simultaneously satisfied if (84) is also satisfied. Therefore, the second non-degeneracy condition in (85) is satisfied by the existence of transversal zeroes of $\Delta^n\widehat{H}_D$. The first condition in (85) is satisfied by the inequality (73).

Finally, it is necessary to verify the following condition to ensure that the landing point of any n-pulse orbit taking off from a slow sink lies in the domain of attraction of one of the sinks. We define a point which is in the interval $[0, 4\pi]$, and is $2k\pi$ apart from the approximate landing point $\gamma^c + n\Delta\gamma$. This point is denoted by

$$\gamma_*^n = \gamma^s + \left[\gamma^c + n\Delta\gamma - \gamma^s\right] \bmod 2\pi, \tag{88}$$

where

$$\gamma^s = \pi + \arcsin\frac{kdI_r}{2}, \qquad \gamma^c = -\arcsin\frac{kdI_r}{2}. \tag{89}$$

If $\gamma_*^n > \gamma^s$, then we redefine γ_*^n by subtracting 2π from it. The aim here is to find $2k\pi$-translation of the landing point which is closest to the saddle point γ^s in the region $[-\pi/2, 3\pi/2]$. Due to the symmetry of the phase portrait $\gamma \to \gamma - 2\pi$, if the energy of point γ_*^n is more than the energy of the saddle point, that is,

$$\widehat{H}_D\left(0, \gamma_*^n\right) > \widehat{H}_D\left(0, \gamma^s\right), \tag{90}$$

then, for $\varepsilon > 0$ small enough, the landing point $\gamma^c + n\Delta\gamma$ will be in the domain of attraction of one of the sinks. Calculating this energy condition yields

$$\cos\gamma_*^n - \cos\gamma^s > \frac{kdI_r}{2}\left(\gamma_*^n - \gamma^s\right). \tag{91}$$

The shape of such an orbit for $n = 3$ is shown in Figure 4. Based on the aforementioned analysis, we summarize the main results in the following theorem which is similar to the theorem obtained by Haller [31].

Theorem 1. *For any integer $n \geq 1$, a positive number $\varepsilon_0(n) > 0$ and a finite union C_n of codimension-one surfaces in the $(\varepsilon_1, a_6, \mu_3, \overline{f}_2, \varepsilon)$ parameter space near the set satisfying $0 < d < 1$, (83) and (91) exist, such that for any $(\varepsilon_1, a_6, \mu_3, \overline{f}_2, \varepsilon) \in C_n$ and $0 < \varepsilon < \varepsilon_0(n)$, the following conclusions hold.*

(1) If the integer

$$R = \operatorname{int}\left[\frac{1}{2} + \frac{n\Delta\gamma - 2\arcsin\left(kdI_r/2\right)}{2\pi}\right] \tag{92}$$

is even, then each of the saddle-focus type equilibrium points contained in the slow manifold M_ε admits two generalized Shilnikov orbits. If the integer R is odd, then there exist two heteroclinic cycles of generalized Shilnikov orbits connecting the saddle foci to each other. In both cases, the n-pulse orbits form pairs that are symmetric with respect to the subspace $(u_1, u_2) = (B, 0)$.

(2) There exists an open set of parameter values containing C_n for which the systems (32a), (32b), (32c), *and* (32d) *admit the Smale horseshoes in its dynamics.*

We give an explanation of statement (1) in Theorem 1.

The main goal is to prove that utilizing an integer R determines which region the landing point will fall in. The regions one considers are bounded by the saddle points in the unperturbed system. If one considers the domain $(0, 4\pi)$, then the chosen two regions are

$$D_1 = \left(\pi + \arcsin\frac{kdI_r}{2}, 3\pi + \arcsin\frac{kdI_r}{2}\right), \tag{93a}$$

$$D_2 = \left(3\pi + \arcsin\frac{kdI_r}{2}, 5\pi + \arcsin\frac{kdI_r}{2}\right). \tag{93b}$$

The landing point $\gamma^c + n\Delta\gamma$ will fall in one of these two regions or a 2π-translation of one of these regions. If the landing point falls in D_1, and conditions (83) *and* (91) *are also satisfied, then each of the saddle foci will have a homoclinic Shilnikov orbit. If, however, the landing point falls in D_2, and conditions* (83) *and* (91) *are also satisfied, then there will exist heteroclinic cycles of Shilnikov orbits connecting the two saddle foci to each other. In each case, one will have pairs of orbits that are symmetric with respect to the planes $(u_1, u_2) = (B, 0)$, due to the existence of the symmetry $(u_1, u_2) \to (-u_1, -u_2)$.*

If the landing point $\gamma^c + n\Delta\gamma$ is in D_1 or a 2π-translation, one has

$$\gamma^c + n\Delta\gamma \in \left(\gamma^s + 2m\pi, \gamma^s + 2\pi + 2m\pi\right). \tag{94}$$

Equation (94) *leads to*

$$\gamma^c + n\Delta\gamma - \gamma^s \in (2m\pi, 2m\pi + 2\pi). \tag{95}$$

Hence, the integer

$$R = \operatorname{int}\left[\frac{1}{2} + \frac{n\Delta\gamma - 2\arcsin\left(kdI_r/2\right)}{2\pi}\right] \tag{96}$$

is even. Reversely, if the landing point falls in D_2 or a 2π-translation, one can similarly obtain

$$\gamma^c + n\Delta\gamma \in \left(\gamma^s + 2m\pi + 2\pi, \gamma^s + 4\pi + 2m\pi\right). \tag{97}$$

From (97), *one has*

$$\gamma^c + n\Delta\gamma - \gamma^s \in (2(m+1)\pi, 2(m+2)\pi). \tag{98}$$

Therefore, it is known that the integer

$$R = \operatorname{int}\left[\frac{1}{2} + \frac{n\Delta\gamma - 2\arcsin\left(kdI_r/2\right)}{2\pi}\right] \tag{99}$$

is odd.

The proof of the second part of Theorem 1 follows from Theorem 2.8.2 presented by Haller [31].

9. Numerical Results of Chaotic Motions

Based on the above qualitative analysis for the multipulse orbits and chaotic dynamics of the laminated composite piezoelectric rectangular plate, the conditions of the chaotic motion under the sense of the Smale horses are obtained. The heteroclinic bifurcations of (16a), (16b), (16c), and (16d) appear when $\eta_1 > 0$. Therefore, the above theoretical analysis is focused on the situation where there exist heteroclinic bifurcations in (16a), (16b), (16c), and (16d). The parameter η_1 is the combination of the parameters a_6, a_7, and b_6, where $\eta_1 = (3a_6a_7)/b_6$. In this section, we have only performed numerical simulations of the multipulse chaotic motions of the laminated composite piezoelectric rectangular plate under heteroclinic bifurcations in order to further verify the theoretical analysis. Consequently, the parameters a_6, a_7, and b_6 are chosen to satisfy $\eta_1 > 0$.

We choose the averaged equations (16a), (16b), (16c), and (16d) to conduct numerical simulations. A numerical approach through the computer software MATLAB is utilized to explore the existence of the Shilnikov type multipulse chaotic motions in the laminated composite piezoelectric rectangular plate. Based on the above qualitative analysis, it is

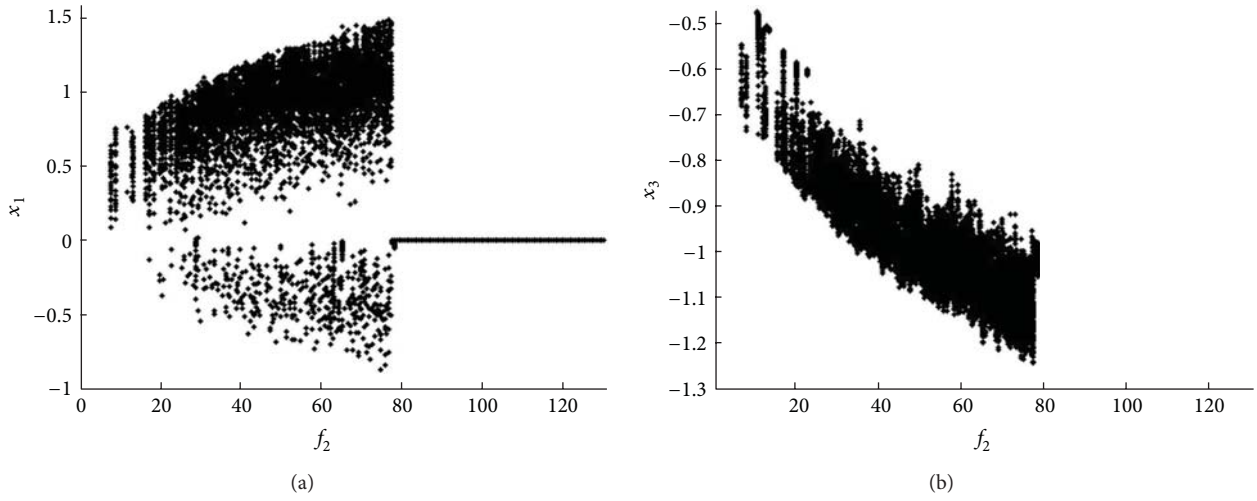

FIGURE 5: The bifurcation diagram is obtained for the excitations $f_2 = 2\sim130$, $x_{10} = -0.01$, $x_{20} = -0.09$, $x_{30} = -0.05$, $x_{40} = -0.6$, $\sigma_1 = 3.31$, $\sigma_2 = 3.23$, $\mu_1 = 0.1$, $\mu_2 = 0.1$, $a_2 = 11.59$, $a_3 = 21.5$, $a_4 = 13.7$, $a_6 = -14.37$, $a_7 = 10.39$, $b_6 = -5.68$, and $b_7 = -14.94$; (a) the bifurcation diagram on the plane (x_1, f_2); (b) the bifurcation diagram on the plane (x_3, f_2).

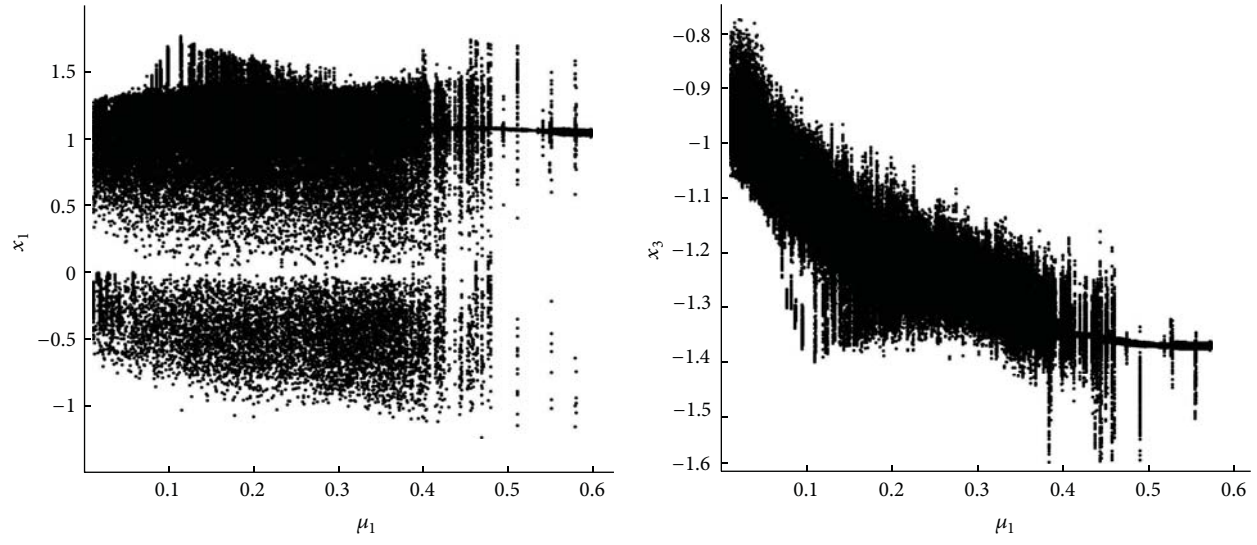

FIGURE 6: The bifurcation diagram is obtained for the damping coefficients $\mu_1 = 0.06\sim0.6$ and $f_2 = 55.1$; (a) the bifurcation diagram on the plane (x_1, μ_1); (b) the bifurcation diagram on the plane (x_3, μ_1).

found that the damping coefficients $\mu_1$and μ_2 and the transverse excitation f_2 play an important role in the multipulse chaotic motions of the laminated composite piezoelectric rectangular plate. In addition, the parameters a_2 and a_3 are related to the in-plane excitation in the x-direction and the in-plane excitation in the y-direction, respectively. The parameter a_4 is the piezoelectric excitation which reflects the characteristics of the piezoelectric material. Hence, the parameters μ_1, μ_2, a_2, a_3, a_4, and f_2 are selected as the controlling parameters to discover the law for complicated nonlinear dynamics of the laminated composite piezoelectric rectangular plate.

Figure 5 illustrates the bifurcation diagram of the laminated composite piezoelectric rectangular plate when the excitation f_2 varies in the interval $f_2 = 2\sim130$. Other parameters and initial conditions are chosen as $\sigma_1 = 3.31$, $\sigma_2 = 3.23$, $\mu_1 = 0.1$, $\mu_2 = 0.1$, $a_2 = 11.59$, $a_3 = 21.5$, $a_4 = 13.7$, $a_6 = -14.37$, $a_7 = 10.39$, $b_6 = -5.68$, $b_7 = -14.94$, $x_{10} = -0.01$, $x_{20} = -0.09$, $x_{30} = -0.05$, and $x_{40} = -0.6$. Figures 5(a) and 5(b) represent the bifurcation diagram on the plane (x_1, f_2) and (x_3, f_2), respectively. It is observed from Figure 5 that the excitation f_2 is an important parameter that influences the nonlinear dynamic responses of the laminated composite piezoelectric rectangular plate. Figure 5 shows that the chaotic motion of the laminated composite piezoelectric rectangular plate appears when the excitation f_2 varies in the interval $f_2 = 20\sim78$, followed by a periodic motion of that. When excitation f_2 continues to increase, Figure 5 presents

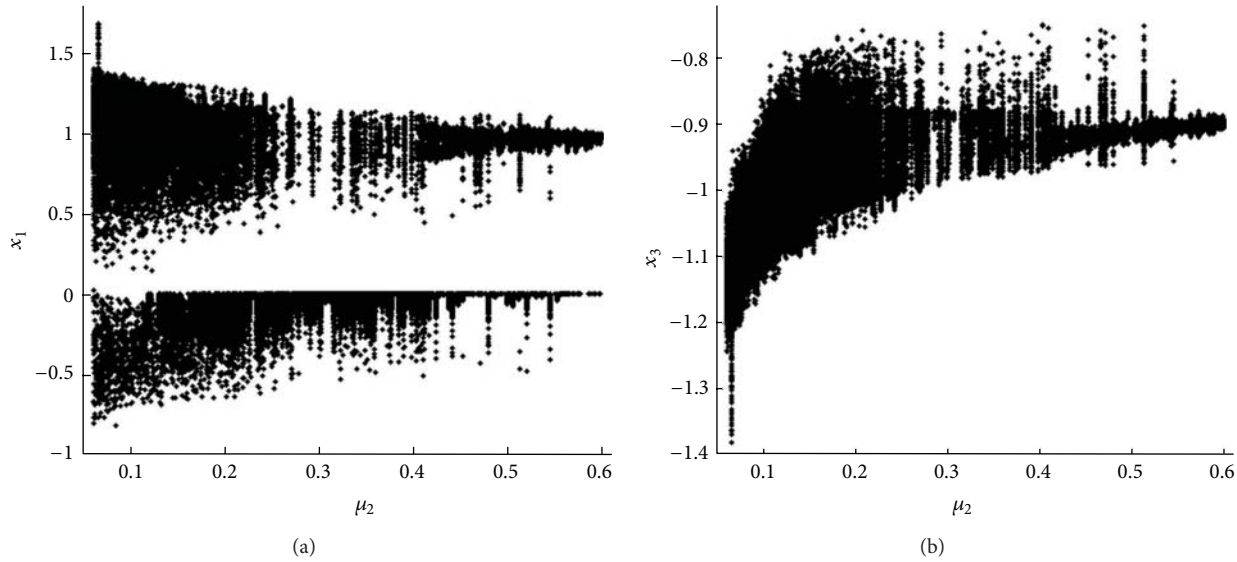

Figure 7: The bifurcation diagram is obtained for the damping coefficients $\mu_2 = 0.06\sim0.6$, $f_2 = 55.1$, and $\mu_1 = 0.1$; (a) the bifurcation diagram on the plane (x_1, μ_2); (b) the bifurcation diagram on the plane (x_3, μ_2).

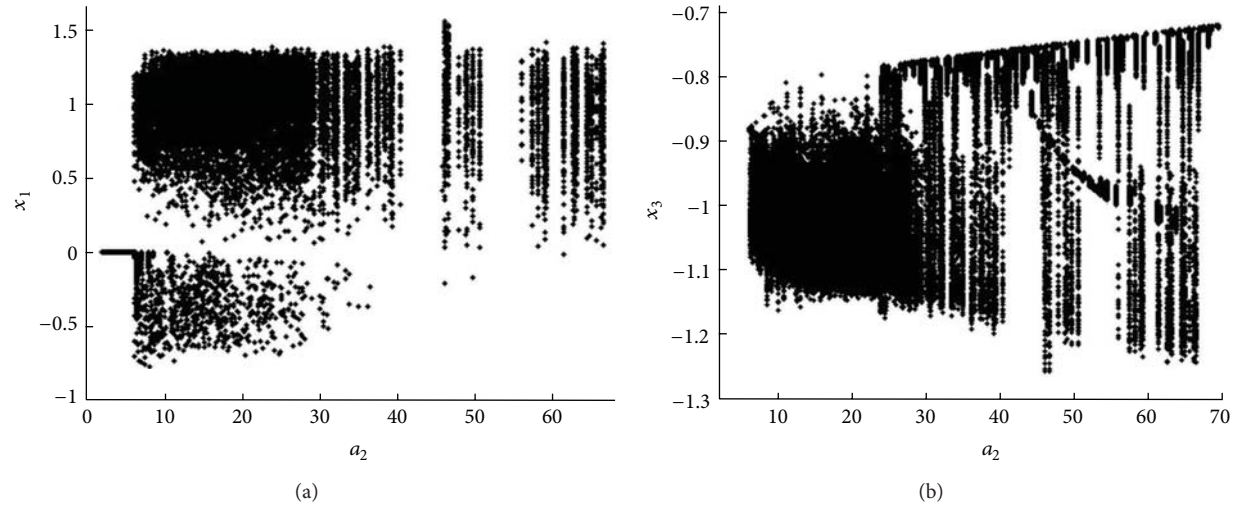

Figure 8: The bifurcation diagram is obtained for the in-plane excitations $a_2 = 2\sim70$, $f_2 = 55.1$, $\mu_1 = 0.1$, and $\mu_2 = 0.1$; (a) the bifurcation diagram on the plane (x_1, a_2); (b) the bifurcation diagram on the plane (x_3, a_2).

that there is the periodic motion of the laminated composite piezoelectric rectangular plate.

We, respectively, study the impact of the two damping parameters since the averaged equations (16a), (16b), (16c), and (16d) have two different damping coefficients. Figure 6 is the bifurcation diagram of the laminated composite piezoelectric rectangular plate with the damping coefficient μ_1. Figure 6 demonstrates that the system is beginning to enter into the region of the chaotic motion and subsequently comes into the region of the periodic motion, as the damping coefficient μ_1 varies in the interval $\mu_1 = 0.06\sim0.6$. Other parameters and initial conditions are the same as those in Figure 5 when the excitation is chosen as $f_2 = 55.1$. Figures 6(a) and 6(b) describe the nonlinear motion of the laminated composite piezoelectric rectangular plate on the planes (x_1, μ_1) and (x_3, μ_1), respectively, as well as the impact of the damping coefficient μ_1 on the system.

Figure 7 represents the bifurcation diagram on the damping coefficient μ_2. Figure 7 shows that the laminated composite piezoelectric rectangular plate has been in a state of chaotic motion as the damping coefficient μ_2 changes in the interval $\mu_2 = 0.06\sim0.6$. Other parameters and initial conditions are the same as those in Figure 6 when the damping coefficient μ_1 is only changed to $\mu_1 = 0.1$. Figures 7(a) and 7(b) depict the nonlinear motion of the laminated composite piezoelectric rectangular plate on the planes (x_1, μ_2) and (x_3, μ_2), respectively. In contrast to Figures 6 and 7, it can be observed that there is a great difference between them. The above numerical analysis proves that the damping coefficients μ_1 and μ_2 make a great impact on the

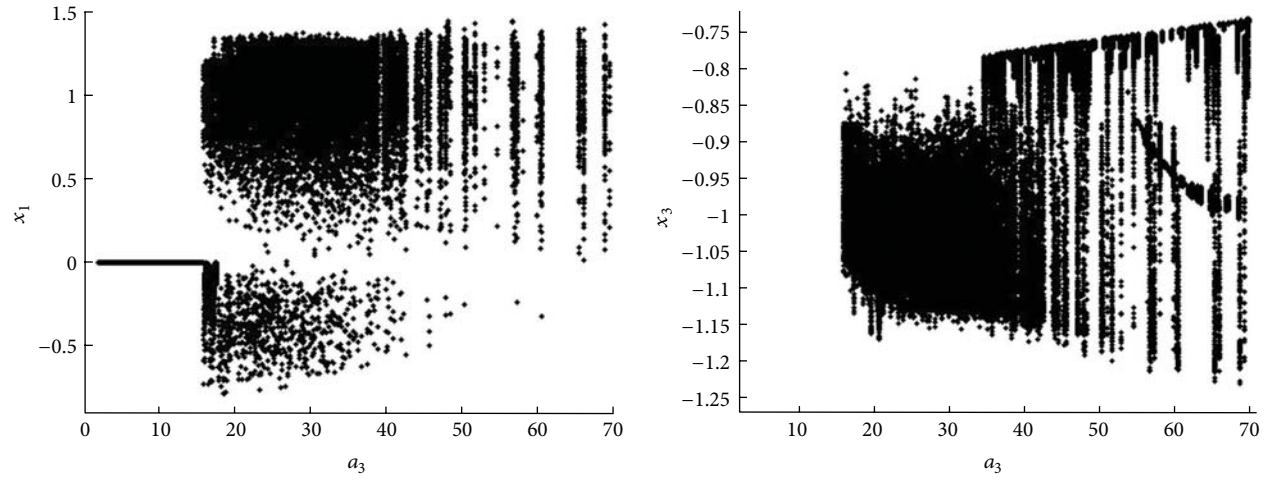

FIGURE 9: The bifurcation diagram is obtained for the in-plane excitations $a_3 = 2\sim70$, $f_2 = 55.1$, $\mu_1 = 0.1$, $\mu_2 = 0.1$, and $a_2 = 11.59$; (a) the bifurcation diagram on the plane (x_1, a_3); (b) the bifurcation diagram on the plane (x_3, a_3).

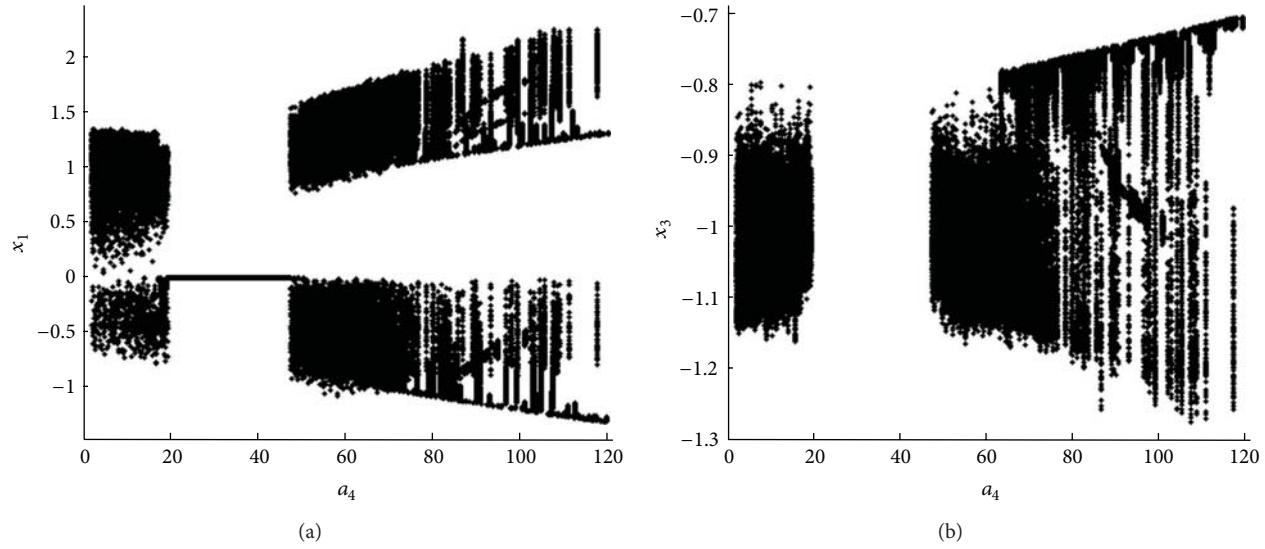

FIGURE 10: The bifurcation diagram is obtained for the piezoelectric excitations $a_4 = 2\sim120$, $f_2 = 55.1$, $\mu_1 = 0.1$, $\mu_2 = 0.1$, $a_2 = 11.59$, and $a_3 = 21.5$; (a) the bifurcation diagram on the plane (x_1, a_4); (b) the bifurcation diagram on the plane (x_3, a_4).

emergence of the multipulse chaotic motions of the laminated composite piezoelectric rectangular plate.

Figure 8 portrays the bifurcation diagram for the laminated composite piezoelectric rectangular plate when the in-plane excitation along the x-direction a_2 varies in the interval $a_2 = 2\sim70$. Other parameters and initial conditions remain the same as those in Figure 7 when the damping coefficient μ_2 is selected as $\mu_2 = 0.1$. Figures 8(a) and 8(b) display the bifurcation diagram on the planes (x_1, a_2) and (x_3, a_2), respectively. Figure 8 presents that periodic motion is just beginning to emerge in the system, followed by a chaotic motion.

Figure 9 denotes the bifurcation diagram for the laminated composite piezoelectric rectangular plate when the in-plane excitation along the y-direction a_3 varies in the interval $a_3 = 2\sim70$. Other parameters and initial conditions are the same as those in Figure 8 when the in-plane excitation a_2 is chosen as $a_2 = 11.59$. Figures 9(a) and 9(b) denote the bifurcation diagram on the planes (x_1, a_3) and (x_3, a_3), respectively. Comparing with Figures 8 and 9, it is found that the evolution law of the nonlinear motion is very similar to each other. This shows that in-plane excitations a_2 and a_3 have the same effect on the existence of the multipulse chaotic motions in the laminated composite piezoelectric rectangular plate under this set of parameters.

Figure 10 indicates the bifurcation diagram for the laminated composite piezoelectric rectangular plate when the piezoelectric excitation a_4 varies from $a_4 = 2$ to $a_4 = 120$. Other parameters and initial conditions remain the same as those in Figure 9 when the in-plane excitation a_3 is chosen as

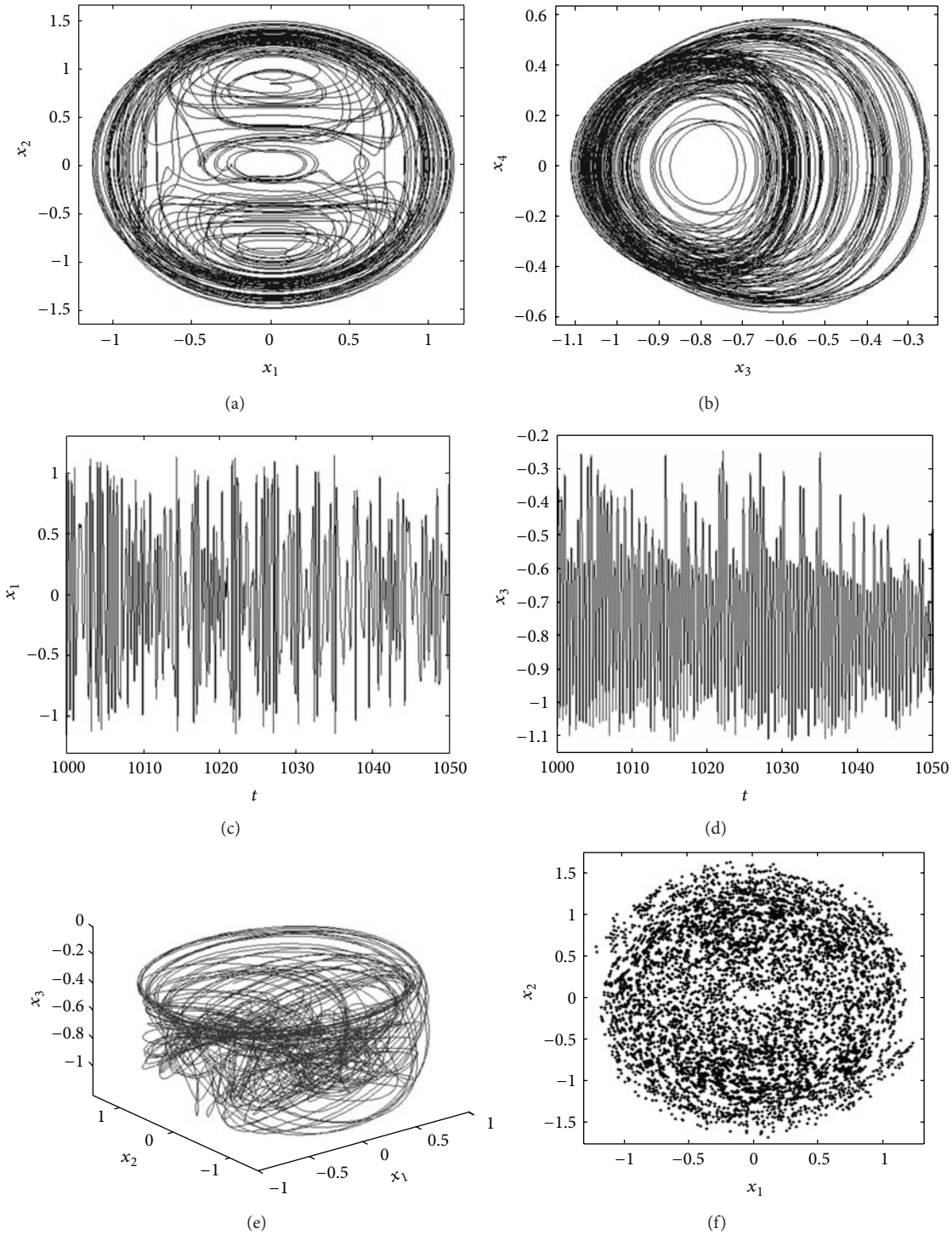

Figure 11: The multipulse chaotic motion is obtained when $f_2 = 55.1$ and $\mu_1 = 0.1$; (a) the phase portrait on the plane (x_1, x_2); (b) the phase portrait on the plane (x_3, x_4); (c) the waveform on the plane (t, x_1); (d) the waveform on the plane (t, x_3); (e) the phase portraits in the three-dimensional space (x_1, x_2, x_3); (f) Poincare map on the plane (x_1, x_2).

$a_3 = 21.5$. Figures 10(a) and 10(b) demonstrate the bifurcation diagram on the planes (x_1, a_4) and (x_3, a_4), respectively. It is observed from Figure 10 that the piezoelectric excitation a_4 has a significant influence on the complicated nonlinear dynamic behaviors of the laminated composite piezoelectric rectangular plate. As the piezoelectric excitation a_4 increases, Figure 10 reveals the following law: chaotic motion $\rightarrow$ periodic motion $\rightarrow$ chaotic motion.

Based on the above bifurcation diagram, the excitations f_2, a_2, a_3, and a_4 and the damping coefficients μ_1 and μ_2

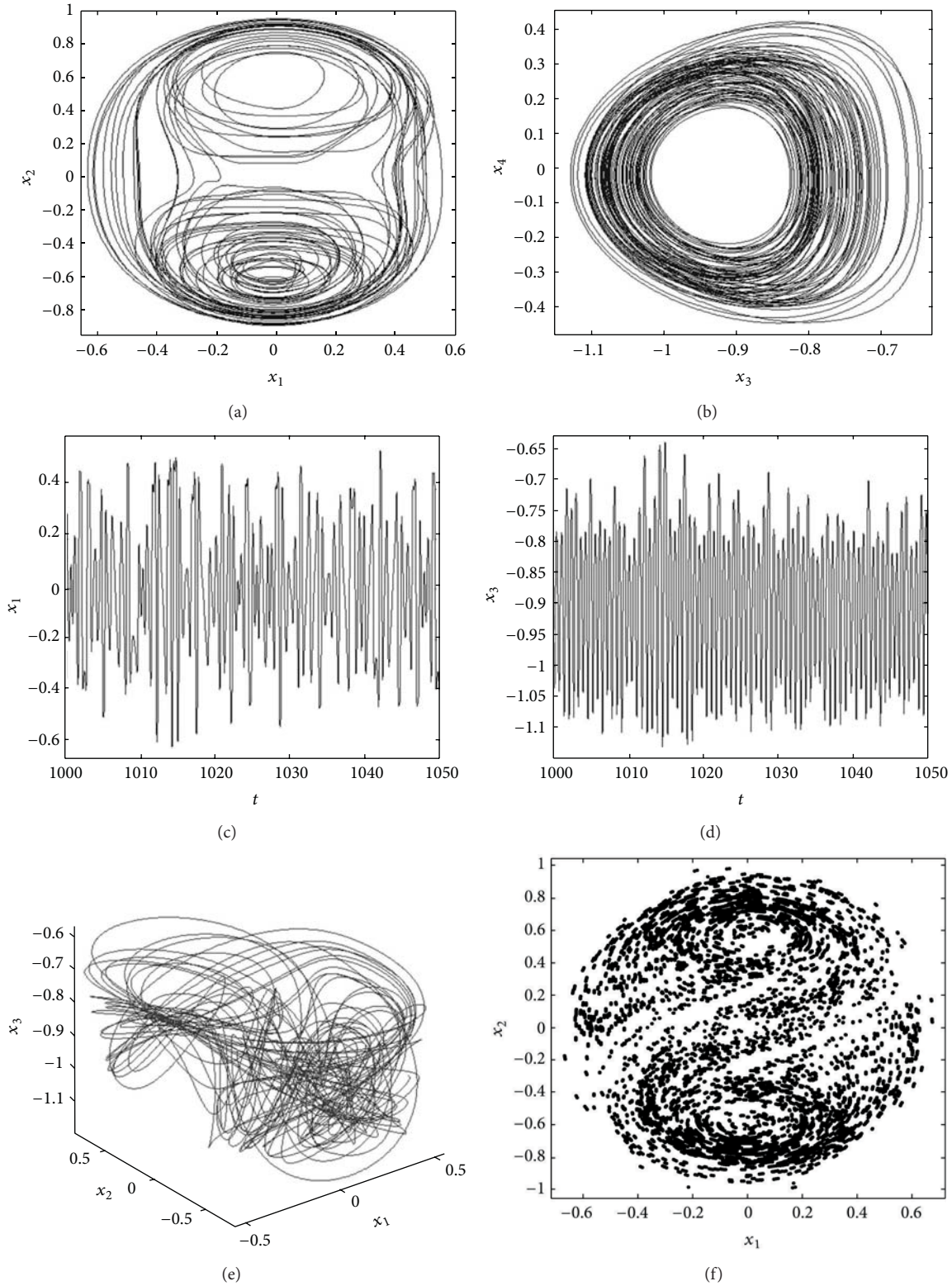

FIGURE 12: The multipulse chaotic motion is obtained when $\sigma_1 = 7.31$, $\sigma_2 = 12.23$, $\mu_1 = 0.3$, $\mu_2 = 0.2$, $a_2 = 20.9$, $a_3 = 13.6$, $a_4 = 17.3$, $a_6 = -7.37$, $a_7 = 13.39$, $f_2 = 35.1$, $b_6 = -3.68$, $b_7 = -11.16$, $x_{10} = -3.1385$, $x_{20} = -4.45$, $x_{30} = -0.59$, and $x_{40} = 0.36$; (a) the phase portrait on the plane (x_1, x_2); (b) the phase portrait on the plane (x_3, x_4); (c) the waveform on the plane (t, x_1); (d) the waveform on the plane (t, x_3); (e) the phase portraits in the three-dimensional space (x_1, x_2, x_3); (f) Poincare map on the plane (x_1, x_2).

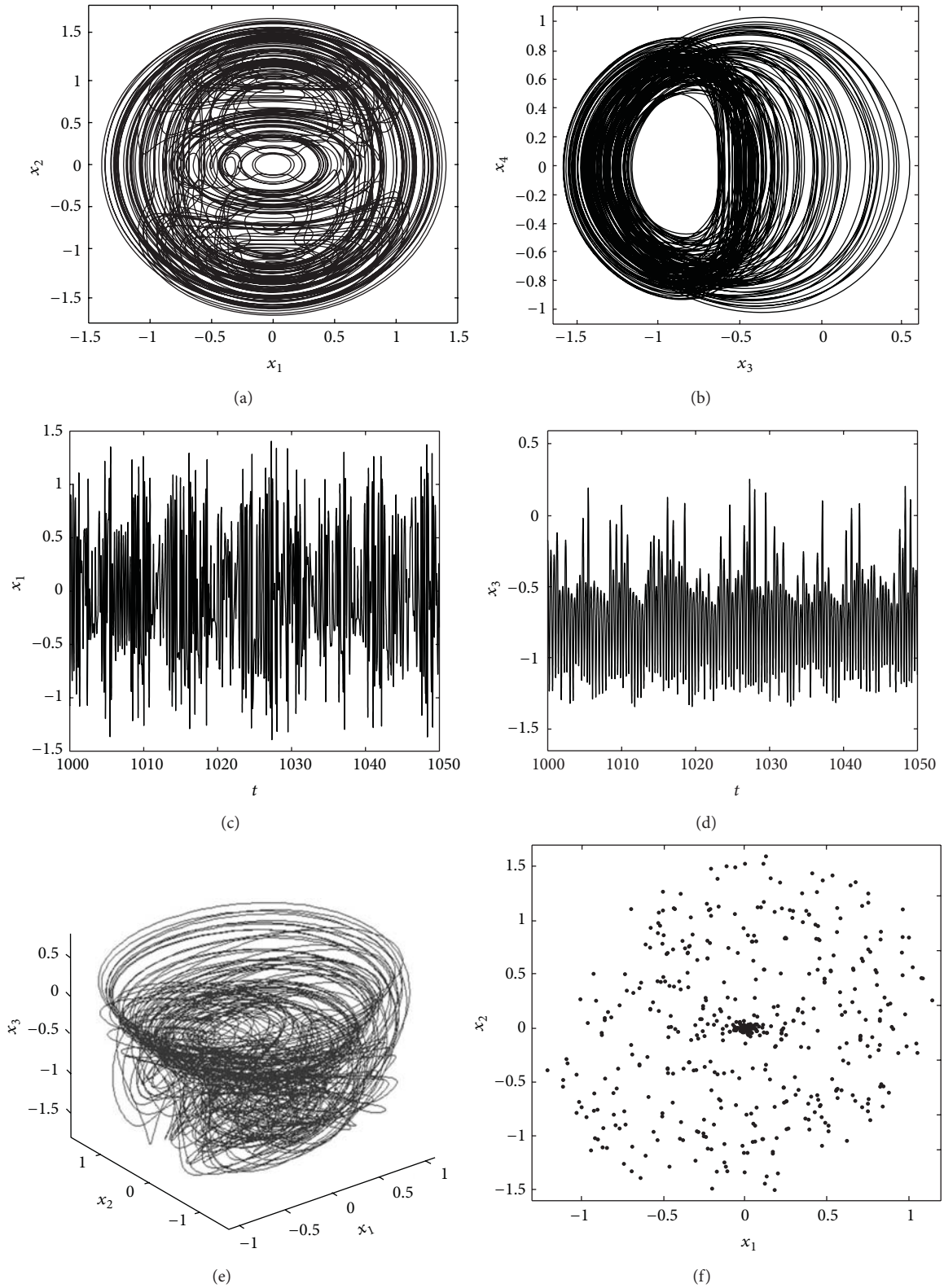

FIGURE 13: The multipulse chaotic motion is obtained when $a_6 = -17.37$ and $b_6 = -13.68$; (a) the phase portrait on the plane (x_1, x_2); (b) the phase portrait on the plane (x_3, x_4); (c) the waveform on the plane (t, x_1); (d) the waveform on the plane (t, x_3); (e) the phase portraits in the three-dimensional space (x_1, x_2, x_3); (f) Poincare map on the plane (x_1, x_2).

are selected as specific values in order to find the multipulse chaotic motions of the laminated composite piezoelectric rectangular plate. Figure 11 indicates the existence of the multipulse chaotic motion of the laminated composite piezoelectric rectangular plate when the excitation f_2 is $f_2 = 55.1$. In this case, the chosen parameters and initial conditions are the same as those in Figure 5. Figures 11(a) and 11(b) represent the phase portraits on the planes (x_1, x_2) and (x_3, x_4), respectively. Figures 11(c) and 11(d) give the waveforms on the planes (t, x_1) and (t, x_3), respectively. Figures 11(e) and 11(f) are the three-dimensional phase portrait in the space (x_1, x_2, x_3) and the Poincare map on the plane (x_1, x_2), respectively. Figure 11 shows that the excitation f_2 has a noticeable effect on the existence of the multipulse chaotic motions on the laminated composite piezoelectric rectangular plate.

Besides the excitations f_2, a_2, a_3, and a_4 and the damping coefficients μ_1 and μ_2, the multipulse chaotic motions of the laminated composite piezoelectric rectangular plate also depend on other parameters. Figure 12 is obtained when the parameters and initial conditions are chosen as $\sigma_1 = 7.31$, $\sigma_2 = 12.23$, $\mu_1 = 0.3$, $\mu_2 = 0.2$, $a_2 = 20.9$, $a_3 = 13.6$, $a_4 = 17.3$, $a_6 = -7.37$, $f_2 = 35.1$, $a_7 = 13.39$, $b_6 = -3.68$, $b_7 = -11.16$, $x_{10} = -3.1385$, $x_{20} = -4.45$, $x_{30} = -0.59$, and $x_{40} = 0.36$. Comparing with Figures 11 and 12, it is found that there are differences in the phase portraits, the waveforms, and the Poincare map, respectively. From the three-dimensional phase portrait in Figure 12, we can see that there exists obvious multi- pulse jumping phenomenon.

In the following numerical simulations, different parameters are given in order to investigate the different shapes of the multipulse chaotic motion. Figure 13 demonstrates the multipulse chaotic response in the laminated composite piezoelectric rectangular plate for $a_6 = -17.37$ and $b_6 = -13.68$. Other parameters and initial conditions are the same as those in Figure 12. From Figure 13, we can see that there is another shape for the multipulse chaotic motion. It is found that the shapes of these two phenomena depicted in Figures 12 and 13 are completely different.

10. Conclusions

In this paper, the nonlinear vibrations of the laminated composite piezoelectric rectangular plate are studied by applying the theories of the global bifurcations and chaotic dynamics for high-dimensional nonlinear systems. The multipulse heteroclinic orbits and chaotic dynamics are investigated using the energy-phase method for the case of primary parametric resonance and 1 : 2 internal resonances. The energy-phase method can be applied to discover the existence of the Shilnikov type multipulse heteroclinic bifurcations and chaotic dynamics of high-dimensional nonlinear systems in engineering applications. The analysis of the multipulse heteroclinic orbits in the laminated composite piezoelectric rectangular plate demonstrates that the unperturbed integrable system contains a normally hyperbolic invariant two-dimensional manifold near the resonance. The resonance brings about a circle of fixed points on the two-dimensional manifold. Two different points on the circle of fixed points are connected by a heteroclinic orbit. The dissipative perturbation can severely change the dynamics near the circle of fixed points. The analysis shows that the existence of heteroclinic orbits depends only on an energy-phase criterion. The studies have led to the following conclusions.

(1) From the aforementioned analytical studies, it is found that the multipulse Shilnikov type orbits depend on the dissipative perturbations and excitations. As the trajectory of motion approaches to the sink point P_ε, every Shilnikov type orbit takes off again and repeats the similar motion in full four-dimensional phase space, which conduces to the Shilnikov type multipulse orbits. In the Shilnikov type multipulse orbits, the final pulse orbit is similar to the one of the single-pulse. It can be conjectured that the transfer of the energy between the different two modes occurs through the Shilnikov type multipulse orbits.

(2) In order to verify the theoretical predictions, numerical simulation is used to examine the bifurcations and chaotic motions of the laminated composite piezoelectric rectangular plate. Several types of the bifurcation diagrams are obtained when the transverse excitation f_2, the in-plane excitations a_2 and a_3, the piezoelectric excitation a_4, and the damping coefficients μ_1 and μ_2 are chosen as several different kinds of control parameters. Based on the bifurcation diagrams, the nonlinear dynamic behavior of the laminated composite piezoelectric rectangular plate is controlled from the chaotic motion to the periodic motion by varying the excitations f_2, a_2, a_3, and a_4 and the damping coefficients μ_1 and μ_2, respectively. Therefore, the excitations f_2, a_2, a_3, a_4, and the damping coefficients μ_1 and μ_2 have important influence on the nonlinear dynamics responses of the laminated composite piezoelectric rectangular plate.

(3) There exist different shapes of the chaotic motions in the nonlinear oscillations of the laminated composite piezoelectric rectangular plate under different excitations, parameters, and initial conditions. It is found from the numerical simulations that the shapes of the chaotic motions are completely different. Therefore, the parameters and the initial conditions have impact on the shapes of the multipulse chaotic motions.

(4) There exist multipulse chaotic motions in the averaged equations. It is well known that the multipulse chaotic motions in the averaged equations can lead to the multipulse amplitude modulated chaotic vibrations in the original system under certain conditions. Therefore, the multipulse amplitude modulated chaotic motions occur in the laminated composite piezoelectric rectangular plate.

In a word, we draw a conclusion through theoretical and numerical investigations that the chaos for the Smale horseshoe sense in nonlinear motion of the simply supported laminated composite piezoelectric rectangular plate exists.

Appendix

A. The Coefficients for Equations (11a)–(11f)

The coefficients presented in (11a), (11b), (11c), (11d), (11e), and (11f) are as follows:

$$k_1 = \frac{896}{225}\frac{aA_{12}}{b^2\pi A_{11}+a^2\pi A_{66}} + \frac{896}{225}\frac{b^2A_{11}}{ab^2\pi A_{11}+a^3\pi A_{66}} - \frac{128}{225}\frac{aA_{66}}{b^2\pi A_{11}+a^2\pi A_{66}},$$

$$k_2 = \frac{2688}{715}\frac{aA_{12}}{b^2\pi A_{11}+a^2\pi A_{66}} + \frac{27264}{715}\frac{b^2A_{11}}{ab^2\pi A_{11}+a^3\pi A_{66}} - \frac{384}{715}\frac{aA_{66}}{b^2\pi A_{11}+a^2\pi A_{66}},$$

$$k_3 = \frac{256}{4725}\frac{aA_{12}}{b^2\pi A_{11}+a^2\pi A_{66}} + \frac{3328}{1575}\frac{b^2A_{11}}{ab^2\pi A_{11}+a^3\pi A_{66}} - \frac{256}{675}\frac{aA_{12}}{b^2\pi A_{11}+a^2\pi A_{66}},$$

$$k_4 = -\frac{32ab^2N_x^p}{b^2\pi^3A_{11}+a^2\pi^3A_{66}} + \frac{32ab^2q_1h}{b^2\pi^3A_{11}+a^2\pi A_{66}},$$

$$k_5 = \frac{128}{15}\frac{aA_{12}}{9b^2\pi A_{11}+a^2\pi A_{66}} + \frac{128}{105}\frac{b^2A_{11}}{9ab^2\pi A_{11}+a^3\pi A_{66}} - \frac{128}{105}\frac{aA_{66}}{9b^2\pi A_{11}+a^2\pi A_{66}},$$

$$k_6 = \frac{896}{225}\frac{aA_{12}}{9b^2\pi A_{11}+a^2\pi A_{66}} + \frac{896}{25}\frac{b^2A_{11}}{9ab^2\pi A_{11}+a^3\pi A_{66}} - \frac{128}{225}\frac{aA_{66}}{9b^2\pi A_{11}+a^2\pi A_{66}},$$

$$k_7 = \frac{2304}{1925}\frac{aA_{66}}{9b^2\pi A_{11}+a^2\pi A_{66}} + \frac{71424}{1925}\frac{b^2A_{11}}{9ab^2\pi A_{11}+a^3\pi A_{66}} + \frac{2304}{275}\frac{aA_{12}}{9b^2\pi A_{11}+a^2\pi A_{66}},$$

$$k_8 = -\frac{32ab^2N_x^p}{9b^2\pi^3A_{11}+a^2\pi^3A_{66}} + \frac{32ab^2q_1h}{9b^2\pi^3A_{11}+a^2\pi^3A_{66}},$$

$$k_9 = \frac{896}{225}\frac{bA_{12}}{a^2\pi A_{22}+b^2\pi A_{66}} + \frac{896}{225}\frac{a^2A_{22}}{a^2b\pi A_{22}+b^3\pi A_{66}} + \frac{128}{225}\frac{bA_{66}}{a^2\pi A_{22}+b^2\pi A_{66}},$$

$$k_{10} = \frac{27264}{715}\frac{bA_{12}}{a^2\pi A_{22}+b^2\pi A_{66}} + \frac{2688}{715}\frac{a^2A_{22}}{a^2b\pi A_{22}+b^3\pi A_{66}} + \frac{384}{715}\frac{bA_{66}}{a^2\pi A_{22}+b^2\pi A_{66}},$$

$$k_{11} = -\frac{3328}{1575}\frac{bA_{12}}{a^2\pi A_{22}+b^2\pi A_{66}} + \frac{256}{675}\frac{a^2A_{22}}{a^2b\pi A_{22}+b^3\pi A_{66}} + \frac{256}{4725}\frac{bA_{66}}{a^2\pi A_{22}+b^2\pi A_{66}},$$

$$k_{12} = -\frac{32a^2bN_y^p}{a^2\pi^3A_{22}+b^2\pi^3A_{66}} + \frac{32a^2bq_2h}{a^2\pi^3A_{22}+b^2\pi^3A_{66}}. \tag{A.1}$$

B. The Coefficients for Equations (13a) and (13b)

The coefficients presented in (13a) and (13b) are as follows:

$$m_1 = I_0 - \frac{J_4k_7}{a\pi c_1} + \frac{I_6}{b^2\pi^2c_1^2} + \frac{I_6}{a^2\pi^2c_1^2} - \frac{J_4k_9}{b\pi c_1},$$

$$m_2 = I_0 - \frac{3J_4k_8}{a\pi c_1} + \frac{9I_6}{a^2\pi^2c_1^2} + \frac{I_6}{b^2\pi^2c_1^2} - \frac{J_4k_{10}}{b\pi c_1},$$

$$\omega_1^2 = \pi^2\frac{F_{44}c_2^2 - 2D_{44}c_2 + A_{44}}{m_1b^2} + \pi^2\frac{-2D_{55}c_2 + A_{55} + F_{55}c_{22}}{m_1a_2} + \pi\frac{A_{55}k_7 + F_{55}c_2^2k_7 - 2D_{55}c_2k_7}{m_1a} + \pi\frac{A_{44}k_9 + F_{44}c_2^2k_9 - 2D_{44}c_2k_9}{m_1b} + \pi^3\frac{-c_1F_{11}k_7 + H_{11}c_1^2k_7}{m_1a^3} + \pi^4\frac{H_{22}c_1^2}{m_1b^4} + \pi^3\frac{H_{22}c_1^2k_9 - c_1F_{22}k_9}{m_1b^3} + \pi^4\frac{H_{11}c_1^2}{m_1a^4} + \pi^4\frac{H_{12}c_1^2 + 4H_{66}c_1^2 + H_{21}c_1^2}{m_1b^2a^2} + \pi^3\frac{H_{12}c_1^2k_9 - c_1F_{12}k_9 - 2c_1F_{66}k_9 + 2\pi^3H_{66}c_1^2k_9}{m_1ba^2} + \pi^3\frac{2c_1F_{66}k_7 + 2H_{66}c_1^2k_7 - c_1F_{21}k_7 + H_{21}c_1^2k_7}{m_1b^2a},$$

$$\omega_2^2 = \pi\frac{A_{44}k_{10} - 2D_{44}c_2k_{10} + F_{44}c_2^2k_{10}}{m_2b} + \pi^2\frac{A_{44} + F_{44}c_2^2 - 2D_{44}c_2}{m_2b^2} + \pi^2\frac{-18D_{55}c_2 + 9F_{55}c_2^2 + 9A_{55}}{m_2a^2}$$

$$+\pi\frac{3A_{55}k_8-6D_{55}c_2k_8+3F_{55}c_2^2k_8}{m_2a}+\frac{\pi^4H_{22}c_1^2}{m_2b^4}$$

$$+\pi^3\frac{-c_1F_{22}k_{10}+H_{22}c_1^2k_{10}}{m_2b^3}$$

$$+\pi^4\frac{36H_{66}c_1^2+9H_{12}c_1^2+9H_{21}c_1^2}{m_2b^2a^2}$$

$$+\pi^3\frac{-3c_1F_{21}k_8+3H_{21}c_1^2k_8-6c_1F_{66}k_8+6H_{66}c_1^2k_8}{m_2b^2a}$$

$$+\frac{81\pi^4H_{11}c_1^2}{m_2a^4}$$

$$+\pi^3\frac{-9c_1F_{12}k_{10}+9H_{12}c_1^2k_{10}-18c_1F_{66}k_{10}+18H_{66}c_1^2k_{10}}{m_2ba^2}$$

$$+\pi^3\frac{-27c_1F_{11}k_8+27H_{11}c_1^2k_8}{m_2a^3},$$

$$a_2=\frac{\pi^2q_x}{a^2},\qquad a_3=\frac{\pi^2q_y}{b^2},\qquad a_4=\frac{\pi^2N_x^p}{a^2}+\frac{\pi^2N_y^p}{b^2},$$

$$\begin{aligned}a_5=&-\frac{208\pi A_{11}k_1}{315a^3}+\frac{112\pi A_{22}k_6}{45b^3}+\frac{64\pi A_{66}k_1}{945ab^2}\\&+\frac{64\pi A_{66}k_4}{225a^2b}+\frac{64\pi A_{21}k_1}{45ab^2}+\frac{\pi^4A_{12}}{32a^2b^2}\\&-\frac{112\pi A_{22}k_4}{225b^3}+\frac{64\pi A_{21}k_1}{945ab^2}+\frac{5\pi^4A_{21}}{32a^2b^2}\\&+\frac{64\pi A_{12}k_6}{45a^2b}+\frac{64\pi A_{66}k_3}{45ab^2}+\frac{3\pi^4A_{66}}{8a^2b^2}\\&-\frac{64\pi A_{12}k_4}{25a^2b}-\frac{64\pi A_{66}k_6}{45a^2b}-\frac{27\pi^4A_{11}}{32a^4}\\&+\frac{9\pi^4A_{22}}{32b^4}+\frac{112\pi A_{11}k_3}{45a^3},\end{aligned}$$

$$\begin{aligned}a_6=&\frac{64\pi A_{66}k_3}{945ab^2}-\frac{64\pi A_{21}k_3}{945ab^2}-\frac{208\pi A_{11}k_3}{315a^3}\\&+\frac{64\pi A_{66}k_6}{225a^2b}+\frac{64\pi A_{21}k_2}{45ab^2}+\frac{112\pi A_{22}k_5}{45b^3}\\&-\frac{9\pi^4A_{22}}{16b^4}-\frac{\pi^4A_{12}}{16ab^2}-\frac{64\pi A_{66}k_5}{45a^2b}\\&-\frac{64\pi A_{66}k_2}{45ab^2}-\frac{112\pi A_{22}k_6}{225b^3}-\frac{81\pi^4A_{11}}{16a^4}\\&+\frac{112\pi A_{11}k_2}{45a^3}+\frac{64\pi A_{12}k_5}{45a^2b}\\&-\frac{208\pi A_{12}k_6}{25a^2b}-\frac{9\pi^4A_{21}}{16a^2b^2},\end{aligned}$$

$$a_7=\frac{64\pi A_{21}k_1}{45ab^2}-\frac{64\pi A_{66}k_4}{45a^2b}+\frac{64\pi A_{12}k_4}{45a^2b}$$

$$\begin{aligned}&-\frac{\pi^4A_{12}}{32a^2b^2}+\frac{112\pi A_{11}}{45ab^2}-\frac{\pi^4A_{21}}{32a^2b^2}\\&-\frac{9\pi^4A_{11}}{32a^4}-\frac{\pi A_{66}k_1}{45ab^2}-\frac{\pi A_{66}}{8a^2b^2}\\&+\frac{112\pi A_{22}k_4}{45b^3}-\frac{9\pi^4A_{22}}{32b^4},\end{aligned}$$

$$\begin{aligned}a_8=&\frac{64\pi A_{21}k_2}{945ab^2}-\frac{208\pi A_{11}k_2}{315a^3}+\frac{64\pi A_{66}k_2}{945ab^2}\\&-\frac{\pi A_{22}k_5}{225b^3}-\frac{64\pi A_{12}k_5}{25a^2b}+\frac{64\pi A_{66}k_5}{225a^2b},\end{aligned}$$

$$f_1=-\frac{16q}{3\pi^2},\qquad b_2=-\frac{9\pi^2q_x}{a^2},$$

$$b_3=-\frac{\pi^2q_y}{b^2},\qquad b_4=\frac{9\pi^2N_x^p}{a^2}+\frac{\pi^2N_y^p}{b^2},$$

$$\begin{aligned}b_5=&-\frac{192\pi A_{66}k_3}{143ab^2}+\frac{3264\pi A_{12}k_6}{175a^2b}-\frac{192\pi A_{66}k_6}{175a^2b}\\&+\frac{48\pi A_{22}k_6}{25a^3}+\frac{192\pi A_{21}k_3}{143ab^2}-\frac{64\pi A_{21}k_2}{945ab^2},\end{aligned}$$

$$\begin{aligned}b_7=&\frac{192\pi\left(-A_{66}k_2+A_{21}k_2\right)}{143ab^2}\\&+\frac{48\pi A_{22}k_5}{25b^3}-\frac{729\pi^4A_{11}}{32a^4}-\frac{9\pi^4A_{22}}{32b^4}\\&+\frac{9\pi^4\left(-4A_{66}-A_{21}-A_{12}\right)}{32a^2b^2}+\frac{3408\pi A_{11}k_2}{143a^3}\\&+\frac{\pi\left(3264A_{12}k_5-192A_{66}k^5\right)}{175a^2b},\end{aligned}$$

$$\begin{aligned}b_8=&\frac{64\pi\left(-A_{21}k_1+A_{66}k_1\right)}{945ab^2}\\&-\frac{112\pi A_{22}k_4}{225b^3}-\frac{9\pi^4A_{11}}{32a^4}+\frac{3\pi^4A_{22}}{32b^4}\\&+\frac{\pi^4\left(-A_{21}+4A_{66}+3A_{12}\right)}{32a^2b^2}\\&-\frac{208\pi A_{11}k_1}{315a^3}+\frac{64\pi\left(-9A_{12}k_4+A_{66}k_4\right)}{a^2b},\end{aligned}$$

$$f_2=-\frac{16q}{3\pi^2}.\tag{B.1}$$

Acknowledgments

The authors gratefully acknowledge the support of the National Natural Science Foundation of China (NNSFC) through Grant nos. 11172009, 10872010, 11290152, 10732020, and 11072008, the National Science Foundation for Distinguished Young Scholars of China (NSFDYSC) through Grant

no. 10425209, the Funding Project for Academic Human Resources Development in Institutions of Higher Learning under the Jurisdiction of Beijing Municipality (PHRIHLB), the Foundation of Beijing University of Technology through Grant no. X4001015201301 and the Ph.D. Programs Foundation of Beijing University of Technology (DPFBUT) through Grant no. 52001015200701.

References

[1] C. K. Lee, W. W. Chiang, and T. C. O'Sullivan, "Piezoelectric modal sensor/actuator pairs for critical active damping vibration control," *Journal of Acoustical Society of America*, vol. 90, pp. 374–384, 1991.

[2] H. S. Tzou and Y. Bao, "Modeling of thick anisotropic composite triclinic piezoelectric shell transducer laminates," *Smart Materials and Structures*, vol. 3, pp. 285–292, 1994.

[3] J. N. Reddy and J. A. Mitchell, "On refined nonlinear theories of laminated composite structures with piezoelectric laminae," *Sādhanā. Academy Proceedings in Engineering Sciences*, vol. 20, no. 2–4, pp. 721–747, 1995.

[4] N. W. Hagood IV and A. J. McFarland, "Modeling of a piezoelectric rotary ultrasonic motor," *IEEE Transactions on Ultrasonics, Ferroelectrics, and Frequency Control*, vol. 42, pp. 210–224, 1995.

[5] A. M. Sadri, J. R. Wright, and R. J. Wynne, "Modelling and optimal placement of piezoelectric actuators in isotropic plates using genetic algorithms," *Smart Materials and Structures*, vol. 8, pp. 490–498, 1999.

[6] S. S. Vel and R. C. Batra, "Cylindrical bending of laminated plates with distributed and segmented piezoelectric actuators/sensors," *AIAA Journal*, vol. 38, pp. 857–867, 2000.

[7] W. B. Yu and D. H. Hodges, "A simple thermopiezoelastic model for smart composite plates with accurate stress recovery," *Smart Materials and Structures*, vol. 13, pp. 926–938, 2004.

[8] X. L. Huang and H. S. Shen, "Nonlinear free and forced vibration of simply supported shear deformable laminated plates with piezoelectric actuators," *International Journal of Mechanical Sciences*, vol. 47, pp. 187–208, 2005.

[9] C. N. Della and D. W. Shu, "Vibration of delaminated composite laminates: a review," *Applied Mechanics Reviews*, vol. 60, pp. 1–20, 2007.

[10] W. Zhang, Z. G. Yao, and M. H. Yao, "Periodic and chaotic dynamics of composite laminated piezoelectric rectangular plate with one-to-two internal resonance," *Science in China E*, vol. 52, pp. 731–742, 2009.

[11] S. K. Sarangi and M. C. Ray, "Active damping of geometrically nonlinear vibrations of doubly curved laminated composite shells," *ComPosite Structures*, vol. 93, pp. 3216–3228, 2011.

[12] S. Wiggins, *Global Bifurcations and Chaos*, Springer, New York, NY, USA, 1988.

[13] G. Kovačič, "Hamiltonian dynamics of orbits homoclinic to a resonance band," *Physics Letters A*, vol. 167, no. 2, pp. 137–142, 1992.

[14] G. Kovačič, "Dissipative dynamics of orbits homoclinic to a resonance band," *Physics Letters A*, vol. 167, no. 2, pp. 143–150, 1992.

[15] K. Yagasaki, "Periodic and homoclinic motions in forced, coupled oscillators," *Nonlinear Dynamics*, vol. 20, no. 4, pp. 319–359, 1999.

[16] Z. C. Feng and K. M. Liew, "Global bifurcations in parametrically excited systems with zero-to-one internal resonance," *Nonlinear Dynamics*, vol. 21, no. 3, pp. 249–263, 2000.

[17] W. Zhang, Z. Liu, and P. Yu, "Global dynamics of a parametrically and externally excited thin plate," *Nonlinear Dynamics*, vol. 24, no. 3, pp. 245–268, 2001.

[18] W. Zhang, "Global and Chaotic dynamics for a parametrically excited thin plate," *Journal of Sound and Vibration*, vol. 239, pp. 1013–1036, 2001.

[19] M. H. Yeo and W. K. Lee, "Evidences of global bifurcations of imperfect circular plate," *Journal of Sound and Vibration*, vol. 293, pp. 138–155, 2006.

[20] A. F. Vakakis, "Relaxation oscillations, subharmonic orbits and chaos in the dynamics of a linear lattice with a local essentially nonlinear attachment," *Nonlinear Dynamics*, vol. 61, no. 3, pp. 443–463, 2010.

[21] G. Haller and S. Wiggins, "Orbits homoclinic to resonances: the Hamiltonian case," *Physica D*, vol. 66, no. 3-4, pp. 298–346, 1993.

[22] G. Haller, "Diffusion at intersecting resonances in Hamiltonian systems," *Physics Letters A*, vol. 200, no. 1, pp. 34–42, 1995.

[23] G. Haller, "Singular perturbation theory for homoclinic orbits in a class of near-integrable dissipative systems," *SIAM Journal on Mathematical Analysis*, vol. 26, no. 6, pp. 1611–1643, 1995.

[24] G. Haller and S. Wiggins, "Multi-pulse jumping orbits and homoclinic trees in a modal truncation of the damped-forced nonlinear Schrödinger equation," *Physica D*, vol. 85, no. 3, pp. 311–347, 1995.

[25] G. Haller and S. Wiggins, "N-pulse homoclinic orbits in perturbations of resonant Hamiltonian systems," *Archive for Rational Mechanics and Analysis*, vol. 130, no. 1, pp. 25–101, 1995.

[26] G. Haller and S. Wiggins, "Geometry and chaos near resonant equilibria of 3-DOF Hamiltonian systems," *Physica D*, vol. 90, no. 4, pp. 319–365, 1996.

[27] G. Haller, "Universal homoclinic bifurcations and chaos near double resonances," *Journal of Statistical Physics*, vol. 86, no. 5-6, pp. 1011–1051, 1997.

[28] G. Haller, "Multi-dimensional homoclinic jumping and the discretized NLS equation," *Communications in Mathematical Physics*, vol. 193, no. 1, pp. 1–46, 1998.

[29] G. Haller, "Homoclinic jumping in the perturbed nonlinear Schrödinger equation," *Communications on Pure and Applied Mathematics LII-*, vol. 52, no. 1, pp. 1–47, 1999.

[30] G. Haller, G. Menon, and V. M. Rothos, "Šilnikov manifolds in coupled nonlinear Schrödinger equations," *Physics Letters A*, vol. 263, no. 3, pp. 175–185, 1999.

[31] G. Haller, *Chaos Near Resonance*, Springer, New York, NY, USA, 1999.

[32] N. Malhotra, N. Sri Namachchivaya, and R. J. McDonald, "Multipulse orbits in the motion of flexible spinning discs," *Journal of Nonlinear Science*, vol. 12, no. 1, pp. 1–26, 2002.

[33] R. J. McDonald and N. Sri Namachchivaya, "Pipes conveying pulsating fluid near a 0:1 resonance: global bifurcations," *Journal of Fluids and Structures*, vol. 21, pp. 665–687, 2005.

[34] M. H. Yao and W. Zhang, "Shilnikov-type multipulse orbits and chaotic dynamics of a parametrically and externally excited rectangular thin plate," *International Journal of Bifurcation and Chaos*, vol. 17, no. 3, pp. 851–875, 2007.

[35] M. H. Yao, W. Zhang, and Z. G. Yao, "Multi-pulse orbits dynamics of composite laminated piezoelectric rectangular plate," *Science in China E*, vol. 54, pp. 2064–2079, 2011.

[36] W. Q. Yu and F. Q. Chen, "Global bifurcations and chaos in externally excited cyclic systems," *Communications in Nonlinear Science and Numerical Simulation*, vol. 15, no. 12, pp. 4007–4019, 2010.

[37] W. Q. Yu and F. Q. Chen, "Orbits homoclinic to resonances in a harmonically excited and undamped circular plate," *Meccanica*, vol. 45, no. 4, pp. 567–575, 2010.

[38] W. Zhang, M. J. Gao, M. H. Yao, and Z. G. Yao, "Higher-dimensional chaotic dynamics of a composite laminated piezoelectric rectangular plate," *Science in China G*, vol. 52, pp. 1989–2000, 2009.

[39] G. Kovačič and T. A. Wettergren, "Homoclinic orbits in the dynamics of resonantly driven coupled pendula," *Zeitschrift für Angewandte Mathematik und Physik*, vol. 47, no. 2, pp. 221–264, 1996.

[40] T. J. Kaper and G. Kovačič, "Multi-bump orbits homoclinic to resonance bands," *Transactions of the American Mathematical Society*, vol. 348, no. 10, pp. 3835–3887, 1996.

[41] R. Camassa, G. Kovačič, and S.-K. Tin, "A Melnikov method for homoclinic orbits with many pulses," *Archive for Rational Mechanics and Analysis*, vol. 143, no. 2, pp. 105–193, 1998.

[42] W. Zhang and M. H. Yao, "Theories of multi-pulse global bifurcations for high-dimensional systems and application to cantilever beam," *International Journal of Modern Physics B*, vol. 22, no. 24, pp. 4089–4141, 2008.

[43] W. Zhang, M. H. Yao, and J. H. Zhang, "Using the extended Melnikov method to study the multi-pulse global bifurcations and chaos of a cantilever beam," *Journal of Sound and Vibration*, vol. 319, pp. 541–569, 2009.

[44] M. H. Yao, W. Zhang, and J. W. Zu, "Multi-pulse chaotic dynamics in non-planar motion of parametrically excited viscoelastic moving belt," *Journal of Sound and Vibration*, vol. 331, pp. 2624–2653, 2012.

[45] J. N. Reddy, *Mechanics of Laminated Composite Plates and Shells*, New York, NY, USA, 2004.

[46] A. Nosir and J. N. Reddy, "A study of non-linear dynamic equations of higher-order deformation plate theories," *International Journal of Non-Linear Mechanics*, vol. 26, pp. 233–249, 1991.

[47] A. Bhimaraddi, "Large-amplitude vibrations of imperfect antisymmetric angle-ply laminated plates," *Journal of Sound and Vibration*, vol. 162, pp. 457–470, 1993.

[48] A. H. Nayfeh and D. T. Mook, *Nonlinear Oscillations*, Wiley-Interscience, New York, NY, USA, 1979.

[49] W. Zhang, F. X. Wang, and J. W. Zu, "Computation of normal forms for high dimensional nonlinear systems and application to nonplanar motions of a cantilever beam," *Journal of Sound and Vibration*, vol. 278, pp. 949–974, 2004.

[50] P. Yu, W. Zhang, and Q. S. Bi, "Vibration analysis on a thin plate with the aid of computation of normal forms," *International Journal of Non-Linear Mechanics*, vol. 36, pp. 597–627, 2001.

Hindawi Publishing Corporation
Discrete Dynamics in Nature and Society
Volume 2013, Article ID 841764, 8 pages
http://dx.doi.org/10.1155/2013/841764

Research Article

Modeling a Tumor Growth with Piecewise Constant Arguments

F. Bozkurt

Department of Mathematics, Faculty of Education, Erciyes University, 38039 Kayseri, Turkey

Correspondence should be addressed to F. Bozkurt; fbozkurt@erciyes.edu.tr

Received 22 February 2013; Accepted 18 April 2013

Academic Editor: Qingdu Li

This study is based on an early brain tumor growth that is modeled as a hybrid system such as (A): $dx(t)/dt = x(t)\{r(1 - \alpha x(t) - \beta_0 x(\llbracket t \rrbracket) - \beta_1 x(\llbracket t-1 \rrbracket)) + \gamma_1 x(\llbracket t \rrbracket) + \gamma_2 x(\llbracket t-1 \rrbracket)\}$, where the parameters α, β_0, β_1, and r denote positive numbers, γ_1 and γ_2 are negative numbers and $\llbracket t \rrbracket$ is the integer part of $t \in [0, \infty)$. Equation (A) explains a brain tumor growth, where γ_1 is embedded to show the drug effect on the tumor and γ_2 is a rate that causes a negative effect by the immune system on the tumor population. Using (A), we have constructed two models of a tumor growth: one is (A) and the other one is a population model at low density by incorporating an Allee function to (A) at time t. To consider the global behavior of (A), we investigate the discrete solutions of (A). Examination of the characterization of the stability shows that increase of the population growth rate decreases the local stability of the positive equilibrium point of (A). The simulations give a detailed description of the behavior of solutions of (A) with and without Allee effect.

1. Introduction

Cancer biology has been revolutionized over the past several decades. Genetic alterations that lead to malignant phenotypes have been identified [1, 2], and mechanisms necessary to sustain a solid tumor [3] and that contribute to tumor-cell invasion [4, 5]. Mathematical modeling of both tumor growth and angiogenesis has been active areas of research. Such models can be classified into one of two categories: those that analyze the remodeling of the vasculature while ignoring changes in the tumor mass and those that predict tumor expansion in the presence of a nonevolving vasculature.

The works in [6, 7] are very important, since they developed a two-dimensional hybrid cellular automaton model of brain tumor growth. Showing a simple model for a single species, the well-known model is constructed by May [8] and May and Oster [9] such as

$$\frac{dx(t)}{dt} = rx(t)\left\{1 - \frac{x(\llbracket t \rrbracket)}{K}\right\}, \tag{1}$$

who obtained that the asymptotic behavior of difference solutions can be complex and "chaotic" for certain parameter values of r. In recent years, several studies have been conducted to investigate the difference solutions of specific logistic differential equations with respect to the parameters [10–19]. When $\gamma_1 = \gamma_2 = 0$ in (A), [13] considered the logistic equation

$$\frac{dx(t)}{dt} = rx(t)\left(1 - \alpha x(t) - \beta_0 x(\llbracket t \rrbracket) - \beta_1 x(\llbracket t-1 \rrbracket)\right), \tag{2}$$

where $t \geq 0$, the parameters α, β_0, β_1, and r denote positive numbers, and $\llbracket t \rrbracket$ denotes the integer part of $t \in [0, \infty)$. Here, the local asymptotic stability of the positive equilibrium point of (2) was proven by using the Linearized Stability Theorem and the global asymptotic stability by using a suitable Lyapunov function.

An investigation of (A) can be shown in [14], where it was obtained that under the condition $3\beta_1 > \alpha + \beta_0 > 2\alpha + \beta_1$ and $\gamma_2 > \gamma_1$ the positive equilibrium point of (A) is locally asymptotically stable if and only if $(\gamma_2 + \gamma_1)/(\alpha + \beta_0 + \beta_1) < r < (\gamma_2/\beta_1)$. Furthermore, under specific conditions the global asymptotic stability, the semicycle, and oscillation results of the solutions of (A) were also studied.

An important research for population models was conducted in 1931, where Allee [20] demonstrated that "Allee effect" occurs when population growth rate is reduced at low population size. The logistic model assumes that per-capita growth rate declines monotonically when the density

increases; it is shown, however, that for population subject to an Allee effect, per-capita growth rate gives a humped curve increasing at low density, up to a maximum intermediate density and then declines again. Many theoretical and laboratory studies have demonstrated the importance of the Allee effect in dynamics of small populations; see, for example, [21–28]. From this reasoning, biological facts lead us to assume the Allee function as follows:

(a) if $N = 0$, then $a(N) = 0$; that is, there is no reproduction without partners,

(b) $a'(N) > 0$ for $N \in (0, \infty)$; that is, Allee effect decreases as density increases,

(c) $\lim_{N\to\infty} a(N) = 1$; that is, Allee effect vanishes at high density [29].

In this paper, a single species population (here especially about an early brain tumor growth) is modeled such as

$$\frac{dx(t)}{dt} = x(t)\{r(1 - \alpha x(t) - \beta_0 x([\![t]\!]) - \beta_1 x([\![t-1]\!])) + \gamma_1 x([\![t]\!]) + \gamma_2 x([\![t-1]\!])\}, \tag{3}$$

where $t \geq 0$, the parameters α, β_0, β_1, and r denote positive numbers, γ_1, γ_2 negative numbers, and $[\![t]\!]$ denotes the integer part of $t \in [0, \infty)$. The parameter r is the population growth rate of this tumor and α, β_0, and β_1 are rates for the delayed tumor volume and basis of a logistic population model. γ_1 is embedded to show the drug effect on the tumor and γ_2 is a rate that causes a negative effect by the immune system on the tumor population. In Section 2 we investigate the local and global behaviors of the nonlinear difference solutions of (3) basin under specific conditions. Additionally, a characterization of the stability when the population growth rate increases was also investigated. Section 3 gives results of the local and global asymptotic behaviors of the nonlinear difference solutions of (3) with Allee effect. The discrepancy of the stability behavior with and without Allee effect of (3) will give interesting results, which is discussed in Section 4.

2. Local and Global Asymptotic Stability Analysis

An integration of (A) on an interval of the form $t \in [n, n+1)$ leads to

$$x(t) = x(n) \cdot e^{\int_n^t (r+(\gamma_1-\beta_0 r)x(n)+(\gamma_2-\beta_1 r)x(n-1)-\alpha r x(s))ds}. \tag{4}$$

In (4) if $x(n) > 0$, then $x(t) > 0$. Let $t \to n+1$; it is clear that $x(n+1) > 0$. This implies that we have positive solutions of (A) for positive initial conditions.

In addition, on an interval of the form $t \in [n, n+1)$ one can write (A) as

$$\frac{dx(t)}{dt} - \{r + (\gamma_1 - \beta_0 r)x(n) + (\gamma_2 - \beta_1 r)x(n-1)\}x(t) = -\alpha r x^2(t). \tag{5}$$

It is well known that (5) is a Bernoulli differential equation, and so for $t \to n+1$ its solutions are

$$x(n+1) = x(n) \cdot e^{\{r+(\gamma_1-\beta_0 r)x(n)+(\gamma_2-\beta_1 r)x(n-1)\}} \times \left(1 + \alpha r x(n)\left\{\frac{e^{\{r+(\gamma_1-\beta_0 r)x(n)+(\gamma_2-\beta_1 r)x(n-1)\}} - 1}{r + (\gamma_1 - \beta_0 r)x(n) + (\gamma_2 - \beta_1 r)x(n-1)}\right\}\right)^{-1}, \quad n = 0, 1, 2, \ldots, \tag{6}$$

where $r + (\gamma_1 - \beta_0 r)x(n) + (\gamma_2 - \beta_1 r)x(n-1) \neq 0$. The solution of (6) does not give any information about the global behavior of the differential equation. Hence, we can continue to investigate more about (6), since (6) is the difference equation of second order. Let $\gamma_1 = -\delta_1$ and $\gamma_2 = -\delta_2$, where δ_1 and δ_2 are positive numbers. It is important to take into account that the drug therapy γ_1 has more destroying effect on the tumor than the immune system. That is why $\delta_1 > \delta_2$. Considering (6) again, we obtain, for $n = 0, 1, 2, \ldots$,

$$\begin{aligned} x(n+1) &= x(n)(r - (\delta_1 + \beta_0 r)x(n) - (\delta_2 + \beta_1 r)x(n-1)) \\ &\quad \times ((r - (\delta_1 + \beta_0 r + \alpha r)x(n) - (\delta_2 + \beta_1 r)x(n-1)) \\ &\qquad \times \exp(-\{r - (\delta_1 + \beta_0 r)x(n) - (\delta_2 + \beta_1 r)x(n-1)\}) \\ &\qquad + \alpha r x(n))^{-1}, \end{aligned} \tag{7}$$

where hereafter

$$r - (\delta_1 + \beta_0 r)x(n) - (\delta_2 + \beta_1 r)x(n-1) \neq 0. \tag{8}$$

Computations reveal that the equilibrium points of (7) are

$$\overline{x}_1 = 0, \qquad \overline{x}_2 = \frac{r}{(\alpha + \beta_0 + \beta_1)r + \delta_1 + \delta_2}. \tag{9}$$

The fundamental study contains the stability analysis of the positive equilibrium point $\overline{x}_2$. For this reason we show only the characteristic equation of (7) by linearizing (7) about $\overline{x}_2$. Computation gives a quadratic equation such as

$$\mu^2 - \left\{\frac{-(\delta_1 + \beta_0 r) + ((\alpha + \beta_0)r + \delta_1) \cdot e^{-A}}{\alpha r}\right\} \times \mu - \left\{\frac{-(\delta_2 + \beta_1 r)(1 - e^{-A})}{\alpha r}\right\} = 0, \tag{10}$$

where $A = \alpha r^2/((\alpha + \beta_0 + \beta_1)r + \delta_1 + \delta_2)$.

Theorem 1. *Let $\beta_0 > \beta_1 + \alpha$ and $\beta_1 > \alpha$. The positive equilibrium point of (7) is locally asymptotically stable if and only if*

$$A < \ln\left(\frac{(\beta_0 - \beta_1 + \alpha)r + \delta_1 - \delta_2}{(\beta_0 - \beta_1 - \alpha)r + \delta_1 - \delta_2}\right). \tag{11}$$

Proof. By the Linearized Stability Theorem [30] we get that the positive equilibrium point of (7) is locally asymptotically stable if and only if

$$\left|\frac{-(\delta_1+\beta_0 r)+((\alpha+\beta_0)r+\delta_1)\cdot e^{-A}}{\alpha r}\right| < 1+\frac{(\delta_2+\beta_1 r)\left(1-e^{-A}\right)}{\alpha r} < 2 \tag{12}$$

holds. We can write (12) such as

(a) $|(-(\delta_1+\beta_0 r)+((\alpha+\beta_0)r+\delta_1)\cdot e^{-A})/\alpha r| < 1+(\delta_2+\beta_1 r)(1-e^{-A})/\alpha r$,

(b) $1+(\delta_2+\beta_1 r)(1-e^{-A})/\alpha r < 2$.

Since $\beta_1 > \alpha$, from (b) we have

$$A < \ln\left(\frac{\delta_2+\beta_1 r}{\delta_2+(\beta_1-\alpha)r}\right). \tag{13}$$

From (a) we get

$$A < \ln\left(\frac{(\beta_0-\beta_1+\alpha)r+\delta_1-\delta_2}{(\beta_0-\beta_1-\alpha)r+\delta_1-\delta_2}\right), \tag{14}$$

where $\beta_0 > \beta_1+\alpha$. Considering both (13) and (14), we will have

$$A < \ln\left(\frac{(\beta_0-\beta_1+\alpha)r+\delta_1-\delta_2}{(\beta_0-\beta_1-\alpha)r+\delta_1-\delta_2}\right) < \ln\left(\frac{\delta_2+\beta_1 r}{\delta_2+(\beta_1-\alpha)r}\right), \tag{15}$$

since $(\beta_0+\alpha-\beta_1)r+\delta_1-\delta_2 > 0$. This completes our proof. □

Theorem 2. *Suppose that* $r-(\delta_1+\beta_0 r+\alpha r)x(n)-(\delta_2+\beta_1 r)x(n-1) > 0$ *for* $n = 0,1,2,\ldots$ *and assume that the conditions in Theorem 1 hold.*

If

$$r-(\delta_1+\beta_0 r)x(n)-(\delta_2+\beta_1 r)x(n-1) < \ln\left(\frac{2\overline{x}_2-x(n)}{x(n)}\right), \quad x(n) < \frac{2r}{(\alpha+\beta_0+\beta_1)r-\gamma_1-\gamma_2}, \tag{16}$$

then the positive equilibrium point of (7) *is globally asymptotically stable.*

Proof. We consider a Lyapunov function $V(n)$ defined by

$$V(n) = \{x(n)-\overline{x}_2\}^2, \quad n = 0,1,2,\ldots. \tag{17}$$

The change along the solutions of (17) is

$$\Delta V(n) = V(n+1)-V(n) = \{x(n+1)-x(n)\}\{x(n+1)+x(n)-2\overline{x}_2\}. \tag{18}$$

Considering (18), we get

$$x(n+1)-x(n) = \frac{U_1}{V}, \tag{19}$$

where

$$\begin{aligned} U_1 &= \left(1-\exp\left(-\{r-(\delta_1+\beta_0 r)x(n)-(\delta_2+\beta_1 r)x(n-1)\}\right)\right) \\ &\quad \times x(n)\cdot\left(r-(\delta_1+\beta_0 r+\alpha r)x(n)-(\delta_2+\beta_1 r)x(n-1)\right), \\ V &= \exp\left(-\{r-(\delta_1+\beta_0 r)x(n)-(\delta_2+\beta_1 r)x(n-1)\}\right) \\ &\quad \cdot\left(r-(\delta_1+\beta_0 r+\alpha r)x(n)-(\delta_2+\beta_1 r)x(n-1)\right) \\ &\quad +\alpha r x(n). \end{aligned} \tag{20}$$

Furthermore, from (18) we will have

$$x(n+1)+x(n)-2\overline{x}_2 = \frac{U_2}{V}, \tag{21}$$

where

$$\begin{aligned} U_2 &= \alpha r x(n)\left(x(n)-2\overline{x}_2\right) \\ &\quad \times\left(1-\exp\left(-\{r-(\delta_1+\beta_0 r)x(n)-(\delta_2+\beta_1 r)x(n-1)\}\right)\right) \\ &\quad +\left(r-(\delta_1+\beta_0 r)x(n)-(\delta_2+\beta_1 r)x(n-1)\right) \\ &\quad \cdot\left(\exp\left(-\{r-(\delta_1+\beta_0 r)x(n)-(\delta_2+\beta_1 r)x(n-1)\}\right)\right. \\ &\quad \cdot x(n)+x(n)-2\overline{x}_2 \\ &\quad \left.\cdot\exp\left(-\{r-(\delta_1+\beta_0 r)x(n)-(\delta_2+\beta_1 r)x(n-1)\}\right)\right). \end{aligned} \tag{22}$$

Since $0 < r-(\delta_1+\beta_0 r-\alpha r)x(n)-(\delta_2+\beta_1 r)x(n-1)$, if

$$x(n) < \overline{x}_2, \quad r-(\delta_1+\beta_0 r)x(n)-(\delta_2+\beta_1 r)x(n-1) < \ln\left(\frac{2\overline{x}_2-x(n)}{x(n)}\right), \tag{23}$$

then

$$x(n+1)-x(n) > 0, \qquad x(n+1)+x(n)-2\overline{x}_2 < 0. \tag{24}$$

This implies that $\Delta V(n) < 0$, which gives the condition for the global asymptotic stability of the positive equilibrium point of (7). □

Theorem 3. *Let* r_1 *and* r_2 *be population growth rates of* (7) *such that* $r_1 < r_2$ *and suppose that* $\overline{x}^*$ *and* $\overline{x}^{**}$ *are positive equilibrium points of* (7) *with respect to* r_1 *and* r_2 *that hold*

the conditions in Theorem 1, respectively. Furthermore, assume that

$$\ln\left(\frac{r_2}{r_1}\right) < A_2 - A_1, \tag{25}$$

where $A_1 = \alpha r_1^2/((\alpha+\beta_0+\beta_1)r_1+\delta_1+\delta_2)$ *and* $A_2 = \alpha r_2^2/((\alpha+\beta_0+\beta_1)r_2+\delta_1+\delta_2)$. *If*

$$\begin{aligned} A_1 &> \ln\left(\frac{(\alpha+\beta_0+\beta_1)r_1+\delta_1+\delta_2}{(\beta_0+\beta_1)r_1+\delta_2+\delta_1}\right), \\ A_2 &< \ln\left(\frac{(\alpha+\beta_0+\beta_1)r_2+\delta_1+\delta_2}{(\beta_0+\beta_1)r_2+\delta_2+\delta_1}\right), \end{aligned} \tag{26}$$

then the local stability of $\overline{x}^{**}$ *is weaker than* $\overline{x}^{*}$. *That is, increase of the population growth rate decreases the local stability of the positive equilibrium point in* (7).

Proof. Let us write from (7)

$$\begin{aligned} &x(n+1) \\ &= x(n)\left(r_1 - (\delta_1+\beta_0 r_1)x(n) - (\delta_2+\beta_1 r_1)x(n-1)\right) \\ &\quad\times\left(\left(r_1 - (\delta_1+\beta_0 r_1+\alpha r_1)x(n) - (\delta_2+\beta_1 r_1)x(n-1)\right)\right. \\ &\qquad\times\exp\left(-\left\{r_1 - (\delta_1+\beta_0 r_1)x(n) - (\delta_2+\beta_1 r_1)x(n-1)\right\}\right) \\ &\qquad\left.+\alpha r_1 x(n)\right)^{-1}, \\ &x(n+1) \\ &= x(n)\left(r_2 - (\delta_1+\beta_0 r_2)x(n) - (\delta_2+\beta_1 r_2)x(n-1)\right) \\ &\quad\times\left(\left(r_2 - (\delta_1+\beta_0 r_2+\alpha r_2)x(n) - (\delta_2+\beta_1 r_2)x(n-1)\right)\right. \\ &\qquad\times\exp\left(-\left\{r_2 - (\delta_1+\beta_0 r_2)x(n) - (\delta_2+\beta_1 r_2)x(n-1)\right\}\right) \\ &\qquad\left.+\alpha r_2 x(n)\right)^{-1}, \end{aligned} \tag{27}$$

where $r_1 < r_2$. In this case, the positive equilibrium points of (27) are

$$\begin{aligned} \overline{x}^{*} &= \frac{r_1}{(\alpha+\beta_0+\beta_1)r_1+\delta_1+\delta_2}, \\ \overline{x}^{**} &= \frac{r_2}{(\alpha+\beta_0+\beta_1)r_2+\delta_1+\delta_2}, \end{aligned} \tag{28}$$

respectively. The characteristic equations of (27) are

$$\begin{aligned} &\mu^2 - \left\{\frac{-(\delta_1+\beta_0 r_1)+((\alpha+\beta_0)r_1+\delta_1)\cdot e^{-A_1}}{\alpha r_1}\right\} \\ &\quad\times\mu - \left\{\frac{-(\delta_2+\beta_1 r_1)\left(1-e^{-A_1}\right)}{\alpha r_1}\right\} = 0, \end{aligned} \tag{29}$$

where $A_1 = \alpha {r_1}^2/((\alpha+\beta_0+\beta_1)r_1+\delta_1+\delta_2)$ and

$$\begin{aligned} &\mu^2 - \left\{\frac{-(\delta_1+\beta_0 r_2)+((\alpha+\beta_0)r_2+\delta_1)\cdot e^{-A_2}}{\alpha r_2}\right\} \\ &\quad\times\mu - \left\{\frac{-(\delta_2+\beta_1 r_2)\left(1-e^{-A_2}\right)}{\alpha r_2}\right\} = 0, \end{aligned} \tag{30}$$

where $A_2 = \alpha r_2^2/((\alpha+\beta_0+\beta_1)r_2+\delta_1+\delta_2)$, respectively. Since $r_1 < r_2$, we can write

$$\frac{1}{\alpha r_2} < \frac{1}{\alpha r_1}, \tag{31}$$

$$\delta_2 + \beta_1 r_1 < \delta_2 + \beta_1 r_2. \tag{32}$$

The inequality (32) can be also written as

$$-(\delta_2+\beta_1 r_2) < -(\delta_2+\beta_1 r_1). \tag{33}$$

Since the inequality

$$(\alpha+\beta_0+\beta_1)r_1 r_2 (r_2-r_1) + (\delta_1+\delta_2)(r_2-r_1)(r_2+r_1) > 0 \tag{34}$$

always holds, we get

$$\frac{\alpha r_2^2}{(\alpha+\beta_0+\beta_1)r_2+\delta_1+\delta_2} > \frac{\alpha r_1^2}{(\alpha+\beta_0+\beta_1)r_1+\delta_1+\delta_2}. \tag{35}$$

The inequality (35) can be also written as

$$\frac{-\alpha r_2^2}{(\alpha+\beta_0+\beta_1)r_2+\delta_1+\delta_2} < \frac{-\alpha r_1^2}{(\alpha+\beta_0+\beta_1)r_1+\delta_1+\delta_2} \tag{36}$$

or

$$-A_2 < -A_1. \tag{37}$$

It is obvious that from (37), we get

$$\delta_2 e^{-A_2} < \delta_2 e^{-A_1}. \tag{38}$$

Furthermore, if

$$\ln\left(\frac{r_2}{r_1}\right) < A_2 - A_1, \tag{39}$$

then the inequality

$$\beta_1 r_2 e^{-A_2} < \beta_1 r_1 e^{-A_1} \tag{40}$$

holds. In view of (39), considering (31), (33), (38), and (40) together, we obtain

$$-1 < \frac{-(\delta_2+\beta_1 r_2)\left(1-e^{-A_2}\right)}{\alpha r_2} < \frac{-(\delta_2+\beta_1 r_1)\left(1-e^{-A_1}\right)}{\alpha r_1}. \tag{41}$$

From the Linearized Stability Theorem we want to obtain the conditions that satisfy the inequality

$$\begin{aligned} -1 &< \frac{-(\delta_1+\beta_0 r_2)+((\alpha+\beta_0)r_2+\delta_1)\cdot e^{-A_2}}{\alpha r_2} \\ &\quad - \frac{-(\delta_2+\beta_1 r_2)\left(1-e^{-A_2}\right)}{\alpha r_2} \\ &< \frac{-(\delta_1+\beta_0 r_1)+((\alpha+\beta_0)r_1+\delta_1)\cdot e^{-A_1}}{\alpha r_1} \\ &\quad - \frac{-(\delta_2+\beta_1 r_1)\left(1-e^{-A_1}\right)}{\alpha r_1}. \end{aligned} \tag{42}$$

Simplifications of (42) give us the inequality

$$\frac{((\beta_1-\beta_0)r_2+\delta_2-\delta_1)+((\alpha+\beta_0-\beta_1)r_2+\delta_1-\delta_2)\cdot e^{-A_2}}{\alpha r_2} < \frac{((\beta_1-\beta_0)r_1+\delta_2-\delta_1)+((\alpha+\beta_0-\beta_1)r_1+\delta_1-\delta_2)\cdot e^{-A_1}}{\alpha r_1}. \tag{43}$$

Since $\beta_0 > \alpha+\beta_1$ and $\delta_1 > \delta_2$, we get

$$((\alpha+\beta_0-\beta_1)r_2+\delta_1-\delta_2)\cdot e^{-A_2} < ((\alpha+\beta_0-\beta_1)r_1+\delta_1-\delta_2)\cdot e^{-A_1}, \tag{44}$$

$$(\beta_1-\beta_0)r_2+\delta_2-\delta_1 < (\beta_1-\beta_0)r_1+\delta_2-\delta_1. \tag{45}$$

Considering both (44) and (45), we get (42).

Furthermore, from the Linearized Stability Theorem we must also show that the inequality

$$\frac{-(\delta_1+\beta_0 r_1)+((\alpha+\beta_0)r_1+\delta_1)\cdot e^{-A_1}}{\alpha r_1} - \frac{(\delta_2+\beta_1 r_1)\left(1-e^{-A_1}\right)}{\alpha r_1} < \frac{-(\delta_1+\beta_0 r_2)+((\alpha+\beta_0)r_2+\delta_1)\cdot e^{-A_2}}{\alpha r_2} - \frac{(\delta_2+\beta_1 r_2)\left(1-e^{-A_2}\right)}{\alpha r_2} < 1 \tag{46}$$

holds. Simplifying (46), we can write

$$-((\beta_0+\beta_1)r_1+\delta_2+\delta_1) + ((\alpha+\beta_0+\beta_1)r_1+\delta_1+\delta_2)\cdot e^{-A_1}(\alpha r_1)^{-1} < -((\beta_0+\beta_1)r_2+\delta_2+\delta_1) + ((\alpha+\beta_0+\beta_1)r_2+\delta_1+\delta_2)\cdot e^{-A_2}(\alpha r_2)^{-1}. \tag{47}$$

If

$$A_1 > \ln\left(\frac{(\alpha+\beta_0+\beta_1)r_1+\delta_1+\delta_2}{(\beta_0+\beta_1)r_1+\delta_2+\delta_1}\right), \quad A_2 < \ln\left(\frac{(\alpha+\beta_0+\beta_1)r_2+\delta_1+\delta_2}{(\beta_0+\beta_1)r_2+\delta_2+\delta_1}\right), \tag{48}$$

then

$$-((\beta_0+\beta_1)r_1+\delta_2+\delta_1) + ((\alpha+\beta_0+\beta_1)r_1+\delta_1+\delta_2)\cdot e^{-A_1} < 0, \quad -((\beta_0+\beta_1)r_2+\delta_2+\delta_1) + ((\alpha+\beta_0+\beta_1)r_2+\delta_1+\delta_2)\cdot e^{-A_2} > 0. \tag{49}$$

The inequalities (49) imply that (46) holds. This result explains that increase of the population growth rate decreases the local stability of the positive equilibrium point in (7), which completes our proof. □

Theorem 4. *Let $\{x(n)\}_{n=0}^{\infty}$ be a positive solution of* (7). *Assume that for $n = 0, 1, \ldots$ the condition*

$$0 < r - (\delta_1+\beta_0 r+\alpha r x(n))\,x(n) - (\delta_2+\beta_1 r)\,x(n-1) \tag{50}$$

holds. Then all positive solutions of (7) *are in the interval*

$$x(n) \in \left(0, \frac{1}{\alpha}\right). \tag{51}$$

Proof. Let (50) hold. Then we can write

$$r - (\delta_1+\beta_0 r)\,x(n) - (\delta_2+\beta_1 r)\,x(n-1) < r. \tag{52}$$

From (52), we will have

$$e^{-(r-(\delta_1+\beta_0 r)x(n)-(\delta_2+\beta_1 r)x(n-1))} > e^{-r}. \tag{53}$$

Considering (52) and (53) together, we get

$$\begin{aligned} x(n+1) &= x(n)\left(r-(\delta_1+\beta_0 r)\,x(n)-(\delta_2+\beta_1 r)\,x(n-1)\right) \\ &\quad\times\left((r-(\delta_1+\beta_0 r+\alpha r)\,x(n)-(\delta_2+\beta_1 r)\,x(n-1)\right) \\ &\qquad\times\exp\left(-\{r-(\delta_1+\beta_0 r)\,x(n)-(\delta_2+\beta_1 r)\,x(n-1)\}\right) \\ &\qquad+\alpha r x(n)\Big)^{-1} \\ &< x(n)\,r \\ &\quad\times\left((r-(\delta_1+\beta_0 r+\alpha r)\,x(n)-(\delta_2+\beta_1 r)\,x(n-1)\right) \\ &\qquad\times\exp(-r)+\alpha r x(n)\Big)^{-1}. \end{aligned} \tag{54}$$

Furthermore, since we have

$$0 < \alpha r x(n) < r - (\delta_1+\beta_0 r)\,x(n) - (\delta_2+\beta_1 r)\,x(n-1) < r, \tag{55}$$

we obtain

$$x(n+1) < \frac{x(n)\,r}{-\alpha r x(n)\exp(-r)+\alpha r x(n)\exp(-r)+\alpha r x(n)} = \frac{1}{\alpha}. \tag{56}$$

This completes the proof. □

3. Local and Global Asymptotic Stability Analysis with Allee Effect

In this section we use an Allee function of time t. Let (3) be written as

$$\frac{1}{x}\frac{dx}{dt} = r - (\delta_1+\delta_2+(\alpha+\beta_0+\beta_1)r)\,x, \tag{57}$$

where $\gamma_1 = -\delta_1$ and $\gamma_2 = -\delta_2$. Applying to (57) an Allee function

$$a(x) = \frac{x}{E+x}, \tag{58}$$

where E is an Allee constant, we get

$$\frac{1}{x}\frac{dx}{dt} = a(x)\left\{r - \left(\delta_1 + \delta_2 + \left(\alpha + \beta_0 + \beta_1\right)r\right)x\right\}. \tag{59}$$

By defining

$$g(x) = a(x)\left\{r - \left(\delta_1 + \delta_2 + \left(\alpha + \beta_0 + \beta_1\right)r\right)x\right\} \tag{60}$$

and taking the derivative of g with respect to x, we obtain

$$\begin{aligned} g'(x) = & -\left(\delta_1 + \delta_2 + \left(\alpha + \beta_0 + \beta_1\right)r\right)x^2 \\ & - 2E\left(\delta_1 + \delta_2 + \left(\alpha + \beta_0 + \beta_1\right)r\right)x \\ & + Er(E+x)^{-2}. \end{aligned} \tag{61}$$

By showing the sign of (61), we get that g is an increasing function for

$$\begin{aligned} x \in \Big(0, \Big(& E^2\left(\delta_1 + \delta_2 + \left(\alpha + \beta_0 + \beta_1\right)r\right)^2 \\ & + Er\left(\left(\alpha + \beta_0 + \beta_1\right)r + \delta_1 + \delta_2\right)\Big)^{-1/2} \\ & - E\left(\left(\alpha + \beta_0 + \beta_1\right)r + \delta_1 + \delta_2\right) \\ & \times \left(\left(\alpha + \beta_0 + \beta_1\right)r + \delta_1 + \delta_2\right)^{-1}\Big) \end{aligned} \tag{62}$$

and g is a decreasing function for

$$\begin{aligned} x \in \Big(\Big(& E^2\left(\delta_1 + \delta_2 + \left(\alpha + \beta_0 + \beta_1\right)r\right)^2 \\ & + Er\left(\left(\alpha + \beta_0 + \beta_1\right)r + \delta_1 + \delta_2\right)\Big)^{-1/2} \\ & - E\left(\left(\alpha + \beta_0 + \beta_1\right)r + \delta_1 + \delta_2\right) \\ & \times \left(\left(\alpha + \beta_0 + \beta_1\right)r + \delta_1 + \delta_2\right)^{-1}, \infty\Big). \end{aligned} \tag{63}$$

This also means that if the density is

$$\begin{aligned} x < \Big(& E^2\left(\delta_1 + \delta_2 + \left(\alpha + \beta_0 + \beta_1\right)r\right)^2 \\ & + Er\left(\left(\alpha + \beta_0 + \beta_1\right)r + \delta_1 + \delta_2\right)\Big)^{-1/2} \\ & - E\left(\left(\alpha + \beta_0 + \beta_1\right)r + \delta_1 + \delta_2\right) \\ & \times \left(\left(\alpha + \beta_0 + \beta_1\right)r + \delta_1 + \delta_2\right)^{-1}, \end{aligned} \tag{64}$$

then a population model without an Allee function will not give realistic results. But if

$$\begin{aligned} x > \Big(& E^2\left(\delta_1 + \delta_2 + \left(\alpha + \beta_0 + \beta_1\right)r\right)^2 \\ & + Er\left(\left(\alpha + \beta_0 + \beta_1\right)r + \delta_1 + \delta_2\right)\Big)^{-1/2} \\ & - E\left(\left(\alpha + \beta_0 + \beta_1\right)r + \delta_1 + \delta_2\right) \\ & \times \left(\left(\alpha + \beta_0 + \beta_1\right)r + \delta_1 + \delta_2\right)^{-1}, \end{aligned} \tag{65}$$

then it is not important to use a model with an Allee function as it is also explained in the introduction. Applying to (3) an Allee function such as

$$a\left(x\left(\left[\left[t\right]\right]\right)\right) = \frac{x\left(\left[\left[t\right]\right]\right)}{E + x\left(\left[\left[t\right]\right]\right)}, \tag{66}$$

where $E > 0$, we obtain

$$\begin{aligned} & \frac{dx(t)}{dt} \\ & = x(t)\left\{r\left(1 - \alpha x(t) - \beta_0 x\left(\left[\left[t\right]\right]\right) - \beta_1 x\left(\left[\left[t-1\right]\right]\right)\right)\right. \\ & \qquad \left. - \delta_1 x\left(\left[\left[t\right]\right]\right) - \delta_2 x\left(\left[\left[t-1\right]\right]\right)\right\} \frac{x\left(\left[\left[t\right]\right]\right)}{E + x\left(\left[\left[t\right]\right]\right)}. \end{aligned} \tag{67}$$

It is clear that (67) is a Bernoulli differential equation on the interval $t \in [n, n+1)$. Solving (67) for $t \in [n, n+1)$ and $t \to n+1$, we get for $n = 0, 1, 2, \ldots$

$$\begin{aligned} & x(n+1) \\ & = x(n)\left(r - \left(\delta_1 + \beta_0 r\right)x(n) - \left(\delta_2 + \beta_1 r\right)x(n-1)\right) \\ & \quad \times \left(\left(r - \left(\delta_1 + \beta_0 r + \alpha r\right)x(n) - \left(\delta_2 + \beta_1 r\right)x(n-1)\right)\right. \\ & \qquad \times \exp(-a(x(n))) \\ & \qquad \times \left\{r - \left(\delta_1 + \beta_0 r\right)x(n) - \left(\delta_2 + \beta_1 r\right)x(n-1)\right\} \\ & \qquad \left. + \alpha r x(n)\right)^{-1}. \end{aligned} \tag{68}$$

It can be shown that the equilibrium points of (68) are also the equilibrium points of (7).

Linearizing (68) about the positive equilibrium point, we obtain the characteristic equation as follows:

$$\begin{aligned} & \mu^2 - \left\{\frac{-\left(\delta_1 + \beta_0 r\right) + \left(\left(\alpha + \beta_0\right)r + \delta_1\right)\cdot e^{-a(\overline{x})A}}{\alpha r}\right\} \\ & \quad \times \mu - \left\{\frac{-\left(\delta_2 + \beta_1 r\right)\left(1 - e^{-a(\overline{x})A}\right)}{\alpha r}\right\} = 0, \end{aligned} \tag{69}$$

where $A = \alpha r^2/((\alpha + \beta_0 + \beta_1)r + \delta_1 + \delta_2)$.

Theorem 5. *Let $\beta_0 > \beta_1 + \alpha$ and $\beta_1 > \alpha$. The positive equilibrium point of* (68) *is locally asymptotically stable if*

$$A < \frac{1}{a(\overline{x})}\ln\left(\frac{\left(\beta_0 - \beta_1 + \alpha\right)r + \delta_1 - \delta_2}{\left(\beta_0 - \beta_1 - \alpha\right)r + \delta_1 - \delta_2}\right). \tag{70}$$

Proof. The proof is similar to that in Theorem 1 and will be omitted. □

Theorem 6. *Suppose that $r - (\delta_1 + \beta_0 r + \alpha r)x(n) - (\delta_2 + \beta_1 r)x(n-1) > 0$ for $n = 0, 1, 2, \ldots$ and assume that the conditions in Theorem 5 hold.*

If

$$r - (\delta_1 + \beta_0 r)\, x(n) - (\delta_2 + \beta_1 r)\, x(n-1) < \ln\left(\frac{2\overline{x}_2 - x(n)}{x(n)}\right), \quad x(n) < \frac{2r}{(\alpha + \beta_0 + \beta_1) r - \gamma_1 - \gamma_2}, \tag{71}$$

then the positive equilibrium point of (68) *is globally asymptotically stable.*

Proof. The proof is similar to that in Theorem 2 and will be omitted. □

Example 7. The goal of this investigation is to examine the development of monoclonal tumors under the effects of treatment. In view of [6], the carrying capacity of a monoclonal tumor is ca. 38 mm. We select $\alpha' = 0.00744$, $\beta_1' = 0.007448$, and $\beta_0' = 0.014896$. By dividing these values by the carrying capacity, we obtain $\alpha = (0.00744/38) = 0.000195789$, $\beta_1 = (0.007448/38) = 0.000196$ and $\beta_0 = (0.014896/38) = 0.000392$. These values are also suitable for the hypotheses in Theorems 1 and 5. To have a compatible result, a relation between the model and the data is constructed by multiplying these values with 10. Thus, the parameters for (7) are in this case $\alpha = 0.00195789$, $\beta_1 = 0.00196$, and $\beta_0 = 0.00392$. For a therapy of ca. 75 mg drug and under the assumption that the effect on the tumor is 1.6% we obtain $\delta_1 = 0.0125$. The effect on the immune is ca. 10% compared with the effect of the drug treatment, so we have $\delta_2 = 0.00125$. Figure 1 shows us the behavior of the solution of (7). Differently from this, we can see Figure 2, where we have used the Allee function for $E = 0.4$. Studies demonstrated that Allee effects play an important role in the stability analysis of equilibrium points of a population dynamics model. Generally, an Allee effect has a stabilizing effect on population dynamics. So, in (68) our expectation is that the chaos begins later as it can be also shown in Figure 2.

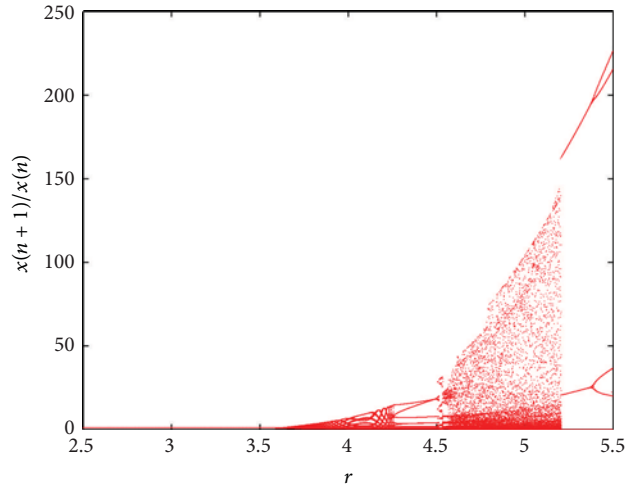

Figure 1: Behavior of the solutions of (7), where $\alpha = 0.00195789$, $\beta_1 = 0.00196$, $\beta_0 = 0.00392$, $\delta_1 = 0.0125$, and $\delta_2 = 0.00125$.

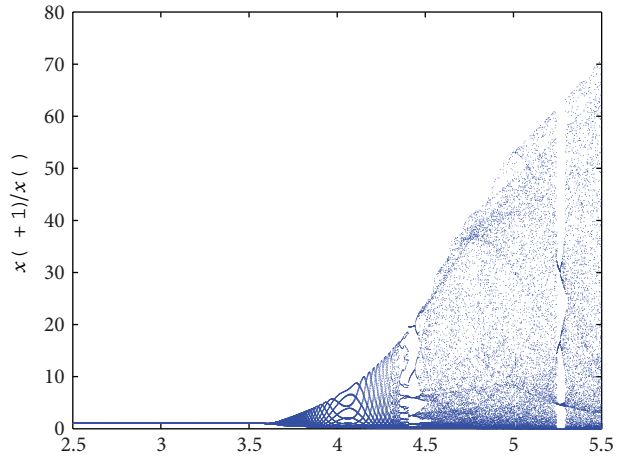

Figure 2: Behavior of the solutions of (68), where $\alpha = 0.00195789$, $\beta_1 = 0.00196$, $\beta_0 = 0.00392$, $\delta_1 = 0.0125$, $\delta_2 = 0.00125$, and $E = 0.4$.

4. Discussion

Section 2 was constructed to obtain specific conditions for local and global asymptotic stability of the positive equilibrium point of (7) without Allee effect by applying the Linearized Stability Theorem and the theory of the use of a Lyapunov function, respectively. Furthermore, we showed that increase of the population growth rate decreases the stability of the positive equilibrium point of (7), which is given in Theorem 3. Finally, in Section 2 we proved Theorem 4, which has given information about the bound of the solutions of (7). By using the data of [6] about the radius of tumor at 111 days, we take the radius as 4.96 mm for a population growth rate $r = 0.31$. By multiplying it with 10, we use the growth rate $r = 3.1$. The volume of such a tumor will be then $(n) = 510.87\,\text{mm}^3$. Considering Theorem 4, we can see that the above mentioned value for α is suitable. For $\alpha = 0.00195789$, $\beta_1 = 0.00196$, $\beta_0 = 0.00392$, $\delta_1 = 0.0125$, and $\delta_2 = 0.00125$ we consider Section 3 in view of $E = 0.4$,

$$x \in \Big(0, \Big(E^2 (\delta_1 + \delta_2 + (\alpha + \beta_0 + \beta_1) r)^2 + Er\left((\alpha + \beta_0 + \beta_1) r + \delta_1 + \delta_2\right)\Big)^{-1/2} - E\left((\alpha + \beta_0 + \beta_1) r + \delta_1 + \delta_2\right) \times \left((\alpha + \beta_0 + \beta_1) r + \delta_1 + \delta_2\right)^{-1}\Big) = (0, 5.322). \tag{72}$$

In this case, for the volume $x(n) = 5\,\text{mm}^3$ the radius of the tumor must be around 1.0609 mm, which the temporal development of a cross-central section of a tumor growing without angiogenesis show a tumor more than at day 80 and the temporal development of a cross-central section of a tumor growing with angiogenesis around 40 days of the tumor (see [6]). This means that during the 90 days of

the tumor we shall use the model given in (68). For days more than 90, both models are suitable ((7) and (68)). Using the above mentioned values, it can be shown that the local stability of both theorems (Theorems 1 and 5) hold. However, Theorem 5 give us that the stable interval for the growth rate is wide as assumed in Theorem 1, which is important for the drug therapy.

References

[1] E. Hulleman and K. Helin, "Molecular mechanisms in gliomagenesis," *Advances in Cancer Research*, vol. 94, no. 1, pp. 1–27, 2005.

[2] E. A. Maher, F. B. Furnari, R. M. Bachoo et al., "Malignant glioma: genetics and biology of a grave matter," *Genes and Development*, vol. 15, no. 11, pp. 1311–1333, 2001.

[3] D. J. Brat, B. Kaur, and E. G. Van Meir, "Genetic modulation of hypoxia induced gene expression and angiogenesis: relevance to brain tumors," *Frontiers in Bioscience*, vol. 8, pp. d100–d116, 2003.

[4] A. Giese and M. Westphal, "Glioma invasion in the central nervous system," *Neurosurgery*, vol. 39, no. 2, pp. 235–252, 1996.

[5] T. Visted, P. O. Enger, M. Lund-Johansen, and R. Bjerkvig, "Mechanisms of tumor cell invasion and angiogenesis in the central nervous system," *Frontiers in Bioscience*, vol. 8, pp. e289–e304, 2003.

[6] J. L. Gevertz and S. Torquato, "Modeling the effects of vasculature evolution on early brain tumor growth," *Journal of Theoretical Biology*, vol. 243, no. 4, pp. 517–531, 2006.

[7] J. E. Schmitz, A. R. Kansal, and S. Torquato, "A cellular automaton model of brain tumor treatment and resistance," *Journal of Theoretical Medicine*, vol. 4, no. 4, pp. 223–239, 2002.

[8] R. M. May, "Biological populations obeying difference equations: stable points, stable cycles, and chaos," *Journal of Theoretical Biology*, vol. 51, no. 2, pp. 511–524, 1975.

[9] R. M. May and G. F. Oster, "Bifurcations and dynamics complexity in simple ecological models," *The American Naturalist*, vol. 110, pp. 573–599, 1976.

[10] K. Gopalsamy and P. Liu, "Persistence and global stability in a population model," *Journal of Mathematical Analysis and Applications*, vol. 224, no. 1, pp. 59–80, 1998.

[11] P. Liu and K. Gopalsamy, "Global stability and chaos in a population model with piecewise constant arguments," *Applied Mathematics and Computation*, vol. 101, no. 1, pp. 63–88, 1999.

[12] K. L. Cooke and W. Huang, "A theorem of george seifert and an equation with State-Dependent Delay," in *Delay and Differential Equations*, A. M. Fink, R. K. Miller, and W. Kliemann, Eds., World Scientific, Ames, Iowa, USA, 1991.

[13] F. Gurcan and F. Bozkurt, "Global stability in a population model with piecewise constant arguments," *Journal of Mathematical Analysis and Applications*, vol. 360, no. 1, pp. 334–342, 2009.

[14] I. Ozturk and F. Bozkurt, "Stability analysis of a population model with piecewise constant arguments," *Nonlinear Analysis: Real World Applications*, vol. 12, no. 3, pp. 1532–1545, 2011.

[15] K. Gobalsamy, *Stability and Oscillation in Delay Differential Equations of Population Dynamics*, Kluwer Academic Publishers, Dodrecht, The Netherlands, 1992.

[16] J. W.-H. So and J. S. Yu, "Global stability in a logistic equation with piecewise constant arguments," *Hokkaido Mathematical Journal*, vol. 24, no. 2, pp. 269–286, 1995.

[17] P. Cull, "Global stability of population models," *Bulletin of Mathematical Biology*, vol. 43, no. 1, pp. 47–58, 1981.

[18] K. Uesugi, Y. Muroya, and E. Ishiwata, "On the global attractivity for a logistic equation with piecewise constant arguments," *Journal of Mathematical Analysis and Applications*, vol. 294, no. 2, pp. 560–580, 2004.

[19] Y. Muroya, "Persistence, contractivity and global stability in logistic equations with piecewise constant delays," *Journal of Mathematical Analysis and Applications*, vol. 270, no. 2, pp. 602–635, 2002.

[20] W. C. Allee, *Animal Aggregations: A Study in General Sociology*, University of Chicago Press, Chicago, Ill, USA, 1931.

[21] G. Wang, X. G. Liang, and F. Z. Wang, "The competitive dynamics of populations subject to an Allee effect," *Ecological Modelling*, vol. 124, no. 2-3, pp. 183–192, 1999.

[22] M. A. Asmussen, "Density-dependent selection II. The Allee effect," *The American Naturalist*, vol. 114, pp. 796–809, 1979.

[23] R. Lande, "Extinction thresholds in demographic models of territorial populations," *American Naturalist*, vol. 130, no. 4, pp. 624–635, 1987.

[24] B. Dennis, "Allee effects: population growth, critical density, and the chance of extinction," *Natural Resource Modeling*, vol. 3, no. 4, pp. 481–538, 1989.

[25] T. Stephan and C. Wissel, "Stochastic extinction models discrete in time," *Ecological Modelling*, vol. 75-76, pp. 183–192, 1994.

[26] I. Hanski, "Single-species metapopulation dynamics: concepts, models and observations," *Biological Journal of the Linnean Society*, vol. 42, no. 1-2, pp. 17–38, 1991.

[27] P. Amarasekare, "Allee effects in metapopulation dynamics," *American Naturalist*, vol. 152, no. 2, pp. 298–302, 1998.

[28] A. P. Dobson and A. M. Lyles, "The population dynamics and conservation of primate populations," *Conservation Biology*, vol. 3, no. 4, pp. 362–380, 1989.

[29] C. Çelik, H. Merdan, O. Duman, and O. Akın, "Allee effects on population dynamics with delay," *Chaos, Solitons & Fractals*, vol. 37, no. 1, pp. 65–74, 2008.

[30] C. H. Gibbons, M. R. S. Kulenović, G. Ladas, and H. D. Voulov, "On the trichotomy character of $x_{n+1} = (\alpha + \beta x_n + \gamma x_{n-1})/(A + x_n)$," *Journal of Difference Equations and Applications*, vol. 8, no. 1, pp. 75–92, 2002.

Hindawi Publishing Corporation
Discrete Dynamics in Nature and Society
Volume 2013, Article ID 408904, 10 pages
http://dx.doi.org/10.1155/2013/408904

Research Article

Bifurcation and Chaos in a Price Game of Irrigation Water in a Coastal Irrigation District

Baogui Xin[1,2] and Yuting Li[1,3]

[1] *Nonlinear Science Center, School of Economics and Management, Shandong University of Science and Technology, Qingdao 266590, China*
[2] *Nonlinear Dynamics and Chaos Group, School of Management, Tianjin University, Tianjin 300072, China*
[3] *College of Mechanical and Electronic Engineering, Shandong University of Science and Technology, Qingdao 266590, China*

Correspondence should be addressed to Baogui Xin; xin@tju.edu.cn

Received 8 March 2013; Accepted 17 April 2013

Academic Editor: Qingdu Li

We propose a price game model of irrigation water in a coastal irrigation district. Then, we discuss the stability and codimension-two period-doubling (flip) bifurcation. Then, the MATLAB package Cl_MatContM is employed to illustrate its numerical bifurcations-based continuation methods. Lastly, the 0-1 test algorithm is used to compute the median value of correlation coefficient which can indicate whether the underlying dynamics is regular or chaotic.

1. Introduction

Water scarcity is one of the key problems affecting most countries in the world. With a burgeoning population, food price volatility, and climate change, water scarcity would also fuel future global conflict. Water scarcity is exacerbated by the indiscriminate discharge of industrial and municipal wastewater and is likely to affect the supply and demand of grain in the years ahead. Irrigation water availability is decreasing in many places where crop and plant production is taking place. Not only is there no set of efficient technique that can suddenly eliminate water scarcity, but also there is no optimal institutional arrangement for water, and rather it is critical to understand the potential contributions, facilitating conditions, and limitations of each [1, 2]. One of the important causes of water scarcity is that the demand exceeds a finite supply. All over the world, water regulations have historically focused on supply management. In fact, pricing mechanism may turn the tide against water scarcity by improving the water use efficiency [3–6]. Thereinto, the price game between water oligopolies is an important pricing mechanism. One of the simplest the price games is price game of irrigation water in a coastal irrigation district because there is little demand diversity of the irrigation water type among farmers. It will be considered in this paper.

In recent years, a lot of research works [7–14] have shown that the game theory plays an important role in the economics and management field. Ji et al., Son et al., and Skoulidas et al. [15–17] studied the game model in an electric power market. Mu et al. [18, 19] analyzed the game model in a real estate market. Liu et al. [20] discussed the minority game in a financial market. Gkonis and Psaraftis [21] proposed a game model in the LNG market. Sun and Ma [22] presented a game model in Chinese cold rolled steel market. Sugawara and Omori [23] considered the duopoly in the Japanese airline market. Chung et al. [24] applied the game model into pollution permit markets. Ma and Zhang [25] build a price game in a property insurance market.

Some references [26–32] have reported the complex dynamics of game model, such as bifurcation and chaos. Analyzing bifurcation and chaos is not an easy task for most of researchers. Fortunately, there are many powerful methods for us to study bifurcation and chaos, such as 0-1 test algorithm for chaos [33–38], MATLAB package MatCont series [39–43] for the bifurcation of discrete, and continuous dynamical systems.

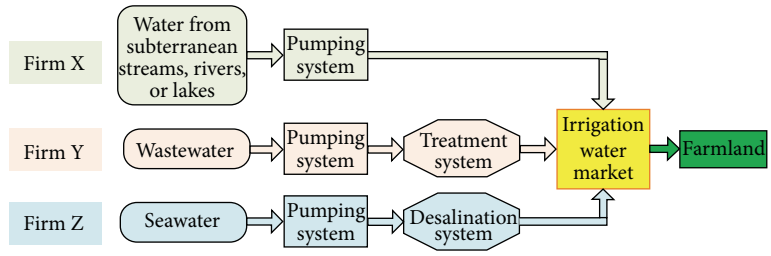

Figure 1: Schematic diagram of water supply in the coastal irrigation district.

This paper is organized as follows. In Section 2, a price game model of irrigation water in a coastal irrigation district is presented. In Section 3, the fixed points and their stabilities are studied. In Section 4, codimension-two period-doubling (flip) bifurcation is discussed. In Section 5, the 0-1 test algorithm and continuation methods are employed to validate the main results. Finally, conclusions in Section 6 close the paper.

2. A Pricing Game Model

In a coastal irrigation district, water mainly exists in ocean, rivers, lakes, or subterranean streams. But seawater and wastewater cannot directly be used for irrigation because the salt and pollutants will not allow the crops to grow. Generally speaking, groundwater can be directly used as irrigation water, but seawater and wastewater need to be pumped to a desalination plant and a wastewater treatment plant, respectively, and to be treated to be suitable for irrigation. Taking such factors as the freshwater scarcity, the high cost of wastewater treatment, and seawater desalination into consideration, wastewater treatment and seawater desalination have to rely on the help of government subsidies or tax breaks.

Assumption 1. As shown in Figure 1, firms X, Y, and Z are the three water oligopolies of the irrigation water market in the coastal irrigation district. Firm X supplies irrigation water by directly pumping from rivers, lakes, or subterranean streams, and firm Y supplies irrigation water by wastewater treatment, and firm Z supplies irrigation water by seawater desalination.

Assumption 2. Firms X, Y, and Z compete with making different price of irrigation water in discrete-time periods $t = 0, 1, 2, \ldots$. Consider that p_{x_t}, p_{y_t}, and p_{z_t} represent, respectively, the irrigation water price of firms X, Y, and Z during period $t = 0, 1, 2, \ldots$.

Assumption 3. The quantities, in which firms X, Y, and Z sell, respectively, Q_{x_t}, Q_{y_t}, and Q_{z_t}, are linear inverse demand functions determined by the following equations:

$$\begin{aligned} Q_{x_t} &= a - bp_{x_t} + d\left(p_{y_t} + p_{z_t}\right), \\ Q_{y_t} &= a - bp_{y_t} + d\left(p_{x_t} + p_{z_t}\right), \\ Q_{z_t} &= a - bp_{z_t} + d\left(p_{x_t} + p_{y_t}\right), \end{aligned} \tag{1}$$

where $a, b, d > 0$. The parameter d denotes the extent to which a firm's irrigation water is substituted by its rivals' water.

Assumption 4. The cost functions of firms X, Y, and Z have the following linear forms:

$$C_{x_t} = c_1 Q_{x_t}, \qquad C_{y_t} = c_2 Q_{y_t}, \qquad C_{z_t} = c_3 Q_{z_t}, \tag{2}$$

where parameters $c_i > 0$ $(i = 1, 2, 3)$ are marginal costs of the firms X, Y, and Z, respectively.

Assumption 5. The profit functions of firms X, Y, and Z have the following forms:

$$\begin{aligned} \Pi_{x_t} &= Q_{x_t} p_{x_t} - C_{x_t} \\ &= \left(p_{x_t} - c_1\right)\left(a - bp_{x_t} + d\left(p_{y_t} + p_{z_t}\right)\right), \\ \Pi_{y_t} &= Q_{y_t} p_{y_t} + Q_{y_t} s_2 - C_{y_t} \\ &= \left(p_{y_t} + s_2 - c_2\right)\left(a - bp_{y_t} + d\left(p_{x_t} + p_{z_t}\right)\right), \\ \Pi_{z_t} &= Q_{z_t} p_{z_t} + Q_{z_t} s_3 - C_{z_t} \\ &= \left(p_{z_t} + s_3 - c_3\right)\left(a - bp_{z_t} + d\left(p_{x_t} + p_{y_t}\right)\right), \end{aligned} \tag{3}$$

where s_2 and $s_3 > 0$ are the intensity coefficients of government support (such as subsidies and tax breaks) for the firms Y and Z, respectively.

Assumption 6. Firms X, Y, and Z always make the optimal price decision for the maximal marginal profit in every single period.

The water prices of firms X, Y, and Z in period $(t + 1)$ are decided by solving the following optimization problem:

$$\begin{aligned} p_{x_{t+1}} &= \arg\max_{p_x} \prod_x \left(p_{x_t}, p^{e_x}_{y_{t+1}}, p^{e_x}_{z_{t+1}}\right), \\ p_{y_{t+1}} &= \arg\max_{p_y} \prod_x \left(p^{e_y}_{x_{t+1}}, p_{y_t}, p^{e_y}_{z_{t+1}}\right), \\ p_{z_{t+1}} &= \arg\max_{p_z} \prod_x \left(p^{e_z}_{x_{t+1}}, p^{e_z}_{y_{t+1}}, p_{z_t}\right), \end{aligned} \tag{4}$$

where $p^{e_x}_{y_{t+1}}$ represents the expectation of firm X about the water price of firm Y during period $t + 1$. Consider that $p^{e_x}_{z_{t+1}}$, $p^{e_y}_{x_{t+1}}$, $p^{e_y}_{z_{t+1}}$, $p^{e_z}_{x_{t+1}}$, and $p^{e_z}_{y_{t+1}}$ may be explained by analogy.

Assumption 7. Each firm expects that its rivals' water price in period $(t+1)$ will remain the same as in period (t).

Thus,

$$p_{y_{t+1}}^{e_x} = p_{y_{t+1}}^{e_z} = p_{y_t}, \qquad p_{z_{t+1}}^{e_x} = p_{z_{t+1}}^{e_y} = p_{z_t},$$
$$p_{x_{t+1}}^{e_y} = p_{x_{t+1}}^{e_z} = p_{x_t}. \tag{5}$$

The margin profits of firms X, Y, and Z in period t are given, respectively, by

$$\frac{\partial \Pi_{x_t}}{\partial p_{x_t}} = a - 2bp_{x_t} + d\left(p_{y_t} + p_{z_t}\right) + bc_1,$$
$$\frac{\partial \Pi_{y_t}}{\partial p_{y_t}} = a - 2bp_{y_t} + d\left(p_{x_t} + p_{z_t}\right) + b\left(c_2 - s_2\right), \tag{6}$$
$$\frac{\partial \Pi_{z_t}}{\partial p_{z_t}} = a - 2bp_{z_t} + d\left(p_{x_t} + p_{y_t}\right) + b\left(c_3 - s_3\right).$$

Let (6) be equal to 0; one can obtain the reaction functions of firms X, Y, and Z; that is, the optimal water prices are as follows:

$$p_x^* = \frac{a + d\left(p_y + p_z\right) + bc_1}{2b},$$
$$p_y^* = \frac{a + d\left(p_x + p_z\right) + b\left(c_2 - s_2\right)}{2b}, \tag{7}$$
$$p_z^* = \frac{a + d\left(p_x + p_y\right) + b\left(c_3 - s_3\right)}{2b}.$$

Assumption 8. Firm X uses bounded rationality to make its price decisions with local information based on the marginal profits $\partial \Pi_x / \partial p_x$ and increase (decrease) its water prices in period $(t+1)$ if the marginal profit is positive (negative) [8, 29, 44].

The above adjustment mechanism of firm X has been called myopic by Dixit [45]. The dynamical adjustment mechanism of firm X can be written as follows:

$$p_{x_{t+1}} = p_{x_t} + \alpha p_{x_t} \frac{\partial \Pi_{x_t}}{\partial p_{x_t}}, \tag{8}$$

where $\alpha > 0$ represents the adjustment speed of firm X.

Assumption 9. Firm Y is an adaptive decision maker and has adaptive expectations. Thus, its price decision in period $(t+1)$ is mainly based on its reaction function and price in period (t).

So, the price adjustment mechanism of firm Y can be written as follows:

$$p_{y_{t+1}} = (1-\beta)\, p_{y_t} + \beta p_{y_t}^*, \tag{9}$$

where $\beta > 0$ represents the adjustment speed of firm Y.

Assumption 10. Firm Z has simple rationality; that is, its price decision in period $(t+1)$ is mainly based on its optimal reaction function in period (t).

Thus, the price adjustment mechanism of firm Z can be expressed as follows:

$$p_{z_{t+1}} = p_{z_t}^*. \tag{10}$$

So, the repeated price game of irrigation water in the coastal irrigation district has the following nonlinear form:

$$p_{x_{t+1}} = p_{x_t} + \alpha p_{x_t}\left(a - 2bp_{x_t} + d\left(p_{y_t} + p_{z_t}\right) + bc_1\right),$$
$$p_{y_{t+1}} = (1-\beta)\, p_{y_t} + \frac{\beta}{2b}\left(a + d\left(p_{x_t} + p_{z_t}\right) + b\left(c_2 - s_2\right)\right),$$
$$p_{z_{t+1}} = \frac{1}{2b}\left(a + d\left(p_{x_t} + p_{y_t}\right) + b\left(c_3 - s_3\right)\right). \tag{11}$$

In what follows, we will focus on how the government supports intensities s_2 and $s_3 > 0$ which have an effect on the complex dynamics of the irrigation water price game.

3. Stability of Fixed Points

The fixed points of the system (11) satisfy the following algebraic system:

$$p_x + \alpha p_x\left(a - 2bp_x + d\left(p_y + p_z\right) + bc_1\right) = 0,$$
$$(1-\beta)\, p_y + \frac{\beta}{2b}\left(a + d\left(p_x + p_z\right) + b\left(c_2 - s_2\right)\right) = 0, \tag{12}$$
$$\frac{1}{2b}\left(a + d\left(p_x + p_y\right) + b\left(c_3 - s_3\right)\right) = 0.$$

By simple computation, one can obtain two fixed points $E_0 = (p_{x_0}, p_{y_0}, p_{z_0})$ and $E_1 = (p_{x_1}, p_{y_1}, p_{z_1})$, where

$$p_{x_0} = 0,$$
$$p_{y_0} = \frac{ad + bdc_3 - bds_3 + 2ab + 2b^2c_2 - 2b^2s_2}{4b^2 - d^2},$$
$$p_{z_0} = \frac{2ab + 2b^2c_3 - 2b^2s_3 + ad + bdc_2 - bds_2}{4b^2 - d^2},$$
$$p_{x_1} = \frac{ad + 2b\left(a + bc_1\right) - bd\left(c_1 - c_2 - c_{3+s_2} + s_3\right)}{2\left(2b + d\right)\left(b - d\right)},$$
$$p_{y_1} = \frac{2b^2\left(c_2 - s_2\right) + bd\left(c_1 - s_3 - c_{2+c_3} + s_2\right) + a\left(2b + d\right)}{2\left(2b + d\right)\left(b - d\right)},$$
$$p_{z_1} = \frac{2b^2\left(c_3 - s_3\right) + bd\left(c_1 + c_2 - c_3 - s_2 + s_3\right) + a\left(2b + d\right)}{2\left(2b + d\right)\left(b - d\right)}. \tag{13}$$

If the characteristic polynomial of a 3-order square matrix can be written as

$$P(\lambda) = (\lambda)^3 + a_2\lambda^2 + a_1\lambda + a_0 = 0, \tag{14}$$

then one can get directly the following Lemma 11 from the Jury stability criterion.

Lemma 11. *A necessary and sufficient condition that the characteristic polynomial of a matrix $A = (a_{ij})_{3\times3}$ has all of its roots inside the unit circle is that*

$$\begin{aligned} &1 + a_0 + a_1 + a_2 > 0,\\ &1 - a_0 + a_1 - a_2 > 0,\\ &1 - a_0^2 > \left|a_1 - a_0 a_2\right|,\\ &\left|a_0\right| < 1. \end{aligned} \tag{15}$$

3.1. Stability of E_0. The Jacobian matrix of system (11) at the point E_0 can be written as

$$A(E_0) = \begin{bmatrix} 1 + \alpha\left(a + d\left(y_0 + z_0\right) + bc_1\right) & 0 & 0\\ \dfrac{\beta d}{2b} & 1 - \beta & \dfrac{\beta d}{2b}\\ \dfrac{d}{2b} & \dfrac{d}{2b} & 0 \end{bmatrix}. \tag{16}$$

Its characteristic polynomial can be written as

$$P(\lambda) = (\lambda)^3 + A_2\lambda^2 + A_1\lambda + A_0 = 0, \tag{17}$$

where $A_2 = \beta - \alpha(a + dy_0 + dz_0 + bc_1) - 2$, $A_1 = \alpha(1 - \beta)bc_1 + ((y_0 + z_0)(1 - \beta)d + a(1 - \beta))\alpha + 1 - \beta - (\beta d^2/4b^2)$, and $A_0 = (-1 - \alpha\beta(a + d(y_0 + z_0) + bc1))d^2/4b^2$.

From Lemma 11, one can get the locally asymptotically stable region $\Omega_{E_0}(s_2, s_3)$ with respect to parameters (s_2, s_3) as follows:

$$\begin{aligned} \Omega_{E_0}(s_2, s_3) = \Big\{&(s_2, s_3) : 1 + A_0 + A_1 + A_2 > 0,\\ &1 - A_0 + A_1 - A_2 > 0,\\ &1 - A_0^2 > \left|A_1 - A_0 A_2\right|, \left|A_0\right| < 1\Big\}. \end{aligned} \tag{18}$$

3.2. Stability of E_1. The Jacobian matrix of system (11) at the point E_1 has the following form:

$$A(E_1) = \begin{bmatrix} 1 + a\alpha - 4\alpha b p_{x_1} + \alpha d p_{y_1} + \alpha d p_{z_1} + \alpha b c_1 & \alpha d p_{x_1} & \alpha d p_{x_1}\\ \dfrac{\beta d}{2b} & 1 - \beta & \dfrac{\beta d}{2b}\\ \dfrac{d}{2b} & \dfrac{d}{2b} & 0 \end{bmatrix}. \tag{19}$$

Its characteristic polynomial can be written as

$$P(\lambda) = (\lambda)^3 + a_2\lambda^2 + a_1\lambda + a_0 = 0, \tag{20}$$

where $a_0 = W_5(W_4(s_2 + s_3) + W_1 + W_2 + W_3)$, $a_1 = W_5(W_{11}(s_2 + s_3) + W_6 + W_7 + W_8 + W_9 + W_{10})$, $a_2 = W_5(W_{13}(s_2 + s_3) + W_{12})$, $W_0 = c_1 - c_2 - c_3$, $W_1 = \beta(\alpha b W_0 - a\alpha - 1)d^4$, $W_2 = (((1 - 4\beta)a\alpha - \beta) - ((2c_2 + 2c_3)\beta + W_0)\alpha b)bd^3$, $W_3 = (2(1 - 2\beta)\alpha b^3 c_1 + ((1 - 2\beta)2a\alpha + 2\beta)b^2)d^2$, $W_4 = 2\alpha\beta b^2 d^3 - \alpha b^2 d^3 + \alpha\beta b d^4$, $W_5 = 1/(8b^4 - 4b^3 d - 4d^2 b^2)$, $W_6 = 8\alpha(\beta - 1)b^5 c_1$, $W_7 = (\alpha(4 - \beta)dW_0 + 8(\beta - 1)(a\alpha - 1))b^4$, $W_8 = 2d((2(\beta - 1)(a\alpha + 1) - \alpha(1 + \beta)c_1 d)b^3$, $W_9 = ((W_0(\beta + 1)\alpha d + 2(\beta - (\beta + 1)a\alpha - 2))b^2 d^2$, $W_{10} = d^4\beta + (\beta - \alpha(\beta + 1))abd^3$, $W_{11} = d^3\alpha b^2 + 4\alpha b^4 d + \alpha b^2 d^3\beta - 4\alpha b^4 d\beta$, $W_{12} = 8\alpha b^5 c_1 + 4(2a\alpha + 2\beta - \alpha d W_0 - 4)b^4 + 4(2 + a\alpha - \beta)db^3 + 4(2 - \beta)b^2 d^2$, and $W_{13} = -4\alpha b^4 d$.

It is obvious that the fixed point E_1 is locally asymptotically stable if and only if Lemma 11 holds. One can get the locally asymptotically stable region $\Omega_{E_1}(s_2, s_3)$ with respect to parameters (s_2, s_3) as follows:

$$\begin{aligned} \Omega_{E_1}(s_2, s_3) = \Big\{&(s_2, s_3) : 1 + a_0 + a_1 + a_2 > 0,\\ &1 - a_0 + a_1 - a_2 > 0,\\ &1 - a_0^2 > \left|a_1 - a_0 a_2\right|, \left|a_0\right| < 1\Big\}. \end{aligned} \tag{21}$$

3.3. Parameter Basin with respect to (s_2, s_3). Let $\alpha = 0.36$, $\beta = 0.2$, $a = 6$, $b = 2.5$, $c_1 = 0.1$, $c_2 = 0.3$, and $c_3 = 0.4$; a parameter basin with respect to the parameters (s_2, s_3) is shown in Figure 2, in which the two red regions correspond to $\Omega_{E_0}(s_2, s_3)$ and $\Omega_{E_1}(s_2, s_3)$, respectively, which are asymptotically stable state, the blue region denotes stable cycles of period two, the yellow region denotes chaotic state, and the white region denotes divergence state, as shown in Table 1.

The regions $\Omega_{E_0}(s_2, s_3)$ and $\Omega_{E_1}(s_2, s_3)$ show that the price game for irrigation water will reach the Nash equilibrium by modulating limited times with random initial prices. Obviously, $E_0 = (p_{x_0}, p_{y_0}, p_{z_0})$ is a bounded equilibrium point [46], which indicates that $p_{x_0} = 0$; that is, free supply of irrigation water is an optimal strategy of firm X. But, in fact, it will never happen in the real word. Thus, E_0 is not considered in the paper. And $E_1 = (p_{x_1}, p_{y_1}, p_{z_1})$ is a Nash equilibrium point, which is practical and feasible. So, we will continue to discuss E_1 in the sections below.

4. Codimension-Two Period-Doubling (Flip) Bifurcation

There are many bifurcation theories [47–49] that can be used into system (11), but the Kuznetsov bifurcation theory [50] is more effective to discuss the bifurcation in system (11). In what follows, we let $\alpha = 0.36$, $\beta = 0.2$, $a = 6$, $b = 2.5$, $c_1 = 0.1$, $c_2 = 0.3$, and $c_3 = 0.4$. The system (11) can be rewritten as follows:

$$\begin{aligned} p_{x_{t+1}} &= p_{x_t} + 1.8p_{x_t}\left(1.25 - p_{x_t} + 0.11\left(p_{y_t} + p_{z_t}\right)\right),\\ p_{y_{t+1}} &= 0.8p_{y_t} + 0.022\left(p_{x_t} + p_{z_t}\right) - 0.1s_2 + 0.27,\\ p_{z_{t+1}} &= 0.11\left(p_{x_t} + p_{y_t}\right) - 0.5s_3 + 1.4. \end{aligned} \tag{22}$$

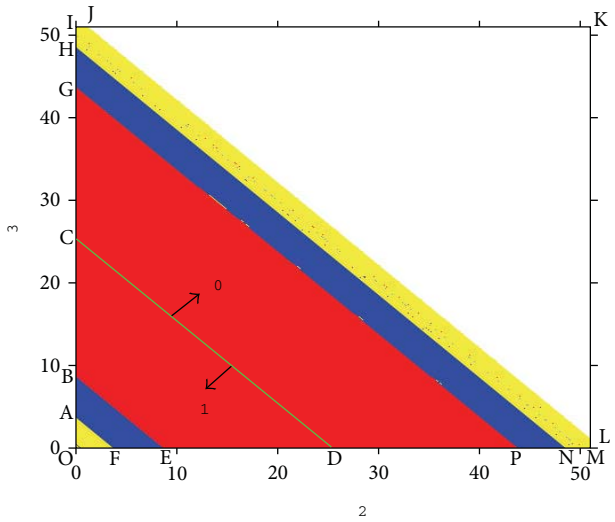

Figure 2: Parameter basin versus the parameters (s_2, s_3).

Table 1: Legend of the color coding for Figure 2.

No.	Polyarea	Color	State type	Fixed point
1	OAF	Yellow	Strange attractor	1
2	ABEF	Blue	Period-twocycle	1
3	BCDE	Red	Stable	1
4	CGPD	Red	Stable	0
5	GHNP	Blue	Period-twocycle	0
6	HIJLMN	Yellow	Strange attractor	0
7	JKL	White	Divergence	0

Its Nash equilibrium $E_1 = (1.096671926, 1.186762016 - 0.4504504505s_2, 2.580653598 + 0.4504504505s_2)$. The Jacobian matrix of system (22) at the point E_1 is

$$A_{pb}(E_1) = \begin{bmatrix} -0.974 & 0.217 & 0.217 \\ 0.022 & 0.8 & 0.022 \\ 0.11 & 0.11 & 0 \end{bmatrix}, \quad (23)$$

which has a simple real eigenvalue $\lambda_1 = -1$ and other two eigenvalues $\lambda_2 = 0.0195$ and $\lambda_3 = 0.807$. From Figures 2, 3, and 4, one can find that a period-doubling bifurcation occurs when a simple real eigenvalue $\lambda_1 = -1$ crosses the boundary BE of the stability region $\Omega_{E_1}(s_2, s_3)$. That is, the critical parameters values s_2 and s_3 satisfy $s_2 + s_3 = 8.463662665$ at the boundary BE of the stability region $\Omega_{E_1}(s_2, s_3)$.

When the fixed point E_1 loses stability via a period-doubling bifurcation point, the restriction of system (22) to a one-dimensional center manifold at the critical parameter value can be transformed to the normal form as follows:

$$X_{n+1} = -X_n + \frac{1}{6}b_1 X_n^3 + O\left(X_n^4\right), \quad X_n \in \mathbb{R}^1, \quad (24)$$

where $b_1 \neq 0$ is called normal form coefficient [50], which is given by

$$b_1 = \frac{1}{6}\left\langle p, C(q,q,q) + 3B\left(q, (I_3 - A)^{-1}B(q,q)\right)\right\rangle, \quad (25)$$

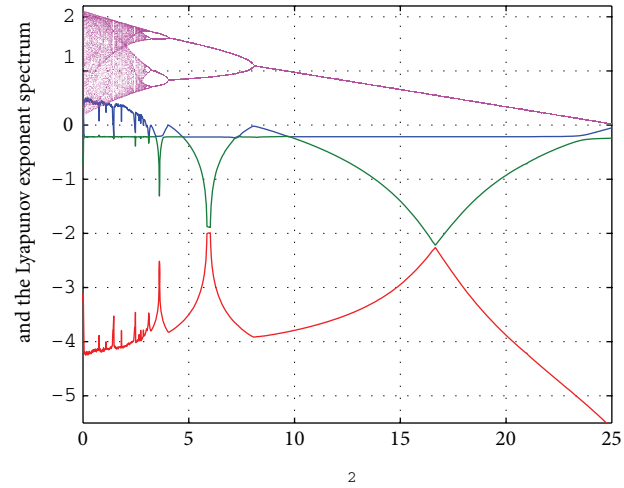

Figure 3: The Lyapunov exponent spectrum (blue, green, and red) and bifurcation of p_x (pinkish red) versus the parameters s_2 when $s_3 = 0.4$.

where I_3 is the unit 3×3 matrix, $Aq = -q$, $A^T p = -p$, $A = A_{pb}(E_1)$, $\langle q, q\rangle = \langle p, q\rangle = 1$, $\langle , \rangle$ denotes the inner product, and the multilinear functions B and C are defined, respectively, by

$$B_i(x,y) = \sum_{j,k=1}^{n} \left.\frac{\partial^2 X_i(\xi,0)}{\partial\xi_j\partial\xi_k}\right|_{\xi=0} x_j y_k, \quad i = 1,2,$$
$$C_i(x,y,z) = \sum_{j,k,l=1}^{n} \left.\frac{\partial^3 X_i(\xi,0)}{\partial\xi_j\partial\xi_k\partial\xi_l}\right|_{\xi=0} x_j y_k z_l, \quad i = 1,2. \quad (26)$$

For the system (22),

$$q = (-0.994075101, 0.01082788553, 0.1081571934)^T,$$
$$p = (-0.9818661631, 0.1055591755, 0.2108811391)^T,$$
$$B(\xi,\eta) = \begin{pmatrix} 0.198\left(\xi_1\eta_2 + \xi_1\eta_3 + \xi_2\eta_1 + \xi_3\eta_1\right) - 3.6\xi_1\eta_1 \\ 0 \\ 0 \end{pmatrix},$$
$$C(\xi,\eta,\zeta) = \begin{pmatrix} 0 \\ 0 \\ 0 \end{pmatrix}. \quad (27)$$

One can obtain

$$B(q,q) = \begin{pmatrix} -3.604306026 \\ 0 \\ 0 \end{pmatrix},$$
$$B\left(q, (I_3 - A)^{-1}B(q,q)\right) = \begin{pmatrix} -6.669763092 \\ 0 \\ 0 \end{pmatrix}, \quad (28)$$
$$C(q,q,q) = \begin{pmatrix} 0 \\ 0 \\ 0 \end{pmatrix}.$$

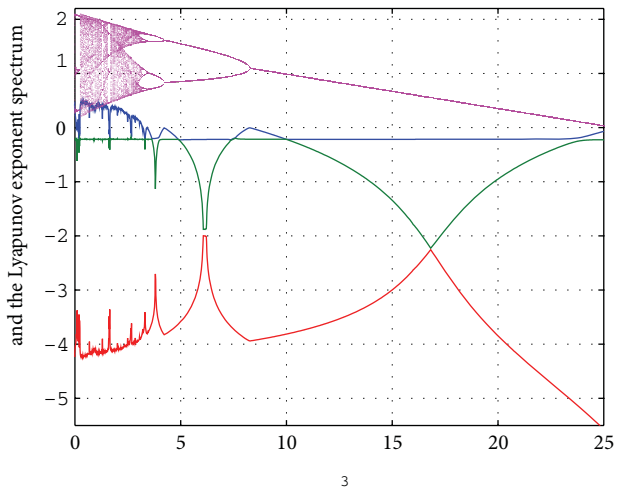

Figure 4: The Lyapunov exponent spectrum (blue, green, and red) and bifurcation of p_x (pinkish red) versus the parameters s_3 when $s_2 = 0.2$.

So, the critical normal form coefficient

$$b_1 = 3.274406 > 0, \tag{29}$$

which means that the period-doubling bifurcation at the fixed point E_1 is supercritical.

5. Numerical Simulation

From Figures 3 and 4, it can be observed that there is a very good agreement between the bifurcation diagram and the Lyapunov exponent spectrum. What is more, it can be find that the Lyapunov exponent spectrum and the bifurcation diagrams in Figures 3 and 4 well coincide with the parameter basin diagram in Figure 2, respectively. In this section, the numerical bifurcation and chaos will be employed to verify the above main results.

5.1. Numerical Bifurcation. In this subsection, based on continuation methods [51], we will discuss numerical bifurcations by using the MATLAB package Cl_MatContM [39–43].

Firstly, we consider that $E_1 = (1.596211596, 1.596211596, 1.551166551)$ which is in the stable region BCDE of Figure 2. We do a numerical continuation of E_1 with s_2 free, and $s_3 = 0.4$ fixed, as shown in Figure 5 and Table 2. Switchings at PD points of the second and fourth iterates are given in Figure 6.

Secondly, from the fixed point $E_1 = (1.596211596, 1.596211596, 1.551166551)$, we do a numerical continuation of E_1 with $s_2 = 0.2$ fixed and s_3 free, as shown in Figure 7 and Table 3.

In Tables 2 and 3, the first three entries of x are the coordinate values of the fixed point E_1, and the last entry of x is the value of the free parameters s_2 or s_3 at the corresponding bifurcation point. It is obvious that the normal form coefficient of the PD point is 3.274406, confirming (29). What is more, the detected bifurcation points in Figures 5 and 6 are in accordance with the statement in Figure 2. In addition, the label "PD" means that a period-doubling (flip) bifurcation occurs. In Table 2, the critical point "2-cycle" means that a stable 2-cycle is born when $s_2 < 8.063663$, "4-cycle" means that a stable 4-cycle is born when $s_2 < 4.045975$, and so on.

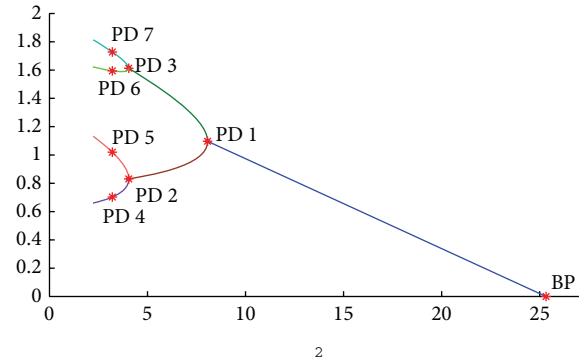

Figure 5: Continuation of E_1 in (s_2,x)-space.

5.2. Numerical Chaos. In the above section, the Wolf algorithm [52] is employed to calculate the Lyapunov exponent spectrum shown in Figures 3 and 4, by which one can find chaos when a largest Lyapunov exponent is greater than 0. In this section, we will use a reliable and efficient binary test for the chaos (called "0-1 test") to detect chaotic attractors.

5.2.1. The 0-1 Test Algorithm. The 0-1 test algorithm [33–38] can be described as follows.

Consider a discrete set of measurement data $\phi(n)$ sampled at times $n = 1, 2, 3, \ldots, N$, where N is the amount of the data.

Step 1. Choose a random number $c \in (\pi/5, 4\pi/5)$, and define the following new coordinates $(p_c(n), s_c(n))$:

$$\begin{aligned} p_c(n) &= \sum_{j=1}^{n} \phi(j) \cos(\theta(j)), \\ s_c(n) &= \sum_{j=1}^{n} \phi(j) \sin(\theta(j)), \end{aligned} \tag{30}$$

where

$$\theta(j) = jc + \sum_{i=1}^{j} \phi(j), \quad j = 1, 2, 3, \ldots, n. \tag{31}$$

Step 2. Define the mean square displacement $M_c(n)$ as follows:

$$\begin{aligned} M_c(n) = \lim_{N\to\infty} \frac{1}{N} \sum_{j=1}^{N} &(p_c(j+n) - p_c(j))^2 \\ &+ (s_c(j+n) - s_c(j))^2, \quad n \in \left[1, \frac{N}{10}\right]. \end{aligned} \tag{32}$$

Table 2: Numerical continuation of E_1 with control parameter s_2 as shown in Figure 5.

No.	Label	x	Normal form coefficient	Critical point
1	PD	(1.096672 −2.445180 1.051627 8.063663)	3.274406e + 00	2-cycle
2	PD	(0.830878 −0.392361 1.333279 4.045975)	1.868612e + 01	4-cycle
3	PD	(1.612503 −0.400875 1.248237 4.045975)	9.352670e + 01	4-cycle
4	PD	(0.702644 0.038991 1.393175 3.208909)	5.559248e + 02	8-cycle
5	PD	(1.019443 0.033503 1.378263 3.208909)	1.160791e + 02	8-cycle
6	PD	(1.594166 0.026410 1.281580 3.208909)	5.498331e + 02	8-cycle
7	PD	(1.727479 0.028661 1.315824 3.208909)	3.265258e + 03	8-cycle

Table 3: Numerical continuation of E_1 with control parameter s_3 as shown in Figure 6.

No.	Label	x	Normal form coefficient	Critical point
1	PD	(1.096672 1.096672 −2.490564 8.263663)	3.274406e + 00	2-cycle
2	PD	(0.830878 1.340060 −0.399142 4.245975)	1.868612e + 01	4-cycle
3	PD	(1.612503 1.331546 −0.484184 4.245975)	9.352670e + 01	4-cycle
4	PD	(0.702644 1.394355 0.037811 3.408909)	5.559248e + 02	8-cycle
5	PD	(1.019443 1.388868 0.022899 3.408909)	1.160791e + 02	8-cycle
6	PD	(1.594166 1.381774 −0.073784 3.408909)	5.498331e + 02	8-cycle
7	PD	(1.727479 1.384026 −0.039540 3.408909)	3.265258e + 03	8-cycle

Step 3. Define the modified mean square displacement $D_c(n)$ as follows:

$$D_c(n) = M_c(n) - \left(\lim_{N\to\infty}\frac{1}{N}\sum_{j=1}^{N}\phi(j)\right)^2\frac{1-\cos nc}{1-\cos c}, \quad (33)$$

Step 4. Define the median value of correlation coefficient K as follows:

$$K = \text{median}(K_c), \quad (34)$$

where

$$K_c = \frac{\text{cov}(\xi,\Delta)}{\sqrt{\text{var}(\xi)\,\text{var}(\Delta)}} \in [-1,1], \quad (35)$$

in which $\xi = (1,2,3,\ldots,n_{\text{cut}})$, $\Delta = (D_c(1),D_c(2),\ldots, D_c(n_{\text{cut}}))$, $n_{\text{cut}} = \text{round}(N/10)$, and the covariance and variance are defined with vectors x, y of length q as follows:

$$\text{cov}(x,y) = \frac{1}{q}\sum_{j=1}^{q}(x(j)-\overline{x})(y(j)-\overline{y}),$$
$$\overline{x} = \frac{1}{q}\sum_{j=1}^{q}x(j), \qquad \text{var}(x) = \text{cov}(x,x). \quad (36)$$

Step 5. Interpret the outputs as follows:

(1) $K \approx 0$ indicates that the underlying dynamics is regular (i.e., periodic or quasiperiodic), whereas $K \approx 1$ indicates that the underlying dynamics is chaotic;

(2) bounded trajectories in the (p,s)-plane imply that the underlying dynamics is regular, whereas the Brownian-like (unbounded) trajectories imply that the underlying dynamics is chaotic.

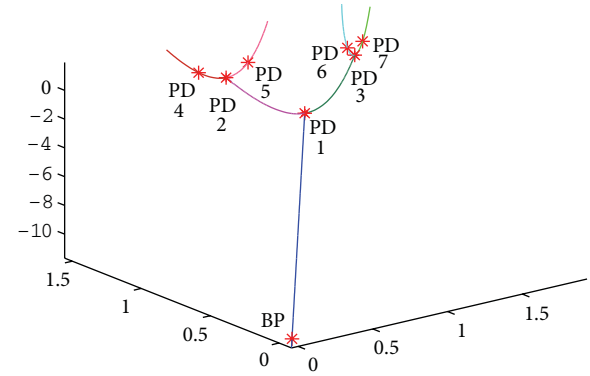

Figure 6: Curves of fixed points of the 1st, 2nd, and 4th iterates.

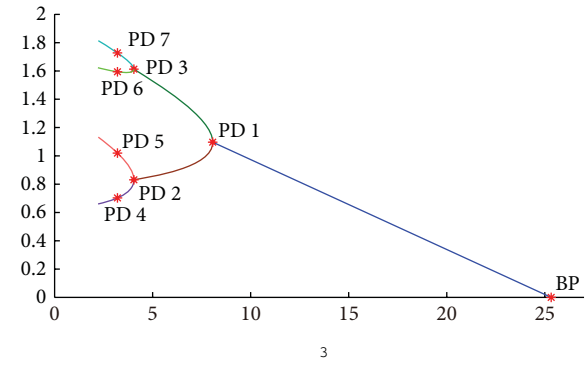

Figure 7: Continuation of E_1 in (s_3,x)-space.

5.2.2. Application. We use the data set p_x of the system (22) to implement the 0-1 test with s_2 and s_2, respectively. The new

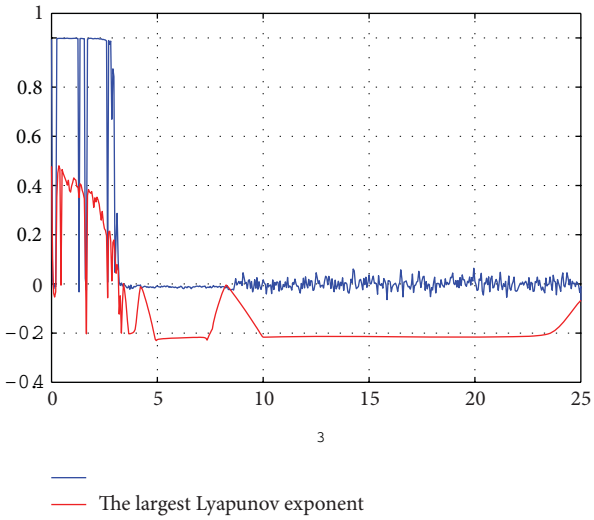

Figure 8: K and the largest Lyapunov exponent versus $s_3 \in [0, 25]$ and $s_2 = 0.2$.

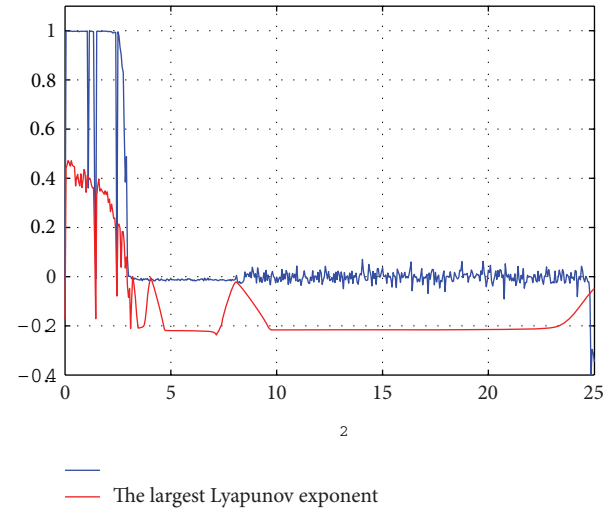

Figure 11: K and the largest Lyapunov exponent versus $s_2 \in [0, 25]$ and $s_3 = 0.4$.

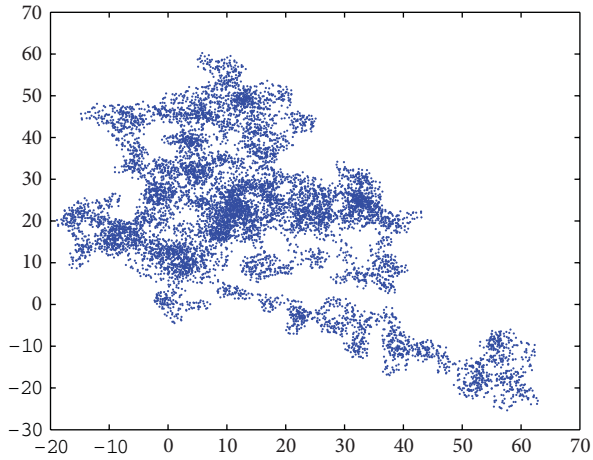

Figure 9: Plots versus $s_2 = 0.2$ and $s_3 = 1$ in new coordinates (p, s) space.

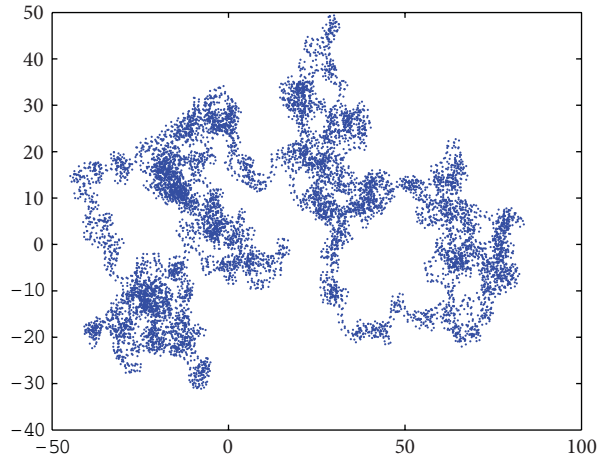

Figure 12: Plots versus $s_2 = 0.1$ and $s_3 = 0.4$ in new coordinates (p, s) space.

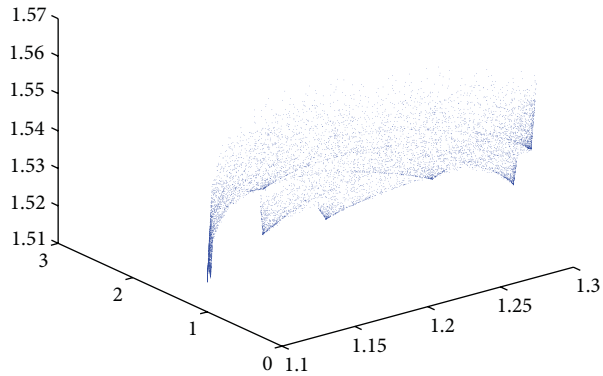

Figure 10: Plots versus $s_2 = 0.1$ and $s_3 = 1$ in the original state space.

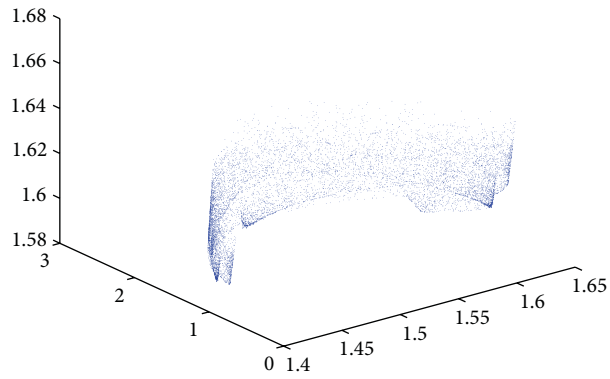

Figure 13: Plots versus $s_2 = 0.1$ and $s_3 = 0.4$ in the original state space.

coordinates variables (p, s) are shown in Figures 8, 9, 10, 11, 12, and 13.

When $s_2 = 0.2$ is fixed and s_3 varies from 0 to 25 in increments of 0.05, one can get the diagram of K value as shown in Figure 8, which is consistent with the numerical simulation in the above sections. If $s_3 = 1$, then $K \approx 1$, which means that the system is chaotic as shown in Figures 9 and 10.

Similarly, fixing $s_3 = 0.4$ and varying s_2 from 0 to 25 in increments of 0.05, one can get the diagram of K value as shown in Figure 11, which well coincides with the numerical simulation in the above sections. If $s_2 = 0.1$, then $K \approx 1$, which means that the system is chaotic as shown in Figures 12 and 13.

From Figures 8 and 11, it can be observed that there is a very good agreement between the largest Lyapunov exponent and the median value of correlation coefficient K.

6. Conclusion

In this paper, we have proposed a nonlinear discrete price game model of irrigation water in a coastal irrigation district. Its stability and codimension-two period-doubling (flip) bifurcation are emphatically discussed. Based on continuation methods, its numerical bifurcations are analyzed by using the MATLAB package Cl_MatContM. Its numerical chaos is shown by means of the 0-1 test algorithm.

Acknowledgments

This work is supported partly by the Excellent Young Scientist Foundation of Shandong Province (Grant no. BS2011SF018), the National Social Science Foundation of China (Grant no. 12BJY103), the Humanities and Social Sciences Foundation of the Ministry of Education of China (Grant no. 11YJCZH200), and the National Natural Science Foundation of China (Grant no. 71272148).

References

[1] D. Merrey, R. Meinzen-Dick, P. Mollinga, and E. Karar, "Policy and institutional reform processes for sustainable agricultural water management: the art of the possible," in *Water for Food Water for Life: A Comprehensive Assessment of Water Management in Agriculture*, D. Molden, Ed., pp. 193–232, Earthscan, London, UK, 2007.

[2] R. Meinzen-Dick, "Beyond panaceas in water institutions," *Proceedings of the National Academy of Sciences of the United States of America*, vol. 104, no. 39, pp. 15200–15205, 2007.

[3] W. Shaw, *Water Resource Economics And Policy: An Introduction*, Edward Elgar, Cheltenham, UK, 2005.

[4] R. Griffin, *Water Resource Economics: The Analysis of Scarcity, Policies, and Projects*, MIT Press, Cambridge, Mass, USA, 2006.

[5] R. Johansson, Y. Tsur, T. Roe, R. Doukkali, and A. Dinar, "Pricing irrigation water: a review of theory and practice," *Water Policy*, vol. 4, no. 2, pp. 173–199, 2002.

[6] K. Schoengold, "Irrigation water pricing: the gap between theory and practice," *American Journal of Agricultural Economics*, vol. 92, no. 5, pp. 1497–1498, 2010.

[7] B. Xin, J. Ma, and Q. Gao, "Complex dynamics of an adnascent-type game model," *Discrete Dynamics in Nature and Society*, vol. 2008, Article ID 467972, 12 pages, 2008.

[8] B. Xin and T. Chen, "Master-slave bertrand game model," *Economic Modelling*, vol. 28, no. 4, pp. 1864–1870, 2011.

[9] W. Ji and D. Xu, "Complexity of discrete investment competition model based on heterogeneous participants," *International Journal of Computer Mathematics*, vol. 89, no. 4, pp. 492–498, 2012.

[10] T. Puu, "Chaos in business cycles," *Chaos, Solitons and Fractals*, vol. 1, no. 5, pp. 457–473, 1991.

[11] G. Bischi, A. Naimzada, and L. Sbragia, "Oligopoly games with local monopolistic approximation," *Journal of Economic Behavior & Organization*, vol. 62, no. 3, pp. 371–388, 2007.

[12] H. N. Agiza and A. A. Elsadany, "Nonlinear dynamics in the Cournot duopoly game with heterogeneous players," *Physica A*, vol. 320, no. 1–4, pp. 512–524, 2003.

[13] J. Wouter and H. Den, "The importance of the number of different agents in a heterogeneous asset-pricing model," *Journal of Economic Dynamics & Control*, vol. 25, no. 5, pp. 721–746, 2001.

[14] A. Elsadany, "Competition analysis of a triopoly game with bounded rationality," *Chaos Solitons & Fractals*, vol. 45, no. 11, pp. 1343–1348, 2012.

[15] W. Ji, "Chaos and control of game model based on heterogeneous expectations in electric power triopoly," *Discrete Dynamics in Nature and Society*, vol. 2009, Article ID 469564, 8 pages, 2009.

[16] Y. Son, R. Baldick, K. Lee, and S. Siddiqi, "Short-term electricity market auction game analysis: uniform and pay-as-bid pricing," *IEEE Transactions on Power Systems*, vol. 19, pp. 1990–1998, 2004.

[17] C. C. Skoulidas, C. D. Vournas, and G. P. Papavassilopoulos, "An adaptive learning game model for interacting electric power markets," *Infor*, vol. 48, no. 4, pp. 261–266, 2010.

[18] L. Mu, P. Liu, Y. Li, and J. Zhang, "Complexity of a real estate game model with a nonlinear demand function," *International Journal of Bifurcation and Chaos*, vol. 21, no. 11, pp. 3171–3179, 2011.

[19] L. Mu, J. Ma, and L. Chen, "A 3-dimensional discrete model of housing price and its inherent complexity analysis," *Journal of Systems Science & Complexity*, vol. 22, no. 3, pp. 415–421, 2009.

[20] X. Liu, X. Liang, and B. Tang, "Minority game and anomalies in financial markets," *Physica A*, vol. 333, pp. 343–352, 2004.

[21] K. Gkonis and H. Psaraftis, "The LNG market: a game theoretic approach to competition in LNG shipping," *Maritime Economics & Logistics*, vol. 11, pp. 227–246, 2009.

[22] Z. Sun and J. Ma, "Complexity of triopoly price game in Chinese cold rolled steel market," *Nonlinear Dynamics*, vol. 67, no. 3, pp. 2001–2008, 2012.

[23] S. Sugawara and Y. Omori, "Duopoly in the Japanese airline market: bayesian estimation for the entry game," *The Japanese Economic Review*, vol. 63, no. 3, pp. 310–332, 2012.

[24] S. Chung, R. Weaver, and T. Friesz, "Oligopolies in pollution permit markets: a dynamic game approach," *International Journal of Production Economics*, vol. 140, no. 1, pp. 48–56, 2012.

[25] J. Ma and J. Zhang, "Price game and chaos control among three oligarchs with dierent rationalities in property insurance market," *Chaos*, vol. 22, no. 4, Article ID 043120, 2012.

[26] F. Tramontana and A. E. A. Elsadany, "Heterogeneous triopoly game with isoelastic demand function," *Nonlinear Dynamics*, vol. 68, no. 1-2, pp. 187–193, 2012.

[27] J. Du, T. Huang, and Z. Sheng, "Analysis of decision-making in economic chaos control," *Nonlinear Analysis*, vol. 10, no. 4, pp. 2493–2501, 2009.

[28] W. Huang, "The long-run benefits of chaos to oligopolistic firms," *Journal of Economic Dynamics & Control*, vol. 32, no. 4, pp. 1332–1355, 2008.

[29] J. Zhang, Q. Da, and Y. Wang, "The dynamics of Bertrand model with bounded rationality," *Chaos, Solitons and Fractals*, vol. 39, no. 5, pp. 2048–2055, 2009.

[30] M. Kopel, "Simple and complex adjustment dynamics in Cournot duopoly models," *Chaos, Solitons and Fractals*, vol. 7, no. 12, pp. 2031–2048, 1996.

[31] F. Tramontana, L. Gardini, and T. Puu, "Cournot duopoly when the competitors operate multiple production plants," *Journal of Economic Dynamics & Control*, vol. 33, no. 1, pp. 250–265, 2009.

[32] F. Tramontana, "Heterogeneous duopoly with isoelastic demand function," *Economic Modelling*, vol. 27, no. 1, pp. 350–357, 2010.

[33] G. A. Gottwald and I. Melbourne, "On the implementation of the 0-1 test for chaos," *SIAM Journal on Applied Dynamical Systems*, vol. 8, no. 1, pp. 129–145, 2009.

[34] G. A. Gottwald and I. Melbourne, "On the validity of the 0-1 test for chaos," *Nonlinearity*, vol. 22, no. 6, pp. 1367–1382, 2009.

[35] G. Gottwald and I. Melbourne, "Comment on Reliability of the 0-1 test for chaos," *Physical Review E*, vol. 77, no. 2, part 2, 3 pages, 2008.

[36] I. Falconer, G. A. Gottwald, I. Melbourne, and K. Wormnes, "Application of the 0-1 test for chaos to experimental data," *SIAM Journal on Applied Dynamical Systems*, vol. 6, no. 2, pp. 395–402, 2007.

[37] K. Sun, X. Liu, and C. Zhu, "The 0-1 test algorithm for chaos and its applications," *Chinese Physics B*, vol. 19, no. 11, Article ID 110510, 2010.

[38] L. Yuan and Q. Yang, "A proof for the existence of chaos in diffusively coupled map lattices with open boundary conditions," *Discrete Dynamics in Nature and Society*, vol. 2011, Article ID 174376, 16 pages, 2011.

[39] W. Govaerts and A. Y. Kuznetsov, "Matcont: a Matlab software project for the numerical continuation and bifurcation study of continuous and discrete parameterized dynamical systems," http://sourceforge.net.

[40] W. Govaerts, R. K. Ghaziani, Yu. A. Kuznetsov, and H. G. E. Meijer, "Numerical methods for two-parameter local bifurcation analysis of maps," *SIAM Journal on Scientific Computing*, vol. 29, no. 6, pp. 2644–2667, 2007.

[41] W. Govaerts and R. K. Ghaziani, "Stable cycles in a Cournot duopoly model of Kopel," *Journal of Computational and Applied Mathematics*, vol. 218, no. 2, pp. 247–258, 2008.

[42] R. K. Ghaziani, W. Govaerts, and C. Sonck, "Resonance and bifurcation in a discrete-time predator-prey system with Holling functional response," *Nonlinear Analysis*, vol. 13, no. 3, pp. 1451–1465, 2012.

[43] R. K. Ghaziani, W. Govaerts, and C. Sonck, "Codimension-two bifurcations of fixed points in a class of discrete prey-predator systems," *Discrete Dynamics in Nature and Society*, vol. 2011, Article ID 862494, 27 pages, 2011.

[44] R. Gibbons, *A Primer in Game Theory*, Simon and Schuster, New York, NY, USA, 1992.

[45] A. Dixit, "Comparative statics for oligopoly," *International Economic Review*, vol. 27, no. 1, pp. 107–122, 1986.

[46] G. Bischi and M. Kopel, "Equilibrium selection in a nonlinear duopoly game with adaptive expectations," *Journal of Economic Behavior & Organization*, vol. 46, pp. 73–100, 2001.

[47] G. Wen, "Criterion to identify Hopf bifurcations in maps of arbitrary dimension," *Physical Review E*, vol. 72, no. 2, Article ID 026201, p. 4, 2005.

[48] G. Wen, D. Xu, and X. Han, "On creation of Hopf bifurcations in discrete-time nonlinear systems," *Chaos*, vol. 12, no. 2, pp. 350–355, 2002.

[49] Q. Lu, *Bifurcation and Singularity*, Shanghai Scientific and Technological Education Publishing House, Shanghai, China, 1995.

[50] Y. A. Kuznetsov, *Elements of Applied Bifurcation Theory*, vol. 112 of *Applied Mathematical Sciences*, Springer, New York, NY, USA, 2nd edition, 1998.

[51] E. L. Allgower and K. Georg, *Numerical Continuation Methods*, vol. 13 of *Springer Series in Computational Mathematics*, Springer, Berlin, Germany, 1990.

[52] A. Wolf, J. B. Swift, H. L. Swinney, and J. A. Vastano, "Determining Lyapunov exponents from a time series," *Physica D*, vol. 16, no. 3, pp. 285–317, 1985.

Hindawi Publishing Corporation
Discrete Dynamics in Nature and Society
Volume 2013, Article ID 385419, 9 pages
http://dx.doi.org/10.1155/2013/385419

Research Article

Bifurcation of Limit Cycles of a Class of Piecewise Linear Differential Systems in $\Re^4$ with Three Zones

Yanyan Cheng

Department of Electronics and Information Engineering, Huazhong University of Science and Technology, Wuhan 430074, China

Correspondence should be addressed to Yanyan Cheng; cdymore@126.com

Received 1 March 2013; Accepted 16 April 2013

Academic Editor: Qingdu Li

We study the bifurcation of limit cycles from periodic orbits of a four-dimensional system when the perturbation is piecewise linear with two switching boundaries. Our main result shows that when the parameter is sufficiently small at most, six limit cycles can bifurcate from periodic orbits in a class of asymmetric piecewise linear perturbed systems, and, at most, three limit cycles can bifurcate from periodic orbits in another class of asymmetric piecewise linear perturbed systems. Moreover, there are perturbed systems having six limit cycles. The main technique is the averaging method.

1. Introduction and Statement of the Main Result

Piecewise linear systems are used extensively to model many physical phenomena, such as switching circuits in power electronics [1, 2] and impact and dry frictions in mechanical systems [3]. These systems exhibit not only standard bifurcations but also complicated dynamical phenomena not existing in smooth systems. The study and classification of various kinds of bifurcation phenomena for piecewise linear systems have attracted great attentions since the last century, see, for example, [4, 5] and the references therein.

In recent years, many papers studied the bifurcation of limit cycles and the number and distribution of these limit cycles. Most of them studied the planar piecewise linear system, see for example, [6–9] and the references quoted there. There are also some papers which studied bifurcation of limit cycles of 3D piecewise linear systems [10, 11]. For high-dimensional cases, there are a few papers [12–16]. Especially in [12] the authors studied the bifurcation of limit cycles of a class of piecewise linear systems in $\Re^4$. They showed that three is an upper bound for the number of limit cycles that bifurcate from periodic orbits.

In this paper, we study the limit cycles bifurcated from periodic orbits of a linear differential system in $\Re^4$ when the perturbation is piecewise linear with two switching boundaries. We consider two classes of asymmetric perturbation. With the first class of asymmetric perturbation, six is the upper bound for the number of limit cycles bifurcated from periodic orbits, and there are perturbed systems having six limit cycles. With the second class of asymmetric perturbation, three is the upper bound for the number of limit cycles bifurcated from periodic orbits, which generalizes the result of the paper [12].

More precisely, we study the maximum number of limit cycles of the 4-dimensional continuous piecewise linear vector fields with three zones of the form

$$\dot{x} = A_0 x + \varepsilon F(x), \tag{1}$$

for $\varepsilon \neq 0$ sufficiently small real parameter, where

$$A_0 = \begin{pmatrix} 0 & -1 & 0 & 0 \\ 1 & 0 & 0 & 0 \\ 0 & 0 & 0 & -1 \\ 0 & 0 & 1 & 0 \end{pmatrix}, \tag{2}$$

and $F : \Re^4 \to \Re^4$ is given by

$$F(x) = Ax + \varphi\left(k^T x\right) b, \tag{3}$$

with $A \in M_4(\Re)$, $k, b \in \Re^4 \setminus \{0\}$, and $\varphi : \Re \to \Re$ the piecewise linear function

if $m_1 < 0 < m_2$,

$$\varphi(x) = \begin{cases} hm_1, & \text{for } x \in (-\infty, m_1), \\ hx, & \text{for } x \in (m_1, m_2), \\ hm_2, & \text{for } x \in (m_2, +\infty); \end{cases} \tag{4}$$

if $m_1 < m_2 < 0$,

$$\varphi(x) = \begin{cases} hm_1 - hm_2, & \text{for } x \in (-\infty, m_1), \\ hx - hm_2, & \text{for } x \in (m_1, m_2), \\ 0, & \text{for } x \in (m_2, +\infty); \end{cases} \tag{5}$$

if $0 < m_1 < m_2$,

$$\varphi(x) = \begin{cases} 0, & \text{for } x \in (-\infty, m_1), \\ hx - hm_1, & \text{for } x \in (m_1, m_2), \\ hm_2 - hm_1, & \text{for } x \in (m_2, +\infty), \end{cases} \tag{6}$$

where $h \in \mathfrak{R} \setminus \{0\}$. The independent variable is denoted by t; vectors of $\mathfrak{R}^4$ are column vectors, and k^T denotes a transposed vector.

For $\varepsilon = 0$, system (1) becomes

$$\dot{x}_1 = -x_2, \qquad \dot{x}_2 = x_1, \qquad \dot{x}_3 = -x_4, \qquad \dot{x}_4 = x_3. \tag{7}$$

Our main results are the following.

Theorem 1. *If $m_1 m_2 > 0$, six is the upper bound for the number of limit cycles of system* (1) *which bifurcate from the periodic orbits of system* (7) *with ε sufficiently small. Moreover, there are systems of form* (1) *having six limit cycles.*

Theorem 2. *If $m_1 m_2 < 0$, three is the upper bound for the number of limit cycles of system* (1) *which bifurcate from the periodic orbits of system* (7) *with ε sufficiently small. Moreover, there are systems of form* (1) *having three limit cycles.*

It is worth to note that Theorem 2 generalizes the result of paper [12]. The method for computing the number of limit cycles bifurcated from periodic orbits is the averaging method, which is obtained by Buică and Llibre [17]. By means of the result of paper [18], we can study the stability of the limit cycles of Theorem 1; for more details see Remark 10.

Theorems 1 and 2 will be proved in Section 3. In Section 2, we review the results from the averaging theory necessary for proving these two theorems. Further discussions on the number of limit cycles of the perturbed system are present in Section 4. There is a conclusion given in the last section.

2. First-Order Averaging Method

The aim of this section is to review the first-order averaging method which is obtained by Buică and Llibre [17]. The advantage of this method is that the smoothness assumptions for the vector field of the differential system are minimal.

Theorem 3 (see [17]). *Consider the following differential system:*

$$\dot{x}(t) = \varepsilon H(t, \varepsilon) + \varepsilon^2 R(t, x, \varepsilon), \tag{8}$$

where $H : \mathfrak{R} \times D \to \mathfrak{R}^n$, $R : \mathfrak{R} \times D \times (-\varepsilon_0, \varepsilon_0) \to \mathfrak{R}^n$ are continuous functions. T-periodic in the first variable, and D is an open subset of $\mathfrak{R}^n$. We define $h : D \to \mathfrak{R}^n$ as

$$h(z) = \int_0^T H(s, z)\, ds, \tag{9}$$

and assume that

(i) *H and R are locally Lipschitz with respect to x;*

(ii) *for $a \in D$ with $h(a) = 0$, there exists a neighborhood V of a such that $h(z) \neq 0$ for all $z \in \overline{V} \setminus \{a\}$ and $d_B(h, V, 0) \neq 0$.*

Then, for $|\varepsilon| > 0$ sufficiently small, there exists an isolated T-periodic solution $\phi(\cdot, \varepsilon)$ of system (8) *such that $\phi(\cdot, \varepsilon) \to a$ as $\varepsilon \to 0$.*

We remind here that $d_B(h, V, a)$ denotes the Brouwer degree of the function h with respect to the set V and the point a, as is defined in [19]. The following fact is useful for the proof of Theorems 1 and 2.

Fact 1. Let $h : D \to \mathfrak{R}^n$ be a C^1 function, with $h(a) = 0$, where D is an open subset of $\mathfrak{R}^n$ and $a \in D$. Whenever a is a simple zero of h (i.e., $J(a) \neq 0$), there exists a neighborhood V of a such that $h(z) \neq 0$ for all $z \in \overline{V} \setminus \{a\}$. Then, $d_B(h, V, 0) \in \{-1, 1\}$.

3. Proof of Main Theorems

The proof of Theorems 1 and 2 is based on the first-order averaging method presented in the previous section. In order to apply this method, we will first reduce the four parameters of the vector k in the definition of the function $F(x)$ to one, and then we will change the variables in order to transform the system into the standard form for the averaging method. After that, we will calculate the number of its isolated zeros.

Lemma 4. *By a linear change of variables, system* (1) *can be transformed into the system*

$$\dot{x} = A_0 x + \varepsilon \overline{A} x + \varepsilon \varphi(x_1)\, \overline{b}, \tag{10}$$

where $\overline{A} \in M_4(\mathfrak{R})$ is an arbitrary matrix and $\overline{b} = (\overline{b}_1, \overline{b}_2, 0, 0)^T$ or $\overline{b} = e_3$.

Proof. A linear change of variables $x = Py$, with P invertible, transforms system (1) into

$$\dot{y} = P^{-1} A_0 P y + \varepsilon P^{-1} A P y + \varepsilon \varphi\left(k^T P y\right) P^{-1} b, \tag{11}$$

where $b = (b_1, b_2, b_3, b_4)^T$, $k = (k_1, k_2, k_3, k_4)^T$.

We have to find P invertible which satisfies

$$\begin{aligned} P^{-1} A_0 P &= A_0, \\ k^T P &= e_1^T. \end{aligned} \tag{12}$$

It is easy to obtain that P^{-1} has the following form:

$$P^{-1} = \begin{pmatrix} k_1 & k_2 & k_3 & k_4 \\ -k_2 & k_1 & -k_4 & k_3 \\ p_{31} & p_{32} & p_{33} & p_{34} \\ -p_{32} & p_{31} & -p_{34} & p_{33} \end{pmatrix}. \tag{13}$$

Thus, we have

$$P^{-1}b = \overline{b}, \tag{14}$$

where

$$\begin{aligned} \overline{b}_1 &= \sum_{i=1}^{4} k_i b_i, \qquad \overline{b}_2 = -k_2 b_1 + k_1 b_2 - k_4 b_3 + k_3 b_4, \\ \overline{b}_3 &= \sum_{i=1}^{4} p_{3i} b_i, \qquad \overline{b}_4 = -p_{32} b_1 + p_{31} b_2 - p_{34} b_3 + p_{33} b_4. \end{aligned} \tag{15}$$

If $\overline{b}_1^2 + \overline{b}_2^2 \neq 0$, it is easy to find P^{-1} invertible with p_{31}, p_{32}, p_{33}, p_{34} satisfying

$$\begin{aligned} \overline{b}_3 &= \sum_{i=1}^{4} p_{3i} b_i = 0, \\ \overline{b}_4 &= -p_{32} b_1 + p_{31} b_2 - p_{34} b_3 + p_{33} b_4 = 0. \end{aligned} \tag{16}$$

If $\overline{b}_1^2 + \overline{b}_2^2 = 0$, it is easy to find P^{-1} invertible with p_{31}, p_{32}, p_{33}, p_{34} satisfying

$$\begin{aligned} \overline{b}_3 &= \sum_{i=1}^{4} p_{3i} b_i = 1, \\ \overline{b}_4 &= -p_{32} b_1 + p_{31} b_2 - p_{34} b_3 + p_{33} b_4 = 0. \end{aligned} \tag{17}$$

Changing variables y to x with $x = y$, then we obtain system (10). □

The standard form of the averaging method is obtained by changing variables (x_1, x_2, x_3, x_4) to (r, θ, ρ, s) with

$$\begin{aligned} x_1 &= r\cos\theta, \qquad x_2 = r\sin\theta, \\ x_3 &= \rho\cos(\theta + s), \qquad x_4 = \rho\sin(\theta + s). \end{aligned} \tag{18}$$

Thus, system (10) is transformed into the following system:

$$\begin{aligned} \frac{dr}{d\theta} &= \varepsilon H_1(\theta, r, \rho, s) + \varepsilon^2 O(1), \\ \frac{d\rho}{d\theta} &= \varepsilon H_2(\theta, r, \rho, s) + \varepsilon^2 O(1), \\ \frac{ds}{d\theta} &= \varepsilon H_3(\theta, r, \rho, s) + \varepsilon^2 O(1), \end{aligned} \tag{19}$$

where H_1, H_2, and H_3 are given by

$$\begin{aligned} H_1 &= \cos\theta F_1 + \sin\theta F_2, \\ H_2 &= \cos(\theta + s) F_3 + \sin(\theta + s) F_4, \\ H_3 &= \frac{1}{r}\sin\theta F_1 - \frac{1}{r}\cos\theta F_2 - \frac{1}{\rho}\sin(\theta + s) F_3 \\ &\quad + \frac{1}{\rho}\cos(\theta + s) F_4 \end{aligned} \tag{20}$$

and for every $i = 1, 2, \ldots, 4$,

$$\begin{aligned} F_i &= a_{i1} r\cos\theta + a_{i2} r\sin\theta + a_{i3}\rho\cos(\theta + s) + a_{i4}\rho\sin(\theta + s) \\ &\quad + \varphi(r\cos\theta)\,\overline{b}_i, \end{aligned} \tag{21}$$

where a_{ij} are elements of the matrix $\overline{A}$ of Lemma 4.

We take ε_0 sufficiently small, m arbitrarily large and

$$D_m = \left\{ (r, \rho, s) \mid (r, \rho, s) \in \left(\frac{1}{m}, m\right)^2 \times S \right\}. \tag{22}$$

Then, the vector of system (19) is well defined and continuous on $S \times D_m \times (-\varepsilon_0, \varepsilon_0)$. Moreover, the system is 2π-periodic with respect to variable θ and locally Lipschitz with respect to variables (r, ρ, s). Our next step is to find the corresponding function $h : D \to \mathfrak{R}^3$, $h = (h_1, h_2, h_3)$, where

$$h_i(r, \rho, s) = \int_0^{2\pi} H_i(r, \theta, \rho, s)\, d\theta, \tag{23}$$

for $i = 1, 2, 3$.

In order to calculate the exact expression of h, we denote

$$I_1(r) = \int_0^{2\pi} \varphi(r\cos\theta)\cos\theta d\theta, \tag{24}$$

$$I_2(r) = \int_0^{2\pi} \varphi(r\cos\theta)\sin\theta d\theta, \tag{25}$$

for each $r > 0$, where φ is the piecewise linear function given by (4)–(6). Without loss of generality, we assume that the slope h of φ is positive.

Lemma 5. *The integrals I_1 and I_2 given by* (24)-(25)*, respectively, have the following expressions:*

$$I_2(r) = 0, \quad \forall r > 0,\ m_1, m_2, \tag{26}$$

and

(1) *if* $0 < m_1 < m_2$,

$$I_1(r) = \begin{cases} 0, & \text{if } 0 < r \le m_1, \\ J(r, m_1), & \text{if } m_1 < r < m_2, \\ K(r, m_1, m_2), & \text{if } r \ge m_2; \end{cases} \tag{27}$$

(2) *if* $m_1 < m_2 < 0$,

$$I_1(r) = \begin{cases} 0, & \text{if } 0 < r \le |m_2|, \\ -J(r, m_2), & \text{if } |m_2| < r < |m_1|, \\ K(r, m_1, m_2), & \text{if } r \ge |m_1|; \end{cases} \tag{28}$$

(3) *if* $m_1 < 0 < m_2$ *and* $|m_1| < |m_2|$,

$$I_1(r) = \begin{cases} \pi hr, & \text{if } 0 < r \le |m_1|, \\ \pi hr + J(r, m_1), & \text{if } |m_1| < r < m_2, \\ \pi hr + K(r, m_1, m_2), & \text{if } r \ge m_2; \end{cases} \quad (29)$$

(4) *if* $m_1 < 0 < m_2$ *and* $|m_1| > |m_2|$,

$$I_1(r) = \begin{cases} \pi hr, & \text{if } 0 < r \le m_2, \\ \pi hr - J(r, m_2), & \text{if } m_2 < r < |m_1|, \\ \pi hr + K(r, m_1, m_2), & \text{if } r \ge |m_1|; \end{cases} \quad (30)$$

(5) *if* $m_1 < 0 < m_2$ *and* $|m_1| = |m_2| = m$,

$$I_1(r) = \begin{cases} \pi hr, & \text{if } 0 < r \le m, \\ \pi hr - 2J(r, m), & \text{if } r > m, \end{cases} \quad (31)$$

where

$$J(r, m_i) = hr\left(\arctan\frac{\sqrt{r^2 - m_i^2}}{m_i} - \frac{m_i\sqrt{r^2 - m_i^2}}{r^2}\right), \quad (32)$$

for $i = 1, 2$, *and*

$$K(r, m_1, m_2) = hr\left(\arctan\frac{\sqrt{r^2 - m_1^2}}{m_1} - \arctan\frac{\sqrt{r^2 - m_2^2}}{m_2} - \frac{m_1\sqrt{r^2 - m_1^2}}{r^2} + \frac{m_2\sqrt{r^2 - m_2^2}}{r^2}\right). \quad (33)$$

The proof of this lemma is given in the appendix.

Remark 6. If $m_1 < 0 < m_2$ and $|m_1| = |m_2|$, system (1) can be transformed into the system which is studied in the paper [12].

Lemma 7. *If* $m_1 m_2 > 0$, *one defines* $\overline{m} = \max(|m_1|, |m_2|)$, $\underline{m} = \min(|m_1|, |m_2|)$ *and consider the equation* $I_1(r) = cr$, $r > 0$ *with* I_1 *given by* (24), *and* c *is a real parameter. Then,*

(1) *if* $c < 0$ *or* $c > h(\arctan(\overline{m}/\underline{m}) - \arctan(\underline{m}/\overline{m}))$, *the equation has no solutions;*

(2) *if* $c = 0$, *then the interval* $(0, \underline{m}]$ *is a continuum of solutions;*

(3) *if* $c = h(\arctan(\overline{m}/\underline{m}) - \arctan(\underline{m}/\overline{m}))$, *there is an unique solution* $r^* = \sqrt{\overline{m}^2 + \underline{m}^2}$;

(4) *if* $c \in (0, h(\arctan(\overline{m}/\underline{m}) - \arctan(\underline{m}/\overline{m})))$, *there are two solutions* $r_1^* < \sqrt{\overline{m}^2 + \underline{m}^2}$ *and* $r_2^* > \sqrt{\overline{m}^2 + \underline{m}^2}$.

Proof. If $0 < m_1 < m_2$, we have $\overline{m} = m_2$ and $\underline{m} = m_1$. It is easy to see that all $r \in (0, \underline{m}]$ are a solution if $c = 0$. If $c \neq 0$ changing the variable $u = \sqrt{r^2 - m_1^2}/m_1$ and defining $g(u) = I_1(r)/hr$, we obtain the equivalent equation

$$g(u) = \begin{cases} \arctan u - \dfrac{u}{1+u^2}, & \text{if } u \in \left(0, \dfrac{\sqrt{m_2^2 - m_1^2}}{m_1}\right], \\ \arctan u - \dfrac{u}{1+u^2} - \arctan\dfrac{\sqrt{(1+u^2)m_1^2 - m_2^2}}{m_2} + \dfrac{m_2\sqrt{(1+u^2)m_1^2 - m_2^2}}{m_1^2(1+u^2)}, & \text{if } u \in \left(\dfrac{\sqrt{m_2^2 - m_1^2}}{m_1}, +\infty\right) \end{cases} \quad (34)$$

with simple computation; we find that the function g is strictly monotonically increasing of variable u when $u \in (0, m_2/m_1)$ and strictly monotonically decreasing when $u \in (m_2/m_1, +\infty)$. The function g gets to the maximal value $g_{\max} = \arctan(m_2/m_1) - \arctan(m_1/m_2)$ when $u = m_2/m_1$. Also we have $f(u) \to 0$ as $u \to 0$ and $u \to +\infty$. The proof is similar if $m_1 < m_2 < 0$. □

Lemma 8. *If* $m_1 m_2 < 0$, *one defines* $\underline{m} = \min(|m_1|, |m_2|)$ *and consider the equation* $I_1(r) = cr$, $r > 0$ *with* I_1 *given by* (24), *and* c *is a real parameter. Then,*

(1) *if* $c < 0$ *or* $c > \pi h$, *the equation has no solutions;*

(2) *if* $c = \pi h$, *then the interval* $(0, \underline{m}]$ *is a continuum of solutions;*

(3) *if* $c \in (0, \pi h)$, *there is an unique solution* r^*.

Proof. We only consider the case when $|m_1| < |m_2|$: the proof is similar when $|m_1| > |m_2|$ and $|m_1| = |m_2|$. It is easy to see that all $r \in (0, |m_1|]$ are a solution if $c = \pi h$. If $c \neq 0$ changing the variable $u = \sqrt{r^2 - m_1^2}/m_1$ and defining $g(u) = I_1(r)/hr$, we obtain the equivalent equation

$$g(u) = \begin{cases} \pi + \arctan u - \dfrac{u}{1+u^2}, & \text{if } u \in \left[\dfrac{m_2^2 - m_1^2}{m_1}, 0\right), \\ \pi + \arctan u - \dfrac{u}{1+u^2} - \arctan\dfrac{\sqrt{(1+u^2)m_1^2 - m_2^2}}{m_2} + \dfrac{m_2\sqrt{(1+u^2)m_1^2 - m_2^2}}{m_1^2(1+u^2)}, & \text{if } u \in \left(-\infty, \dfrac{\sqrt{m_2^2 - m_1^2}}{m_1}\right). \end{cases} \quad (35)$$

With simple computation, we find that the function g is strictly monotonically increasing of variable u. It is easy to know $f(u) \to \pi$ as $u \to 0$ and $f(u) \to 0$ as $u \to -\infty$. □

With Lemma 5, we obtain the expressions for the components of function h,

$$h_1(r, \rho, s) = c_1 r + c_2 \rho \cos s + c_3 \rho \sin s + \overline{b}_1 I_1(r),$$

$$h_2(r,\rho,s) = c_7\rho + c_5 r\cos s + c_6 r\sin s + \bar{b}_3\cos s I_1(r),$$
$$h_3(r,\rho,s) = c_4 + (c_3\cos s - c_2\sin s)\frac{\rho}{r} + (c_6\cos s - c_5\sin s)\frac{r}{\rho} - \bar{b}_3\sin s\frac{I_1(r)}{\rho} - \bar{b}_2\frac{I_1(r)}{r}, \tag{36}$$

where c_i are constants that depend linearly on a_{ij}

$$c_1 = (a_{11}+a_{22})\pi, \quad c_2 = (a_{13}+a_{24})\pi,$$
$$c_3 = (a_{14}-a_{23})\pi, \quad c_4 = (a_{43}+a_{12}-a_{34}-a_{21})\pi,$$
$$c_5 = (a_{31}+a_{42})\pi, \quad c_6 = (a_{41}-a_{32})\pi, \tag{37}$$
$$c_7 = (a_{33}+a_{44})\pi.$$

According to Theorem 3 and Fact 1, for each simple zero (r^*,ρ^*,s^*) of (36) there is an isolated 2π-periodic solution $\phi(\cdot,\varepsilon)$ of system (19) with $|\varepsilon|\neq 0$ sufficiently small such that $\phi(\cdot,\varepsilon)\to(r^*,\rho^*,s^*)$ as $\varepsilon\to 0$. Any isolated 2π-periodic solution of system (19) with $|\varepsilon|\neq 0$ sufficiently small corresponds to a limit cycle of system (10). Thus, the most important task is to calculate the number of the simple zeros of function h. We solve the two first equations of (36), then, we get

$$I_1(r) = \frac{k_2(s)}{d(s)}\rho, \qquad r = \frac{k_1(s)}{d(s)}\rho, \tag{38}$$

where

$$d(s) = \left(\bar{b}_1c_5 - \bar{b}_3c_1\right)\cos s + \bar{b}_1c_6\sin s,$$
$$k_1(s) = \bar{b}_3\cos s\left(c_2\cos s + c_3\sin s\right) + \bar{b}_1c_7,$$
$$k_2(s) = c_1c_7 - c_2c_5\cos^2 s - c_3c_6\sin^2 s - \left(c_2c_6 + c_3c_5\right)\sin s\,\cos s. \tag{39}$$

Substituting (38) into the third equation, we obtain

$$h_3(r,\rho,s) = \frac{f(s)}{d(s)k_1(s)} = 0, \tag{40}$$

where

$$f(s) = c_4d(s)k_1(s) + (c_3\cos - c_2\sin s)d^2(s) + (c_6\cos s - c_5\sin s)k_1^2(s) - \bar{b}_3\sin s k_1(s)k_2(s) - \bar{b}_2d(s)k_2(s). \tag{41}$$

It is necessary to study the zeros of f instead of the zeros of h.

Lemma 9. *The function $f:[0,2\pi)\to\mathfrak{R}$ given by formula (41) can have at most six isolated zeros, and they appear in pairs $\{s^*, s^*+\pi(\mathrm{mod}\,2\pi)\}$.*

Proof. Substituting $\cos s = x$ and $\sin s = \sqrt{1-x^2}$ in $f(s)=0$ we get

$$D_1x + D_3x^3 + \left(D_0 + D_2x^2\right)\sqrt{1-x^2} = 0, \tag{42}$$

where

$$D_0 = \bar{b}_1^2\left(c_2c_6^2 - c_4c_6c_7 + c_5c_7^2\right) + \bar{b}_1\bar{b}_2\left(c_3c_6^2 - c_1c_6c_7\right),$$
$$D_1 = \bar{b}_1^2\left(2c_2c_5c_6 - c_3c_6^2 - c_4c_5c_7 - c_6c_7^2\right) + \bar{b}_3^2\left(c_1c_3c_7 - c_6c_3^2\right) + \bar{b}_1\bar{b}_2\left(2c_2c_5c_6 + c_3c_5^2 - c_1c_5c_7\right),$$
$$D_2 = \bar{b}_1^2\left(c_2c_5^2 - c_2c_6^2 - 2c_3c_5c_6\right) + \bar{b}_3^2\left(c_1c_2c_7 + c_2c_1^2 - c_1c_3c_4 - 2c_2c_3c_6\right) + \bar{b}_1\bar{b}_2\left(2c_2c_5c_6 + c_3c_5^2 - c_3c_6^2\right),$$
$$D_3 = \bar{b}_1^2\left(c_3c_6^2 - c_3c_5^2 - 2c_2c_5c_6\right) + \bar{b}_3^2\left(c_3^2c_6 - c_3c_1^2 - c_1c_2c_4 - c_1c_3c_7 - c_6c_2^2\right) + \bar{b}_1\bar{b}_2\left(c_2c_5^2 - 2c_3c_5c_6 - c_2c_6^2\right). \tag{43}$$

When we consider the case $\cos s = x$ and $\sin s = -\sqrt{1-x^2}$, $f(s)=0$ becomes

$$D_1x + D_3x^3 - \left(D_0 + D_2x^2\right)\sqrt{1-x^2} = 0. \tag{44}$$

It follows that we have to find solutions of (42) or (44) in the interval $[-1,1]$. This is equivalent to

$$D_1x + D_3x^3 - \left(D_0 + D_2x^2\right)^2\left(1-x^2\right) = 0 \tag{45}$$

which is the polynomial equation

$$\left(D_3^2 + D_2^2\right)x^6 + \left(2D_1D_3 + 2D_0D_2 - D_2^2\right)x^4 + \left(D_1^2 + D_0^2 - 2D_0D_2\right)x^2 - D_0^2 = 0. \tag{46}$$

This equation can have at most six roots in the interval $[-1,1]$. Then, $f(s)=0$ has at most six solutions $s\in[0,2\pi)$. Since $f(s+\pi) = -f(s)$ for all $s\in[0,2\pi)$, it is clear that if s^* is a zero of f then $s^*+\pi(\mathrm{mod}\,2\pi)$ is also a zero. □

The functions $f(s)$, $d(s)$, $k_1(s)$, and $k_2(s)$ have the properties $f(s+\pi) = -f(s)$, $d(s+\pi) = -d(s)$, $k_1(s+\pi) = k_1(s)$, and $k_2(s+\pi) = k_2(s)$. So, we have

$$\frac{k_1(s)}{d(s)} > 0 \Longrightarrow \frac{k_1(s+\pi)}{d(s+\pi)} < 0. \tag{47}$$

Thus, the equation $h_3 = 0$ at most three zeros that satisfy $k_1(s)/d(s) > 0$. With Lemma 7 for a fixed s^*, we at most find two isolated value of r^* from $I_1(r)/r = k_2(s^*)/d(s^*)$. With Lemma 8 for a fixed s^*, we at most find one isolated value of r^* from $I_1(r)/r = k_2(s^*)/d(s^*)$. For fixed s^* and fixed r^*, $\rho/r = k_1(s^*)/d(s^*)$ gives at most one isolated value for ρ^*. Thus, we conclude that if $m_1m_2 > 0$ the maximum number of limit cycles for system (1) is six, and if $m_1m_2 < 0$ the maximum number of limit cycles for system (1) is three.

Remark 10. Using the main result of [18], the stability of the limit cycles associated with the solution (r^*, ρ^*, s^*) is given by the eigenvalues of the matrix

$$\left.\frac{\partial(h_1, h_2, h_3)}{\partial(r, \rho, s)}\right|_{(r,\rho,s)=(r^*,\rho^*,s^*)}. \tag{48}$$

In order to show that there exist examples with exactly six limit cycles, we consider the following values of the coefficients:

$$\begin{gathered} c_1 = -1, \qquad c_2 = \frac{-4\sqrt{3}}{3}, \qquad c_3 = 0, \\ c_4 = \frac{-4\sqrt{3}}{3}, \qquad c_5 = 0, \quad c_6 = 1, \qquad c_7 = -1, \\ \bar{b}_1 = 1, \qquad \bar{b}_2 = \bar{b}_3 = \bar{b}_4 = 0, \qquad h = 6, \\ m_1 = 1, \qquad m_2 = \sqrt{3}. \end{gathered} \tag{49}$$

More precisely, the system has the following form:

$$\dot{x} = A_0 x + \varepsilon A x + \varepsilon \varphi(x_1)\bar{b}, \tag{50}$$

where

$$\varphi(x_1) = \begin{cases} 0, & \text{for } x_1 \in (-\infty, 1), \\ 6x_1 - 6, & \text{for } x_1 \in \left(1, \sqrt{3}\right), \\ 6\sqrt{3} - 6, & \text{for } x_1 \in \left(\sqrt{3}, +\infty\right), \end{cases}$$

$$A_0 = \begin{pmatrix} 0 & -1 & 0 & 0 \\ 1 & 0 & 0 & 0 \\ 0 & 0 & 0 & -1 \\ 0 & 0 & 1 & 0 \end{pmatrix}, \tag{51}$$

$$A = \begin{pmatrix} a_{11} & a_{12} & a_{13} & a_{14} \\ a_{21} & a_{22} & a_{14} & a_{24} \\ a_{31} & a_{32} & a_{33} & a_{34} \\ a_{41} & -a_{31} & a_{43} & a_{44} \end{pmatrix}, \qquad \bar{b} = \begin{pmatrix} 1 \\ 0 \\ 0 \\ 0 \end{pmatrix},$$

and $a_{ij} \in \mathfrak{R}$ satisfy

$$\begin{gathered} (a_{11} + a_{22})\pi = -1, \qquad (a_{13} + a_{24})\pi = \frac{-4\sqrt{3}}{3}, \\ (a_{43} + a_{12} - a_{34} - a_{21})\pi = \frac{-4\sqrt{3}}{3}, \\ (a_{41} - a_{32})\pi = 1, \qquad (a_{33} + a_{44})\pi = -1. \end{gathered} \tag{52}$$

It is easy to know $6(\arctan\sqrt{3} - \arctan(\sqrt{3}/3)) = \pi$. Computing the six solutions of $f(s) = 0$, we get $\{\pi/6, \pi/3, \pi/2, 7\pi/6, 4\pi/3, 3\pi/2\}$. The values of $d(s^*)$, $k_1(s^*)$ and $k_2(s^*)$ are given in Table 1.

There are three values of s^* that satisfy $k_1(s^*)/d(s^*) > 0$ and $0 < k_2(s^*)/k_1(s^*) < \pi$. These three solutions are $\{\pi/6, \pi/3, \pi/2\}$.

The six values of solution s^*, r^*, ρ^* and the value of the Jacobian at the solution (r^*, ρ^*, s^*) are given in Table 2.

Table 1: The values of s^*, $d(s^*)$, $k_1(s^*)$, and $k_2(s^*)$.

s^*	$k_1(s^*)$	$d(s^*)$	$k_2(s^*)$
$\pi/6$	1	$1/2$	2
$\pi/3$	1	$\sqrt{3}/2$	2
$\pi/2$	1	1	1
$7\pi/6$	1	$-1/2$	2
$4\pi/3$	1	$-\sqrt{3}/2$	2
$3\pi/2$	1	-1	1

Table 2: The values of solution s^*, r^*, ρ^* and the Jacobian $Jh(r^*, \rho^*, s^*)$.

s^*	r^*	ρ^*	$Jh(r^*, \rho^*, s^*)$
$\pi/6$	1.484	0.742	11.957
$\pi/6$	4.139	2.07	−4.688
$\pi/3$	1.484	1.285	−3.27
$\pi/3$	4.139	3.585	−1.144
$\pi/2$	1.254	1.254	5.732
$\pi/2$	8.672	8.672	−0.964

4. Conclusion

In this paper, we have studied the limit cycles bifurcated from periodic orbits of a linear differential system in $\mathfrak{R}^4$ when the perturbation is piecewise linear with two switching boundaries. We considered two classes of asymmetric perturbation. We have found that the perturbed system could have at most six limit cycles with one class of the asymmetric perturbation and three limit cycles with the other class of asymmetric perturbation, which generalized the result of paper [12].

Appendix

The Proof of Lemma 5

Case 1 $(0 < m_1 < m_2)$. We have $|r\sin\theta| \le m_1$ and $|r\cos\theta| \le m_1$ for all $\theta \in [0, 2\pi)$ if $0 < r \le m_1$. Then, $\varphi(r\cos\theta) = 0$ for every θ. Thus,

$$I_1(r) = I_2(r) = 0. \tag{A.1}$$

We now fix $m_1 < r < m_2$ and consider $\theta_c \in (0, \pi/2)$ which satisfies $r\cos\theta_c = m_1$. Then, we have

$$\begin{aligned} I_1(r) &= \int_0^{\theta_c} (hr\cos\theta - hm_1)\cos\theta d\theta \\ &\quad + \int_{2\pi-\theta_c}^{2\pi} (hr\cos\theta - hm_1)\cos\theta d\theta \\ &= hr\theta_c - hm_1\sin\theta_c, \\ I_2(r) &= \int_0^{\theta_c} (hr\cos\theta - hm_1)\sin\theta d\theta \\ &\quad + \int_{2\pi-\theta_c}^{2\pi} (hr\cos\theta - hm_1)\sin\theta d\theta \\ &= 0. \end{aligned} \tag{A.2}$$

We now fix $r \geq m_2$ and consider $0 < \widetilde{\theta}_c < \theta_c < \pi/2$ which satisfies $r\cos\widetilde{\theta}_c = m_2$. Then, we have

$$\begin{aligned} I_1(r) &= \int_{-\widetilde{\theta}_c}^{\widetilde{\theta}_c} (hm_2 - hm_1)\cos\theta d\theta \\ &\quad + \int_{\widetilde{\theta}_c}^{\theta_c} (hr\cos\theta - hm_1)\cos\theta d\theta \\ &\quad + \int_{2\pi-\theta_c}^{2\pi-\widetilde{\theta}_c} (hr\cos\theta - hm_1)\cos\theta d\theta, \\ I_2(r) &= \int_{-\widetilde{\theta}_c}^{\widetilde{\theta}_c} (hm_2 - hm_1)\sin\theta d\theta \\ &\quad + \int_{\widetilde{\theta}_c}^{\theta_c} (hr\cos\theta - hm_1)\sin\theta d\theta \\ &\quad + \int_{2\pi-\theta_c}^{2\pi-\widetilde{\theta}_c} (hr\cos\theta - hm_1)\sin\theta d\theta. \end{aligned} \tag{A.3}$$

With simple computation, we get

$$\begin{aligned} I_1(r) &= hm_2\sin\widetilde{\theta}_c - hm_1\sin\theta_c + hr\theta_c - hr\widetilde{\theta}_c, \\ I_2(r) &= 0, \end{aligned} \tag{A.4}$$

where

$$\sin\theta_c = \frac{\sqrt{r^2 - m_1^2}}{r}, \qquad \sin\widetilde{\theta}_c = \frac{\sqrt{r^2 - m_2^2}}{r}, \tag{A.5}$$

$$\theta_c = \arctan\frac{\sqrt{r^2 - m_1^2}}{m_1}, \qquad \widetilde{\theta}_c = \arctan\frac{\sqrt{r^2 - m_2^2}}{m_2}. \tag{A.6}$$

Case 2 ($m_1 < m_2 < 0$). We have $|r\sin\theta| \leq |m_2|$ and $|r\cos\theta| \leq |m_2|$ for all $\theta \in [0, 2\pi)$ if $0 < r \leq |m_2|$. Then, $\varphi(r\cos\theta) = 0$ for every θ. Thus,

$$I_1(r) = I_2(r) = 0. \tag{A.7}$$

We fix now $|m_2| < r < |m_1|$ and consider $\theta_c \in (\pi/2, \pi)$ which satisfies $r\cos\theta_c = m_2$. Then, we have

$$\begin{aligned} I_1(r) &= \int_{\theta_c}^{2\pi-\theta_c} (hr\cos\theta - hm_2)\cos\theta d\theta \\ &= \pi hr - hr\theta_c + hm_2\sin\theta_c, \\ I_2(r) &= \int_{\theta_c}^{2\pi-\theta_c} (hr\cos\theta - hm_2)\sin\theta d\theta = 0. \end{aligned} \tag{A.8}$$

We now fix $r \geq |m_1|$ and consider $\widetilde{\theta}_c \in (\pi/2, \pi)$ which satisfies $r\cos\widetilde{\theta}_c = m_1$. Obviously, $\theta_c < \widetilde{\theta}_c$. Then, we have

$$\begin{aligned} I_1(r) &= \int_{\theta_c}^{\widetilde{\theta}_c} (hr\cos\theta - hm_2)\cos\theta d\theta \\ &\quad + \int_{\widetilde{\theta}_c}^{2\pi-\widetilde{\theta}_c} (hm_1 - hm_2)\cos\theta d\theta \\ &\quad + \int_{2\pi-\widetilde{\theta}_c}^{2\pi-\theta_c} (hr\cos\theta - hm_2)\cos\theta d\theta, \\ I_2(r) &= \int_{\theta_c}^{\widetilde{\theta}_c} (hr\cos\theta - hm_2)\sin\theta d\theta \\ &\quad + \int_{\widetilde{\theta}_c}^{2\pi-\widetilde{\theta}_c} (hm_1 - hm_2)\sin\theta d\theta \\ &\quad + \int_{2\pi-\widetilde{\theta}_c}^{2\pi-\theta_c} (hr\cos\theta - hm_2)\sin\theta d\theta. \end{aligned} \tag{A.9}$$

With simple computation, we get

$$\begin{aligned} I_1(r) &= hm_2\sin\theta_c - hm_1\sin\widetilde{\theta}_c - hr\theta_c + hr\widetilde{\theta}_c, \\ I_2(r) &= 0, \end{aligned} \tag{A.10}$$

where

$$\sin\theta_c = \frac{\sqrt{r^2 - m_2^2}}{r}, \qquad \sin\widetilde{\theta}_c = \frac{\sqrt{r^2 - m_1^2}}{r},$$

$$\theta_c = \pi + \arctan\frac{\sqrt{r^2 - m_2^2}}{m_2}, \qquad \widetilde{\theta}_c = \pi + \arctan\frac{\sqrt{r^2 - m_1^2}}{m_1}. \tag{A.11}$$

Case 3 ($m_1 < 0 < m_2$ and $|m_1| < |m_2|$). We have $|r\sin\theta| \leq |m_1|$ and $|r\cos\theta| \leq |m_1|$ for all $\theta \in [0, 2\pi)$ if $0 < r \leq |m_1|$. Then, $\varphi(r\cos\theta) = hr\cos\theta$ for every θ. Thus,

$$\begin{aligned} I_1(r) &= \int_0^{2\pi} hr\cos^2\theta d\theta = \pi hr, \\ I_2(r) &= \int_0^{2\pi} hr\cos\theta\sin\theta d\theta = 0. \end{aligned} \tag{A.12}$$

We fix now $|m_1| < r < |m_2|$ and consider $\theta_c \in (\pi/2, \pi)$ which satisfies $r\cos\theta_c = m_1$. Then, we have

$$\begin{aligned} I_1(r) &= \int_{-\theta_c}^{\theta_c} hr\cos^2\theta d\theta \\ &\quad + \int_{\theta_c}^{2\pi-\theta_c} hm_1\cos\theta d\theta = hr\theta_c - hm_1\sin\theta_c, \\ I_2(r) &= \int_{-\theta_c}^{\theta_c} hr\sin\theta\cos\theta d\theta + \int_{\theta_c}^{2\pi-\theta_c} hm_1\sin\theta d\theta = 0. \end{aligned} \tag{A.13}$$

We now fix $r \geq m_2$ and consider $\widetilde{\theta}_c \in (0, \pi/2)$ which satisfies $r\cos\widetilde{\theta}_c = m_2$. Then, we can write

$$\begin{aligned} I_1(r) &= \int_{-\widetilde{\theta}_c}^{\widetilde{\theta}_c} hm_2\cos\theta d\theta + \int_{\widetilde{\theta}_c}^{\theta_c} hr\cos^2\theta d\theta \\ &\quad + \int_{\theta_c}^{2\pi-\theta_c} hm_1\cos\theta d\theta + \int_{2\pi-\theta_c}^{2\pi-\widetilde{\theta}_c} hr\cos^2\theta d\theta, \end{aligned} \tag{A.14}$$

$$\begin{aligned} I_2(r) &= \int_{-\widetilde{\theta}_c}^{\widetilde{\theta}_c} hm_2\sin\theta d\theta + \int_{\widetilde{\theta}_c}^{\theta_c} hr\cos\theta\sin\theta d\theta \\ &\quad + \int_{\theta_c}^{2\pi-\theta_c} hm_1\sin\theta d\theta + \int_{2\pi-\theta_c}^{2\pi-\widetilde{\theta}_c} hr\cos\theta\sin\theta d\theta. \end{aligned} \tag{A.15}$$

With simple computation, we get

$$I_1(r) = hm_2\sin\widetilde{\theta}_c - hm_1\sin\theta_c + hr\theta_c - hr\widetilde{\theta}_c, \tag{A.16}$$

$$I_2(r) = 0, \tag{A.17}$$

where

$$\sin\theta_c = \frac{\sqrt{r^2-m_1^2}}{r}, \qquad \sin\widetilde{\theta}_c = \frac{\sqrt{r^2-m_2^2}}{r}, \tag{A.18}$$

$$\theta_c = \pi + \arctan\frac{\sqrt{r^2-m_1^2}}{m_1}, \qquad \widetilde{\theta}_c = \arctan\frac{\sqrt{r^2-m_2^2}}{m_2}. \tag{A.19}$$

Case 4 ($m_1 < 0 < m_2$ and $|m_1| > |m_2|$). We have $|r\sin\theta| \leq m_2$ and $|r\cos\theta| \leq m_2$ for all $\theta \in [0, 2\pi)$ if $0 < r \leq m_2$. Then, $\varphi(r\cos\theta) = hr\cos\theta$ for every θ. Thus,

$$\begin{aligned} I_1(r) &= \int_0^{2\pi} hr\cos^2\theta d\theta = \pi hr, \\ I_2(r) &= \int_0^{2\pi} hr\cos\theta\sin\theta d\theta = 0. \end{aligned} \tag{A.20}$$

We fix now $m_2 < r < |m_1|$ and consider $\theta_c \in (0, \pi/2)$ which satisfies $r\cos\theta_c = m_2$. Then, we have

$$\begin{aligned} I_1(r) &= \int_{-\theta_c}^{\theta_c} hm_2\cos\theta d\theta + \int_{\theta_c}^{2\pi-\theta_c} hr\cos^2\theta d\theta \\ &= \pi hr - hr\theta_c + hm_2\sin\theta_c, \\ I_1(r) &= \int_{-\theta_c}^{\theta_c} hm_2\sin\theta d\theta + \int_{\theta_c}^{2\pi-\theta_c} hr\cos\theta\sin\theta d\theta = 0. \end{aligned} \tag{A.21}$$

We now fix $r \geq |m_1|$ and consider $\widetilde{\theta}_c \in (\pi/2, \pi)$ which satisfies $r\cos\widetilde{\theta}_c = m_1$. Then, we have

$$\begin{aligned} I_1(r) &= \int_{-\theta_c}^{\theta_c} hm_2\cos\theta d\theta + \int_{\theta_c}^{\widetilde{\theta}_c} hr\cos^2\theta d\theta \\ &\quad + \int_{\widetilde{\theta}_c}^{2\pi-\widetilde{\theta}_c} hm_1\cos\theta d\theta + \int_{2\pi-\widetilde{\theta}_c}^{2\pi-\theta_c} hr\cos^2\theta d\theta, \\ I_2(r) &= \int_{-\theta_c}^{\theta_c} hm_2\sin\theta d\theta + \int_{\theta_c}^{\widetilde{\theta}_c} hr\cos\theta\sin\theta d\theta \\ &\quad + \int_{\widetilde{\theta}_c}^{2\pi-\widetilde{\theta}_c} hm_1\sin\theta d\theta + \int_{2\pi-\widetilde{\theta}_c}^{2\pi-\theta_c} hr\cos\theta\sin\theta d\theta. \end{aligned} \tag{A.22}$$

With simple computation, we get

$$\begin{aligned} I_1(r) &= hm_2\sin\theta_c - hm_1\sin\widetilde{\theta}_c - hr\theta_c + hr\widetilde{\theta}_c, \\ I_2(r) &= 0, \end{aligned} \tag{A.23}$$

where

$$\sin\theta_c = \frac{\sqrt{r^2-m_2^2}}{r}, \qquad \sin\widetilde{\theta}_c = \frac{\sqrt{r^2-m_1^2}}{r},$$

$$\theta_c = \arctan\frac{\sqrt{r^2-m_2^2}}{m_2}, \qquad \widetilde{\theta}_c = \pi + \arctan\frac{\sqrt{r^2-m_1^2}}{m_1}. \tag{A.24}$$

Case 5 ($m_1 < 0 < m_2$ and $|m_1| = |m_2| = m$). We have $|r\sin\theta| \leq m$ and $|r\cos\theta| \leq m$ for all $\theta \in [0, 2\pi)$ if $0 < r \leq m$. Then, $\varphi(r\cos\theta) = hr\cos\theta$ for every θ. Thus,

$$\begin{aligned} I_1(r) &= \int_0^{2\pi} hr\cos^2\theta d\theta = \pi hr, \\ I_2(r) &= \int_0^{2\pi} hr\cos\theta\sin\theta d\theta = 0. \end{aligned} \tag{A.25}$$

We fix now $r > m$ and consider $\theta_c \in (0, \pi/2)$ which satisfies $r\cos\theta_c = m$. Then, we have

$$\begin{aligned} I_1(r) &= \int_{-\theta_c}^{\theta_c} hm\cos\theta d\theta + \int_{\theta_c}^{\pi-\theta_c} hr\cos^2\theta d\theta \\ &\quad - \int_{\pi-\theta_c}^{\pi+\theta_c} hm\cos\theta d\theta + \int_{\pi+\theta_c}^{2\pi-\theta_c} hr\cos^2\theta d\theta, \\ I_1(r) &= \int_{-\theta_c}^{\theta_c} hm\sin\theta d\theta + \int_{\theta_c}^{\pi-\theta_c} hr\cos\theta\sin\theta d\theta \\ &\quad - \int_{\pi-\theta_c}^{\pi+\theta_c} hm\sin\theta d\theta + \int_{\pi+\theta_c}^{2\pi-\theta_c} hr\cos\theta\sin\theta d\theta. \end{aligned} \tag{A.26}$$

With simple computation, we get

$$\begin{aligned} I_1(r) &= \pi hr + 2hm\sin\theta_c - 2hr\theta_c, \\ I_2(r) &= 0, \end{aligned} \tag{A.27}$$

where

$$\sin\theta_c = \frac{\sqrt{r^2 - m^2}}{r}, \qquad \theta_c = \arctan\frac{\sqrt{r^2 - m^2}}{m}. \tag{A.28}$$

This completes the proof of the lemma.

Acknowledgment

This work is supported in part by the National Natural Science Foundation of China (1097 2082).

References

[1] J. Llibre and M. A. Texeira, "On the stable limit cycle of a weight-driven pendulum clock," *European Journal of Physics*, vol. 31, no. 1, pp. 249–1254, 2010.

[2] M. Vidyasagar, *Nonlinear Systems Analysis*, Poelltice-Hall, 2nd edition, 1993.

[3] M. di Bernardo, C. J. Budd, A. R. Champneys, and P. Kowalczyk, *Piecewise-Smooth Dynamical Systems*, vol. 163 of *Applied Mathematical Sciences*, Springer, London, UK, 2008, Theory and applications.

[4] V. Carmona, E. Freire, E. Ponce, and F. Torres, "Bifurcation of invariant cones in piecewise linear homogeneous systems," *International Journal of Bifurcation and Chaos in Applied Sciences and Engineering*, vol. 15, no. 8, pp. 2469–2484, 2005.

[5] S. Huan and X.-S. Yang, "Generalized Hopf bifurcation emerged from a corner in general planar piecewise smooth systems," *Nonlinear Analysis. Theory, Methods & Applications*, vol. 75, no. 17, pp. 6260–6274, 2012.

[6] C. Chritopher and C. Li, *Limit Cycles in Differential Equations*, Birkhauser, Boston, Mass, USA, 2007.

[7] S.-M. Huan and X.-S. Yang, "On the number of limit cycles in general planar piecewise linear systems," *Discrete and Continuous Dynamical Systems A*, vol. 32, no. 6, pp. 2147–2164, 2012.

[8] J. Li, "Hilbert's 16th problem and bifurcations of planar polynomial vector fields," *International Journal of Bifurcation and Chaos in Applied Sciences and Engineering*, vol. 13, no. 1, pp. 47–106, 2003.

[9] J. Llibre and A. Makhlouf, "Bifurcation of limit cycles from a two-dimensional center inside $\mathfrak{R}^4$," *Nonlinear Analysis. Theory, Methods & Applications*, vol. 72, no. 3-4, pp. 1387–1392, 2010.

[10] E. Freire, E. Ponce, and J. Ros, "The focus-center-limit cycle bifurcation in symmetric 3D piecewise linear systems," *SIAM Journal on Applied Mathematics*, vol. 65, no. 6, pp. 1933–1951, 2005.

[11] V. Carmona, S. Fernández-García, F. Fernández-Sánchez, E. García-Medina, and A. E. Teruel, "Reversible periodic orbits in a class of 3D continuous piecewise linear systems of differential equations," *Nonlinear Analysis. Theory, Methods & Applications*, vol. 75, no. 15, pp. 5866–5883, 2012.

[12] A. Buică and J. Llibre, "Bifurcation of limit cycles from a four-dimensional center in control systems," *International Journal of Bifurcation and Chaos in Applied Sciences and Engineering*, vol. 15, no. 8, pp. 2653–2662, 2005.

[13] C. A. Buzzi, J. Llibre, and J. C. Medrado, "On the limit cycles of a class of piecewise linear differential systems in $\mathfrak{R}^4$ with two zones," *Mathematics and Computers in Simulation*, vol. 82, no. 4, pp. 533–539, 2011.

[14] C. A. Buzzi, J. Llibre, J. C. Medrado, and J. Torregrosa, "Bifurcation of limit cycles from a centre in $\mathfrak{R}^4$ in resonance 1:*N*," *Dynamical Systems*, vol. 24, no. 1, pp. 123–137, 2009.

[15] P. T. Cardin, T. de Carvalho, and J. Llibre, "Bifurcation of limit cycles from an *n*-dimensional linear center inside a class of piecewise linear differential systems," *Nonlinear Analysis. Theory, Methods & Applications*, vol. 75, no. 1, pp. 143–152, 2012.

[16] J. Llibre, E. Ponce, and J. Ros, "Algebraic determination of limit cycles in a family of three-dimensional piecewise linear differential systems," *Nonlinear Analysis. Theory, Methods & Applications*, vol. 74, no. 17, pp. 6712–6727, 2011.

[17] A. Buică and J. Llibre, "Averaging methods for finding periodic orbits via Brouwer degree," *Bulletin des Sciences Mathématiques*, vol. 128, no. 1, pp. 7–22, 2004.

[18] A. Buică, J. Llibre, and O. Makarenkov, "Asymptotic stability of periodic solutions for nonsmooth differential equations with application to the nonsmooth van der Pol oscillator," *SIAM Journal on Mathematical Analysis*, vol. 40, no. 6, pp. 2478–2495, 2009.

[19] F. E. Browder, "Fixed point theory and nonlinear problems," *American Mathematical Society*, vol. 9, no. 1, pp. 1–39, 1983.

Hindawi Publishing Corporation
Discrete Dynamics in Nature and Society
Volume 2013, Article ID 705601, 8 pages
http://dx.doi.org/10.1155/2013/705601

Research Article

Bifurcation and Chaotic Behavior of a Discrete-Time SIS Model

Junhong Li and Ning Cui

Department of Mathematics and Sciences, Hebei Institute of Architecture and Civil Engineering, Zhangjiakou, Hebei 075000, China

Correspondence should be addressed to Junhong Li; lijunhong27@yahoo.com.cn

Received 5 January 2013; Accepted 8 April 2013

Academic Editor: Qingdu Li

The discrete-time epidemic model is investigated, which is obtained using the Euler method. It is verified that there exist some dynamical behaviors in this model, such as transcritical bifurcation, flip bifurcation, Hopf bifurcation, and chaos. The numerical simulations, including bifurcation diagrams and computation of Lyapunov exponents, not only show the consistence with the theoretical analysis but also exhibit the rich and complex dynamical behaviors.

1. Introduction

Epidemic models have been widely used in different forms for studying epidemiological processes such as the spread of HIV [1], SARS [2], and influenza [3]. It is well known that dynamical systems with simple dynamical behavior in the constant parameter case display very complex behaviors including chaos when they are periodically perturbed [4, 5]. The continuous-time epidemic models have been widely investigated in many articles (e.g., [6–10] and the references cited therein). In recent years, we have found that more attention is paid to the discrete-time epidemic models (see [11–15] and the references cited therein). The reasons are as follows: first, difference models are more realistic than continuous differential ones because the epidemic statistics are compiled from given time intervals and are discontinuous. Second, the discrete-time models can provide natural simulators for the continuous cases. One can thus not only study the behaviors of the continuous-time model with good accuracy, but also assess the effect of lager time steps. At last, the use of discrete -time models makes it possible to use the entire arsenal of methods recently developed for the study of mappings and lattice equations, either from the integrability and/or chaos points of view.

On the other hand, daily treatments are frequently done for some infections, such as the group of those being responsible for the common cold, which do not confer any long lasting immunity. Such infections do not have a recovered state and individuals become susceptible again after infection. For such reasons, according to [16], we firstly consider the SIS epidemic model with nonlinear incidence rate:

$$\begin{aligned} \frac{dS}{dt} &= bS\left(1-\frac{S}{K}\right)-\beta S^2 I+\gamma I, \\ \frac{dI}{dt} &= \beta S^2 I-dI-\gamma I, \end{aligned} \tag{1}$$

where S denotes the susceptible population, I is the infected population, and b is the intrinsic birth rate constant. K, β are the carrying capacity and the infection rate, respectively. $\gamma \geq 0$ is the recovery rate constant ($1/\gamma$ is the average infective time).

Let

$$S=\sqrt{\frac{d+\gamma}{\beta}}x, \qquad I=\sqrt{\frac{d+\gamma}{\beta}}y, \qquad d\tau=(d+\gamma)\,dt. \tag{2}$$

We obtain the following system analogous to (1):

$$\begin{aligned} \frac{dx}{d\tau} &= a_0 x-a_1 x^2-x^2 y+a_2 y, \\ \frac{dy}{d\tau} &= x^2 y-y, \end{aligned} \tag{3}$$

where

$$a_0=\frac{b}{d+\gamma}, \qquad a_1=\frac{b}{K\sqrt{\beta(d+\gamma)}}, \qquad a_2=\frac{\gamma}{d+\gamma}. \tag{4}$$

Applying Euler scheme to (3), we obtain the following equation:

$$x_{n+1} = (a_0 + 1)\, x_n - a_1 x_n^2 - x_n^2 y_n + a_2 y_n,$$
$$y_{n+1} = x_n^2 y_n. \tag{5}$$

This paper is organized as follows. In Section 2, we give sufficient conditions of existence for transcritical bifurcation, flip bifurcation, and Hopf bifurcation. In Section 3, a series of numerical simulations show that there are bifurcation and chaos in the discrete-time epidemic model. Finally, we give remarks to conclude this paper in Section 4.

2. Bifurcations

It is easy to visualize that system (5) has three fixed points $P_0(0,0)$, $P_1(a_0/a_1, 0)$, and $P_2(1, (a_0 - a_1)/(1 - a_2))$ when a_1, a_0 are fixed. We can see that the fixed point $P_0(0,0)$ is a saddle. In the following paper, we focus on investigating the bifurcations of P_1, P_2.

Theorem 1. *If $a_0 = a_1$ and $a_0 \neq 2$, (5) undergo a transcritical bifurcation at P_1. Furthermore, the system has three fixed points when $a_0 > a_1$ and has two fixed points when $a_0 \leq a_1$.*

Proof. The Jacobian matrix of (5) at P_1 takes the form

$$J(P_1) = \begin{pmatrix} 1 - a_0 & a_2 - \dfrac{a_0^2}{a_1^2} \\ 0 & \dfrac{a_0^2}{a_1^2} \end{pmatrix}. \tag{6}$$

$J(P_1)$ has eigenvalues $\lambda_1 = 1 - a_0$, $\lambda_2 = a_0^2/a_1^2$. And $a_0 \neq 2$ implies that $|\lambda_1| \neq 1$.

Let

$$\xi_n = x_n - \frac{a_0}{a_1}, \qquad \eta_n = y_n, \qquad c_n = a_0 - a_1, \tag{7}$$

equation (5) becomes

$$\xi_{n+1} = (1 - a_1)\, \xi_n + (a_2 - 1)\, \eta_n + F_1(\xi_n, \eta_n, c_n),$$
$$\eta_{n+1} = \eta_n + F_2(\xi_n, \eta_n, c_n), \tag{8}$$
$$c_{n+1} = c_n,$$

where

$$F_1(\xi_n, \eta_n, c_n) = -(a_1 + \eta_n)\, \xi_n^2 - \frac{2\xi_n \eta_n c_n}{a_1} - (2\eta_n + c_n)\, \xi_n - \frac{\eta_n c_n^2}{a_1^2} - \frac{2c_n \eta_n}{a_1},$$
$$F_2(\xi_n, \eta_n, c_n) = 2\xi_n \eta_n + \frac{2c_n \eta_n}{a_1} + \xi_n^2 \eta_n + \frac{\eta_n c_n^2}{a_1^2} + \frac{2\xi_n \eta_n c_n}{a_1}. \tag{9}$$

By the following transformation:

$$\begin{pmatrix} \xi_n \\ \eta_n \\ c_n \end{pmatrix} = \begin{pmatrix} 1 & 1 & 0 \\ 1 & \dfrac{a_1}{a_2 - 1} & 0 \\ 0 & 0 & 1 \end{pmatrix} \begin{pmatrix} p_n \\ q_n \\ \sigma_n \end{pmatrix}, \tag{10}$$

equation (8) becomes

$$\begin{pmatrix} p_{n+1} \\ q_{n+1} \\ \sigma_{n+1} \end{pmatrix} = \begin{pmatrix} 1 - a_1 & 0 & 0 \\ 0 & 1 & 0 \\ 0 & 0 & 1 \end{pmatrix} \begin{pmatrix} p_n \\ q_n \\ \sigma_n \end{pmatrix} + \begin{pmatrix} f_1(p_n, q_n, \sigma_n) \\ f_2(p_n, q_n, \sigma_n) \\ 0 \end{pmatrix}, \tag{11}$$

where

$$f_1(p_n, q_n, \sigma_n) = \left(\frac{a_1 + a_2 - 1}{1 - a_2} q_n - a_1\right) p_n^2 + \left[\frac{2(a_1 + a_2 - 1)(\sigma_n + 1)(q_n + q_n^2)}{a_1(1 - a_2)} - \sigma_n - 2a_1 q_n\right] p_n + \frac{2(a_1 + a_2 - 1) q_n^3}{a_1(1 - a_2)} + \left[\frac{2(a_1 + a_2 - 1)(\sigma_n + a_1)}{a_1(1 - a_2)} - a_1\right] q_n^2 + \left[\frac{(a_1 a_2 + 2a_2 - 2)\sigma_n}{a_1(1 - a_2)} + \frac{2(a_1 + a_2 - 1)\sigma_n^2}{a_1^3(1 - a_2)}\right] q_n,$$
$$f_2(p_n, q_n, \sigma_n) = q_n^3 + 2\left(1 + p_n + \frac{\sigma_n}{a_1}\right) q_n^2 + 2p_n q_n + \frac{2q_n \sigma_n}{a_1} + \frac{(a_1 p_n + \sigma_n)^2 q_n}{a_1^2}. \tag{12}$$

Then, we can consider

$$p_n = g(q_n, \sigma_n) = \varepsilon_1 q_n^2 + \varepsilon_2 q_n \sigma_n + \varepsilon_3 \sigma_n^2 + o\left((|p_n| + |q_n|)^3\right), \tag{13}$$

which must satisfy

$$g(q_{n+1}, \sigma_{n+1}) = g(q_n + f_2(g(q_n, \sigma_n), q_n, \sigma_n), \sigma_{n+1}) = (1 - a_1)\, g(q_n, \sigma_n) + f_1(g(q_n, \sigma_n), q_n, \sigma_n). \tag{14}$$

Thus, we have

$$\varepsilon_1 = \frac{a_1 a_2 + 2a_2 - 2}{a_1(1 - a_2)}, \qquad \varepsilon_2 = \frac{a_1 a_2 + 2a_2 - 2}{a_1^2(1 - a_2)}, \qquad \varepsilon_3 = 0. \tag{15}$$

And (8) is restricted to the center manifold, which is given by

$$f : q_{n+1} = \frac{2\left(a_1a_2 + 2a_2 - 2\right)}{a_1\left(1 - a_2\right)}\left(q_n^3 + \frac{q_n^2\sigma_n}{a_1}\right) + q_n^3 + 2q_n^2 + q_n + \frac{2q_n^2\sigma_n}{a_1} + \frac{2q_n\sigma_n}{a_1} + o\left(\left(|q_n| + |\sigma_n|\right)^4\right). \tag{16}$$

Since

$$f\left(0, \sigma_n\right) = 0, \qquad \left.\frac{\partial f}{\partial q}\right|_{(0,0)} = 1, \qquad \left.\frac{\partial^2 f}{\partial q^2}\right|_{(0,0)} = 4, \qquad \left.\frac{\partial^2 f}{\partial q \partial \sigma}\right|_{(0,0)} = -\frac{2}{a_1} \neq 0, \tag{17}$$

system (5) undergoes a transcritical bifurcation at P_1. This proves the theorem. □

Theorem 2. *Equation* (5) *undergoes a flip bifurcation at* P_1 *when* $a_0 = 2$, $a_1 \neq a_0$. *Furthermore, the stable periodic-2 point bifurcates from this fixed point.*

Proof. Let

$$\xi_n = x_n - \frac{a_0}{a_1}, \qquad \rho_n = y_n, \qquad c_n = a_0 - 2, \tag{18}$$

system (5) becomes

$$\begin{aligned} \xi_{n+1} &= -\xi_n + \left(a_2 - \frac{4}{a_1^2}\right)\rho_n + F_1\left(\xi_n, c_n, \rho_n\right), \\ c_{n+1} &= -c_n, \\ \rho_{n+1} &= \frac{4}{a_1^2}\rho_n + F_2\left(\xi_n, c_n, \rho_n\right), \end{aligned} \tag{19}$$

where

$$\begin{aligned} F_1\left(\xi_n, c_n, \rho_n\right) = & -\left(a_1 + \rho_n\right)\xi_n^2 - \left(c_n + \frac{2\left(c_n + 2\right)\rho_n}{a_1}\right)\xi_n - \frac{4c_n + c_n^2}{a_1^2}\rho_n, \\ F_2\left(\xi_n, c_n, \rho_n\right) = & \rho_n\xi_n^2 + \frac{4c_n + c_n^2}{a_1^2}\rho_n + \frac{2\left(c_n + 2\right)\rho_n}{a_1}\xi_n. \end{aligned} \tag{20}$$

By the following transformation:

$$\begin{pmatrix} \xi_n \\ c_n \\ \rho_n \end{pmatrix} = \begin{pmatrix} 1 & 0 & 1 \\ 0 & 1 & 0 \\ 0 & 0 & \dfrac{\left(a_1^2 + 4\right)}{\left(a_2a_1^2 - 4\right)} \end{pmatrix}\begin{pmatrix} \phi_n \\ u_n \\ v_n \end{pmatrix}, \tag{21}$$

equation (19) becomes

$$\begin{pmatrix} \phi_{n+1} \\ u_{n+1} \\ v_{n+1} \end{pmatrix} = \begin{pmatrix} -1 & 0 & 0 \\ 0 & -1 & 0 \\ 0 & 0 & \dfrac{4}{a_1^2} \end{pmatrix}\begin{pmatrix} \phi_n \\ u_n \\ v_n \end{pmatrix} + \begin{pmatrix} f_1\left(\phi_n, u_n, v_n\right) \\ 0 \\ f_2\left(\phi_n, u_n, v_n\right) \end{pmatrix}, \tag{22}$$

where

$$\begin{aligned} & f_1\left(\phi_n, u_n, v_n\right) \\ &= \left(\frac{a_1^2 + a_2a_1^2}{4 - a_2a_1^2}v_n - a_1\right)\phi_n^2 \\ &\quad + \left[\frac{2\left(1 + a_2\right)a_1^2v_n^2}{4 - a_2a_1^2} + \frac{2a_1\left(u_n - 2 + a_2a_1^2 + a_2u_n + 2a_2\right)v_n}{4 - a_2a_1^2} - u_n\right]\phi_n \\ &\quad + \frac{a_1^2 + a_2a_1^2}{4 - a_2a_1^2}v_n^3 + \frac{a_1\left(a_2a_1^2 + 2a_2u_n + 4a_2 + 2u_n\right)}{4 - a_2a_1^2}v_n^2 \\ &\quad + \frac{\left(1 + a_2\right)u_n^2v_n}{4 - a_2a_1^2} + \frac{a_2\left(4 + a_1^2\right)u_nv_n}{4 - a_2a_1^2}, \\ & f_2\left(\phi_n, u_n, v_n\right) = v_n^3 + 2\left(\phi_n + \frac{u_n + 4}{a_1}\right)v_n^2 + \frac{\left(a_1\phi_n + u_n\right)\left(a_1\phi_n + u_n + 4\right)v_n}{a_1^2}. \end{aligned} \tag{23}$$

Then, we can consider $v_n = g(\phi_n, u_n) = \varepsilon_1\phi_n^2 + \varepsilon_2\phi_nu_n + \varepsilon_3u_n^2 + o((|\phi_n| + |u_n|)^3)$, which must satisfy

$$\begin{aligned} & g\left(-\phi_n + f_1\left(\phi_n, g\left(\phi_n, u_n\right), v_n\right), u_{n+1}\right) \\ &= \frac{4}{a_1^2}g\left(\phi_n, u_n\right) + g^3\left(\phi_n, u_n\right) \\ &\quad + 2\left(\phi_n + \frac{u_n + 4}{a_1}\right)g^2\left(\phi_n, u_n\right) \\ &\quad + \frac{\left(a_1\phi_n + u_n\right)\left(a_1\phi_n + u_n + 4\right)g\left(\phi_n, u_n\right)}{a_1^2}. \end{aligned} \tag{24}$$

Thus, we have $\varepsilon_k = 0$, $k = 1, 2, 3$. We obtain the center manifold as follows:

$$v_n = g\left(\phi_n, u_n\right) = \varepsilon_4\phi_n^2u_n + \varepsilon_5\phi_nu_n^2 + \varepsilon_6u_n^3 + o\left(\left(|\phi_n| + |u_n|\right)^4\right). \tag{25}$$

And (19) is restricted to the center manifold, which is given by

$$f : \phi_{n+1} = -\phi_n + f_1\left(\phi_n, g\left(\phi_n, u_n\right), v_n\right). \tag{26}$$

Direct calculations show that

$$\left(\frac{\partial f}{\partial \sigma}\frac{\partial^2 f}{\partial p^2}+2\frac{\partial^2 f}{\partial p\partial \sigma}\right)\Big|_{(0,0)}=-2,$$
$$\left(\frac{1}{2}\left(\frac{\partial^2 f}{\partial p^2}\right)^2+\frac{1}{3}\left(\frac{\partial^3 f}{\partial p^3}\right)\right)\Big|_{(0,0)}=\frac{a_1^2}{2}. \tag{27}$$

Hence, system (5) undergoes a flip bifurcation at P_1. This completes the proof. □

The positive fixed point is so important to the biological system that people usually are very interested in it. We will next pay attention to the only positive fixed point P_2 of (5).

Theorem 3. *Equation* (5) *undergoes a transcritical bifurcation at* P_2 *when* $a_1 = a_0$, $a_1 \neq 2$, *and* $\Delta > 0$, *where*

$$\Delta=\frac{(1+a_2)^2a_0^2}{(1-a_2)^2}+8(a_1-a_0)+\frac{4a_1^2a_2^2-4a_2(a_2+1)}{(1-a_2)^2}. \tag{28}$$

Theorem 4. *If* $\Delta > 0$, $a_1 \neq a_0$, *and* $a_0 = (2 - 2a_2 - a_1 + 3a_1a_2)/2a_2$, (5) *undergoes a flip bifurcation at* P_2.

Since the analysis is similar to the case at P_1, the previously mentioned proofs are omitted.

We next give the condition of existence of Hopf bifurcation by using the hopf bifurcation theorem in [17].

The characteristic equation of the Jacobian matrix $J(P_2)$ can be written as $\lambda^2 - t_2\lambda + d_2 = 0$, where

$$t_2=2+a_0-2a_1-\frac{2(a_0-a_1)}{1-a_2},$$
$$d_2=t_2-1+2a_0-2a_1. \tag{29}$$

The eigenvalues of the Jacobian matrix of (5) at P_2 are $\lambda_{1,2} = (t_2 \pm \sqrt{t_2^2 - 4d_2})/2$. The eigenvalues $\lambda_{1,2}$ are complex conjugates for $\Delta < 0$. We translate the fixed point $P_2(1, (a_0 - a_1)/(1 - a_2))$ to the origin by $x_n = \varphi_n - 1$, $y_n = \delta_n - ((a_0 - a_1)/(1 - a_2))$, and the system (5) becomes

$$\varphi_{n+1}=(t_2-1)\varphi_n+(a_2-1)\delta_n-\left(\delta_n+\frac{a_0-a_1a_2}{1-a_2}\right)\varphi_n^2-2\varphi_n\delta_n,$$
$$\delta_{n+1}=\frac{2(a_0-a_1)}{1-a_2}\varphi_n+\delta_n+2\varphi_n\delta_n+\left(\delta_n+\frac{a_0-a_1}{1-a_2}\right)\varphi_n^2. \tag{30}$$

The eigenvalues of the matrix associated with the linearized map (30) at fixed point $(0, 0)$ are complex conjugates which are written as $\lambda, \overline{\lambda} = (t_2 \pm i\sqrt{4d_2 - t_2^2})/2$, where

$$|\lambda|=\sqrt{1+3a_0-4a_1-\frac{2(a_0-a_1)}{1-a_2}}. \tag{31}$$

Now assume that $3a_2 < 1$, and let $a_{00} = (2a_1(1 - 2a_2))/(1 - 3a_2)$. Then we have

$$\frac{d(|\lambda|)}{da_0}\Big|_{a_0=a_{00}}=\frac{1-3a_2}{2(1-a_2)}>0,\quad |\lambda(a_{10})|=1,$$
$$\lambda(a_{00})=1+\frac{a_1a_2-a_1}{1-3a_2}\pm i\frac{\sqrt{a_1(1-a_2)(2-a_1+a_1a_2-6a_2)}}{1-3a_2},$$
$$\lambda^j\neq 1,\quad j=1,2,3,4. \tag{32}$$

Let

$$\mathrm{T}=\begin{pmatrix}a_2-1 & 0\\ \frac{2-t_2}{2} & -\frac{\sqrt{4d_2-t_2^2}}{2}\end{pmatrix},$$
$$\begin{pmatrix}\varphi_n\\ \delta_n\end{pmatrix}=\mathrm{T}\begin{pmatrix}\phi_n\\ \sigma_n\end{pmatrix}. \tag{33}$$

The system (30) becomes

$$\begin{pmatrix}\phi_{n+1}\\ \sigma_{n+1}\end{pmatrix}=\begin{pmatrix}\frac{t_2}{2} & -\frac{\sqrt{4d_2-t_2^2}}{2}\\ \frac{\sqrt{4d_2-t_2^2}}{2} & \frac{t_2}{2}\end{pmatrix}\begin{pmatrix}\phi_n\\ \sigma_n\end{pmatrix}+\begin{pmatrix}f_1(\phi_n,\sigma_n)\\ f_2(\phi_n,\sigma_n)\end{pmatrix}, \tag{34}$$

where

$$\begin{aligned}f_1(\phi_n,\sigma_n)&=\left(\frac{a_0+a_0a_2}{2}-a_1a_2\right)\phi_n^3\\&\quad+\left[\frac{(a_2-1)\sqrt{4d_2-t_2^2}}{2}\sigma_n+\frac{a_2(2a_0-a_1-a_1a_2)}{a_2-1}\right]\phi_n^2\\&\quad+\sqrt{4d_2-t_2^2}\sigma_n\phi_n,\\ f_2(\phi_n,\sigma_n)&=\frac{(2-t_2)(2a_2-t_2)(a_2-1)}{2\sqrt{4d_2-t_2^2}}\phi_n^3\\&\quad+(a_2-1)\left(a_2-\frac{t_2}{2}\right)\phi_n^2\sigma_n-\frac{(2-t_2)(2-t_2+a_1a_2-a_0)}{\sqrt{4d_2-t_2^2}}\phi_n^2\\&\quad-\frac{2(a_2-1)(2-t_2-a_0+a_1)}{\sqrt{4d_2-t_2^2}}\phi_n^2+(2a_2-t_2)\sigma_n\phi_n.\end{aligned} \tag{35}$$

Notice that (34) is exactly on the center manifold in the form, in which the coefficient l [18] is given by $l = -\mathrm{Re}[((1-2\lambda)\bar{\lambda}^2/(1-\lambda))l_{11}l_{20}] - (1/2)|l_{11}|^2 - |l_{02}|^2 + \mathrm{Re}(\bar{\lambda}l_{21})$, where

$$\begin{aligned}
l_{11} &= \frac{1}{4}\left[\left(f_{1\phi\phi}+f_{1\sigma\sigma}\right)+\left(f_{2\phi\phi}+f_{2\sigma\sigma}\right)i\right] \\
&= \frac{3a_0a_2-2a_1a_2^2-a_0}{4a_2-4}-\frac{1}{4\sqrt{4d_2-t_2^2}} \\
&\quad\times\left[\left(4-2t_2\right)\left(2-t_2+a_1a_2-a_0\right)\right. \\
&\qquad\left.+\left(a_2-1\right)\left(4-2t_2-2a_0+2a_1\right)\right]i, \\
l_{20} &= \frac{1}{8}\left[\left(f_{1\phi\phi}-f_{1\sigma\sigma}+2f_{2\phi\sigma}\right)+\left(f_{2\phi\phi}-f_{2\sigma\sigma}-2f_{1\phi\sigma}\right)i\right] \\
&= \frac{1}{4}\left(a_2-a_1a_2-2+2a_0\right)-\frac{1}{8\sqrt{4d_2-t_2^2}} \\
&\quad\times\left[\left(4-2t_2\right)\left(2-t_2+a_1a_2-a_0\right)+\left(a_2-1\right)\right. \\
&\qquad\left.\times\left(4-2t_2-2a_0+2a_1\right)-8d_2+2t_2^2\right]i, \\
l_{02} &= \frac{1}{8}\left[\left(f_{1\phi\phi}-f_{1\sigma\sigma}-2f_{2\phi\sigma}\right)+\left(f_{2\phi\phi}-f_{2\sigma\sigma}+2f_{1\phi\sigma}\right)i\right] \\
&= \frac{1}{8}\left(2a_0-2a_0a_2-2-4a_2+3t_2\right) \\
&\quad+\frac{1}{8}\left(2a_0-a_1a_2-2+t_2+2\sqrt{4d_2-t_2^2}\right)i, \\
l_{21} &= \frac{1}{16}\left[\left(f_{1\phi\phi\phi}+f_{1\phi\sigma\sigma}+f_{2\phi\phi\sigma}+f_{2\sigma\sigma\sigma}\right)\right. \\
&\qquad\left.+\left(f_{2\phi\phi\phi}+f_{2\phi\sigma\sigma}-f_{1\phi\phi\sigma}-f_{1\sigma\sigma\sigma}\right)i\right] \\
&= \frac{1}{8}\left(1-a_2\right)\left(3+a_2-2t_2\right) \\
&\quad+\frac{1}{8\sqrt{4d_2-t_2^2}}\left(6a_2-3t_2+3a_2t_2+8d_2+t_2^2\right)i.
\end{aligned} \tag{36}$$

From the previous analysis, we have Theorem 5.

Theorem 5. *System* (5) *undergoes a Hopf bifurcation at fixed point* P_2*, if* $l \neq 0$*,* $\Delta < 0$ *and*

$$a_1 \neq \frac{2\left(1-a_2\right)+2a_2a_1}{1+a_3}. \tag{37}$$

3. Numerical Simulations

With development of scientific computation, computer becomes a powerful tool to study nonlinear systems, especially for a system without explicit solution. It not only is able to explore new complex dynamical behaviors, for example, periodic orbits and chaos in different regions [16, 19], but also can do rigorous analysis by combining modern dynamical systems theory and reliable computation, for example, topological horseshoes [20–23]. In this section, we use the bifurcation diagrams, Lyapunov exponents, and phase portraits to illustrate the previous analytic results and find new dynamics of the model (5) as the parameters vary. The attractors of (5) are also given by using the method in [20]. The bifurcation parameters are considered in the following three cases:

(I) varying a_0 in range $1.6 \leq a_0 \leq 2.2$ and fixing $a_1 = 0.9$, $a_3 = 0.01$;

(II) varying a_1 in range $0.8 \leq a_1 \leq 1.2$ and fixing $a_0 = 2$, $a_3 = 0.01$;

(III) varying a_2 in range $0.3 \leq a_2 \leq 0.6$ and fixing $a_0 = 2$, $a_1 = 0.9$.

For case (I). The bifurcation diagram of (5) in a_0-x_n and a_0-y_n space for $a_1 = 0.9$, $a_3 = 0.01$ is given in Figures 1(a) and 1(b) to show the dynamical changes of susceptible and infective, respectively, as a_0 varies. There is obvious phenomenon of bifurcation when we select the stepsize to be 10^{-4}. The spectrum of Lyapunov exponents of the system (5) with respect to parameter a_1 is given in Figure 1(c).

Moreover, we can see that the orbit with initial values $(1, 1)$ approaches to the stable fixed point P_2 for $a_0 < 1.8$ approximately, and Hopf bifurcation occurs at $a_0 \approx 1.8$. When increased to $a_0 \approx 2.05$, (5) becomes stable. In Figures 1(b) and 1(c), we observe the period -4,8 windows within the chaotic regions and boundary crisis at $a_0 \approx 2.05$. For $a_0 \in (1.95, 2.05)$ the maximum Lyapunov exponents are positive which correspond to chaotic region. To well see the dynamics, the attractor in the system (5) and time series of x_n and y_n are given in Figures 1(d) and 1(e), respectively.

For case (II). Figure 2(a) is the bifurcation diagram of (5) for x_n and y_n and depicts that there are period -4,5 windows within the chaotic regions and boundary crisis at $a_1 \approx 1$. Figure 2(b) shows the spectrum of Lyapunov exponents of the system (5) with respect to parameter a_1. For $a_1 \in (0.85, 0.95)$ the maximum Lyapunov exponents are positive which correspond to chaotic region.

For case (III). Figures 3(a) and 3(b) are the bifurcation diagrams of (5) for x_n and y_n, respectively, and depict that there are period -2,4 windows within the chaotic regions and boundary crisis at $a_2 = 0.5$. Figure 3(c) shows the spectrum of Lyapunov exponents of (5) with respect to parameter a_2. Figure 3(d) is the attractor of (5) with $a_2 = 0.46$.

4. Conclusion

In this paper, we investigate the behaviors of a discrete-time SIS epidemic model with nonlinear incidence rate, and find many complex and new interesting dynamical phenomena. Without the recovery rate of infectious hosts, (1) becomes the SI model (see [16]). Our theoretical analysis and numerical simulations have demonstrated that the model exhibits the variety of dynamical behaviors, which includes that the discrete epidemic model undergoes transcritical bifurcation,

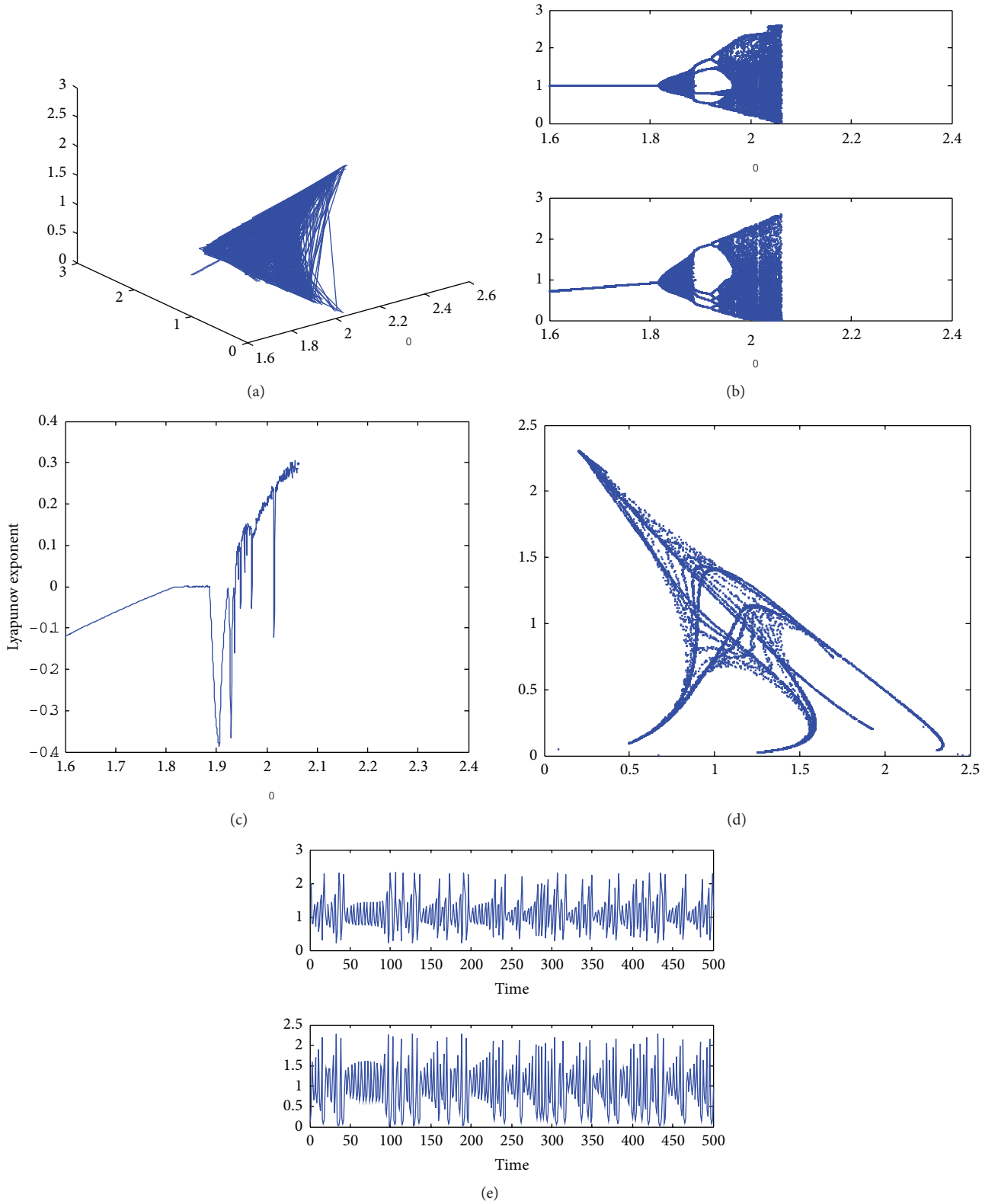

FIGURE 1: (a) Bifurcation diagram in (a_0, x_n, y_n) space. (b) The bifurcation diagram in a_0-x_n plane and in a_0-y_n plane. (c) Spectrum of Lyapunov exponents corresponding to (b). (d) The attractor of (5) with $a_0 = 2$ (e) Time series of x_n and y_n of the same parameters.

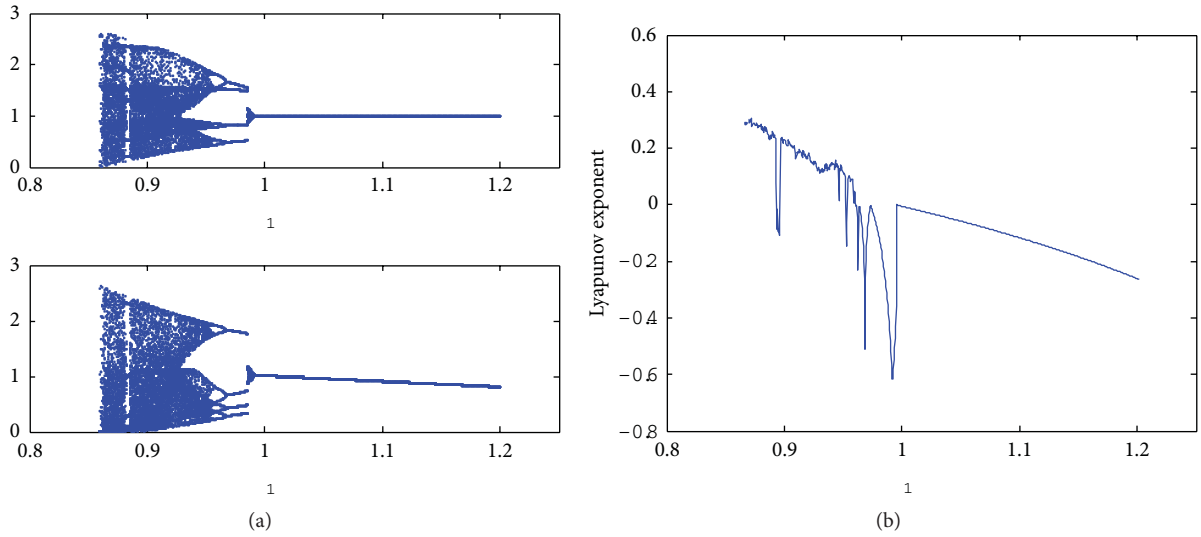

(a) (b)

Figure 2

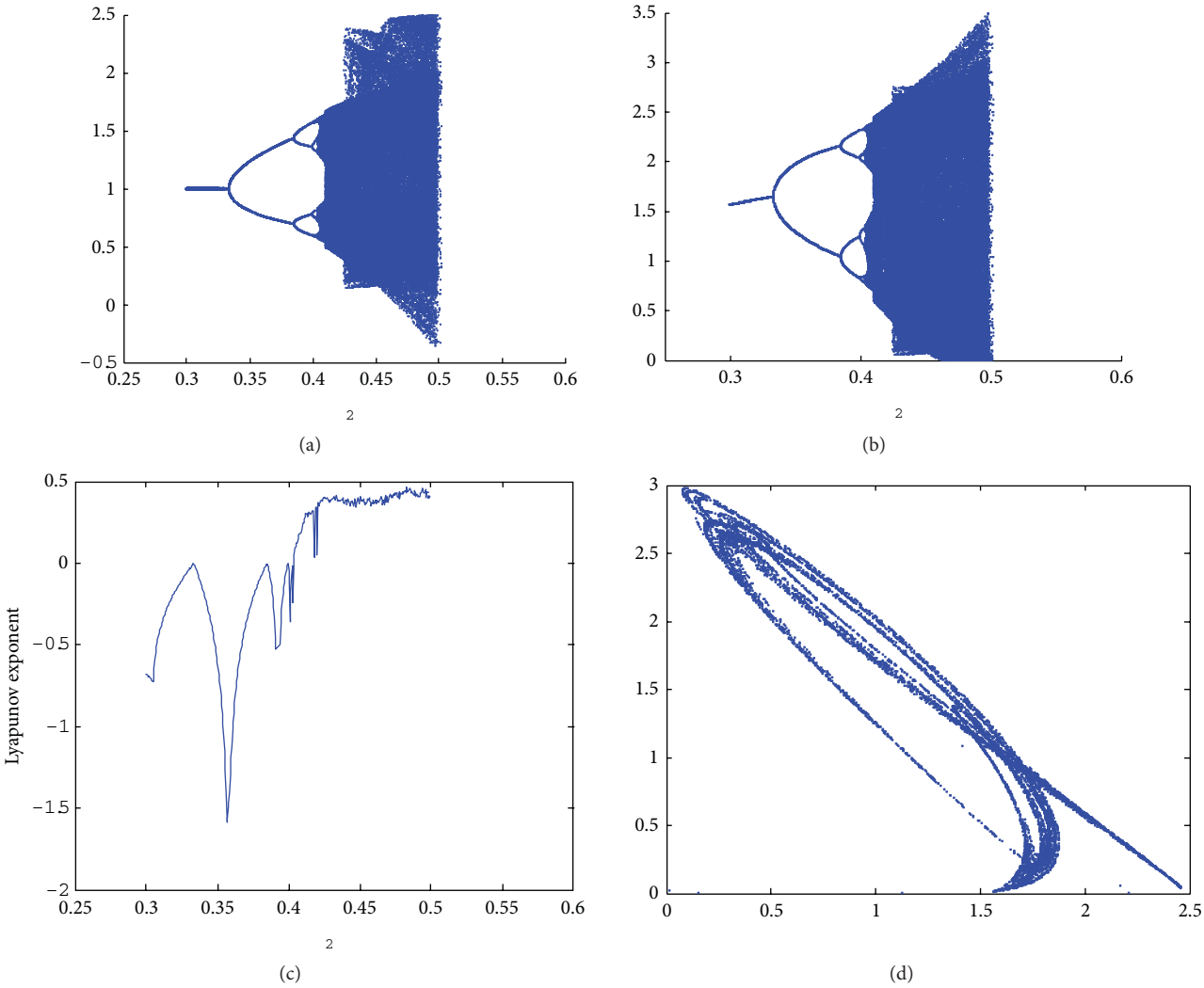

(a) (b)

(c) (d)

Figure 3

flip bifurcation, Hopf bifurcation, and chaos. Furthermore, chaos can cause the population to run a higher risk of extinction due to the unpredictability [24, 25]. Thus, how to control chaos in the epidemic model is very important, which needs further consideration.

Acknowledgments

The authors are very grateful to the reviewers for their valuable comments and suggestions. This work was supported by the Youth Science Foundations of Education Department of Hebei Province (nos. 2010233, 2011236).

References

[1] L. Cai, X. Li, M. Ghosh, and B. Guo, "Stability analysis of an HIV/AIDS epidemic model with treatment," *Journal of Computational and Applied Mathematics*, vol. 229, no. 1, pp. 313–323, 2009.

[2] Y.-H. Hsieh, C.-C. King, C. W. S. Chen, M.-S. Ho, S.-B. Hsu, and Y.-C. Wu, "Impact of quarantine on the 2003 SARS outbreak: a retrospective modeling study," *Journal of Theoretical Biology*, vol. 244, no. 4, pp. 729–736, 2007.

[3] S. Iwami, Y. Takeuchi, X. Liu, and S. Nakaoka, "A geographical spread of vaccine-resistance in avian influenza epidemics," *Journal of Theoretical Biology*, vol. 259, no. 2, pp. 219–228, 2009.

[4] D. Summers, J. G. Cranford, and B. P. Healey, "Chaos in periodically forced discrete-time ecosystem models," *Chaos, Solitons and Fractals*, vol. 11, no. 14, pp. 2331–2342, 2000.

[5] J. Vandermeer, L. Stone, and B. Blasius, "Categories of chaos and fractal basin boundaries in forced predator-prey models," *Chaos, Solitons and Fractals*, vol. 12, no. 2, pp. 265–276, 2001.

[6] A. Gray, D. Greenhalgh, X. Mao, and J. Pan, "The SIS epidemic model with Markovian switching," *Journal of Mathematical Analysis and Applications*, vol. 394, no. 2, pp. 496–516, 2012.

[7] A. Gray, D. Greenhalgh, L. Hu, X. Mao, and J. Pan, "A stochastic differential equation SIS epidemic model," *SIAM Journal on Applied Mathematics*, vol. 71, no. 3, pp. 876–902, 2011.

[8] J. Liu and T. Zhang, "Bifurcation analysis of an SIS epidemic model with nonlinear birth rate," *Chaos, Solitons & Fractals*, vol. 40, no. 3, pp. 1091–1099, 2009.

[9] D. Gao and S. Ruan, "An SIS patch model with variable transmission coefficients," *Mathematical Biosciences*, vol. 232, no. 2, pp. 110–115, 2011.

[10] Y. Li and J. Cui, "The effect of constant and pulse vaccination on SIS epidemic models incorporating media coverage," *Communications in Nonlinear Science and Numerical Simulation*, vol. 14, no. 5, pp. 2353–2365, 2009.

[11] Q. Wu and X. Fu, "Modelling of discrete-time SIS models with awareness interactions on degree-uncorrelated networks," *Physica A*, vol. 390, no. 3, pp. 463–470, 2011.

[12] P. L. Salceanu and H. L. Smith, "Persistence in a discrete-time stage-structured fungal disease model," *Journal of Biological Dynamics*, vol. 3, no. 2-3, pp. 271–285, 2009.

[13] J. E. Franke and A.-A. Yakubu, "Disease-induced mortality in density-dependent discrete-time S-I-S epidemic models," *Journal of Mathematical Biology*, vol. 57, no. 6, pp. 755–790, 2008.

[14] J. Li, Z. Ma, and F. Brauer, "Global analysis of discrete-time SI and SIS epidemic models," *Mathematical Biosciences and Engineering*, vol. 4, no. 4, pp. 699–710, 2007.

[15] L. J. S. Allen, Y. Lou, and A. L. Nevai, "Spatial patterns in a discrete-time SIS patch model," *Journal of Mathematical Biology*, vol. 58, no. 3, pp. 339–375, 2009.

[16] L. Li, G.-Q. Sun, and Z. Jin, "Bifurcation and chaos in an epidemic model with nonlinear incidence rates," *Applied Mathematics and Computation*, vol. 216, no. 4, pp. 1226–1234, 2010.

[17] J. Guckenheimer and P. Holmes, *Nonlinear Oscillations, Dynamical Systems, and Bifurcations of Vector Fields*, vol. 42, Springer, New York, NY, USA, 1983.

[18] S. Wiggins, *Introduction to Applied Nonlinear Dynamical Systems and Chaos*, vol. 2, Springer, New York, NY, USA, 1990.

[19] T. Chen, J. He, and Q. Yin, "Dynamics evolution of credit risk contagion in the CRT market," *Dynamics in Nature and Society*, vol. 2013, Article ID 206201, 9 pages, 2013.

[20] Q. Li, L. Zhang, and F. Yang, "An algorithm to automatically detect the Smale horseshoes," *Discrete Dynamics in Nature and Society*, Article ID 283179, 9 pages, 2012.

[21] Q. Li and X.-S. Yang, "A simple method for finding topological horseshoes," *International Journal of Bifurcation and Chaos in Applied Sciences and Engineering*, vol. 20, no. 2, pp. 467–478, 2010.

[22] X.-S. Yang, "Topological horseshoes and computer assisted verification of chaotic dynamics," *International Journal of Bifurcation and Chaos in Applied Sciences and Engineering*, vol. 19, no. 4, pp. 1127–1145, 2009.

[23] L. Qingdu and T. Song, "Algorithm for finding horseshoes in three-dimensinal hyperchaltic maps and its application," *Acta Physica Sinica*, vol. 62, no. 2, Article ID 020510, 2013.

[24] M. P. Hassell, H. N. Comins, and R. M. May, "Spatial structure and chaos in insect population dynamics," *Nature*, vol. 353, pp. 255–258, 1991.

[25] A. A. Berryman and J. A. Millstein, "Are ecological systems chaotic and if not, why not?" *Trends in Ecology & Evolution*, vol. 4, no. 1, pp. 26–28, 1989.

Hindawi Publishing Corporation
Discrete Dynamics in Nature and Society
Volume 2013, Article ID 430963, 6 pages
http://dx.doi.org/10.1155/2013/430963

Research Article

Horseshoe Chaos in a 3D Neural Network with Different Activation Functions

Fangyan Yang,[1] Song Tang,[2] and Guilan Xu[2]

[1] *School of Optoelectronic Engineering, Chongqing University of Posts and Telecommunications, Chongqing 400065, China*
[2] *Key Laboratory of Industrial Internet of Things & Networked Control of Ministry of Education, Chongqing University of Posts and Telecommunications, Chongqing 400065, China*

Correspondence should be addressed to Song Tang; kao_123@163.com

Received 22 February 2013; Accepted 20 March 2013

Academic Editor: Xiao-Song Yang

This paper studies a small neural network with three neurons. First, the activation function takes the sign function. Although the network is a simple hybrid system with all subsystems being exponentially stable, we find that it can exhibit very complex dynamics such as limit cycles and chaos. Since the sign function is a limit case of sigmoidal functions, we find that chaos robustly exists with some different activation functions, which implies that such chaos in this network is more related to its weight matrix than the type of activation functions. For chaos, we present a rigorous computer-assisted study by virtue of topological horseshoe theory.

1. Introduction

Since substantial evidence of chaos is found in biological studies of natural neuronal systems, researchers have realized that chaos is much helpful for neural networks escaping the local minima and may play an essential role in the storage and retrieval of information [1–3]. Thus, a thorough investigation on chaotic dynamics of neural networks is significant for neural networks studies, which has become a popular research field in recent decades. A lot of artificial neural networks have been proposed in order to realize chaotic and hyperchaotic attractors [4–12].

Generally, neural networks in real world have very high dimension, which is too hard to study. Fortunately, research in anatomy and physiology shows that neurons in biological brains are grouped together into functional circuits [13, 14]. This implies that a first step before studying chaos in high-dimensional neural networks should be to have detailed investigations on chaos in low-dimensional networks with only a few nerons [15–19].

The nonlinearity of neural systems usually comes from the activation functions, which is the reason causing chaos. There are many types of sigmoid functions used in literature, such as the hyperbolic tangent function, piecewise linear functions, the Logistic (sigmoid) function, and the sign functions. So, we are interested in whether chaos in a neural network can take place with all these functions or whether chaos can take place for any type sigmoidal activation function.

In order to answer the two questions, this paper will take a limit of the sigmoidal functions by zooming out the input scale and study a small Hopfield neural network (HNN) with hard switches. Such sign function is not only extremely easy to implement, but also of dynamical and biological significance in gene regulatory networks [4, 5]. An interesting phenomenon we find in this paper is that the HNN can demonstrate chaos, although it is a switching system that only consisted of stable subsystems; such chaos still exists even when we replace the sign function with many other activation functions.

The following paper is organized as follows. Section 2 presents the HNN and demonstrates its chaotic behavior with different activation functions; Section 3 first recalls some theoretical results of topological horseshoe and then presents computer-assisted proof of the existence of chaos; Section 4 draws conclusions.

2. Chaos in the Small Network with Different Activation Functions

The Hopfield neural network is described by [20]

$$\dot{x}_i = -a_i x_i + \sum_{j=1}^{n} w_{ij} f_i(x_i) + b_i, \quad i = 1, 2, \ldots, n, \tag{1}$$

where f_i is a sigmoidal activation function and $W = (w_{ij})$ is an $n \times n$ matrix, called weight matrix or connection matrix describing the strength of connections between neurons.

In this paper, we only consider three neurons, that is, $n = 3$ and take $b_i = 0$, then the small network can be written with the following equation in vector form:

$$\dot{x} = -\operatorname{diag}(a)\, x + W f(x), \tag{2}$$

where $a = [a_1, a_2, a_3]^T$, $f(x) = [f(x_1), f(x_2), f(x_3)]^T$.

Now let $a = [1, 1, 2]^T$, $f(x_i) = \operatorname{sign}(x_i)$, $i = 1, 2, 3$, and

$$W = \begin{pmatrix} 0.3 & 0.8 & 0.4 \\ -0.97 & 0.31 + p & 0.05 \\ 0.23 & -0.2 & 0.198 \end{pmatrix}, \tag{3}$$

where p is a parameter. Then we can easily solve the isolated equilibrium points of (2) while the parameter p from $-\infty$ to $+\infty$, as illustrated in Table 1. Since (2) is symmetric with respect to the origin, its equilibria appears in pairs, and the origin is always an equilibrium. Numerical computation suggests that the origin is always unstable. Since f only takes value of -1, 0, and 1, it is easy to see from the equation that the other equilibria are always exponentially stable.

To explore complex dynamics in (2), we simulate the system with $p < 0.61$ then numerically find that there are limit circles and strange attractors, as illustrated with the bifurcation plot in Figure 1. The dynamics relies greatly on its initial condition; that is, different initial value may result in different kind of dynamics. During our simulation, we chose $x(0) = [0.2, 0.3, -0.4]^T$. The bifurcation diagram indicates that the system (2) is very likely to be chaotic when p is near to zero.

After careful numerical computation, we obtain an invariant set called attractor in the sense that almost every trajectory with initial point near this set tends to this set, while this set contains a trajectory, that is, dense in it, as illustrated in Figure 2 for $p = 0$. It seems a chaotic attractor. In the next section, we will prove that this attractor is indeed chaotic with the topological horseshoe theory.

Since the sign function is a limit of most sigmoidal functions with large-scale input, we in this section will study existence of chaos for the HNN (1) with other sigmoidal activation function. For this purpose, we considerate the following equations:

$$\dot{x} = -\operatorname{diag}(a)\, x + W f(kx), \tag{4}$$

where k is a positive scale factor. Replacing x with $k^{-1}x$, we have the equivalent system

$$\dot{x} = -\operatorname{diag}(a)\, x + kW f(x). \tag{5}$$

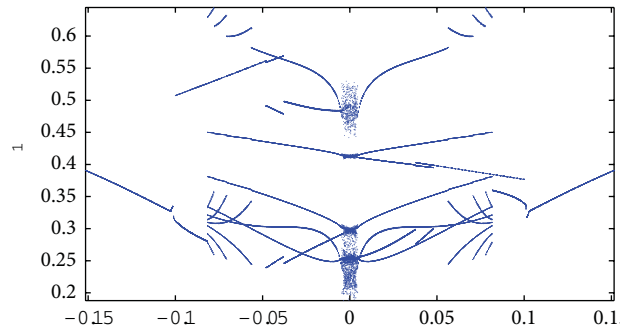

Figure 1: The bifurcation plot of (2) on the crossplane $x_2 = 0$.

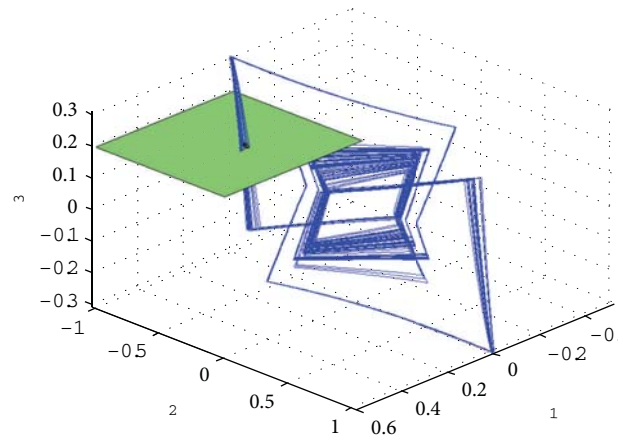

Figure 2: The phase portrait of system (2) and the poincaré plane $P : x_3 = 0.2$.

Table 1: Equilibrium points of (2) as we adjust p from $-\infty$ to $+\infty$.

Region of p	Number of isolated equilibrium points	Stable	Unstable
$p \le 0.61$	1	0	1
$0.61 < p < 0.71$	3	2	1
$0.71 \le p$	5	4	1

So for any type sigmoidal activation function $f(x)$ with its output range from -1 to 1, if k is great enough, $f(kx)$ will be sufficiently close to the discontinuous sign function. The robustness of (2) suggests that (4) could exhibit chaos with the same weight matrix (3). Taking the consideration of the bias, (1) may exhibit chaos for any type sigmoidal activation function when $n = 3$.

To illustrate this fact, we will give examples with a hyperbolic tangent function, a Logistic function, a piecewise linear function, and a very complicated function.

Case 1. f takes the hyperbolic tangent function. Let $f(x) = \tanh(x)$. In order to make the neural system (5) chaos, we take $k = 60$. Then we get an attractor shown in Figure 3. The Lyapunov exponents are 0.156, 0.000, and -1.4273. The first

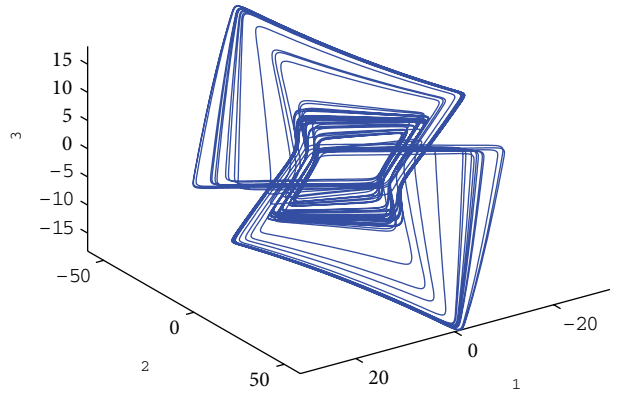

Figure 3: The phase portrait of (5) with $f(x) = \tanh(x)$ and $k = 60$.

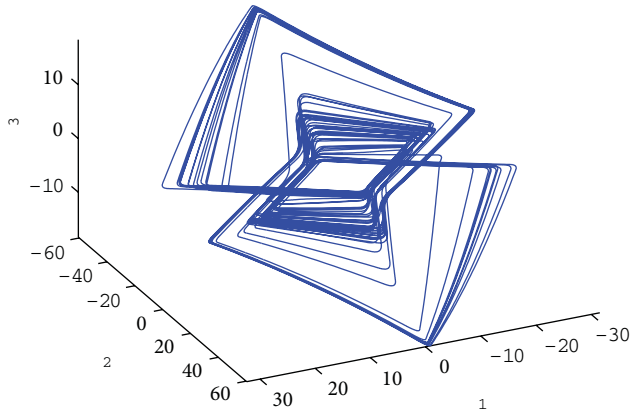

Figure 4: The phase portrait of (5) with $f(x) = 0.5(|x+1| - |x-1|)$ and $k = 60$.

one is positive showing that the attractor is most likely chaotic.

Case 2. f takes the Logistic (sigmoid) function. Take $f(x) = 1/(1+e^{-x}) = 0.5\tanh(x)+0.5$, then $\tanh(x) = 2f(x)+1$. From the previous subsection, we have a Hopfield neural network with the Logistic (sigmoid) activation function:

$$\dot{x} = -\operatorname{diag}(a)\, x + 2kWf(x) + b. \tag{6}$$

Here, $b = kW[1, 1, 1]^T$ is the bias.

Case 3. f is a piecewise linear function. Let $f(x) = 0.5(|x+1| - |x-1|)$. In order to make the neural system (5) chaos, we also take $k = 60$. Then we get an attractor shown in Figure 4. The three Lyapunov exponents are 0.169, 0.000, and −1.450. The first one is positive suggesting the attractor is chaotic.

Case 4. f is a complicated piecewise linear function. For the system (4) and the weight matrix (3) at $p = 0$, we take a more complicated $f(x_i)$ randomly as shown in Figure 5. Let $k = 100$, a chaotic attractor appears as shown in Figure 6. Since the activation function is too complicate, it is not easy to compute the Lyapunov exponent of the attractor in Figure 6

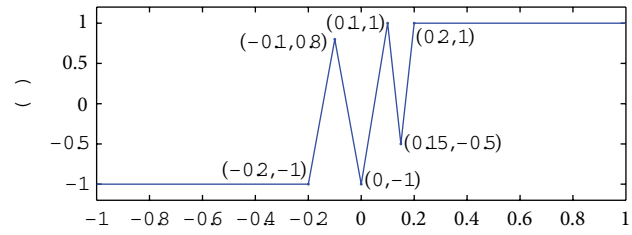

Figure 5: The plot of the piecewise function $f(x_i)$.

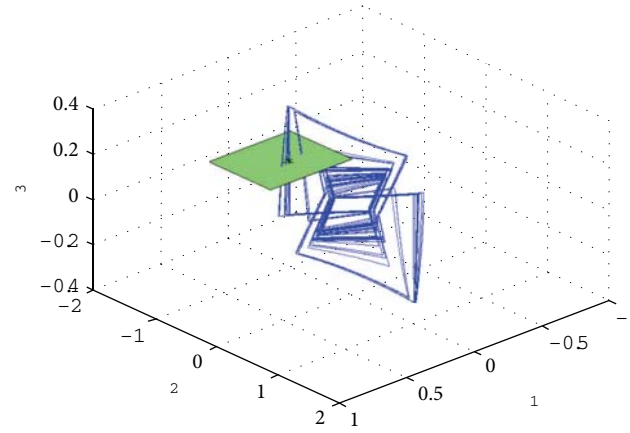

Figure 6: The attractor we observed and the poincaré plane $P : x_3 = 0.2$.

with enough accuracy; so, in next section we will prove that this attractor is indeed chaotic with the topological horseshoe theory.

It is clear to see from Figures 3 to 6 that although their activation functions are much different, the chaotic attractor exists in all four cases and they all look similar. All the above four cases suggest that the existence of chaos in this neural network is robust on the type of activation functions. In another word, the complex dynamics of a small neural network should be more related to its weight matrix.

3. Computer-Assisted Proof of Chaos

The existence of a topological horseshoe is recognized as one of the most important signatures of chaos. With the horseshoe theory, one can not only prove chaos rigorously but also reveal the mechanism of chaos with its invariant set. So we will present computer-assisted proof of chaos in the HNN in this section. First, let us recall a theorem on topological horseshoe and the m-shift and then present our main results.

Let X be a metric space, Q is a compact subset of X, and $g : Q \to X$ is map satisfying the assumption that there exist m mutually disjoint compact subsets $Q_1, Q_2, \ldots, Q_m$ of Q, the restriction of g to each Q_i, that is, $g \mid Q_i$ is continuous.

Definition 1. Let γ be a compact subset of Q, such that for each $1 \le i \le m$, $\gamma_i = \gamma \cap Q_i$ is nonempty and compact; then

γ is called a connection with respect to $Q_1, Q_2, \ldots, Q_m$. Let F be a family of connections γs with respect to $Q_1, Q_2, \ldots, Q_m$ satisfying property: $\gamma \in F \Rightarrow g(\gamma_i) \in F$. Then F is said to be g-connected family with respect to $Q_1, Q_2, \ldots, Q_m$.

Theorem 2. *Suppose that there exists a g-connected family with respect to $Q_1, Q_2, \ldots, Q_m$. Then there exists a compact invariant set $K \subset Q$, such that K is semiconjugate to m-shift.*

In this theorem, the m-shift is also called Bernoulli shift sometimes, denoted by $\sigma : \Sigma_m \to \Sigma_m$, where Σ_m is the collection of all bi-infinite sequences

$$s = \{\ldots, s_{-n}, \ldots, s_{-1}; s_0, s_1, \ldots, s_n, \ldots\}, \quad s_i \in \{0, 1, \ldots, m-1\}, \tag{7}$$

and the shift map σ is defined as

$$\sigma(s) = \{\ldots, s_{-n+1}, \ldots, s_0; s_1, s_2, \ldots, s_{n+1}, \ldots\}. \tag{8}$$

It is well known that Σ_m is a Cantor set, which is compact, totally disconnected, and perfect. As a dynamical system defined on Σ_m, σ has a countable infinity of periodic orbits consisting of orbits of all periods, an uncountable infinity of aperiodic orbits, and a dense orbit. A direct consequence of these three properties is that the dynamics generated by the shift map is sensitive to initial conditions. Since g is topologically semiconjugate to σ, which means that there exists a continuous surjection $h : \Sigma_m \to X$ such that $f \circ h = h \circ \sigma$, g must be also sensitive to initial conditions. Mathematically, the complexity of the system g can be measured by its topological entropy, which roughly means the exponential growth rate of the number of distinguishable orbits as time advances. As another result of the semiconjugate, the topological entropy of g, denoted by ent(g), is not less then m. When $m > 1$, ent(g) > 0, therefore the system is chaotic. For more details of the above symbolic dynamics and horseshoe theory, we refer the reader to [21–24].

In what follows we will study existence of horseshoes embedded in the attractor in Figure 2. For this purpose, we will utilize the technique of cross section and the corresponding Poincaré map. Consider the section plane $P : x_3 = 0.2$, as shown in Figure 2. The Poincaré map $\pi : P \to P$ is chosen as follows. For each $x \in P$, $\pi(x)$ is taken to be the second return point in P under the flow with the initial condition x.

To find the horseshoe, we use the efficient method proposed in [21, 25] which has been implemented with a MATLAB toolbox called "a toolbox for finding horseshoes in 2D map" (download: http://www.mathworks.com/matlabcentral/fileexchange/14075). The method is so powerful that it has been successfully applied in a number of chaotic systems [26–29], a fractional-order system [30],even a hyperchaotic system [31].

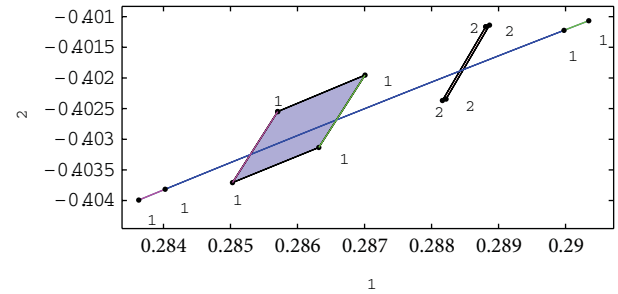

Figure 7: The image $\pi(|A_1B_1C_1D_1|)$ lies wholly across $|A_1B_1C_1D_1|$ and $|A_2B_2C_2D_2|$.

After many attempts, we carefully pick two quadrangles $|A_1B_1C_1D_1|$ and $|A_2B_2C_2D_2|$ in this section plane P with their vertices as follows:

$$\begin{aligned} A_1 &= (0.28570, -0.40254, 0.2), \\ B_1 &= (0.28700, -0.40195, 0.2), \\ C_1 &= (0.28631, -0.40313, 0.2), \\ D_1 &= (0.28502, -0.40370, 0.2), \\ A_2 &= (0.28880, -0.40116, 0.2), \\ B_2 &= (0.28886, -0.40114, 0.2), \\ C_2 &= (0.28821, -0.40234, 0.2), \\ D_2 &= (0.28816, -0.40237, 0.2). \end{aligned} \tag{9}$$

By means of interval analysis, we compute the Poincaré map on $|A_1B_1C_1D_1|$ and $|A_2B_2C_2D_2|$ and then have the following statement.

Theorem 3. *For the Poincaré map π corresponding to the cross sections $|A_1B_1C_1D_1|$ and $|A_2B_2C_2D_2|$, there exists a closed invariant set $\Lambda \subset Q \triangleq |A_1B_1C_1D_1| \cup |A_2B_2C_2D_2|$ for which $\pi \mid \Lambda$ is semiconjugate to the 2-shift map.*

Proof. To prove this statement, we will find two disjoint compact subsets Q_1 and Q_2 of Q, such that the existence of a π-connected family can be easily derived.

The first subset Q_1 takes $|A_1B_1C_1D_1|$ as shown in Figure 7, and the Poincaré map sends this subset to its image $|A_1'B_1'C_1'D_1'|$ as follows:

$$A_1D_1 \longrightarrow A_1'D_1', \qquad B_1C_1 \longrightarrow B_1'C_1', \tag{10}$$

showing that A_1D_1 is mapped left of the side A_1D_1 and B_1C_1 is mapped right of the side B_2C_2. In this case, we say that the image $\pi(|A_1B_1C_1D_1|)$ lies wholly across the quadrangles $|A_1B_1C_1D_1|$ and $|A_2B_2C_2D_2|$ with respect to A_1D_1 and B_2C_2.

The second subset Q_2 takes $|A_2B_2C_2D_2|$ as shown in Figure 8, and the Poincaré map sends this subset to its image $|A_2'B_2'C_2'D_2'|$ as follows:

$$A_2D_2 \longrightarrow A_2'D_2', \qquad B_2C_2 \longrightarrow B_2'C_2', \tag{11}$$

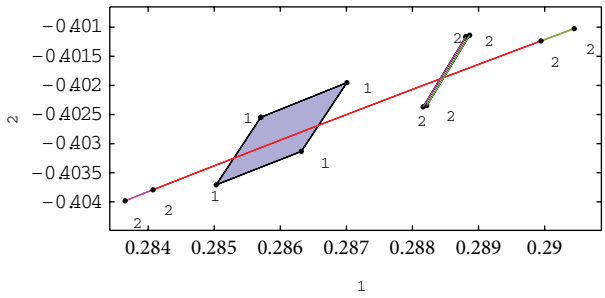

FIGURE 8: The image $\pi(|A_2B_2C_2D_2|)$ lies wholly across $|A_1B_1C_1D_1|$ and $|A_2B_2C_2D_2|$.

showing that A_2D_2 is mapped left of the side A_1D_1 and B_2C_2 is mapped right of the side B_2C_2. In this case, we say that the image $\pi(|A_2B_2C_2D_2|)$ lies wholly across the quadrangles $|A_1B_1C_1D_1|$ and $|A_2B_2C_2D_2|$ with respect to A_1D_1 and B_2C_2.

Generally, (2) can be regarded as a switching system consisting of eight very simple continuous subsystems and 12 quarter planes called switching planes; for detail, see [5]. In this system, every trajectory in the neighborhood of the attractor transversely intersects with the switching plane, and the Poincaré map π can be regarded as a composition of a series of continuous submaps by the subsystems. Since each subsystem is linear, it is easy to prove that for the quadrangle region $|A_1B_1C_1D_1|$ or $|A_2B_2C_2D_2|$ all submaps are continuous; consequently, $\pi \mid Q$ is continuous.

Note that the subsets $|A_1B_1C_1D_1|$ and $|A_2B_2C_2D_2|$ are mutually disjointed. It is easy to see from the whole acrossness of $\pi(|A_1B_1C_1D_1|)$ and $\pi(|A_2B_2C_2D_2|)$ with respect to A_1D_1 and B_2C_2 that there exists a π-connected family with respect to $Q_1 = |A_1B_1C_1D_1|$ and $Q_2 = |A_2B_2C_2D_2|$. In view of Theorem 2, this means that the Poincaré map π is semiconjugate to 2-shift map.

It is easy to see from Theorem 3 that the entropy of π is not less than log 2, so the attractor in Figure 2 is a chaotic attractor indeed.

So we can prove the existence of chaos in the attractor shown in Figure 6 by the same way in Section 3. The new vertices of the two subsets $|A_1B_1C_1D_1|$ and $|A_2B_2C_2D_2|$ are

$$\begin{aligned} A_1 &= (0.28589, -0.40149, 0.2), \\ B_1 &= (0.28766, -0.40075, 0.2), \\ C_1 &= (0.28730, -0.40122, 0.2), \\ D_1 &= (0.28555, -0.40196, 0.2), \\ A_2 &= (0.28999, -0.39985, 0.2), \\ B_2 &= (0.29007, -0.39982, 0.2), \\ C_2 &= (0.28996, -0.40002, 0.2), \\ D_2 &= (0.28988, -0.40005, 0.2). \end{aligned} \tag{12}$$

The images of $|A_1B_1C_1D_1|$ and $|A_2B_2C_2D_2|$ are shown in Figure 9, from which we can see easily that the images of $|A_1B_1C_1D_1|$ and $|A_2B_2C_2D_2|$ across simultaneously $|A_1B_1C_1D_1|$ and $|A_2B_2C_2D_2|$, that is, analogous to Figures 7 and 8. From Theorem 2, we infer that there exists

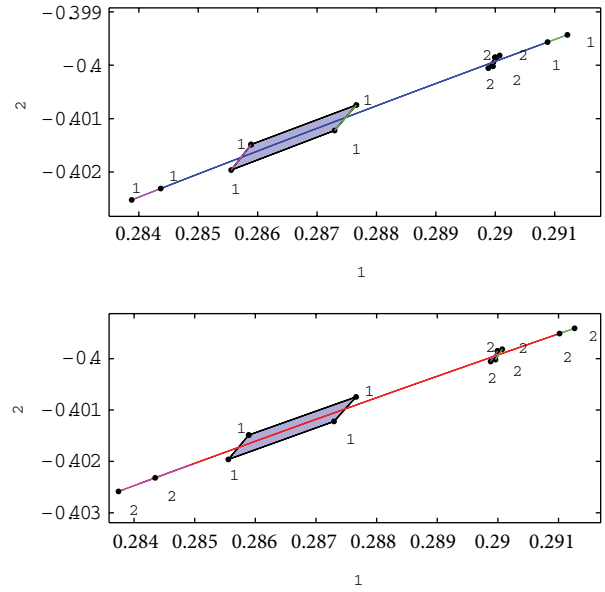

FIGURE 9: The new topological horseshoe.

a β-connected family with respect to $|A_1B_1C_1D_1|$ and $|A_2B_2C_2D_2|$, where β is the corresponding Poincaré map. From the topological horseshoe theory we have $\mathrm{ent}(\pi) \geqslant \log 2$ after similar arguments. The positive entropy suggests that the attractor in Figure 6 is chaotic indeed. □

4. Conclusions

In this paper, we have studied a 3D Hopfield neural network with the sign activation function. Computer simulation shows that this HNN can exhibit chaotic attractors and limit cycles with respect to p. In order to verify the chaotic behavior, we present a computer-assisted verification for the existence of horseshoes imbedded in this system. We also show evidence that chaos could possibly be exhibited by the HNN with any type of sigmoidal activation function. In another word, such chaos should be more related to its weight matrix than the type of activation functions. In addition, since the HNN is a switching system only consisting of stable subsystems, this fact suggests that the dynamics of a hybrid system could be much more complex than we used to think. This may be of interest to researchers of neural networks, nonlinear dynamics, and so on.

Acknowledgments

This work is supported in part by the National Natural Science Foundation of China (61104150), Natural Science Foundation Project of Chongqing (cstcjjA40044), and Doctoral Fund of CQUPT (A2009-12).

References

[1] M. R. Guevara, L. Glass, M. C. Mackey, and A. Shrier, "Chaos in neurobiology," *IEEE Transactions on Systems, Man and Cybernetics*, vol. 13, no. 5, pp. 790–798, 1983.

[2] A. Babloyantz and C. Lourenço, "Brain chaos and computation," *International Journal of Neural Systems*, vol. 7, no. 4, pp. 461–471, 1996.

[3] J. Guckenheimer and R. A. Oliva, "Chaos in the Hodgkin-Huxley model," *SIAM Journal on Applied Dynamical Systems*, vol. 1, no. 1, pp. 105–114, 2002.

[4] J. E. Lewis and L. Glass, "Nonlinear dynamics and symbolic dynamics of neural networks," *Neural Computation*, vol. 4, no. 5, pp. 621–642, 1992.

[5] R. Edwards, "Analysis of continuous-time switching networks," *Physica D*, vol. 146, no. 1–4, pp. 165–199, 2000.

[6] H. Bersini and P. Sener, "The connections between the frustrated chaos and the intermittency chaos in small Hopfield networks," *Neural Networks*, vol. 15, no. 10, pp. 1197–1204, 2002.

[7] Q. Li and X.-S. Yang, "Chaotic dynamics in a class of three dimensional Glass networks," *Chaos*, vol. 16, no. 3, Article ID 033101, 5 pages, 2006.

[8] X.-S. Yang and Q. Li, "Chaos in simple cellular neural networks with connection matrices satisfying Dale's rule," *International Journal of Bifurcation and Chaos in Applied Sciences and Engineering*, vol. 17, no. 2, pp. 583–587, 2007.

[9] Q. Li, X. S. Yang, and F. Yang, "Hyperchaos in a simple CNN," *International Journal of Bifurcation and Chaos*, vol. 16, no. 8, pp. 2453–2457, 2006.

[10] Q. Li and X. S. Yang, "Two kinds of horseshoes in a hyperchaotic neural network," *International Journal of Bifurcation and Chaos*, vol. 22, no. 8, Article ID 1250200, 2012.

[11] L. Li and L. Chong-xin, "Application of chaos and neural network in power load forecasting," *Discrete Dynamics in Nature and Society*, vol. 2011, Article ID 597634, 12 pages, 2011.

[12] T. Kanamaru and K. Aihara, "Rewiring-induced chaos in pulse-coupled neural networks," *Neural Computation*, vol. 24, no. 4, pp. 1020–1046, 2012.

[13] M. A. Arbib, P. Erdi, and J. Szentagothai, *Neural Organization: Structure, Function, and Dynamics*, MIT Press, Cambridge, Mass, USA, 1997.

[14] F. Pasemann, "Complex dynamics and the structure of small neural networks," *Network*, vol. 13, no. 2, pp. 195–216, 2002.

[15] A. Das, P. Das, and A. B. Roy, "Chaos in a three-dimensional general model of neural network," *International Journal of Bifurcation and Chaos in Applied Sciences and Engineering*, vol. 12, no. 10, pp. 2271–2281, 2002.

[16] Q. Li and X. Yang, "Complex dynamics in a simple hopfield-type neural network," in *Advances in Neural Networks—ISNN 2005*, vol. 3496 of *Lecture Notes in Computer Science*, pp. 357–362, Springer, Berlin, Germany, 2005.

[17] X. S. Yang and Y. Huang, "Complex dynamics in simple Hopfield neural networks," *Chaos*, vol. 16, no. 3, Article ID 033114, 2006.

[18] Q. Yuan, Q. Li, and X.-S. Yang, "Horseshoe chaos in a class of simple Hopfield neural networks," *Chaos, Solitons and Fractals*, vol. 39, no. 4, pp. 1522–1529, 2009.

[19] Z. H. Guan, F. Liu, J. Li, and T. Li, "A new chaotic hopfield neural network and its synthesis via parameter switchings ," *Neurocomputing*. In press.

[20] J. J. Hopfield, "Neurons with graded response have collective computational properties like those of two-state neurons," *Proceedings of the National Academy of Sciences of the United States of America*, vol. 81, no. 10, pp. 3088–3092, 1984.

[21] Q. Li and X.-S. Yang, "A simple method for finding topological horseshoes," *International Journal of Bifurcation and Chaos in Applied Sciences and Engineering*, vol. 20, no. 2, pp. 467–478, 2010.

[22] Q. Li, L. Zhang, and F. Yang, "An algorithm to automatically detect the Smale horseshoes," *Discrete Dynamics in Nature and Society*, vol. 2012, Article ID 283179, 9 pages, 2012.

[23] X.-S. Yang, "Topological horseshoes and computer assisted verification of chaotic dynamics," *International Journal of Bifurcation and Chaos in Applied Sciences and Engineering*, vol. 19, no. 4, pp. 1127–1145, 2009.

[24] X.-S. Yang and Y. Tang, "Horseshoes in piecewise continuous maps," *Chaos, Solitons and Fractals*, vol. 19, no. 4, pp. 841–845, 2004.

[25] Q. Li, "A topological horseshoe in the hyperchaotic Rössler attractor," *Physics Letters A*, vol. 372, no. 17, pp. 2989–2994, 2008.

[26] C. Lia, L. Wub, H. Lic, and Y. Tongc, "A novel chaotic system and its topological horseshoe," *Nonlinear Analysis*, vol. 18, no. 1, pp. 66–77, 2013.

[27] Q.-j. Fan, "Horseshoe in a modified Van der Pol-Duffing circuit," *Applied Mathematics and Computation*, vol. 210, no. 2, pp. 436–440, 2009.

[28] Q. Li and X.-S. Yang, "New walking dynamics in the simplest passive bipedal walking model," *Applied Mathematical Modelling*, vol. 36, no. 11, pp. 5262–5271, 2012.

[29] Q. Fan, "Horseshoe chaos in a hybrid planar dynamical system," *International Journal of Bifurcation and Chaos*, vol. 22, no. 8, Article ID 1250202, 2012.

[30] Q. D. Li, S. Chen, and P. Zhou, "Horseshoe and entropy in a fractional-order unified system," *Chinese Physics B*, vol. 20, no. 1, Article ID 010502, 2011.

[31] Q. Li, X. S. Yang, and S. Chen, "Hyperchaos in a spacecraft power system," *International Journal of Bifurcation and Chaos*, vol. 21, no. 6, pp. 1719–1726, 2011.

Hindawi Publishing Corporation
Discrete Dynamics in Nature and Society
Volume 2013, Article ID 875749, 6 pages
http://dx.doi.org/10.1155/2013/875749

Research Article

Perturbation of Stochastic Boussinesq Equations with Multiplicative White Noise

Chunde Yang and Xin Zhao

Institute of System Theory and Application, Chongqing University of Posts and Telecommunications, Chongqing 400065, China

Correspondence should be addressed to Chunde Yang; yangcqupt@yeah.net

Received 28 December 2012; Accepted 28 March 2013

Academic Editor: Xiaofeng Liao

This paper studies the Boussinesq equations perturbed by multiplicative white noise and shows the existence and uniqueness of the global solution. It also gets some regularity results for the unique solution.

1. Introduction

The Boussinesq equation is a mathematics model of thermohydraulics, which consists of equations of fluid and temperature in the Boussinesq approximation. The deterministic case has been studied systematically by many authors (e.g., see [1–3]). However, in many practical circumstances, small irregularity has to be taken into account. Thus, it is necessary to add to the equation a random force, which is in general a space-time white noise, as considered recently by many authors for other equations (see [4–11]). The random attractors of boussinesq equations with multiplicative noise have been investigated by [12]. In this paper, We will study the perturbation of stochastic boussinesq equations with multiplicative white noise.

We will consider the following stochastic two-dimension a Boussinesq equations perturbed by a multiplicative white noise of Stratonovich form:

$$\begin{aligned} dv + \left[(v\cdot\nabla)\, v - v\Delta v + \nabla p\right] dt \\ = e_2 \left(T - T_1\right) dt + \sigma v \circ dw\,(t)\,, \\ dT + \left[(v\cdot\nabla)\, T - \lambda\Delta T\right] dt = 0, \\ \operatorname{div} v = 0. \end{aligned} \tag{1}$$

The domain occupied by the fluid is $D = (0,1)\times(0,1)$, and e_1, e_2 is the canonical basis of $\mathbb{R}^2$. The unknown $v = (v_1, v_2)$, T, and p stand for the velocity vector, temperature, and pressure, respectively. T_1 is the temperature at the top, $x_2 = 1$, while $T_0 = T_1 + 1$ is the temperature at the boundary below, $x_2 = 0$. The constant numbers $\lambda > 0$, $\beta > 0$, and $\sigma > 0$ are related to the usual Prandtl, Grashof, and Rayleigh numbers.

$W(t)$ is two-sided Wiener processes on the probability space $(\Omega, \mathbb{F}, P)$, where $\Omega = \{\omega \in C(\mathbb{R},\mathbb{R}) : \omega(0) = 0\}$, $\mathbb{F}$ is the Borel sigma-algebra induced by the compact-open topology of Ω, and P is a Wiener measure.

We supplement (1) with the following boundary condition:

$$\begin{gathered} v = 0 \quad \text{at } x_2 = 0,\ x_2 = 1, \\ T = T_0 \quad \text{at } x_2 = 0, \qquad T = T_1 = T_0 - 1 \quad \text{at } x_2 = 1, \\ \psi|_{x_1=0} = \psi|_{x_1=1} \quad \text{for } \psi = v,\ T,\ p,\ \frac{\partial v}{\partial x_1},\ \frac{\partial T}{\partial x_1}. \end{gathered} \tag{2}$$

When an initial-valued problem is considered, we supplement these equations with

$$v(x,0) = v_0(x), \quad T(x,0) = T_0(x) \quad \text{for } x \in D. \tag{3}$$

The existence of a compact random attractor and its Hausdorff, fractal dimension estimates have been investigated by [12]. We will solve pathwise (1)–(3). By using the Faedo-Galerkin approximation and a priori estimates, we prove the existence and uniqueness of the global solution and show that the solution continuously depends on the initial value. We also get some regularity results of the solutions.

2. Mathematical Setting and Basic Estimates

Let

$$\eta := T - T_0 + x_2, \tag{4}$$

and change p to $p - x_2 + x_2^2/2$; then (1) can be rewritten as

$$\begin{aligned} dv + \left[(v\cdot\nabla)\, v - \beta\Delta v + \nabla p\right] dt &= e_2\eta dt + \sigma v \circ dW, \\ d\eta + \left[(v\cdot\nabla)\,\eta\right] dt &= v_2 dt, \\ \operatorname{div} v &= 0. \end{aligned} \tag{5}$$

Let the process be

$$\alpha(t) := e^{-\sigma W(t)}. \tag{6}$$

Then $d\alpha = -\sigma\alpha \circ dW$, and if we let

$$\xi := \alpha v, \tag{7}$$

we get the new equations (no stochastic differential appears here)

$$\frac{d\xi}{dt} + \alpha^{-1}(\xi\cdot\nabla)\,\xi - \beta\Delta\xi + \alpha\nabla p = \alpha e_2\eta, \tag{8}$$

$$\frac{d\eta}{dt} + \alpha^{-1}(\xi\cdot\nabla)\,\eta - \lambda\Delta\eta = \alpha^{-1}\xi_2, \tag{9}$$

$$\operatorname{div}\xi = 0, \tag{10}$$

with the boundary conditions

$$\begin{aligned} &\xi = 0 \quad \text{at } x_2 = 0,\ x_2 = 1, \\ &\eta = 0 \quad \text{at } x_2 = 0,\ x_2 = 1, \\ &\psi|_{x_1=0} = \psi|_{x_1=1} \quad \text{for } \psi = \xi, \eta, p, \frac{\partial\xi}{\partial x_1}, \frac{\partial\eta}{\partial x_1} \end{aligned} \tag{11}$$

and the initial value conditions

$$\xi(0) = \xi_0, \qquad \eta(0) = \eta_0. \tag{12}$$

To solve (8)–(12), we consider the Hilbert space $H = H_1 \times H_2$ with the scalar products $(\cdot,\cdot)$ and norms $|\cdot|$, where $H_2 = L^2(D)$ and

$$H_1 = \left\{\xi \in L^2(D) : \operatorname{div}\xi = 0,\ \xi_i|_{x_i=0} = \xi_i|_{x_i=1},\ i = 1,2\right\}. \tag{13}$$

We also consider the subspace $V = V_1 \times V_2$ of H, where V_2 is the space of functions in $H^1(D)$ vanishing at $x_2 = 0$ and $x_2 = 1$ and periodic in the direction of x_1. V_2 is a Hilbert space for the scalar product and the norm

$$((\eta_1,\eta_2)) = \int_D \operatorname{grad}\eta_1 \operatorname{grad}\eta_2\, dx,\ \|\eta\| = ((\eta,\eta))^{1/2}, \tag{14}$$

and $V_1 = \{\xi \in V_2^2 : \operatorname{div}\xi = 0\}$. We also denote by $((\cdot,\cdot))$ and $\|\cdot\|$ the canonical scalar product and norm in V_1 and V.

The bilinear form

$$\begin{aligned} \mu(u_1,u_2) &= \beta((\xi_1,\xi_2)) + \lambda((\eta_1,\eta_2)), \\ &\forall \{\xi_i,\eta_i\} \in V,\ i = 1,2, \end{aligned} \tag{15}$$

determines a linear isomorphism A from $D(A)$ into H and from V into the dual space V', defined by

$$(Au_1,u_2) = \mu(u_1,u_2), \quad \forall u_i = \{\xi_i,\eta_i\} \in V,\ i = 1,2, \tag{16}$$

with $D(A) = D(A_1) \times D(A_2)$, where

$$\begin{aligned} D(A_1) &= \left\{\xi \in V_1 \cap H^2(D)^2 : \frac{\partial\xi}{\partial x_1}\bigg|_{x_1=0} = \frac{\partial\xi}{\partial x_1}\bigg|_{x_1=1}\right\} \\ D(A_2) &= \left\{\eta \in V_2 \cap H^2(D) : \frac{\partial\eta}{\partial x_1}\bigg|_{x_1=0} = \frac{\partial\eta}{\partial x_1}\bigg|_{x_1=1}\right\}. \end{aligned} \tag{17}$$

Four spaces $D(A)$, V, H, and V' satisfy

$$D(A) \subset V \subset H \subset V' \tag{18}$$

and all embedding injections are densely continuous. It is well known that $A : D(A) \to H$ is self-adjoint and positive and A^{-1} is a compact self-adjoint in H.

We also consider the trilinear forms γ on V defined by

$$\begin{aligned} \gamma(u_1,u_2,u_3) &= ((\xi_1\cdot\nabla)\,\xi_2,\xi_3) + ((\xi_1\cdot\nabla)\,\eta_2,\eta_3), \\ &\forall u_i = \{\xi_i,\eta_i\} \in V,\ i = 1,2,3. \end{aligned} \tag{19}$$

The trilinear form γ is continuous on V or even on $H^1(D)^2 \times H^1(D)$. We associate with the form γ the bilinear continuous operator B which map $V \times V$ into V' and $D(A) \times D(A)$ into H, defined by

$$\begin{aligned} (B(u_1,u_2),u_3) &= \gamma(u_1,u_2,u_3), \\ &\forall u_i = \{\xi_i,\eta_i\} \in V,\ i = 1,2,3. \end{aligned} \tag{20}$$

Finally, we define the continuous operators $R(t)$ in H

$$R(t) : u = \{\xi,\eta\} \longrightarrow Ru = \left\{\alpha(t)\, e_2\eta, \alpha^{-1}(t)\,\xi_2\right\}. \tag{21}$$

Now, we can set (8) in the operator form. If $u = \{\xi,\eta\}$ is the solution of (8) and $\psi = \{f,g\}$ is a test function in V, we multiply (8) by f and (9) by g, integrate over D, and add the resulting equation. The pressure term disappears and after simplification we find

$$\begin{aligned} &\frac{d}{dt}(u,\psi) + \alpha^{-1}(u,u,\psi) + \mu(u,\psi) + (R(t)\,u,\psi) = 0, \\ &\forall \psi \in V, \end{aligned} \tag{22}$$

which can be reinterpreted as

$$\frac{du}{dt} + Au + \alpha^{-1}(t)\, B(u,u) + R(t)\,u = 0. \tag{23}$$

Note that this equation differs from the determined case, and in determined case, the family $R(t)$ of operator is independent of the time t. Initial condition (12) can be reinterpreted as

$$u(0) = u_0 := \{\xi_0, \eta_0\}. \tag{24}$$

To solve (23)-(24), we also need some Sobolev norm estimates on the bilinear B and the operators R and A.

Lemma 1. *The bilinear operators $B : V \times V \to V'$ and $D(A) \times D(A) \to H$ are continuous and satisfy*

(i) $(B(u,v),v) = 0$, *for all* $u, v \in V$,

(ii) $|(B(u,v),w)| \le c_1 |u|^{\theta_1} \|u\|^{1-\theta_1} \|v\| \|w\|^{\theta_1} |w|^{1-\theta_1}$, *for all* $u, v, w \in V$,

(iii) $|B(u,v)| + |B(v,u)| \le c_2 \|u\| \|v\|^{1-\theta_2} |Av|^{\theta_2}$, *for all* $u \in V$, $v \in D(A)$,

(iv) $|B(u,v)| \le c_3 |u|^{\theta_3} \|u\|^{1-\theta_3} |Av|^{\theta_3} \|v\|^{1-\theta_3}$, *for all* $u \in V$, $v \in D(A)$,

where c_1, c_2, c_3 are appropriate constants and $\theta_i \in [0,1)$, $i = 1,2,3$.

Proof. The proof is the same as the deterministic case (see [10]). □

Lemma 2. *The linear continuous operators $R : V \to V'$ and $D(A) \to H$ satisfy*

$$|R(t)u| \le c_4 (\alpha(t)) + \alpha^{-1}(t) \|u\|, \quad \forall u \in V, \ \forall t \ge 0, \tag{25}$$

$$|(R(t)u, u)| \le c_4 \left(\alpha(t) + \alpha^{-1}(t)\right) \|u\| |u|, \quad \forall u \in V, \ \forall t \ge 0. \tag{26}$$

Proof. By (21), we have

$$\begin{aligned} |Ru| &= \left|\alpha e_2 \eta\right| + \left|\alpha^{-1} \xi_2\right| \\ &\le \alpha |\eta| + \alpha^{-1} |\xi| \le \left(\alpha + \alpha^{-1}\right) (|\xi| + |\eta|) \end{aligned} \tag{27}$$

which implies by the Poincare inequality

$$|u| \le c_4 \|u\|, \quad \text{for } u \in V \tag{28}$$

that (25) holds true. Since $|(Ru,u)| \le |Ru||u|$, it follows from (25) that (26) holds true. □

Lemma 3. *The bilinear form μ on $V \times V$ satisfies*

$$c_5 \|u\|^2 \le \mu(u,u) \le c_6 \|u\|^2, \quad \text{for } u \in V. \tag{29}$$

Proof. By (15), we have

$$\begin{aligned} \mu(u,u) &= \beta \|\xi\|^2 + \lambda \|\eta\|^2 \le (\beta + \lambda) (\|\xi\| + \|\eta\|)^2 \\ &= (\beta + \lambda) \|u\|^2, \\ \mu(u,u) &\ge \min\{\beta, \lambda\} \left(\|\xi\|^2 + \|\eta\|^2\right) \\ &\ge \frac{1}{2} \min\{\beta, \lambda\} \left(\|\xi\|^2 + \|\eta\|^2\right), \end{aligned} \tag{30}$$

which imply (28). □

3. Existence and Uniqueness

In this section, we will prove the existence and uniqueness of the global solution of (23)-(24), equivalently (8)–(12) or (1)–(3). We are working almost surely for $\omega \in \Omega$.

Theorem 4. *Assume that $u_0 \in H$, then there exists a unique solution of* (23)-(24), *such that*

$$u \in C([0,\infty), H) \cap L^2_{\text{loc}}(0,\infty; V), \tag{31}$$

and the mapping $u_0 \mapsto u(t)$ is continuous from H into $D(A)$, for all $t > 0$.

Proof. Since $A^{-1} : H \to D(A)$ is a self-adjoint compact operator in H, it follows from a classical spectral theorem that there exists a sequence $\lambda_j : 0 < \lambda_1 \le \lambda_2 \le \cdots, \lambda_j \to \infty$ and a family of elements $w_j \in D(A)$ which is completely orthogonal in H such that

$$Aw_j = \lambda_j w_j, \quad \forall j. \tag{32}$$

For each m, we look for an approximate solution u_m of the following form:

$$u_m(t) = \sum_{i=1}^{m} g_{im}(t) w_i \tag{33}$$

satisfying

$$\begin{aligned} &\frac{d}{dt}\left(u_m, w_j\right) + \mu\left(u_m, w_j\right) \\ &\quad + \alpha^{-1} \gamma\left(u_m, u_m, w_j\right) + \left(Ru_m, w_j\right) = 0, \quad j = 1, 2, \ldots, m \end{aligned} \tag{34}$$

and initial condition

$$u_m(0) = P_m u_0, \tag{35}$$

where P_m is the projector in H (or V) on the space spanned by $w_1, w_2, \ldots, w_m$. Since A and P_m commute, the above equation is also equivalent to

$$\frac{du_m}{dt} + Au_m + \alpha^{-1} P_m B\left(u_m, u_m\right) + P_m\left(Ru_m\right) = 0, \tag{36}$$

where

$$P_m\left(Ru_m\right) = \sum_{j=1}^{m} g_{jm}(t) P_m R w_j, \tag{37}$$

in view of the linearity of P_m, R.

The existence of u_m on any finite interval $[0, T_m)$ follows from standard results of the existence of solutions of ordinary differential equations that $T_m = +\infty$ is a consequence of these results and of the following priori estimates:

$$\begin{aligned} &u_m \text{ remains bounded in } L^\infty(0,T;H) \cap L^2(0,T;V), \\ &\qquad \forall T > 0. \end{aligned} \tag{38}$$

Indeed, multiplying (34) by g_{jm}, summing these relations for $j = 1, 2, \ldots, m$, and noting that $\alpha^{-1}\mu(u_m, u_m, u_m) = 0$ (by Lemma 1), we find

$$\frac{1}{2}\frac{d}{dt}|u_m|^2 + \mu(u_m, u_m) + (Ru_m, u_m) = 0, \tag{39}$$

which implies by Lemma 2, (29), and the Young inequality that

$$\begin{aligned}
&\frac{1}{2}\frac{d}{dt}|u_m|^2 + c_5\|u_m\|^2 \\
&\quad \le |(Ru_m, u_m)| \\
&\quad \le c_4 \sup_{0\le t\le T}\left(\alpha(t) + \alpha^{-1}(t)\right)\|u_m\| \cdot |u_m| \\
&\quad \le \frac{c_5}{2}\|u_m\|^2 + c_4'|u_m|^2,
\end{aligned} \tag{40}$$

that is,

$$\frac{d}{dt}|u_m|^2 + c_5\|u_m\|^2 \le c'|u_m|^2, \tag{41}$$

where c_5 is defined in (29) and c' is a appropriate constant. Using the classical Gronwall lemma we find

$$|u_m(t)|^2 \le |u_m(0)|^2 e^{c'T} \le |u_0|^2 e^{c'T} = M_1, \quad \forall 0 < t \le T. \tag{42}$$

Integrating (41) for t from 0 to T and using above estimates we have

$$\begin{aligned}
&\int_0^T \|u_m\|^2 dt \\
&\quad \le \frac{1}{c_5}\left(|u_m(0)|^2 - |u_m(T)|^2\right) + \frac{1}{c_5}\int_0^T |u_m(t)|^2 dt \\
&\quad \le M_2,
\end{aligned} \tag{43}$$

where M_1 and M_2 are independent of m. Thus, we have proved (38).

We also claim that

$$\frac{du_m}{dt} \text{ remains bounded in } L^2\left(0, T;\ V'\right). \tag{44}$$

Indeed, it follows from Lemma 1 that $|B(u_m, u_m)|V' \le c|u_m|\|u_m\|$ with appropriate constant c, which, together with (38), implies that $B(u_m, u_m)$ and thus $P_m B(u_m, u_m)$ remain bounded in $L^2(0, T; V')$. Since both operators $R : V \to V'$ and $A : V \to V'$ are continuous (Lemmas 2 and 3), it follows from (38) that Au_m, Ru_m and thus $P_m Ru_m$ remain bounded in $L^2(0, T; V')$. Therefore, by (36),

$$\frac{du_m}{dt} = -Au_m - \alpha^{-1}P_m B(u_m, u_m) - P_m(Ru_m) \tag{45}$$

remains bounded in $L^2(0, T; V')$, which proved (44).

By weak compactness, it follows from (38) and (44) that there exists a $u \in L^\infty(0, T; H) \cap L^2(0, T; V)$, for all $T > 0$ subsequence still denoted by u_m, such that

$$\begin{aligned}
u_m &\longrightarrow u \quad \text{in } L^2(0, T; V) \text{ weakly}, \\
u_m &\longrightarrow u \quad \text{in } L^\infty(0, T; H) \text{ weakly star}, \\
\frac{du_m}{dt} &\longrightarrow \frac{du}{dt} \quad \text{in } L^2\left(0, T; V'\right) \text{ weakly}.
\end{aligned} \tag{46}$$

We pass to the limit in (34) and find that

$$\frac{d}{dt}(u, \varphi) + \mu(u, \varphi) + \alpha^{-1}\gamma(u, u, \varphi) + (Ru, \varphi), \quad \forall \varphi \in V, \tag{47}$$

which implies that u satisfies (23). In particular, $u' = (du/dt) \in L^2(0, T; V') \in L^1(0, T; V')$. This implies by [10, Lemma II.3.1] that u is almost everywhere equal to a continuous function from $[0, T]$ into V'. Therefore initial condition (24) follows by a passage to the limit in (35). $u \in C([0, T], H)$ follows from [10, Lemma II.3.2] and the facts that $H \subset V \subset V'$ and $u' \in L^2(0, T; V')$. Furthermore, if we show that uniqueness, then the fact that $u \in C([0, T], H)$, for all $T > 0$, implies that $u \in C([0, \infty), H)$.

To prove the uniqueness and continuous dependence of $u(t)$ on u_0 (in H), we let u be a solution of (23)-(24) such that $u \in C([0, \infty), H) \cap L^2_{\text{loc}}(0, \infty; V)$. Similar to (39), u must satisfy the energy equality

$$\frac{1}{2}\frac{d}{dt}|u|^2 + \mu(u, u) + (Ru, u) = 0. \tag{48}$$

By using Lemmas 1–3 and Gronwall lemma, we get the following similar estimates:

$$|u(t)|^2 \le |u(0)|^2 e^{ct}, \tag{49}$$

which has proved the continuous dependence. For the uniqueness, we let u_1, u_2 be two solutions of (23)-(24) and $u = u_1 - u_2$. Then u is also a solution with $u(0) = 0$. Thus, (49) implies that $|u(t)|^2 \le 0$, that is, $u_1 = u_2$. □

4. Regularity Results

In this section, we will consider further regularity results for the unique solution. The main result is that $u \in D(A)$, and thus $u \in H^2(D)^2 \times H^2(D)$ provided the initial function $u_0 \in V$. More precisely, we have the following.

Theorem 5. *Assume that $u_0 \in V$, and let u be the unique solution of* (23)-(24). *Then,*

$$u \in C([0, \infty), V) \cap L^2_{\text{loc}}(0, \infty; D(A)). \tag{50}$$

Proof. Let u_m be the approximate solution (33) in the proof of Theorem 4. We first claim that

$$u_m \text{ remains bounded in } L^\infty(0, T;\ V) \cap L^2(0, T; D(A)), \quad \forall T > 0. \tag{51}$$

Indeed, multiplying (34) by $\lambda_j g_{jm}$, summing these relations for $j = 1, 2, \ldots, m$, and using (32), we find

$$\left(\frac{du_m}{dt}, Au_m\right) + \mu\left(u_m, Au_m\right) + \alpha^{-1}\gamma\left(u_m, u_m, Au_m\right) + \left(Ru_m, Au_m\right) = 0. \tag{52}$$

By Lemma 1(iv) and the Young inequality, we find

$$\begin{aligned}
&\left|\alpha^{-1}\gamma\left(u_m, u_m, Au_m\right)\right| \\
&= \left|\alpha^{-1}\left(B\left(u_m, u_m\right), Au_m\right)\right| \\
&\le \sup_{0\le s\le T} \alpha^{-1}(s) \cdot c_3 |u_m|^{\theta_3} \|u_m\|^{2(1-\theta_3)} |Au_m|^{(1+\theta_3)} \\
&\le \frac{1}{4}|Au_m|^2 + c_3'(T)\|u_m\|^4 |u|^{2\theta_3/(1-\theta_3)}.
\end{aligned} \tag{53}$$

For $0 \le t \le T$, by Lemma 2, (25), and the Young inequality, we have

$$\begin{aligned}
&\left|\left(Ru_m, Au_m\right)\right| \\
&\le \sup_{0\le s\le T}\left(\alpha(s) + \alpha^{-1}(s)\right) c_4 \|u_m\| \, |Au_m| \\
&\le \frac{1}{4}|Au_m|^2 + c_4'\|u_m\|^2.
\end{aligned} \tag{54}$$

Noting also that

$$\begin{aligned}
\left(\frac{du_m}{dt}, Au_m\right) &= \left(Au_m, u_m'\right) \\
&= \mu\left(u_m, u_m'\right) = \frac{1}{2}\frac{d}{dt}\mu\left(u_m, u_m\right)
\end{aligned} \tag{55}$$

and $\mu(u_m, Au_m) = |Au_m|^2$, we find from (52) and all the above estimates that

$$\begin{aligned}
&\frac{d}{dt}\mu\left(u_m, u_m\right) + |Au_m|^2 \\
&\quad \le 2c_4'\|u_m\|^2 + 2c_3'\|u_m\|^4 |u_m|^{2\theta_3/(1-\theta_3)}.
\end{aligned} \tag{56}$$

By (38), u_m is bounded in $L^\infty(0, T; H)$. This, together with Lemma 3, implies that (56) can be rewritten as

$$\begin{aligned}
&\frac{d}{dt}\mu\left(u_m, u_m\right) + |Au_m|^2 \\
&\quad \le 2c\left(1 + \|u_m\|^2\right)\mu\left(u_m, u_m\right), \quad 0 \le t \le T
\end{aligned} \tag{57}$$

for some appropriate constant $c > 0$. By Gronwall lemma, it follows from (57) and (38) that

$$\begin{aligned}
&\mu\left(u_m(t), u_m(t)\right) \\
&\le \|u_m(0)\|^2 \exp\left(\int_0^t c\left(1 + \|u_m(s)\|^2\right) ds\right) \\
&\le M_1(T), \quad 0 \le t \le T,
\end{aligned} \tag{58}$$

which implies by Lemma 3 again that u_m remains bounded in $L^\infty(0, T; V)$. Integrating in (57) from $t = 0$ to $t = T$, we have

$$\int_0^T |Au_m(t)|^2 ds \le 2M_1 + \int_0^T M_1\left(1 + \|u_m(t)\|^2\right) ds \le M_2. \tag{59}$$

which proved the second argument of (51), and thus (51) holds.

Taking the limit in (51) (by weak compactness), we then find that u is in $L^\infty(0, T; V) \cap L^2(0, T; D(A))$. We need also to prove that u is continuous from $[0, T]$ into V. This is proved as follows.

Since $u \in C([0, T], H) \cap L^\infty(0, T; V)$ and $V \subset H$ with densely continuous injection, it follows from [10, Lemma II.3.3] that $u : [0, T] \to V$ is weakly continuous; that is, $t \mapsto ((u(t), v))$ is continuous for every $v \in V$. Similarly $t \mapsto \mu((u(t), v))$ is continuous for every $v \in V$. Thus, by taking the limit in (52) and applying [10, Lemma II.3.2], we obtain an equality similar to (52) for u:

$$\frac{d}{dt}\mu(u, u) + 2|Au|^2 + 2\alpha^{-1}\lambda(u, u, Au) + 2(Ru, u) = 0, \tag{60}$$

which holds in the distribution sense on $(0, T)$. Since $u \in L^\infty(0, T; V) \cap L^2(0, T; D(A))$, it follows from Lemma 1 and Lemma 2 that

$$|Au|^2 + \alpha^{-1}\gamma(u, u, Au) + (Ru, u) \in L^1(0, T; \mathbb{R}) \tag{61}$$

and thus $(d/dt)\mu(u(t), u(t)) \in L^1(0, T; \mathbb{R})$, which implies by [10, Lemma II.3.1] that the function $t \mapsto \mu(u(t), u(t))$ is continuous. Therefore, since $\mu(\varphi, \varphi)^{1/2}$ is a norm on V equivalent to $\|\varphi\|$ (by Lemma 3), it follows that $u : [0, T] \to V$ is continuous for the norm topology. □

Acknowledgment

This work was supported by the Foundation of Science and Technology Project of Chongqing Education Commission (KJ100513).

References

[1] R. Temam, *Infinite-Dimensional Dynamical Systems in Mechanics and Physics*, vol. 68 of *Applied Mathematical Sciences*, Springer, New York, NY, USA, 1988.

[2] B. Guo, "Nonlinear Galerkin methods for solving two-dimensional Newton-Boussinesq equations," *Chinese Annals of Mathematics B*, vol. 16, no. 3, pp. 379–390, 1995.

[3] B. L. Guo, "Spectral method for solving two-dimensional Newton-Boussinesq equations," *Acta Mathematicae Applicatae Sinica*, vol. 5, no. 3, pp. 208–218, 1989.

[4] Y. R. Li and B. L. Guo, "Random attractors for quasi-continuous random dynamical systems and applications to stochastic reaction-diffusion equations," *Journal of Differential Equations*, vol. 245, no. 7, pp. 1775–1800, 2008.

[5] L. Arnold, *Random Dynamical Systems*, Springer Monographs in Mathematics, Springer, Berlin, Germany, 1998.

[6] T. Caraballo, J. A. Langa, and J. C. Robinson, "Stability and random attractors for a reaction-diffusion equation with multiplicative noise," *Discrete and Continuous Dynamical Systems*, vol. 6, no. 4, pp. 875–892, 2000.

[7] T. Caraballo, J. A. Langa, and J. C. Robinson, "Upper semicontinuity of attractors for small random perturbations of dynamical systems," *Communications in Partial Differential Equations*, vol. 23, no. 9-10, pp. 1557–1581, 1998.

[8] H. Crauel, A. Debussche, and F. Flandoli, "Random attractors," *Journal of Dynamics and Differential Equations*, vol. 9, no. 2, pp. 307–341, 1997.

[9] X. Fan, "Random attractor for a damped sine-Gordon equation with white noise," *Pacific Journal of Mathematics*, vol. 216, no. 1, pp. 63–76, 2004.

[10] G. Da Prato, A. Debussche, and R. Temam, "Stochastic Burger's equation," *Nonlinear Differential Equations and Applications*, vol. 1, no. 4, pp. 389–402, 1994.

[11] J. C. Robinson, "Stability of random attractors under perturbation and approximation," *Journal of Differential Equations*, vol. 186, no. 2, pp. 652–669, 2002.

[12] Y. R. Li and B. L. Guo, "Random attractors of Boussinesq equations with multiplicative noise," *Acta Mathematica Sinica*, vol. 25, no. 3, pp. 481–490, 2009.

Hindawi Publishing Corporation
Discrete Dynamics in Nature and Society
Volume 2013, Article ID 910189, 6 pages
http://dx.doi.org/10.1155/2013/910189

Research Article

A Fractional-Order Chaotic System with an Infinite Number of Equilibrium Points

Ping Zhou,[1,2] Kun Huang,[2] and Chun-de Yang[1]

[1] *Center of System Theory and Its Applications, Chongqing University of Posts and Telecommunications, Chongqing 400065, China*
[2] *Key Laboratory of Network Control and Intelligent Instrument of Ministry of Education, Chongqing University of Posts and Telecommunications, Chongqing 400065, China*

Correspondence should be addressed to Ping Zhou; zhouping@cqupt.edu.cn

Received 18 February 2013; Accepted 21 March 2013

Academic Editor: Xiao-Song Yang

A new 4D fractional-order chaotic system, which has an infinite number of equilibrium points, is introduced. There is no-chaotic behavior for its corresponded integer-order system. We obtain that the largest Lyapunov exponent of this 4D fractional-order chaotic system is 0.8939 and yield the chaotic attractor. A chaotic synchronization scheme is presented for this 4D fractional-order chaotic system. Numerical simulations is verified the effectiveness of the proposed scheme.

1. Introduction

Because the chaotic (hyperchaotic) signal can be used in electrical engineering, telecommunications, information processing, material engineering, and so forth much attention has been paid to effectively generating chaotic and hyperchaotic systems. Many chaotic (hyperchaotic) systems and fractional-order chaotic (hyperchaotic) systems are reported in recent years [1–14], such as Lorenz chaotic (hyperchaotic) system and its corresponded fractional-order system, and integer-order and fractional-order Chen chaotic (hyperchaotic) system, integer-order and fractional-order Lü chaotic (hyperchaotic) system.

However, for all the previous integer-order and fractional-order chaotic (hyperchaotic), many systems have a finite number of equilibrium points. For example, some chaotic systems have one equilibrium point [15–17], some chaotic systems have two equilibrium points [18], and some chaotic systems have three equilibrium points [1, 2, 5, 6, 9, 10], so a natural and interesting question is can we construct a chaotic (hyperchaotic) system which has an infinite number of equilibrium points? Moreover, many fractional-order chaotic and hyperchaotic systems also possess chaotic attractor for its corresponded integer-order system, so the other question is as follows: are the fractional-order chaotic and hyperchaotic systems no-chaotic behavior for its corresponded integer-order system? To the best of our knowledge, few results on the above mentioned two questions are reported.

Motivated by the above discussions, a new 4D fractional-order chaotic system is presented in this paper. This new 4D fractional-order chaotic system has an infinite number of equilibrium points, and no-chaotic behavior for its corresponded integer-order system. The largest Lyapunov exponent and chaotic attractor are yielded for the new 4D fractional-order chaotic system. A chaotic synchronization scheme is presented for this new 4D fractional-order chaotic system.

2. A New 4D Fractional-Order Chaotic System

Now, a new 4D fractional-order chaotic system is constructed, which is described as follows:

$$\frac{d^q x_1}{dt^q} = 10\left(x_2 - x_1\right) + x_4$$

$$\frac{d^q x_2}{dt^q} = 15x_1 - x_1 x_3$$

$$\frac{d^q x_3}{dt^q} = -2.5x_3 + 4{x_1}^2$$
$$\frac{d^q x_4}{dt^q} = -10x_2 - x_4, \tag{1}$$

where $q = 0.95$ is the fractional-order, and $x_i\,(i = 1, 2, 3, 4)$ are real state variables.

The real equilibrium points of system (1) is calculated by

$$\begin{aligned} 10(x_2 - x_1) + x_4 &= 0 \\ 15x_1 - x_1x_3 &= 0 \\ -2.5x_3 + 4{x_1}^2 &= 0 \\ -10x_2 - x_4 &= 0. \end{aligned} \tag{2}$$

Obviously, $(x_1, x_2, x_3, x_4) = (0, x_2, 0, -10x_2)$ is the real equilibrium points of system (1), where x_2 is a any real numbers, so system (1) has an infinite number of real equilibrium points. To the best of our knowledge, this result is different from all the previous fractional-order chaotic and hyperchaotic systems. It implies that we yield a new 4D fractional-order system, which has an infinite number of real equilibrium points.

The Jacobian J at all equilibrium points is

$$J = \begin{pmatrix} -10 & 10 & 0 & 1 \\ 15 & 0 & 0 & 0 \\ 0 & 0 & -2.5 & 0 \\ 0 & -10 & 0 & -1 \end{pmatrix} \tag{3}$$

and its eigenvalues are $\lambda_1 = -18.548$, $\lambda_2 = -2.5$, $\lambda_3 = 0$, and $\lambda_4 = 7.548$ for all x_2. Therefore, all the equilibrium points in system (1) are unstable.

The dynamical behaviors of system (1) for its corresponded integer-order system ($q = 1$) can be characterized by its Lyapunov exponents. The Lyapunov exponents for its corresponded integer-order system are 0, 0, −0.779, and −12.724, respectively. Therefore, the fractional-order system (1) no-chaotic behaviors for $q = 1$, and which is periodic orbit for its corresponded integer-order system. Figure 1 shows the periodic orbit of fractional-order system (1) for its corresponded integer-order system ($q = 1$).

Now, we discuss the numerical solution of fractional differential equations. It is well known that there are direct time domain approximation (the improved version of Adams-Bashforth-Moulton numerical algorithm) and frequency domain approximation for nonlinear fractional-order system [6]. However, frequency domain approximation may result in wrong consequences [19], so the direct time domain approximation [6] numerical simulation is used to solve the fractional-order system in this paper. Let $h = T/N$, $t_n = nh\,(n = 0, 1, 2 \ldots, N)$, and initial condition $(x_1(0), x_2(0), x_3(0), x_4(0))$, so the fractional-order chaotic system (1) can be discretized as follows:

$$\begin{aligned} x_1(n+1) &= x_1(0) + \frac{h^q}{\Gamma(q+2)} \\ &\quad \times \left[10\left(x_2^p(n+1) - x_1^p(n+1)\right) + x_4^p(n+1) \right. \\ &\quad \left. + \sum_{j=0}^{n} \alpha_{1,j,n+1} \times \left(10\left(x_2(j) - x_1(j)\right) + x_4(j)\right) \right] \\ x_2(n+1) &= x_2(0) + \frac{h^q}{\Gamma(q+2)} \\ &\quad \times \left[15x_1^p(n+1) - x_1^p(n+1)\, x_3^p(n+1) \right. \\ &\quad \left. + \sum_{j=0}^{n} \alpha_{2,j,n+1} \left(15x_1(j) - x_1(j)\, x_3(j)\right) \right] \\ x_3(n+1) &= x_3(0) + \frac{h^q}{\Gamma(q+2)} \\ &\quad \times \left[4\left(x_1^p(n+1)\right)^2 - 2.5x_3^p(n+1) \right. \\ &\quad \left. + \sum_{j=0}^{n} \alpha_{3,j,n+1} \left(4\left(x_1(j)\right)^2 - 2.5x_3(j)\right) \right] \\ x_4(n+1) &= x_4(0) + \frac{h^q}{\Gamma(q+2)} \\ &\quad \times \left[-10x_2^p(n+1) - x_4^p(n+1) \right. \\ &\quad \left. + \sum_{j=0}^{n} \alpha_{4,j,n+1} \times \left(-10x_2(j) - x_4(j)\right) \right], \end{aligned} \tag{4}$$

where

$$x_1^p(n+1) = x_1(0) + \frac{1}{\Gamma(q)} \times \sum_{j=0}^{n} b_{1,j,n+1} \times \left[10\left(x_2(j) - x_1(j)\right) + x_4(j)\right]$$

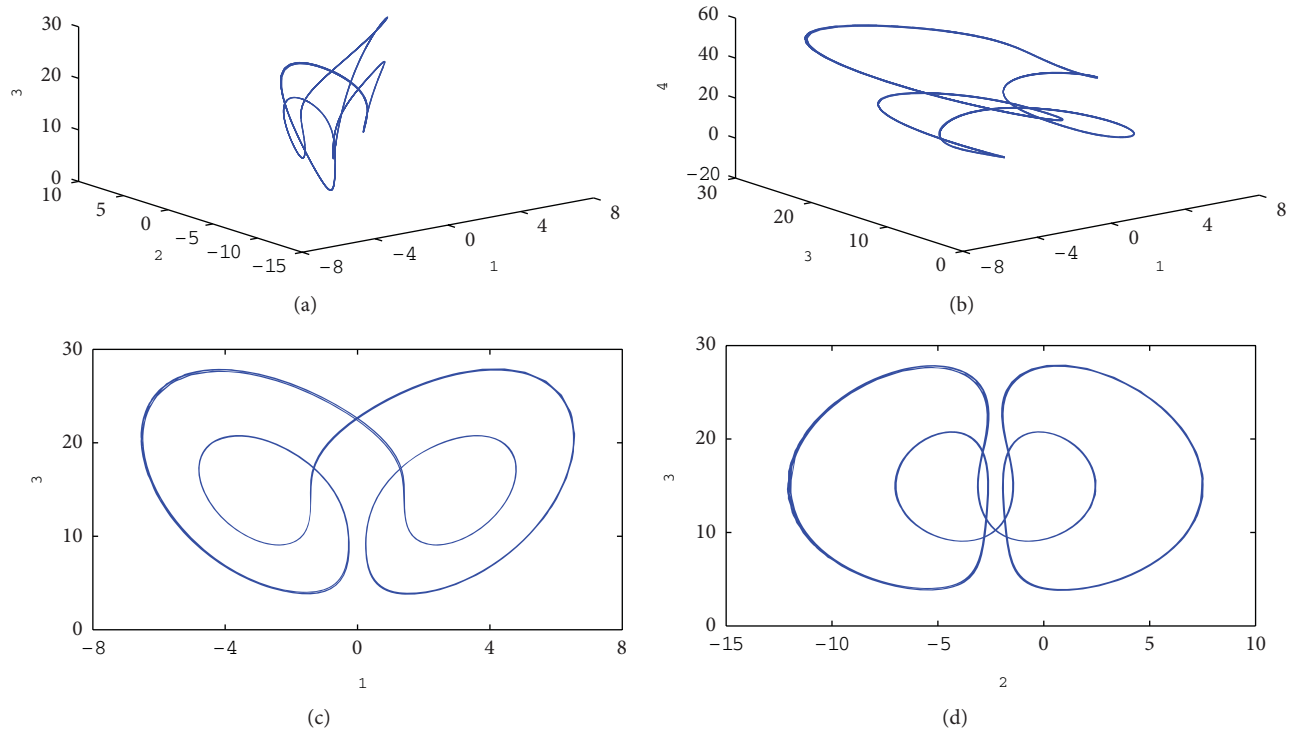

Figure 1: The periodic orbit of fractional-order system (1) for its corresponded integer-order system ($q = 1$).

$$
\begin{aligned}
x_2^p(n+1) &= x_2(0) + \frac{1}{\Gamma(q)} \\
&\quad \times \sum_{j=0}^{n} b_{2,j,n+1} \left[15x_1(j) - x_1(j)\, x_3(j)\right] \\
x_3^p(n+1) &= x_3(0) + \frac{1}{\Gamma(q)} \\
&\quad \times \sum_{j=0}^{n} b_{3,j,n+1} \left[4(x_1(j))^2 - 2.5x_3(j)\right] \\
x_4^p(n+1) &= x_4(0) + \frac{1}{\Gamma(q)} \\
&\quad \times \sum_{j=0}^{n} b_{4,j,n+1} \times \left[-10x_2(j) - x_4(j)\right],
\end{aligned}
\tag{5}
$$

and for $i = 1, 2, 3, 4$

$$
\begin{aligned}
&\alpha_{i,j,n+1} \\
&= \begin{cases} n^{q+1} - (n-q)(n+1)^q, & j = 0 \\ (n-j+2)^{q+1} + (n-j)^{q+1} - 2(n-j+1)^{q+1}, & 1 \le j \le n \\ 1, & j = n+1, \end{cases} \\
&b_{i,j,n+1} = \frac{h^q}{q}\left[(n-j+1)^q - (n-j)^q\right], \quad 0 \le j \le n.
\end{aligned}
\tag{6}
$$

The error of this approximation is described as follows:

$$
\left|x_i(t_n) - x_i(n)\right| = o\left(h^p\right), \qquad p = \min(2, 1+q). \tag{7}
$$

The dynamical behaviors of 4D fractional-order system (1) can be characterized by its largest Lyapunov exponent. By computer simulation, we can obtain that the largest Lyapunov exponent of fractional-order system (1) is 0.8939, so the 4D fractional-order system (1) is chaotic. The chaotic attractor is shown in Figure 2.

According to the above mentioned, we obtain a new 4D fractional-order chaotic system, which has an infinite number of real equilibrium points. Moreover, the 4D fractional-order chaotic system is no-chaotic behaviors for its corresponded integer-order system ($q = 1$). The result in our paper is different from all the previous fractional-order chaotic and hyperchaotic systems.

3. Chaotic Synchronization for the New 4D Fractional-Order Chaotic System

In this section, the chaotic synchronization for the new 4D fractional-order chaotic system (1) is considered. Based on the stability theory of nonlinear fractional-order systems [20–24], one synchronization scheme is proposed, and some numerical simulations are performed.

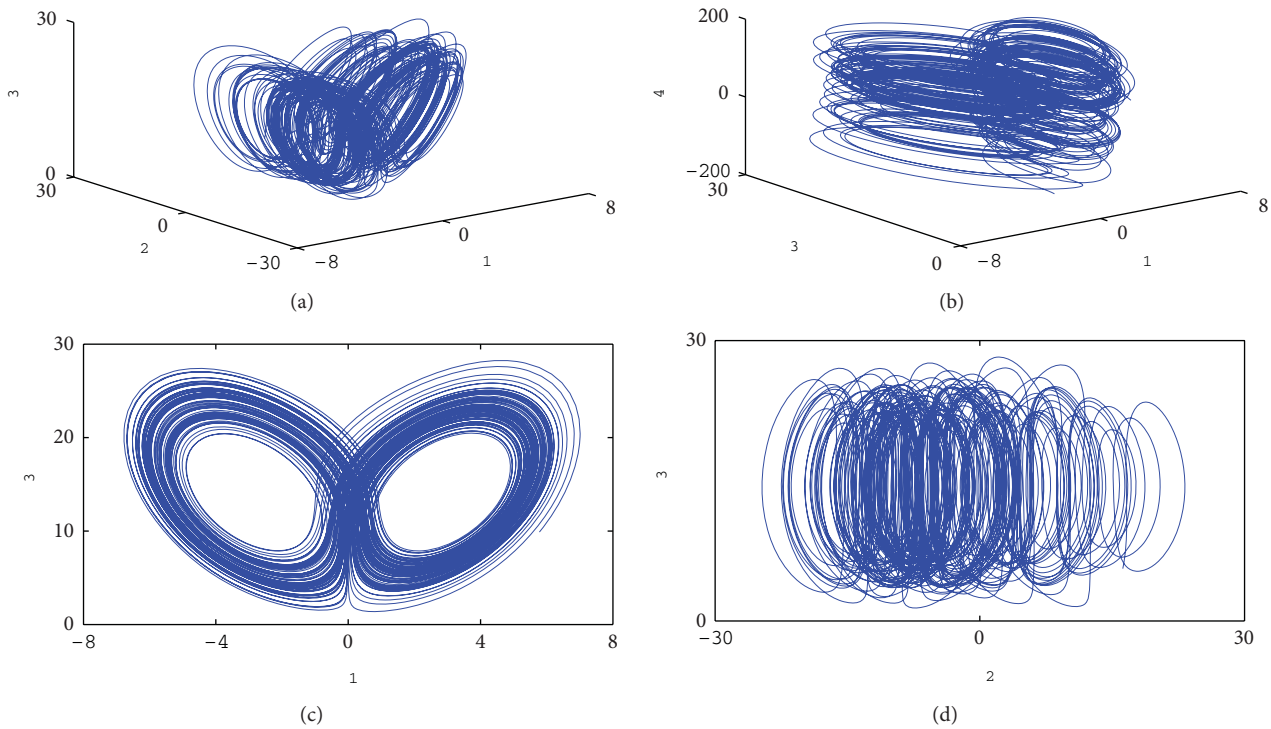

Figure 2: The chaotic attractor of 4D fractional-order system (1).

Now, the response fractional-order chaotic system is considered as

$$\begin{aligned} D^q y_1 &= 10(y_2 - y_1) + y_4 + u_1 \\ D^q y_2 &= 15y_1 - y_1 y_3 + u_2 \\ D^q y_3 &= -2.5y_3 + 4{y_1}^2 + u_3 \\ D^q y_4 &= -10y_2 - y_4 + u_4, \end{aligned} \tag{8}$$

where $u_i\,(i = 1, 2, 3, 4)$ is the feedback controller, and $y_i\,(i = 1, 2, 3, 4)$ are real state variables. Our goal is to choose suitable $u_i\,(i = 1, 2, 3, 4)$ such that drive system (1) and response system (8) can be achieved with chaotic synchronization.

Definition the synchronization errors are $e_i = y_i - x_i\,(i = 1, 2, 3, 4)$. The following Theorem 1 is given in order to achieve the chaotic synchronization between the fractional-order chaotic system (1) and the fractional-order chaotic system (8).

Theorem 1. *If the feedback controllers are*

$$\begin{aligned} u_1 &= (y_3 - 25)e_2 - 4(y_1 + x_1)e_3 \\ u_2 &= 10e_4 \\ u_3 &= x_1 e_2 \\ u_4 &= -e_1, \end{aligned} \tag{9}$$

then the chaotic synchronization between fractional-order chaotic system (1) *and fractional-order chaotic system* (8) *can be arrived.*

Proof. Combining the fractional-order chaotic system (1), fractional-order chaotic system (8), and the feedback controller (9), we can obtain the following error system

$$\begin{aligned} &\begin{pmatrix} D^q e_1 \\ D^q e_2 \\ D^q e_3 \\ D^q e_4 \end{pmatrix} \\ &= \begin{pmatrix} -10 & -15 + y_3 & -4(y_1 + x_1) & 1 \\ 15 - y_3 & 0 & -x_1 & 10 \\ 4(y_1 + x_1) & x_1 & -2.5 & 0 \\ -1 & -10 & 0 & -1 \end{pmatrix} \\ &\quad \times \begin{pmatrix} e_1 \\ e_2 \\ e_3 \\ e_4 \end{pmatrix} \\ &\triangleq A(x, y) \begin{pmatrix} e_1 \\ e_2 \\ e_3 \\ e_4 \end{pmatrix}, \end{aligned} \tag{10}$$

where matrix

$$A(x, y) \triangleq \begin{pmatrix} -10 & -15 + y_3 & -4(y_1 + x_1) & 1 \\ 15 - y_3 & 0 & -x_1 & 10 \\ 4(y_1 + x_1) & x_1 & -2.5 & 0 \\ -1 & -10 & 0 & -1 \end{pmatrix}, \tag{11}$$

$\mathrm{x} = (\mathrm{x}_1, \mathrm{x}_2, \mathrm{x}_3, \mathrm{x}_4)^{\mathrm{T}}$, $\mathrm{y} = (\mathrm{y}_1, \mathrm{y}_2, \mathrm{y}_3, \mathrm{y}_4)^{\mathrm{T}}$.

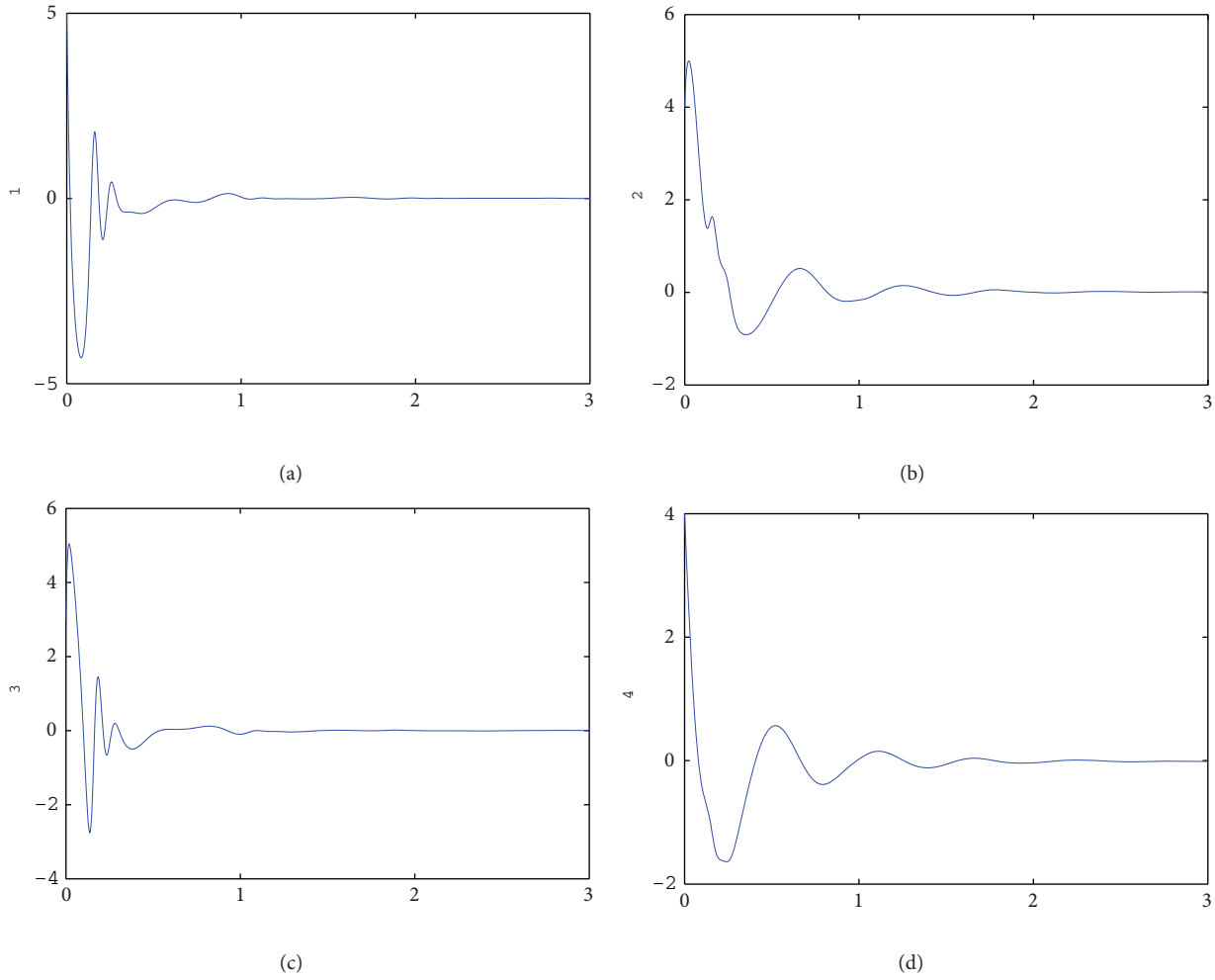

Figure 3: The synchronization errors between the drive systems (1) and the response system (8).

Let λ be one of the eigenvalues of $A(x, y)$ and ψ is the corresponding nonzero eigenvector, so

$$\begin{aligned} A(x, y)\psi &= \lambda\psi, \\ \psi^{\mathbf{H}} A(x, y)^{\mathbf{H}} &= \overline{\lambda}\psi^{\mathbf{H}}, \end{aligned} \tag{12}$$

where $\mathbf{H}$ is conjugate transpose, and $\overline{\lambda}$ is the conjugate for eigenvalues λ.

According to (12), one can obtain

$$\psi^{\mathbf{H}} A(x, y)\psi + \psi^{\mathbf{H}} A(x, y)^{\mathbf{H}}\psi = \psi^{\mathbf{H}}\lambda\psi + \overline{\lambda}\psi^{\mathbf{H}}\psi. \tag{13}$$

Therefore

$$\lambda + \overline{\lambda} = \frac{\psi^{\mathbf{H}}\left[\operatorname{diag}(-20, 0, -5, -2)\right]\psi}{\psi^{\mathbf{H}}\psi}, \tag{14}$$

so

$$\lambda + \overline{\lambda} \le 0. \tag{15}$$

That is

$$\arg|\lambda| \ge \frac{\pi}{2} > \frac{q\pi}{2}. \tag{16}$$

Using the stability theory of nonlinear fractional-order systems, one can yield that the error system (10) is asymptotically stable, so

$$\lim_{t \to +\infty} e_i = 0 \quad (i = 1, 2, 3, 4). \tag{17}$$

Equation (17) indicates that the chaotic synchronization between fractional-order chaotic system (1) and fractional-order chaotic system (8) can be achieved. The proof is completed. □

Now, numerical simulations are considered. The numerical results are shown as Figure 3, in which the initial conditions are $\mathbf{x} = (3, 3, 1, 2)^{\mathbf{T}}$ for drive system (1), and $\mathbf{y} = (8, 7, 4, 6)^{\mathbf{T}}$ for response system (8), respectively.

4. Conclusions

In this paper, we obtain a new 4D fractional-order chaotic system, which has an infinite number of equilibrium points and no-chaotic behavior for its corresponded integer-order system. We yield the largest Lyapunov exponent of the new

4D fractional-order system and the Lyapunov exponents for its corresponded integer-order system. The chaotic attractor for the new 4D fractional-order chaotic system and the periodic orbit for its corresponded integer-order system are given. Finally, we realize the chaotic synchronization for the new 4D fractional-order chaotic system, and some numerical simulations are performed.

Acknowledgments

This work was supported by the Foundation of Science and Technology Project of Chongqing Education Commission (KJ110525, KJ100513) and by the National Natural Science Foundation of China (61104150).

References

[1] E. N. Lorenz, "Deterministic nonperodic flow," *Journal of the Atmospheric Sciences*, vol. 20, no. 2, pp. 130–141, 1963.

[2] I. Grigorenko and E. Grigorenko, "Chaotic dynamics of the fractional Lorenz system," *Physical Review Letters*, vol. 91, no. 3, Article ID 034101, 4 pages, 2003.

[3] Q. Jia, "Hyperchaos generated from the Lorenz chaotic system and its control," *Physics Letters A*, vol. 366, no. 3, pp. 217–222, 2007.

[4] X. Y. Wang and J. M. Song, "Synchronization of the fractional order hyperchaos Lorenz systems with activation feedback control," *Communications in Nonlinear Science and Numerical Simulation*, vol. 14, no. 8, pp. 3351–3357, 2009.

[5] G. Chen and T. Ueta, "Yet another chaotic attractor," *International Journal of Bifurcation and Chaos in Applied Sciences and Engineering*, vol. 9, no. 7, pp. 1465–1466, 1999.

[6] C. Li and G. Peng, "Chaos in Chen's system with a fractional order," *Chaos, Solitons & Fractals*, vol. 22, no. 2, pp. 443–450, 2004.

[7] Z. Y. Yan, "Controlling hyperchaos in the new hyperchaotic Chen system," *Applied Mathematics and Computation*, vol. 168, no. 2, pp. 1239–1250, 2005.

[8] X. J. Wu and Y. Lu, "Generalized projective synchronization of the fractional-order Chen hyperchaotic system," *Nonlinear Dynamics*, vol. 57, no. 1-2, pp. 25–35, 2009.

[9] J. Lü and G. Chen, "A new chaotic attractor coined," *International Journal of Bifurcation and Chaos in Applied Sciences and Engineering*, vol. 12, no. 3, pp. 659–661, 2002.

[10] J. G. Lu, "Chaotic dynamics of the fractional-order Lü system and its synchronization," *Physics Letters A*, vol. 354, no. 4, pp. 305–311, 2006.

[11] P. Zhou, R. Ding, and Y. X. Cao, "Multi drive-one response synchronization for fractional-order chaotic systems," *Nonlinear Dynamics*, vol. 70, no. 2, pp. 1263–1271, 2012.

[12] Q. Li and X.-S. Yang, "New walking dynamics in the simplest passive bipedal walking model," *Applied Mathematical Modelling*, vol. 36, no. 11, pp. 5262–5271, 2012.

[13] Q. Li, "A topological horseshoe in the hyperchaotic Rössler attractor," *Physics Letters A*, vol. 372, no. 17, pp. 2989–2994, 2008.

[14] Q. Li, X.-S. Yang, and S. Chen, "Hyperchaos in a spacecraft power system," *International Journal of Bifurcation and Chaos*, vol. 21, no. 6, pp. 1719–1726, 2011.

[15] S. Dadras, H. R. Momeni, G. Qi, and Z.-l. Wang, "Four-wing hyperchaotic attractor generated from a new 4D system with one equilibrium and its fractional-order form," *Nonlinear Dynamics*, vol. 67, no. 2, pp. 1161–1173, 2012.

[16] Z. Ping, C. Yu-Xia, and C. Xue-Feng, "A new hyperchaos system and its circuit simulation by EWB," *Chinese Physics B*, vol. 18, no. 4, pp. 1394–1398, 2009.

[17] D. R. Zhu, C. X. Liu, and B. N. Yan, "Controlling and synchronization of hyperchaotic system based on passive control," *Chinese Physics B*, vol. 21, no. 9, Article ID 090509, 7 pages, 2012.

[18] J. C. Sprott, "Some simple chaotic flows," *Physical Review E*, vol. 50, no. 2, pp. R647–R650, 1994.

[19] M. S. Tavazoei and M. Haeri, "A necessary condition for double scroll attractor existence in fractional-order systems," *Physics Letters A*, vol. 367, no. 1-2, pp. 102–113, 2007.

[20] M. S. Tavazoei and M. Haeri, "Chaos control via a simple fractional-order controller," *Physics Letters A*, vol. 372, no. 6, pp. 798–807, 2008.

[21] X.-Y. Wang, Y.-J. He, and M.-J. Wang, "Chaos control of a fractional order modified coupled dynamos system," *Nonlinear Analysis. Theory, Methods & Applications A*, vol. 71, no. 12, pp. 6126–6134, 2009.

[22] C.-M. Chang and H.-K. Chen, "Chaos and hybrid projective synchronization of commensurate and incommensurate fractional-order Chen-Lee systems," *Nonlinear Dynamics*, vol. 62, no. 4, pp. 851–858, 2010.

[23] Z. M. Odibat, "Adaptive feedback control and synchronization of non-identical chaotic fractional order systems," *Nonlinear Dynamics*, vol. 60, no. 4, pp. 479–487, 2010.

[24] Z. Odibat, "A note on phase synchronization in coupled chaotic fractional order systems," *Nonlinear Analysis. Real World Applications. An International Multidisciplinary Journal*, vol. 13, no. 2, pp. 779–789, 2012.

Hindawi Publishing Corporation
Discrete Dynamics in Nature and Society
Volume 2013, Article ID 287371, 6 pages
http://dx.doi.org/10.1155/2013/287371

Research Article

Complexity Analysis of a Cournot-Bertrand Duopoly Game Model with Limited Information

Hongwu Wang[1,2] and Junhai Ma[1]

[1] *School of Management, Tianjin University, Tianjin 300072, China*
[2] *College of Science, Tianjin University of Science and Technology, Tianjin 300457, China*

Correspondence should be addressed to Junhai Ma; mjhtju@yahoo.com.cn

Received 11 December 2012; Accepted 21 January 2013

Academic Editor: Qingdu Li

A Cournot-Bertrand mixed duopoly game model with limited information about the market and opponent is considered, where the market has linear demand and two firms have the same fixed marginal cost. The principles of decision-making are bounded rational. One firm chooses output and the other chooses price as decision variable, with the assumption that there is a certain degree of differentiation between the products offered by firms to avoid the whole market being occupied by the one that applies a lower price. The existence of Nash equilibrium point and its local stability of the game are investigated. The complex dynamics, such as bifurcation scenarios and route to chaos, are displayed using parameter basin plots by numerical experiment. The influences of the parameters on the system performance are discussed from the perspective of economics.

1. Introduction

An *oligopoly* is a market structure between monopoly and perfect competition, in which the market is completely controlled by only a few number of firms producing the same or homogeneous productions [1, 2]. If there are two firms, it is called a *duopoly* while if there are three competitors, it is known as a *triopoly*.

Cournot oligopoly [3] and Bertrand oligopoly [4] are the two most notable models in oligopoly theory. In the Cournot model, firms control their production level, which influences the market price, while in the Bertrand model, firms choose the price of a unit of product to affect the market demand.

A large amount of the literature deals with Cournot or Bertrand competition in oligopolistic market [1, 2, 5–7], but there are only a considerably lower number of works devoted to Cournot-Bertrand competition, which are characterized by the fact that the market can be subdivided into two groups of firms, the first of which optimally adjusts prices and the other one optimally adjusts their output to ensure maximum profit [8].

Cournot-Bertrand model exists in realistic economy. For instance, in duopoly market, one firm competes in a dominant position, and it chooses output as decision variable while the other one is in disadvantage, and it chooses price as decision variable in order to gain more market share. As we have known so far, Bylka and Komar [9] and Singh and Vives [10] are the first authors to analyze duopolies, where one firm competes on quantities and the other on prices. Häckner [11], Zanchettin [12], and Arya et al. [13] pointed that in some cases Cournot-Bertrand competition may be optimal. Recently, C. H. Tremblay and V. J. Tremblay [14] analyzed the role of product differentiation for the static properties of the Nash equilibrium of a Cournot-Bertrand duopoly. Naimzada and Tramontana [8] considered a Cournot-Bertrand duopoly model, which is characterized by linear difference equations. They also analyzed the role of best response dynamics and of the adaptive adjustment mechanism for the stability of the equilibrium.

In this paper, we set up a Cournot-Bertrand duopoly model, assuming that two firms choose output and price as decision variable, respectively, and they all have bounded

rational expectations. The gaming system can be described by nonlinear difference equations, which modifies and extends the results of Naimzada and Tramontana [8], which considered the firms with static expectations and described by linear difference equations. The research will lead to a good guidance for the enterprise decision-makers to do the best decision-making.

The paper is organized as follows the Cournot-Bertrand game model with bounded rational expectations is described in Section 2. In Section 3, the existence and stability of equilibrium points are studied. Dynamical behaviors under some change of control parameters of the game are investigated by numerical simulations in Section 4. Finally, a conclusion is drawn in Section 5.

2. The Cournot-Bertrand Game Model with Bounded Rational Expectations

We consider a market served by two firms and firm i produces good x_i, $i = 1, 2$. There is a certain degree of differentiation between the products x_1 and x_2. Firm 1 competes in output q_1 as in a Cournot duopoly, while firm 2 fixes its price p_2 like in the Bertrand case. Suppose that firms make their strategic choices simultaneously and each firm knows the production and the price of each other firm.

The inverse demand functions of products of variety 1 and 2 come from the maximization by the representative consumer of the following utility function:

$$U(q_1, q_2) = q_1 + q_2 - \frac{1}{2}\left(q_1^2 + 2dq_1q_2 + q_2^2\right) \tag{1}$$

subject to the budget constraint $p_1q_1 + p_2q_2 + y = M$ and are given by the following equations (the detailed proof see [15]):

$$\begin{aligned} p_1(t) &= 1 - q_1(t) - dq_2(t), \\ p_2(t) &= 1 - q_2(t) - dq_1(t), \end{aligned} \tag{2}$$

where the parameter $d \in (0, 1)$ denotes the index of product differentiation or product substitution. The degree of product differentiation will increase as $d \to 0$. Products x_1 and x_2 are homogeneous when $d = 1$, and each firm is a monopolist when $d = 0$, while a negative $d \in (-1, 0)$ implies that products are complements. Assume that the two firms have the same marginal cost $c > 0$, and the cost function has the linear form:

$$C_i(q_i(t)) = cq_i(t), \quad i = 1, 2. \tag{3}$$

We can write the demand system in the two strategic variables, $q_1(t)$ and $p_2(t)$:

$$\begin{aligned} p_1(t) &= 1 - d - \left(1 - d^2\right)q_1(t) + dp_2(t), \\ q_2(t) &= 1 - p_2(t) - dq_1(t). \end{aligned} \tag{4}$$

The profit functions of firm 1 and 2 are in the form:

$$\begin{aligned} \Pi_1(t) &= q_1(t)\left(1 - d + dp_2(t) - q_1(t) + d^2q_1(t)\right) \\ &\quad - cq_1(t), \\ \Pi_2(t) &= p_2(t)\left(1 - p_2(t) - dq_1(t)\right) \\ &\quad - c\left(1 - p_2(t) - dq_1(t)\right). \end{aligned} \tag{5}$$

We assume that the two firms do not have a complete knowledge of the market and the other player, and they build decisions on the basis of the expected marginal profit. If the marginal profit is positive (negative), they increases (decreases) their production or price in the next period; that is, they are bounded rational players [5, 15, 16]. Then the Cournot-Bertrand mixed dynamical system can be described by the nonlinear difference equations:

$$\begin{aligned} q_1(t+1) &= q_1(t) + \alpha q_1(t)\left(1 - c - d + dp_2(t)\right. \\ &\qquad \left. -2q_1(t) + 2d^2q_1(t)\right), \\ p_2(t+1) &= p_2(t)(t) + \beta p_2(t)\left(1 + c - 2p_2(t) - dq_1(t)\right), \end{aligned} \tag{6}$$

where $\alpha > 0$ and $\beta > 0$ represent the two players' adjustment speed in each relation, respectively.

3. Equilibrium Points and Local Stability

The system (6) has four equilibrium points:

$$\begin{aligned} &E_0 = (0, 0), \qquad E_1\left(0, \frac{1+c}{2}\right), \\ &E_2\left(\frac{1-c-d}{2\left(1-d^2\right)}, 0\right), \qquad E^*\left(q_1^*, p_2^*\right), \end{aligned} \tag{7}$$

where $q_1^* = (2 - 2c - d + cd)/(4 - 3d^2)$, $p_2^* = (2 + 2c - d + cd - d^2 - 2cd^2)/(4 - 3d^2)$. E_0, E_1, and E_2 are the boundary equilibrium points, and E^* is the unique Nash equilibrium point provided that $q_1^* > 0$ and $p_2^* > 0$, that requires $c < 1$. Otherwise, there will be one firm out of the market.

In order to investigate the local stability of the equilibrium points, let J be the Jacobian matrix of system (6) corresponding to the state variables (q_1, p_2), then

$$J(q_1, p_2) = \begin{pmatrix} J_{11} & \alpha d q_1 \\ -\beta d p_2 & J_{22} \end{pmatrix}, \tag{8}$$

where $J_{11} = 1 + \alpha(1 - c - d + dp_2 + 4(d^2 - 1)q_1)$, $J_{22} = 1 + \beta(1 + c - 4p_2 - dq_1)$. The stability of equilibrium points will be determined by the nature of the equilibrium eigenvalues of the Jacobian matrix evaluated at the corresponding equilibrium points.

Proposition 1. *The boundary equilibria E_0, E_1, and E_2 of system (6) are unstable equilibrium points when $c < 1$.*

Proof. For equilibrium E_0, the Jacobian matrix of system (6) is equal to

$$J(E_0) = \begin{pmatrix} 1+\alpha(1-c-d) & 0 \\ 0 & 1+\beta(1+c) \end{pmatrix}. \quad (9)$$

These eigenvalues that correspond to equilibrium E_0 are as follows:

$$\lambda_1 = 1+\alpha(1-c-d), \qquad \lambda_2 = 1+\beta(1+c). \quad (10)$$

Evidently $\lambda_2 > 1$, then the equilibrium point E_0 is unstable.

Also at E_1 the Jacobian matrix J becomes a triangular matrix

$$J(E_1) = \begin{pmatrix} 1+\alpha(1-c)\left(1-\dfrac{d}{2}\right) & 0 \\ -\dfrac{1}{2}\beta d(1+c) & 1-\beta(1+c) \end{pmatrix}. \quad (11)$$

These eigenvalues that correspond to equilibrium E_1 are as follows:

$$\lambda_1 = 1+\alpha(1-c)\left(1-\frac{d}{2}\right), \qquad \lambda_2 = 1-\beta(1+c). \quad (12)$$

When $c < 1$, evidently $\lambda_1 > 1$. So, the equilibrium point E_1 is unstable. Similarly we can prove that E_2 is also unstable. □

From an economic point of view we are more interested to the study of the local stability properties of the Nash equilibrium point E^*, whose properties have been deeply analyzed in [14].

The Jacobian matrix evaluated at the Nash equilibrium point E^* is as follows

$$J(E^*) = \begin{pmatrix} \dfrac{-4+3d^2+2\alpha(1-c)\left(2-d-2d^2+d^3\right)}{\left(3d^2-4\right)} & \dfrac{\alpha d(c-1)(2-d)}{4-3d^2} \\ \dfrac{\beta d\left(2-d-d^2+c\left(2+d-2d^2\right)\right)}{\left(3d^2-4\right)} & \dfrac{-4+3d^2-2\beta\left(-2+d+d^2+c\left(-2-d+2d^2\right)\right)}{\left(3d^2-4\right)} \end{pmatrix}. \quad (13)$$

The trace and determinant of $J(E^*)$ are denoted as $\mathrm{Tr}(J(E^*))$ and $\mathrm{Det}(J(E^*))$, respectively. With respect to the point E_0, E_1, and E_2, now it is more difficult to explicitly calculate the eigenvalues, but it is still possible to evaluate the stability of the Nash equilibrium point by using the following stability conditions, known as Jury's conditions [17]:

$$\begin{aligned} &\text{(i)} \quad A := 1+\mathrm{Tr}\left(J\left(E^*\right)\right)+\mathrm{Det}\left(J\left(E^*\right)\right) > 0, \\ &\text{(ii)} \quad B := 1-\mathrm{Tr}\left(J\left(E^*\right)\right)+\mathrm{Det}\left(J\left(E^*\right)\right) > 0, \\ &\text{(iii)} \quad C := 1-\mathrm{Det}\left(J\left(E^*\right)\right) > 0. \end{aligned} \quad (14)$$

The above inequalities define a region in which the Nash equilibrium point E^* is local stable. Also, we can learn more about the stability region via numerical simulations. In order to study the complex dynamics of system (6), it is convenient to take the parameters values as follows:

$$c = 0.1, \qquad d = 0.2. \quad (15)$$

Figure 1 shows in the (α, β) parameters plane the stability and instability regions. From the figure, we can find that too high speed of adjustment will make the Nash equilibrium point E^* lose stability. We also find that the adjustment speed of price is more sensitive than the speed of output, and when about $\alpha > 2.5$, the Nash equilibrium point will lose stability, while about $\beta > 2.0$ the Nash equilibrium point will do that.

4. The Effects of Parameters on System Stability

The parameter basin plots (also called 2D bifurcation diagrams) are a more powerful tool in the numerical analysis of nonlinear dynamics than the 1D bifurcation diagrams [18], which assigns different colors in a 2D parameter space to stable cycles of different periods. In this section, the parameter basin plots will be used to analyze the effects of players' adjustment speed and index of product differentiation on system stability. We set $c = 0.1$ and the initial values are chosen as $(q_1(0), p_2(0)) = (0.2, 0.1)$.

4.1. The Effects of Players' Adjustment Speed on System Stability. Figure 2 presents the parameter basin with respect to the parameters (α, β) when $d = 0.1$ and assigns different colors to stable steady states (dark blue); stable cycles of periods 2 (light blue), 4 (purple), and 8 (green) (the first four cycles in a period-doubling bifurcation route to chaos) and periods 3 (red), 5 (orange), and 7 (pink) (low order stable cycles of odd period); chaos (yellow); divergence (white) (which means one of the players will be out of the market in economics).

We can find that when the parameters (α, β) pass through the borders as the black arrows A and C, system (6) loses its stability through flip bifurcation (called period-doubling bifurcation in continuous system), as shown in Figures 3 and 4. But when the parameters cross the borders as the arrow B, the system's dynamic behavior is more complicated, and it first enters into chaos through Neimark-Sacker bifurcation

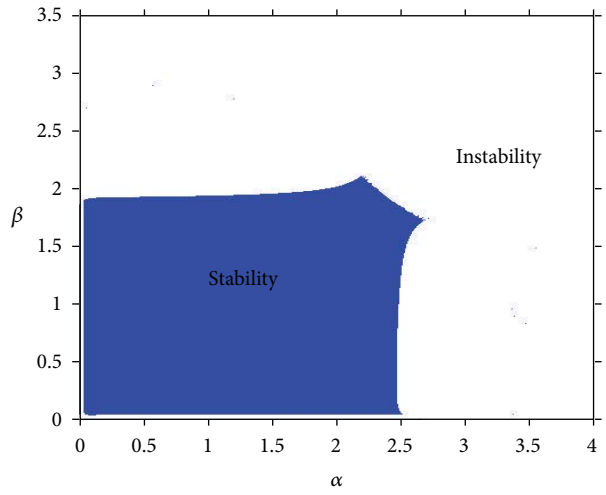

Figure 1: The stability and instability region.

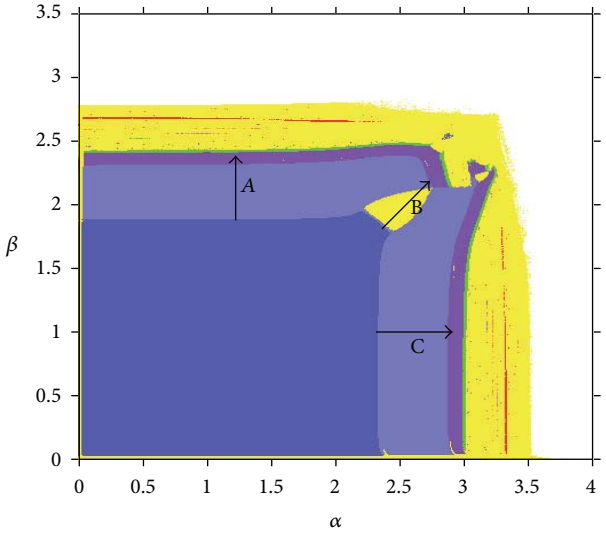

Figure 2: The parameter basin for $d = 0.1$.

(called Hopf bifurcation in continuous system) [19–21], second enters period 2, and then evolves into chaos through flip bifurcation separately, as shown in Figure 5. We also notice that in the yellow region (chaos) there is red line and orange points (odd cycle); that is, there is intermittent odd cycle in the chaos as shown in Figure 3 to Figure 5. It is well known that, for 1D continuous maps, a cycle with odd period implies chaotic dynamical behavior (the so-called topological chaos) according to the famous "period 3 implies chaos" result of Li and Yorke [22].

From the perspective of economics, the firms' adjustment speed α and β should be in a certain range; otherwise, the system will come forth the cycle fluctuation, and then into chaos, which means irregular, sensitive to initial values, unpredictable and bad for the economy. We also find that the adjustable range of α is larger than that of β, which means the

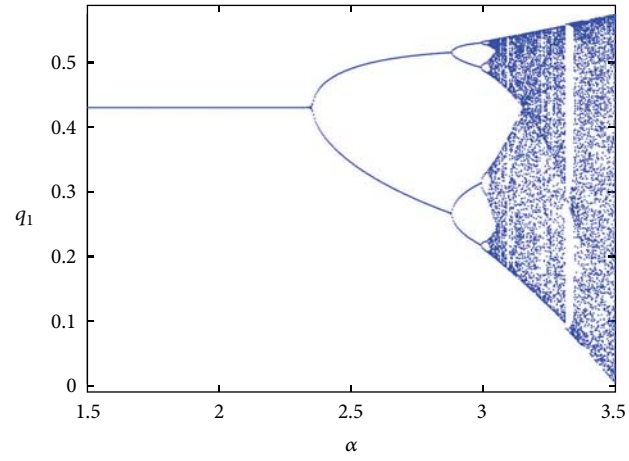

Figure 3: Bifurcation diagram for $\beta = 1$ and α varies from 1.5 to 3.5.

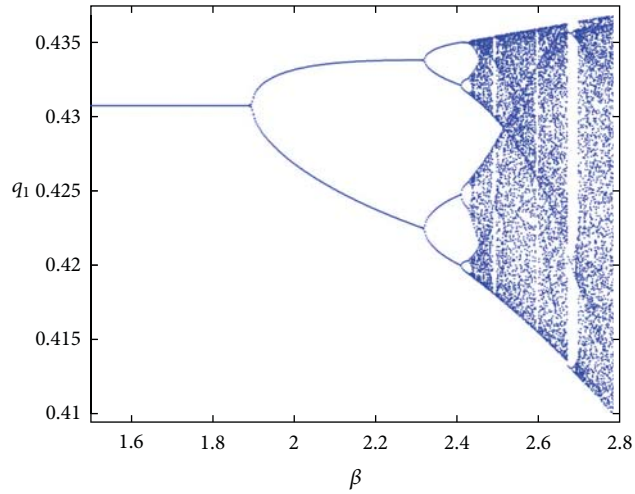

Figure 4: Bifurcation diagram for $\alpha = 1$ and β varies from 1.5 to 2.8.

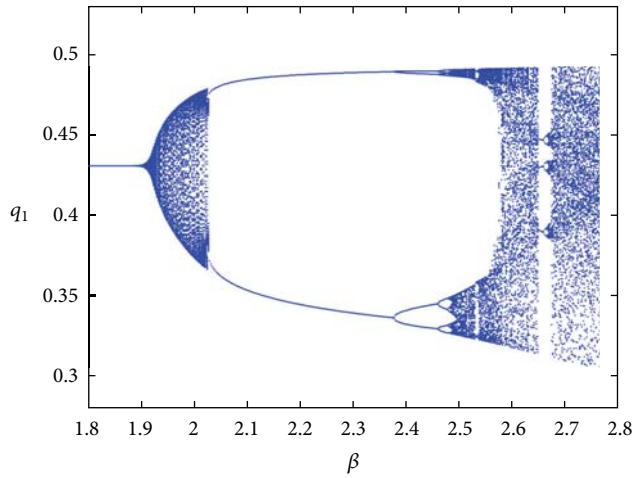

Figure 5: Bifurcation diagram for $\alpha = 2.3$ and β varies from 1.8 to 2.8.

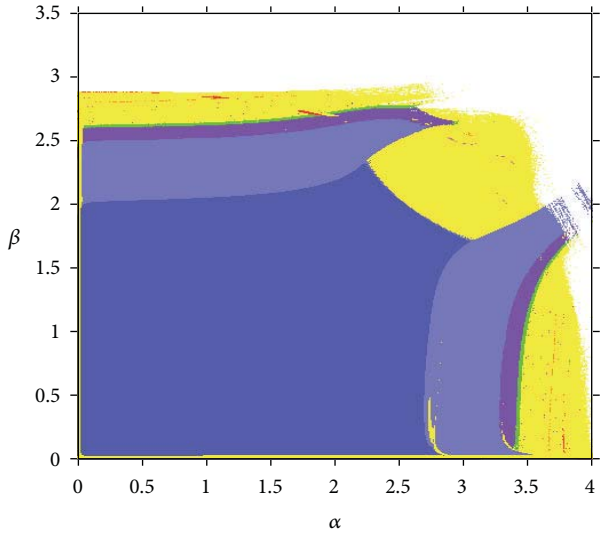

Figure 6: The parameter basin for $d = 0.3$.

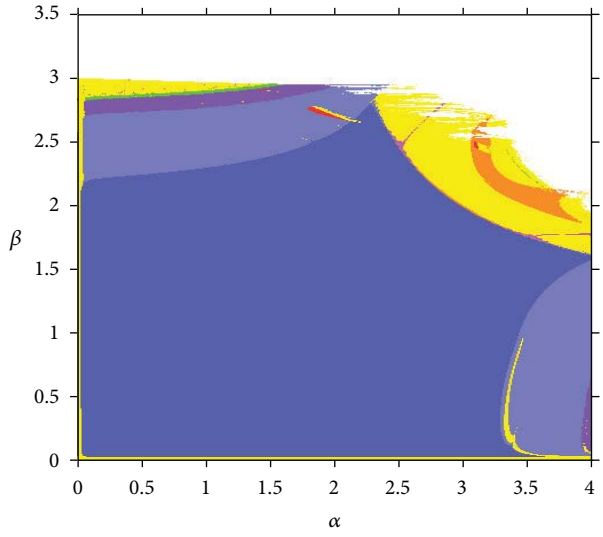

Figure 7: The parameter basin for $d = 0.5$.

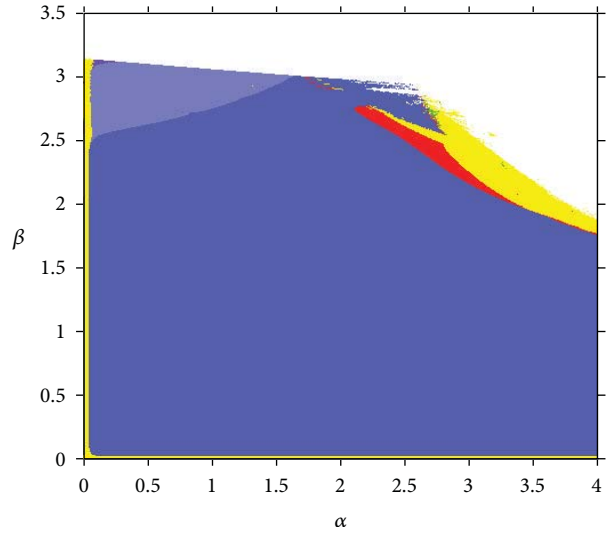

Figure 8: The parameter basin for $d = 0.7$.

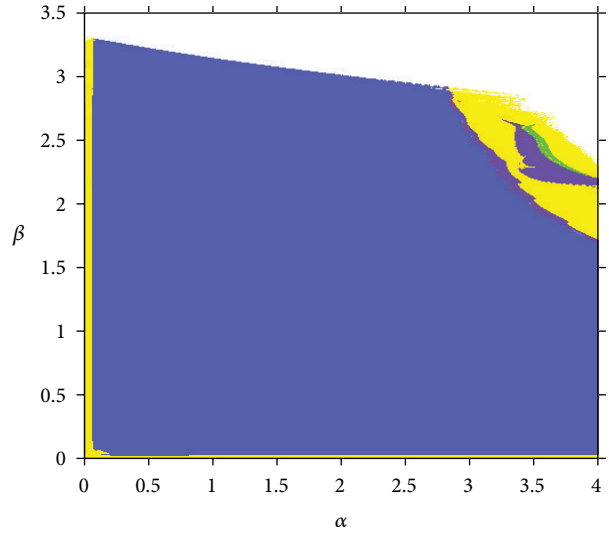

Figure 9: The parameter basin for $d = 0.9$.

adjustment of price is more sensitive than that of output, and price war is easier to get market into chaos.

4.2. The Effects of the Index of Product Differentiation on System Stability. In order to find the influences of the index of product differentiation d on the system stability, Figures 6, 7, 8, and 9 give the parameter basins for $d = 0.3, 0.5, 0.7$, and 0.9 separately.

From the comparison we can see the dark blue area becomes bigger and the yellow area becomes smaller with the increasing of the index of product differentiation d; that is, the degree of product differentiation is smaller, and the adjustable range of parameters α and β to make the system remain stable will become bigger, which means more competition between the two firms' products.

5. Conclusions

In this paper, we propose a Cournot-Bertrand mixed game model, supposing that the firms do not have the complete information of the market and opponent, and they make their decisions according to their own marginal profit. The demand and cost function is assumed to be linear and the model can be described by difference equations. The boundary equilibrium is always unstable and the existence and local stability of the Nash equilibrium are analyzed. Moreover, we analyze the effects of the parameters (adjustment speed and the index of product differentiation) on the system stability, and different bifurcations and routes to chaos are analyzed using parameter basin plots. The Cournot-Bertrand game models under different marketing environment need to be considered, and it will be an interesting topic for future study.

Acknowledgments

The authors thank the reviewers for their careful reading and providing some pertinent suggestions. The research was supported by the National Natural Science Foundation of China (no. 61273231).

References

[1] G. I. Bischi, C. Chiarella, M. O. Kopel, and F. Szidarovszky, *Nonlinear Oligopolies: Stability and Bifurcations*, Springer, New York, NY, USA, 2009.

[2] T. Puu and I. Sushko, *Oligopoly Dynamics: Models and Tools*, Springer, New York, NY, USA, 2002.

[3] A. A. Cournot, *Recherches sur les principes mathmatiques de la thorie des richesses*, L. Hachette, 1838.

[4] L. Walras, *Thorie Mathmatique de la Richesse Sociale*, Guillaumin, 1883.

[5] J. Ma and X. Pu, "Complex dynamics in nonlinear triopoly market with different expectations," *Discrete Dynamics in Nature and Society*, vol. 2011, Article ID 902014, 12 pages, 2011.

[6] Z. Sun and J. Ma, "Complexity of triopoly price game in Chinese cold rolled steel market," *Nonlinear Dynamics*, vol. 67, no. 3, pp. 2001–2008, 2012.

[7] J. Zhang and J. Ma, "Research on the price game model for four oligarchs with different decision rules and its chaos control," *Nonlinear Dynamics*, vol. 70, no. 1, pp. 323–334, 2012.

[8] A. K. Naimzada and F. Tramontana, "Dynamic properties of a Cournot-Bertrand duopoly game with differentiated products," *Economic Modelling*, vol. 290, pp. 1436–1439, 2012.

[9] S. Bylka and J. Komar, "Cournot-Bertrand mixed oligopolies," in *Warsaw Fall Seminars in Mathematical Economics*, M. Beckmann HP Kunzi, Ed., vol. 133 of *Lecture Notes in Economics and Mathematical Systems*, pp. 22–33, Springer, New York, NY, USA, 1976.

[10] N. Singh and X. Vives, "Price and quantity competition in a differentiated duopoly," *The RAND Journal of Economics*, vol. 15, pp. 546–554, 1984.

[11] J. Häckner, "A note on price and quantity competition in differentiated oligopolies," *Journal of Economic Theory*, vol. 93, no. 2, pp. 233–239, 2000.

[12] P. Zanchettin, "Differentiated duopoly with asymmetric costs," *Journal of Economics and Management Strategy*, vol. 15, no. 4, pp. 999–1015, 2006.

[13] A. Arya, B. Mittendorf, and D. E. M. Sappington, "Outsourcing, vertical integration, and price vesus quantity competition," *International Journal of Industrial Organization*, vol. 26, no. 1, pp. 1–16, 2008.

[14] C. H. Tremblay and V. J. Tremblay, "The Cournot-Bertrand model and the degree of product differentiation," *Economics Letters*, vol. 111, no. 3, pp. 233–235, 2011.

[15] L. Fanti and L. Gori, "The dynamics of a differentiated duopoly with quantity competition," *Economic Modelling*, vol. 29, pp. 421–427, 2012.

[16] E. Ahmed, H. N. Agiza, and S. Z. Hassan, "On modifications of Puu's dynamical duopoly," *Chaos, Solitons and Fractals*, vol. 11, no. 7, pp. 1025–1028, 2000.

[17] T. Puu, *Attractors, Bifurcations, & Chaos: Nonlinear Phenomena in Economics*, Springer, New York, NY, USA, 2003.

[18] C. Diks, C. Hommes, V. Panchenko, and R. van der Weide, "E&F chaos: a user friendly software package for nonlinear economic dynamics," *Computational Economics*, vol. 32, no. 1-2, pp. 221–244, 2008.

[19] A. Medio and G. Gallo, *Chaotic Dynamics: Theory and Applications to Economics*, Cambridge University Press, Cambridge, UK, 1995.

[20] G. Gandolfo, *Economic Dynamics*, Springer, New York, NY, USA, 2010.

[21] Y. A. Kuznetsov, *Elements of Applied Bifurcation Theory*, Springer, New York, NY, USA, 1998.

[22] T. Y. Li and J. A. Yorke, "Period three implies chaos," *The American Mathematical Monthly*, vol. 82, no. 10, pp. 985–992, 1975.

Hindawi Publishing Corporation
Discrete Dynamics in Nature and Society
Volume 2013, Article ID 206201, 9 pages
http://dx.doi.org/10.1155/2013/206201

Research Article

Dynamics Evolution of Credit Risk Contagion in the CRT Market

Tingqiang Chen, Jianmin He, and Qunyao Yin

School of Economics and Management, Southeast University, Nanjing, Jiangsu 211189, China

Correspondence should be addressed to Tingqiang Chen; tingqiang88888888@163.com

Received 3 October 2012; Revised 4 December 2012; Accepted 20 December 2012

Academic Editor: Qingdu Li

This work introduces a nonlinear dynamics model of credit risk contagion in the credit risk transfer (CRT) market, which contains time delay, the contagion rate of credit risk, and nonlinear resistance. The model depicts the dynamics behavior characteristics of evolution of credit risk contagion through numerical simulation. Meanwhile, numerical simulations show that, in the CRT market, the contagion rate of credit risk and the nonlinear resistance among CRT activities participants have some significant effects on the dynamics behaviors of evolution of credit risk contagion. Specifically, on the one hand, we find that the status curve of credit risk contagion that causes some significant changes with the increase in the contagion rate of credit risk, moreover, emerges a series of Hopf bifurcation and chaotic phenomena in the process of credit risk contagion. On the other hand, Hopf bifurcation and chaotic phenomena appear in advance with the increase in the nonlinear resistance coefficient and time-delay. In addition, there are a series of periodic windows in the chaotic interval inside, including Hopf bifurcation, inverse bifurcation, and chaos.

1. Introduction

Over the past few years, with the significant development of nonlinear science, economists have gradually started to use nonlinear theory to study the complex phenomena of social economic system [1–7]. Some far-sighted economists began to apply the nonlinear science research results into economics, which produced the nonlinear economics and the chaos economics. The latest studies of nonlinear theory show that whether interpersonal network, computer network, ecological system, economic system, or disease spread, computer virus spread, forest fire spread, risk spread, complex nonlinear dynamics phenomena, and so forth, can be observed in these social phenomena [8, 9]. The aforementioned phenomena present complex dynamical behavior, involving Hopf bifurcation, inverse bifurcation, chaos, and fractals. Among these behavior types, chaos and bifurcation are complex phenomena that exist in the nonlinear financial system and are important issues in economic and financial dynamics research [10]. Credit risk transfer (CRT) market is a third-party market that connects with the credit markets, the securities market, and the insurance market, in which credit risk contagion has some complex nonlinear characteristics obviously.

At present, participants of the CRT market covered mainly universal banks, commercial banks, securities dealers, insurance companies, investment funds, and parts of nonfinancial institutions. Among them exist close and complicated network relations directly or indirectly, and that constituted a nonlinear giant system. Because the interactions between individuals that have complex nonlinear dynamic properties. Moreover, credit risk contagion is dependent on CRT behaviors of participants of the CRT market and market information dissemination of the relationship network. With the rapid development of the CRT market, the quantity of participants, and the depth and breadth of CRT trading all rapidly increase. This will lead to the increase in the complexity of the CRT market and make the distribution of information and risk of terminal undertaker of credit risk change more complicate. Meanwhile, the rapid development structured products will also increase the complexity. These will make the financial institutions extremely easily cause the superposition or clustering of credit risk in credit risk transfer and cause credit risk contagion. However, credit risk

contagion also has complex nonlinearity. It will increase the difficulty of the prediction and control of credit risk in CRT market and bring great challenges to credit risk management departments.

Generally, some participants do not fully understand the potential risk of CRT market or lack of corresponding risk management ability into the CRT market, which will lead to some new risks in the process of CRT behaviors. Moreover, the systemic risk can increase in the CRT market. In the imperfect competition market, CRT behaviors not only did not spread risk, but also added to the system risk and increased the likelihood of the credit risk contagion [11]. The existing literature also showed that the rapid development of the CRT market increased the possibility of credit risk contagion across departments and trade. For example, credit risk transfer in creating contagion between banking and insurance systems and caused contagion, and the spread in systemic risk made everybody worse off. At the same time, credit risk transfer induced insurance companies to hold the same assets as banks [12]. Banks' motive of extensive using CDS (Credit Default Swap) is that improve the diversification of their credit risk. However, this might reduce banks' stability. The main reasons behind these negative impacts are firstly, that banks are induced to increase their investment in an illiquid, risky credit portfolio and secondly, that these CDS create a possible channel of credit risk contagion [13].

The theory and practice have recognized the serious consequences of the credit default contagion by the US subprime mortgage crisis in 2008. Moreover, a number of studies are also aware of credit risk contagion in the CRT process [11–14]. At present, the study of credit risk contagion mainly focus on the interbank market and credit market. However, the existing credit risk model have not yet discussed and involved nonlinear dynamic problems of the risk contagion process. However, nonlinear dynamic behaviors are obvious in credit risk contagion due to the complex network relationships, the continuous innovation of CRT tools, and the asymmetric information in CRT market. Moreover, network relations of CRT market exist time delay and nonlinear resistance. Therefore, we try to put the nonlinear system theory into the study of the credit risk contagion in CRT market and construct the nonlinear dynamic model of credit risk contagion in CRT market. Then, we conduct numerical simulation to analyze the dynamic behaviors characteristics of evolution of credit risk contagion in CRT market.

The remainder of this paper is organized as follows. In Section 2, the model of credit risk contagion in CRT market and dynamics behavior characteristics of evolution of credit risk contagion are discussed through numerical simulation. In Section 3, we discuss the bifurcation and chaotic behaviors of credit risk contagion. Finally, we conclude the paper in Section 4.

2. Dynamics Evolution of Credit Risk Contagion Based on the Vector Field

With the development of network theory, a number of studies have taken into account the spread and response characters of events in a long-distance connection of network. Newman and Watts [15], Moukarzel [16] have given the dynamic model of constant speed transmission of the events in the network. However, they have not taken into account time-delay and various nonlinear factors. Yang [17] took into account the nonlinear factor and time-delay of events in the long connection and constructed the reasonable dynamic model.

2.1. The Contagion Model of Credit Risk in the CRT Market. We are enlightened by the works [17–19] and propose the dynamic model of credit risk contagion in the CRT market. On the one hand, we assume that the complex network connections among CRT activities participants are Newman-Watts length scale connections and long-distance connections. On the other hand, we take into account the time-delay and nonlinear resistance of long-distances connection between CRT activities participants. In fact, the model is also a nonlinear time-delay differential equation. Therefore, the dynamic model of credit risk contagion is described by the following time-delay differential equation:

$$\begin{aligned} \frac{dN(t)}{dt} &= \lambda k_1 - N(t) + \lambda k_2 N(t-\tau) \\ &\quad - \mu\xi\left[\lambda k_2 N(t-\tau)\right]^2 \quad t \geq 0, \\ N(t) &= c \quad -\tau \leq t \leq 0, \end{aligned} \tag{1}$$

where $N(t)$ denotes the number of CRT activities participants that are infected by credit risk in the CRT market, ξ refers to Newman-Watts length scale, k_1 is the number of instances that the connection distance from the participant infected by credit risk is a Newman-Watts length scale, k_2 is the number of instances that the connection distance from the participant infected by credit risk is a long-distance connection, λ is the effective contagion rate of credit risk in the CRT market, μ is the nonlinear resistance coefficient of the relationship network comprising CRT market participants, $c \in \mathbb{R}^+$ is a real parameter, and τ is the time-delay of credit risk contagion in the long-distance connection. Therefore, the mechanism of the time-delay and the nonlinear resistance of credit risk contagion in Newman-Watts length scale connection and long-distance connection can be described by the time-delay differential equation (1).

According to the general definition, we can derive the balance position and stable point of credit risk contagion when the left side of equation (1) is equal to zero. In fact, this kind of nonlinear dynamics system can be denoted by equation (1), where balance positions may become unstable, periodic solution and the system vibration may emerge, and the phenomenon of Hopf bifurcation and chaos may occur, along with the change in various parameters [20]. Torelli [21], Liu and Spijker [22] have given a numerical Euler method for the solution of delay differential equation as equation (1). We still use the method in this paper. Now, let the stepsize h is such that $h = \tau/m$ and $\theta \in [0, 1]$, where τ is a time-delay, and m is a positive integer. Therefore, according to the one-point

collocation rule for delay differential equation (1), we can get

$$\begin{aligned} N_{n+1} &= N_n + \lambda k_1 h - h\left[(1-\theta)N_n + \theta N_{n+1}\right] \\ &\quad + \lambda k_2 h\left[(1-\theta)N_{n-m} + \theta N_{n-m+1}\right] \\ &\quad - \mu\xi\lambda^2 k_2^2 h\left[(1-\theta)N_{n-m} + \theta N_{n-m+1}\right]^2, \end{aligned} \tag{2}$$

where N_n denotes the approximate value of $N(t)$ at the point t_n. Let $= (m-\delta)h + h/2 (0 \le \delta < 1)$, then $\Omega_h = \{t_n = nh, n \in Z\}$. Thus, we can get $t_n + \theta h \in [t_n, t_{n+1}]$ and $t_n + \theta h - \tau \in [t_{n-m}, t_{n-m+1}]$. We apply the θ-collocation method to define the approximate value of $N(t)$ at the point $t_n + \theta h$ and $t_n + \theta h - \tau$ as follows:

$$\begin{aligned} N(t_n + \theta h) &\approx \theta\left[N(t_n) + N(t_{n+1})\right], \\ N(t_n + \theta h - \tau) &\approx \theta\left[N(t_{n-m}) + N(t_{n-m+1})\right]. \end{aligned} \tag{3}$$

We apply the midpoint collocation method (one-point collocation with $\theta = 1/2$) to equation (1), and can get

$$\begin{aligned} N_{n+1} &= N_n + \lambda k_1 h - h\left[\frac{N_n + N_{n+1}}{2}\right] \\ &\quad + \lambda k_2 h\left[\frac{N_{n-m} + N_{n-m+1}}{2}\right] \\ &\quad - \mu\xi\lambda^2 k_2^2 h\left[\frac{N_{n-m} + N_{n-m+1}}{2}\right]^2. \end{aligned} \tag{4}$$

Namely,

$$\begin{aligned} N(t_{n+1}) &= N(t_n) + \lambda k_1 h - h\left[\frac{N(t_n) + N(t_{n+1})}{2}\right] \\ &\quad + \lambda k_2 h\left[\frac{N(t_{n-m}) + N(t_{n-m+1})}{2}\right] \\ &\quad - \mu\xi\lambda^2 k_2^2 h\left[\frac{N(t_{n-m}) + N(t_{n-m+1})}{2}\right]^2. \end{aligned} \tag{5}$$

Put equation (3) into equation (5), we can get

$$\begin{aligned} N(t_{n+1}) &\approx N(t_n) + \lambda k_1 h - hN\left(t_n + \frac{h}{2}\right) \\ &\quad + \lambda k_2 hN\left(t_n + \frac{h}{2} - \tau\right) \\ &\quad - \mu\xi\lambda^2 k_2^2 h\left[N\left(t_n + \frac{h}{2} - \tau\right)\right]^2. \end{aligned} \tag{6}$$

We put $h = \tau/m$ into equation (6), we can get

$$\begin{aligned} N(t_{n+1}) &\approx N(t_n) + \frac{\lambda k_1 \tau}{m} - \frac{\tau}{m}N\left(t_n + \frac{\tau}{2m}\right) \\ &\quad + \frac{\lambda k_2 \tau}{m}N\left(t_n + \frac{(1-2m)\tau}{2m}\right) \\ &\quad - \frac{\mu\xi\lambda^2 k_2^2 \tau}{m}\left[N\left(t_n + \frac{(1-2m)\tau}{2m}\right)\right]^2. \end{aligned} \tag{7}$$

To understand the effect of nonlinear factors on credit risk contagion further, we have to use equation (7) to conduct numerical simulations under the given parameters μ, ξ, k_1, k_2, λ, and τ and the initial condition $N(t) = c\ (-\tau \le t \le 0)$.

2.2. Simulation Analysis of the Dynamics Behavior of Evolution of Credit Risk Contagion in the CRT Market. We try to describe the dynamics behavior characteristics of evolution of credit risk contagion and its influencing factors by the nonlinear time-delayed differential equation in this paper. According to the solving process of equation (1), we know that parameters μ, ξ, k_1, k_2, and λ and the initial condition $N(t) = c\ (-\tau \le t \le 0)$ will affect the stability of the solution of time-delayed differential equations and the trajectory of the process of credit risk contagion. In order to describe the dynamic behaviors and its influencing factors of the process of credit risk contagion in CRT market, we take parameters λ and μ as the bifurcation parameter. Then, we conduct numerical simulations to the dynamics system (1) and analyze the dynamics behavior of credit risk contagion in CRT market. Let $\tau = 1$, $h = 0.01$, $m = 100$, $\delta = 0.5$, $\xi = 3$, $k_1 = 10$, $k_2 = 25$, and the initial condition $N(t) = 2 (t \in (-\tau, 0))$. Figure 1 depicts the effect of the effective contagion rate λ of credit risk on the trajectory curve of credit risk contagion in the CRT market. We find that the status of credit risk contagion changes gradually from "hyperbolic attenuation" (a piece of the hyperbolic) to "logarithm Gauss attenuation," and the influence strength and range of credit risk contagion emerge nonlinear velocity increasing with the increase in the effective contagion rate λ of credit risk in CRT market. However, the influence strength and range attenuate rapidly after a period of time and emerge the fat-tail characteristic. This shows that the effect of the default behaviors of CRT activities participants on other participants weakened gradually after a period of time and the default intensity and default state depend on the company oneself and macroeconomic factors. Figure 2 shows that oscillation amplitude and frequency increase gradually with the increase in the effective contagion rate λ of credit risk in CRT market. However, the oscillation will weaken after a period of time. Figure 3 shows that the stable state of credit risk contagion will trend to unstable and emerge periodic solution and Hopf bifurcation with the increase in the effective contagion rate λ of credit risk in CRT market. Namely, the contagion amplitude and range of credit risk will emerge periodic oscillation with the increase in the effective rate of credit risk contagion in CRT market. Moreover, the limit cycle radius of the attractive domain increases gradually, and the shape of the limit cycle becomes increasingly irregular, such that the bifurcation and chaos phenomena occur with the increase in the effective contagion rate λ of credit risk contagion. In Figure 4, we find that the process of credit risk contagion present different "logarithm Gauss attenuation" feature under the influence of the nonlinear resistance of the relationship network comprising CRT activities participants. In Figure 5, we find that the oscillation of the process of credit risk contagion is not affected with the increase in the nonlinear resistance coefficient μ. However, the number of CRT activities

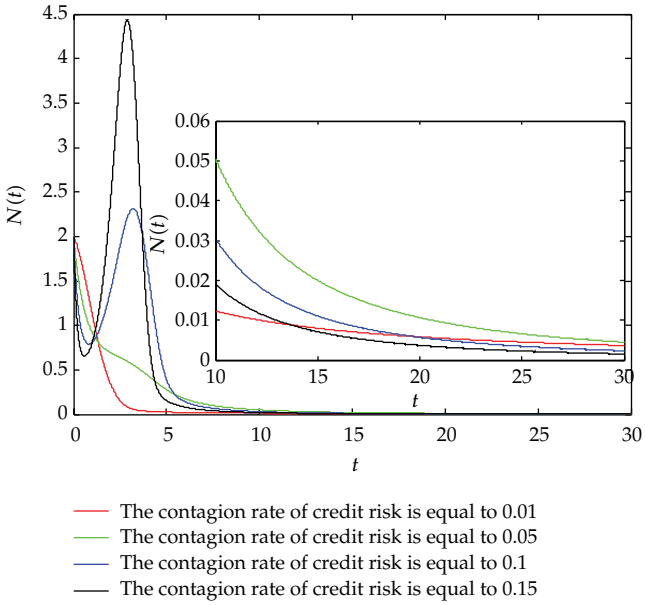

Figure 1: The trajectory curve of credit risk contagion where $\mu = 0.03$.

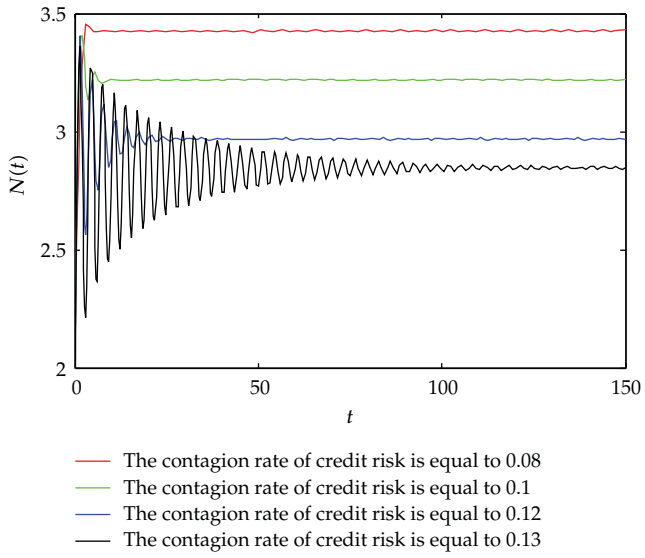

Figure 2: The step response of the process of credit risk contagion where $\mu = 0.03$.

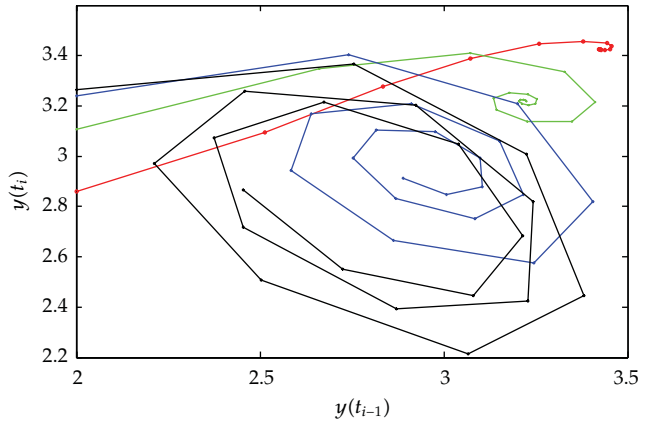

Figure 3: The phase diagram of the process of credit risk contagion where $\mu = 0.03$.

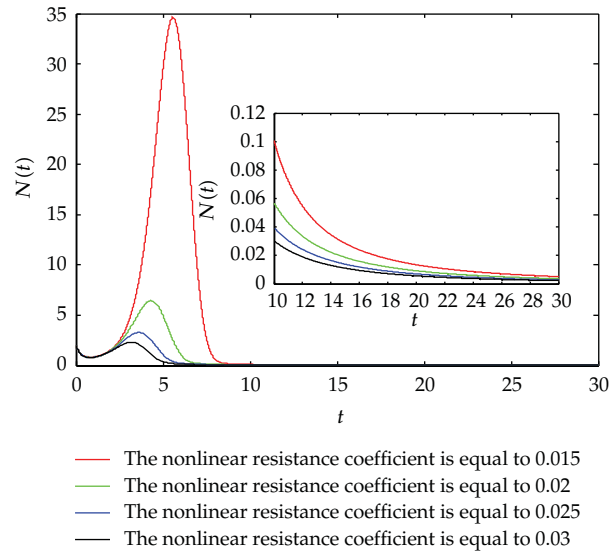

Figure 4: The state trajectory curve of the process of credit risk contagion where $\lambda = 0.1$.

participants $N(t)$ gradually reduces with the increase in the nonlinear resistance coefficient μ. In Figure 6, we find that the effect of the nonlinear resistance coefficient μ on the attract factor of balance position of credit risk contagion, and the number of CRT activities participants $N(t)$ is very sensitive. Namely, the attractive factor of credit risk contagion and the number of CRT activities participants $N(t)$ will decrease rapidly with the increase in nonlinear resistance coefficient μ.

3. Bifurcation and Chaotic Analysis of Credit Risk Contagion Based on Logistic Mapping

3.1. The Model Analysis of Credit Risk Contagion Based on Logistic Mapping. The model (1) of credit risk contagion used the form of vector field to discuss credit risk contagion in credit risk transfer. However, the previous figures are not intuitive and are difficult to interpret. Thus, analyzing the properties of the dynamic system of credit risk contagion, such as the difference of the trajectory curve of period doubling, may be challenging. However, given the intuition, legibility, and geometrical features of the logistic mapping, we often discretize the nonlinear problem of the continuous vector

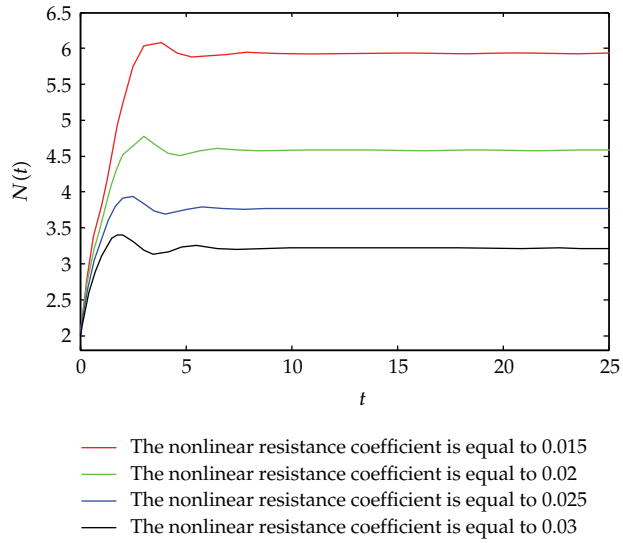

Figure 5: The step response of the process of credit risk contagion where $\lambda = 0.1$.

field to the logistic mapping by using a numerical approximation method to analyze the periodic bifurcation and chaos of nonlinear dynamics system. A number of studies use the Euler [23–25] to analyze bifurcation, periodic solution, and chaotic phenomena of nonlinear time-delayed system. We also adopt the Euler method and take step length h. Therefore, equation (1) can be transformed into the form following form:

$$\begin{aligned} &N(t-\tau+h) - N(t-\tau) \\ &\quad = h\{\lambda k_1 - N(t) + \lambda k_2 N(t-\tau) \\ &\qquad -\mu\xi[\lambda k_2 N(t-\tau)]^2\}. \end{aligned} \tag{8}$$

Let $h = \tau$, $N(t) = N_{n+1}$, and $N(t-\tau) = N_n$. Thus, equation (8) can be transformed into the form following form:

$$N_{n+1} = \frac{\lambda k_1 \tau}{1+\tau} + \frac{1+\lambda k_2 \tau}{1+\tau} N_n - \frac{\mu\xi\tau\lambda^2 k_2^2}{1+\tau}(N_n)^2. \tag{9}$$

Therefore, there exists the logistic mapping f as follow:

$$f : N_n \longmapsto N_{n+1}. \tag{10}$$

According to the definition of the fixed point of the logistic mapping, we know that the fixed point of the logistic mapping f should meet $N_{n+1} = N_n = N^*$. Therefore, we can get the analytic equation of the fixed point of the logistic mapping as follow:

$$\frac{\mu\xi\tau\lambda^2 k_2^2}{1+\tau}(N^*)^2 - \frac{\lambda k_2 \tau - \tau}{1+\tau} N^* - \frac{\lambda k_1 \tau}{1+\tau} = 0. \tag{11}$$

Therefore, we can get the fixed point of the logistic mapping f by equation (11) as follow:

$$\begin{aligned} N_1^* &= \frac{(\lambda k_2 \tau - \tau) + \sqrt{(\lambda k_2 \tau - \tau)^2 + 4\mu\xi k_1 \tau^2 \lambda^3 k_2^2}}{2\mu\xi\tau\lambda^2 k_2^2}, \\ N_2^* &= \frac{(\lambda k_2 \tau - \tau) - \sqrt{(\lambda k_2 \tau - \tau)^2 + 4\mu\xi k_1 \tau^2 \lambda^3 k_2^2}}{2\mu\xi\tau\lambda^2 k_2^2}. \end{aligned} \tag{12}$$

Obviously, $N_2^* < 0$ is unrealistic. Therefore, the fixed point N_1^* is sole fixed point of the logistic mapping f. According to the definition of the logistic mapping and the Lyapunov movement stability, we know that the movement stability of the fixed point depends on the characteristic root of the derived operator of the logistic mapping, which is Floquet multiplier [26, 27]. Therefore, the Floquet multiplier will determine the stability of the fixed point N_1^*. Namely,

$$Dg|_{N^*} = 1 - \frac{\sqrt{(\lambda k_2 \tau - \tau)^2 + 4\mu\xi k_1 \tau^2 \lambda^3 k_2^2}}{1+\tau}. \tag{13}$$

According to the nonlinear system theory [27, 28], if $|Dg|_{N^*} > 1$, then the fixed point N^* will become unstable; if $|Dg|_{N^*} < 1$, then the fixed point N^* is asymptotically stable; if $|Dg|_{N^*} = 1$, then the fixed point N^* is criticality stable. So, for the fixed point N^* of the mapping f, the fixed point N^* is asymptotically stable when $\mu < (4(1+\tau)^2 - (\lambda k_1 \tau - \tau)^2)/4\xi k_1 k_2^2 \tau^2 \lambda^3$, is criticality stability when $\mu = (4(1+\tau)^2 - (\lambda k_1 \tau - \tau)^2)/4\xi k_1 k_2^2 \tau^2 \lambda^3$, or is unstable when $\mu > (4(1+\tau)^2 - (\lambda k_1 \tau - \tau)^2)/4\xi k_1 k_2^2 \tau^2 \lambda^3$.

According to the nonlinear dynamic related theory [26–28], if there exists a series of period-doubling bifurcation phenomena, then a series of period-doubling bifurcation leads to chaos. In recent years, much works used topological horseshoes embedded method to study chaos rigorously [28–34]. By this method, one can not only prove the existence of chaos, but also reveal the mechanism of chaotic phenomena by showing the structure of chaotic attractors [31–34]. Beyond that, some works used the Lyapunov exponents [35] and set oriented numerical methods [36, 37] to prove the existence of chaos. Li and Yorke [38] gave a definition of chaos that the existence of a point of period 3 implies the existence of chaos. Therefore, according to this definition, we use numerical simulation to discuss the fixed point and its stability, bifurcation, and chaos of the mapping from the intuitive.

3.2. Numerical Simulation Analysis. Let $\xi = 3$, $\tau = 1$, $k_1 = 10$, $k_2 = 25$, and the initial condition $N(t) = 2$ ($t \in (-\tau, 0)$). We use equation (8) to conduct numerical simulations. The Figure 3 reflects the Hopf bifurcation process and its variation characteristics of credit risk contagion with parameter λ and μ. Figures 7(a) and 7(b) reflect the Hopf bifurcation and chaos characteristics of credit risk contagion with the increase in the effective contagion rate λ of credit risk. Figure 7(a) reflects that the process of credit risk contagion exists the only stable constant state when parameter λ is kept at a proper level.

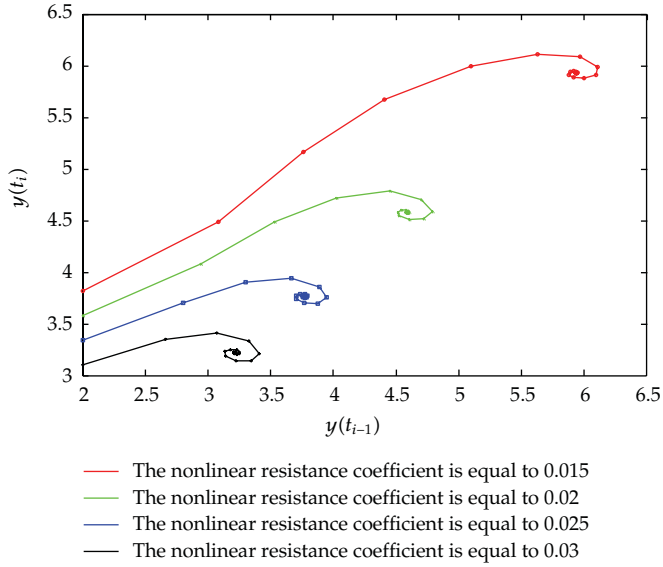

Figure 6: The phase diagram of the process of credit risk contagion where $\lambda = 0.1$.

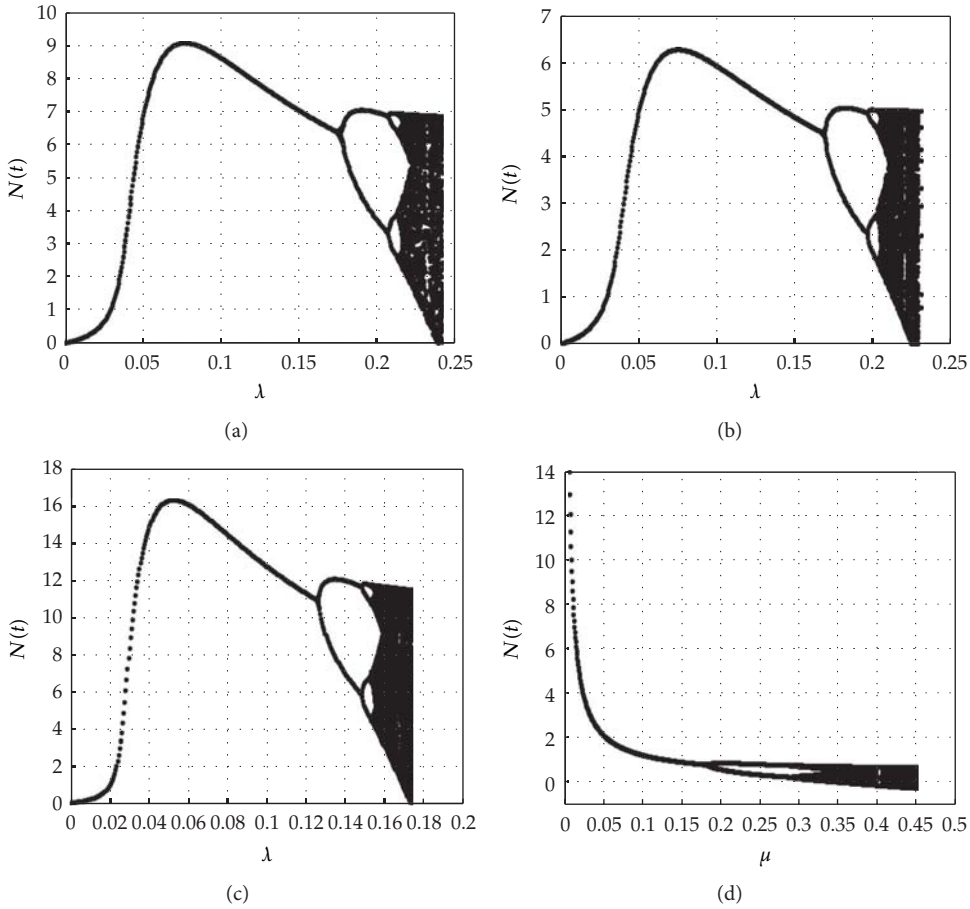

Figure 7: (a) The bifurcation diagram of the process of credit risk contagion with λ when $\mu = 0.01$; (b) the bifurcation diagram of the process of credit risk contagion with λ when $\mu = 0.015$; (c) the bifurcation diagram of the process of credit risk contagion with λ when $\mu = 0.01$, $\tau = 1.5$; (d) the bifurcation diagram of the process of credit risk contagion with μ when $\lambda = 0.1$.

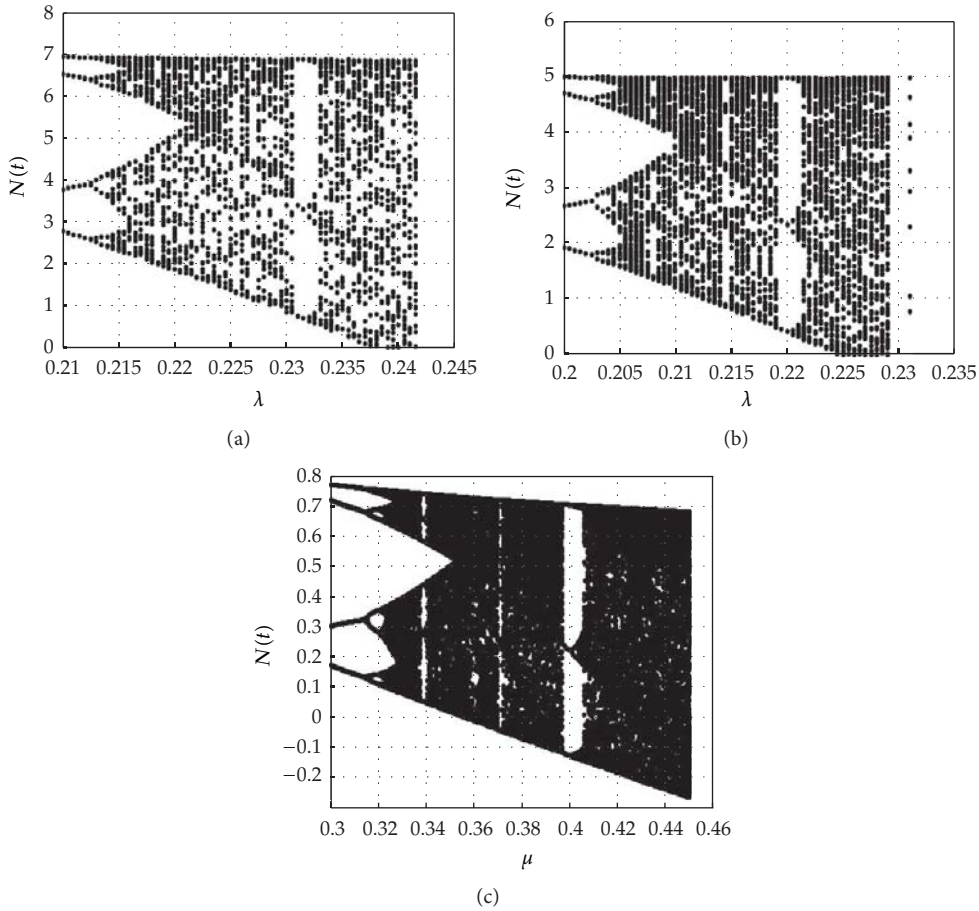

Figure 8: (a) The bifurcation diagram in the chaos area when $\mu = 0.01$; (b) the bifurcation diagram in the chaos area when $\mu = 0.015$; (c) the bifurcation diagram in the chaos area when $\lambda = 0.1$.

Moreover, the process of credit risk contagion emerge different types of period bifurcation and periodic oscillation with the increase in the effective contagion rate λ of credit risk in CRT market. According to the definition of Li-Yorke [29], the process of credit risk contagion can occur chaos phenomenon when the effective contagion rate λ reaches to a proper value. Figure 7(b) reflects a series of similar characteristics with Figure 7(a). However, we also find that the Hopf bifurcation and chaotic phenomena of credit risk contagion emerge in advance with the increase in the nonlinear resistance coefficient μ. In Figure 7(c), we find that the Hopf bifurcation and chaotic phenomena of credit risk contagion emerge in advance with the increase in time-delay τ. In Figure 7(d), we find that the process of credit risk contagion exists the only stable constant state when parameter λ is kept at a proper level. Moreover, the process of credit risk contagion emerges different types of period bifurcation and periodic oscillation with the increase in the nonlinear resistance coefficient μ among CRT activities participants. According to the definition of Li-Yorke [29], the process of credit risk contagion can occur chaos phenomenon when the nonlinear resistance coefficient μ reaches to a proper value.

According to numerical simulation and comparative analysis, we find that the process of credit risk contagion can emerge three states, including the stable constant state, Hopf bifurcation, and chaos with the increase in parameter λ and μ. However, these cannot more directly depict the nonlinear dynamic behavior characteristics after occurring chaotic phenomena. Therefore, we further discuss the effect of these parameters on the chaotic state and the period window of the process of credit risk contagion. In Figures 8(a) and 8(b), we find that Hopf bifurcation, pour bifurcation, and chaos mixed emerge in chaotic interval internal period window. Moreover, Hopf bifurcation, pour bifurcation, and chaos phenomena emerge in advance in chaos interval inside with the increase in nonlinear resistance coefficient μ. Figure 8(c) shows that chaos states are significant in the process of credit risk contagion with the increase in nonlinear resistance coefficient μ. However, Hopf bifurcation and pour bifurcation features become relatively obscure comparing to the Figures 8(a) and 8(b).

4. Conclusion

In this paper, we constructed a nonlinear dynamic model of credit risk contagion based on literatures [17–19]. Moreover, the dynamical properties of the nonlinear dynamics system

of credit risk contagion were investigated. We found that the effective rate of credit risk contagion and nonlinear resistance between CRT market participants have significant effect on dynamics behavior of credit risk contagion. Moreover, we found a series of complex Hopf bifurcation, inverse bifurcation, and chaos phenomena in the nonlinear dynamics system of credit risk contagion through a numerical simulation. At the same time, there are a series of period window in chaos interval inside, and that emerge intertwined state including Hopf bifurcation, pour bifurcation, and chaos. The study of dynamics behavior of evolution of credit risk contagion can help us to understand the effect of the interaction between the internal nonlinear factors and external disturbance of credit risk contagion, which has important theoretical and practical value.

There is still much work that is worth further research. For example, in the real world, a variety of noises usually influence the process of credit risk contagion and its dynamics behaviors, such as Gaussian noise, random noises, and so forth. For the kind of credit risk contagion with both time-delay and noises, we leave it for the future work.

Acknowledgments

The authors wish to express their gratitude to the referees for their invaluable comments. This work was supported by the National Natural Science Foundation of China Grant (nos. 71071034, 71173103, and 71201023), the Humanities and Social Science Youth Foundation of the Ministry of Education of China (no. 12YJC630101), the Funding of Jiangsu Innovation Program for Graduate Education (no. CXZZ12-0131), and the Scientific Research Foundation of Graduate School of Southeast University (no. YBJJ1238).

References

[1] O. Gomes, "Routes to chaos in macroeconomic theory," *Journal of Economic Studies*, vol. 33, no. 6, pp. 437–468, 2006.

[2] P. Holmes, "A nonlinear oscillator with a strange attractor," *Philosophical Transactions of the Royal Society of London*, vol. 292, no. 1394, pp. 419–448, 1979.

[3] S. Serrano, R. Barrio, A. Dena, and M. Rodríguez, "Crisis curves in nonlinear business cycles," *Communications in Nonlinear Science and Numerical Simulation*, vol. 17, no. 2, pp. 788–794, 2012.

[4] B. H. Kim, H. G. Min, and Y. K. Moh, "Nonlinear dynamics in exchange rate deviations from the monetary fundamentals: an empirical study," *Economic Modelling*, vol. 27, no. 5, pp. 1167–1177, 2010.

[5] T. O. Awokuse and D. K. Christopoulos, "Nonlinear dynamics and the exports-output growth nexus," *Economic Modelling*, vol. 26, no. 1, pp. 184–190, 2009.

[6] W. Wu, Z. Chen, and W. H. Ip, "Complex nonlinear dynamics and controlling chaos in a Cournot duopoly economic model," *Nonlinear Analysis: Real World Applications*, vol. 11, no. 5, pp. 4363–4377, 2010.

[7] L. F. Petrov, "Nonlinear effects in economic dynamic models," *Nonlinear Analysis: Theory Methods & Applications*, vol. 71, no. 12, pp. e2366–e2371, 2009.

[8] B. Liu, Y. Duan, and S. Luan, "Dynamics of an SI epidemic model with external effects in a polluted environment," *Nonlinear Analysis: Real World Applications*, vol. 13, no. 1, pp. 27–38, 2012.

[9] S. Reitz and M. P. Taylor, "The coordination channel of foreign exchange intervention: a nonlinear microstructural analysis," *European Economic Review*, vol. 52, no. 1, pp. 55–76, 2008.

[10] B. Xin, J. Ma, and Q. Gao, "The complexity of an investment competition dynamical model with imperfect information in a security market," *Chaos, Solitons & Fractals*, vol. 42, no. 4, pp. 2425–2438, 2009.

[11] F. Allen and D. Gale, "Systemic risk and regulation," Wharton Financial Institutions Center Working Paper No. 95-124, 2005.

[12] F. Allen and E. Carletti, "Credit risk transfer and contagion," *Journal of Monetary Economics*, vol. 53, no. 1, pp. 89–111, 2006.

[13] U. Neyer and F. Heyde, "Credit default swaps and the stability of the banking sector," *International Review of Finance*, vol. 10, no. 1, pp. 27–61, 2010.

[14] T. Santos, "Comment on: credit risk transfer and contagion," *Journal of Monetary Economics*, vol. 53, no. 1, pp. 113–121, 2006.

[15] M. E. J. Newman and D. J. Watts, "Scaling and percolation in the small-world network model," *Physical Review E*, vol. 60, no. 6, pp. 7332–7342, 1999.

[16] C. F. Moukarzel, "Spreading and shortest paths in systems with sparse long-range connections," *Physical Review E*, vol. 60, no. 6, part A, pp. R6263–R6266, 1999.

[17] X. S. Yang, "Chaos in small-world networks," *Physical Review E*, vol. 63, no. 4, Article ID 046206, 4 pages, 2001.

[18] S. R. Pastor, A. Vázquez, and A. Vespignani, "Dynamical and correlation properties of the internet," *Physical Review Letters*, vol. 87, no. 25, Article ID 258701, 4 pages, 2001.

[19] S. R. Pastor and A. Vespignani, "Epidemic dynamics and endemic states in complex networks," *Physical Review E*, vol. 63, no. 6, Article ID 066117, 8 pages, 2001.

[20] J. Guckenheimer and P. Holmes, *Nonlinear Oscillations, Dynamical Systems, and Bifurcations of Vector Fields*, vol. 42 of *Applied Mathematical Sciences*, Springer, Berlin, Germany, 1990.

[21] L. Torelli, "Stability of numerical methods for delay differential equations," *Journal of Computational and Applied Mathematics*, vol. 25, no. 1, pp. 15–26, 1989.

[22] M. Z. Liu and M. N. Spijker, "The stability of the θ-methods in the numerical solution of delay differential equations," *IMA Journal of Numerical Analysis*, vol. 10, no. 1, pp. 31–48, 1990.

[23] N. J. Ford and V. Wulf, "The use of boundary locus plots in the identification of bifurcation points in numerical approximation of delay differential equations," *Journal of Computational and Applied Mathematics*, vol. 111, no. 1-2, pp. 153–162, 1999.

[24] T. Koto, "Periodic orbits in the Euler method for a class of delay differential equations," *Computers & Mathematics with Applications*, vol. 42, no. 12, pp. 1597–1608, 2001.

[25] M. Peng, "Bifurcation and chaotic behavior in the Euler method for a Uçar prototype delay model," *Chaos Solitons Fractals*, vol. 22, no. 2, pp. 483–493, 2004.

[26] R. Seydel, *Practical Bifurcation and Stability Analysis: From Equilibrium to Chaos*, Springer, 1999.

[27] D. Rugh, *Nonlinear System Theory*, The John Hopkins University Press, Baltimore, Md, USA, 1980.

[28] S. Wiggins, *Introduction to Applied Nonlinear Dynamical Systems and Chaos*, vol. 2 of *Texts in Applied Mathematics*, Springer Academic Press, New York, NY, USA, 1990.

[29] J. Kennedy and J. A. Yorke, "Topological horseshoes," *Transactions of the American Mathematical Society*, vol. 353, no. 6, pp. 2513–2530, 2001.

[30] X.-S. Yang and Y. Tang, "Horseshoes in piecewise continuous maps," *Chaos, Solitons & Fractals*, vol. 19, no. 4, pp. 841–845, 2004.

[31] Q. Li, "A topological horseshoe in the hyperchaotic Rössler attractor," *Physics Letters A*, vol. 372, no. 17, pp. 2989–2994, 2008.

[32] Q. Li and X.-S. Yang, "A simple method for finding topological horseshoes," *International Journal of Bifurcation and Chaos in Applied Sciences and Engineering*, vol. 20, no. 2, pp. 467–478, 2010.

[33] Q. Li and X.-S. Yang, "New walking dynamics in the simplest passive bipedal walking model," *Applied Mathematical Modelling*, vol. 36, no. 11, pp. 5262–5271, 2012.

[34] Q. Li and X. Yang, "Two kinds of horseshoes in a hyperchaotic neural network," *International Journal of Bifurcation and Chaos*, vol. 22, no. 8, Article ID 1250200, 14 pages, 2012.

[35] K. Tomasz, M. Konstantin, and M. Marian, *Computational homology*, vol. 157 of *Applied Mathematical Sciences*, Springer, New York, NY, USA, 2004.

[36] T. Csendes, B. M. Garay, and B. Bánhelyi, "A verified optimization technique to locate chaotic regions of Hénon systems," *Journal of Global Optimization*, vol. 35, no. 1, pp. 145–160, 2006.

[37] S. Sertl and M. Dellnitz, "Global optimization using a dynamical systems approach," *Journal of Global Optimization*, vol. 34, no. 4, pp. 569–587, 2006.

[38] T. Y. Li and J. A. Yorke, "Period three implies chaos," *The American Mathematical Monthly*, vol. 82, no. 10, pp. 985–992, 1975.